PYROLYSIS OF THERMAL PROTECTION SYSTEM MATERIALS: MOLAR YIELDS OF VOLATILE PRODUCTS DERIVED FROM IN SITU MASS SPECTROMETRIC MEASUREMENTS

by

Brody Kelly Bessire

A dissertation submitted in partial fulfillment
of the requirements for the degree

of

Doctor of Philosophy

in

Chemistry

MONTANA STATE UNIVERSITY
Bozeman, Montana

April 2018

DEDICATION

This work is dedicated to Hanni Bessire. Our journey to Montana State University began with a long road trip down the Alaska-Canada highway. Our first night on the road was spent inside a tent with two cats, at a campground in Destruction Bay, that was closed for bear activity. Hanni has been a dedicated companion and friend throughout our time in graduate school. This work would not have been accomplished without her support and patience over the course of the past few years. She has taught me what it means to be loved and how to care for other people. Thank you for being such a beautiful person, I love you.

Leo, I love you buddy, and you will never be forgotten.

I would like to thank my parents for always being available to give good advice, and for their encouragement over the years. I would also like to thank Betty, Dan, Sam, and Inga, for accepting me into their family, and caring for me as if I were one of their own. I would also like to thank my beautiful sisters for their support. Grandma and Grandpa Bessire, thank you for your love and for taking an interest in my research. Granny June, I bet you can hear the ducks now!

Brooks Marshall and Tino Woodburn, thank you for your general enthusiasm for life and for taking the time to teach me the fundamentals of the lab. Our long conversations about science and life have broadened my perspective, and I am a better person as a result.

I would also like to thank the scientists and engineers at the NASA Ames Research Center for supporting this research.

I would also like to thank all the great teachers that I have had over the years. I would like to thank Mr. Scow for introducing me to AutoCAD and 3D studio max. A special thank you to Dr. Tarter for inspiring me to become a chemist. Dr. Bronson deserves a special thank you for demanding excellence in organic chemistry and providing quality lectures and labs.

Finally, I have a fortunate position in life. It is not lost on me that I have been surrounded by the best of the best, and this alone has led directly to my success. Thank you all.

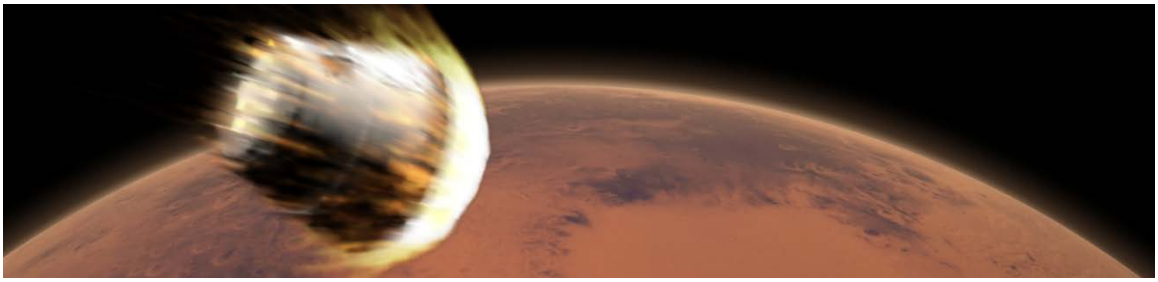

ACKNOWLEDGMENTS

I would like to thank my graduate advisor, Dr. Timothy K. Minton. His desire for excellence is unequaled and has been a constant source of motivation. Thank you for providing me with the opportunity to perform research in a world-class setting and for teaching me how to think critically about science, experimentation, and even art! Thank you to Dr. Sridhar Lahankar for getting me started with this research and for our many conversations. I am thankful to my committee members: Dr. Pat Callis, Dr. Robert Walker, Dr. Nicholas Stadie, and Dr. Berk Knighton. I would also like to thank the members of the Minton Lab Group. I have been very fortunate to have been surrounded by talented colleagues who have pushed me to be a better scientist. Thank you to Dr. Poovathingal for your kindness and willingness to talk about science and life. Finally, a special thank you is extended to Dr. Mansour, Dr. Wright, and the rest of the staff at the NASA Ames Research Center for providing me with the opportunity to work on this research project.

TABLE OF CONTENTS

TABLE OF CONTENTS – CONTINUED

TABLE OF CONTENTS – CONTINUED

LIST OF TABLES

LIST OF TABLES – CONTINUED

Table Page

LIST OF FIGURES

LIST OF FIGURES – CONTINUED

Figure Page

LIST OF FIGURES – CONTINUED

Figure Page

LIST OF FIGURES – CONTINUED

Figure Page

LIST OF FIGURES – CONTINUED

Figure Page

LIST OF FIGURES – CONTINUED

Figure Page

LIST OF FIGURES – CONTINUED

Figure Page

LIST OF FIGURES – CONTINUED

Figure Page

LIST OF FIGURES – CONTINUED

Figure Page

ABSTRACT

Mass spectrometric techniques have been developed to measure the molar yields of pyrolysis products from ablative resins and composite materials at heating rates that are relevant to flight conditions. Thermal decomposition mechanisms of phenolic and an epoxy-novolac resin systems are reviewed. New insights into the thermal decomposition mechanisms of PICA (Phenolic Impregnated Carbon Ablator) and epoxy-novolac D.E.N. 438 (Dow Epoxy-Novolac) are proposed and are based on the measurements of molar yields from these materials. Molar yield data have been provided in the appendices of this thesis for use in material response models.

The thermal decomposition of phenolic impregnated carbon ablator (PICA) has been investigated with the objective of measuring molar yields of pyrolysis products at heating rates that are relevant to MSL flight conditions. The relative molar yields of 14 pyrolysis gases were obtained in conjunction with mass loss measurements. These measurements allowed for the calculation of absolute molar yields and mass yields as a function of temperature and heating rate, as well as the simulation of TGA curves. Pyrolysis product yields change as a function of heating rate, and this behavior has been attributed to two mechanisms that compete during the initial stages of thermal decomposition. The results of this study are now available for use in material response models.

The thermal decomposition of an epoxy-novolac resin system has also been investigated. Samples of D.E.N. 438 were cured using NMA (methyl-5-norbornene-2,3-dicarboxylic anhydride) as a crosslinking agent and BDMA (N-benzyldimethylamine) as a catalyst. A radiative heating method was developed to minimize experimental uncertainties that may emerge from thermal gradients that are established across the samples as they experience high rates of heating. The molar yields of the six dominant pyrolysis products were measured at a heating rate of 8 °C s^{-1}. The molar yields of pyrolysis products provide new insight, and a new thermal decomposition mechanism is proposed

CHAPTER ONE

INTRODUCTION

1.1 THE ATMOSPHERIC ENTRY ENVIRONMENT AND THERMAL PROTECTION SYSTEM MODELLING

When a spacecraft transitions from orbit to the surface of a planet, it must withstand the extremely high temperatures in the shock layer between the leading edge of the spacecraft and the planet's atmosphere.[1] At 11km/s, (Apollo space capsule) the tremendous kinetic energy of the freestream is converted to internal energy of the gas across the bow shock wave.[1] This phenomenon creates temperatures that can be as high as 11,600 K in the shock layer.[1] Some of this energy is absorbed by the heat shield and is conducted internally.

To prevent catastrophic failure, spacecraft need materials that mitigate the transfer of thermal energy to the substructure of the vehicle. Ablative thermal protection systems (TPSs) have been developed to mitigate the effects of the harsh atmospheric-entry environment. In general, ablative TPSs are manufactured by infiltrating a network of carbon with a sacrificial resin that is meant to absorb energy through the thermal decomposition of molecular bonds. Figure 1.1 represents theoretical core TPS samples collected from a spacecraft heatshield during atmospheric entry, and it helps to illustrate the complex process by which TPSs operate.

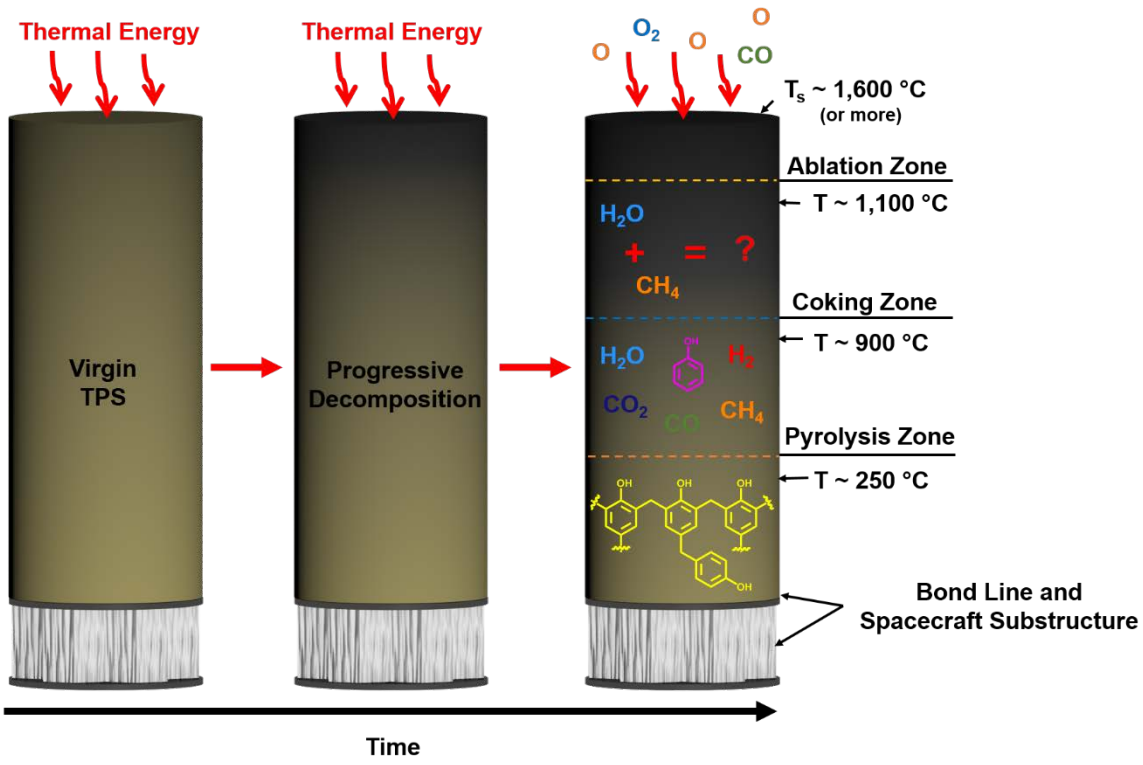

Figure 1.1. Schematic representation the thermal decomposition process for an ablative thermal protection system.

At the onset of heating, thermal energy is absorbed by the virgin material and is conducted towards the bondline between the TPS and the spacecraft substructure. As time progresses, the interface between the char and the virgin material advances closer to the bond line. In concert with this progression, several zones are formed, with all zones present after the initial decomposition of the virgin material. In the pyrolysis zone, chemical bonds in the polymer begin to break down into gaseous molecules. These gaseous molecules then diffuse through a hot carbonaceous char layer. Some of these molecules may coke the char layer through heterogeneous reactions, and therefore, the distribution of molecules that make it to the boundary layer can be altered. The final distribution of pyrolysis products

enters the boundary layer where they may participate in gas-phase reactions. Boundary layer gases, such as dissociated O_2, or CO_2 if the spacecraft is traversing the Martian atmosphere, may react with the TPS and ablate the outer char layer.

With the retirement of the space shuttle and a renewed focus on blunt body spacecraft that enter planetary atmospheres at high velocity, there has been a renewed development of TPS material response models. Ideal material response models can accurately predict the recession rate of the TPS front, the in-depth temperature response, and the maximum temperature of the bondline between the TPS and the spacecraft substructure. The validation of emerging material response codes requires accurate experimental data from pyrolysis and thermogravimetric analysis (TGA) experiments.[2-3] Accurate measurements of the molar yields from the pyrolysis of TPS materials are especially useful to inform high-fidelity models that take chemical reactions in the decomposing TPS material into account.[3-4]

State-of-the-art material response models require Arrhenius rate constants, which are typically derived from TGA mass loss measurements.[5] The majority of relevant TGA studies have been performed at much lower rates (<0.3 °C s^{-1}) than the in-depth heating rates measured during flight (frequently >10 °C s^{-1}).[6-8] In general, for lower heating rates (<5 °C s^{-1}), TGA curves shift to higher temperatures as the heating rate increases. It has been suggested that this behavior is caused by the large thermal gradients that develop between the crucible and the sample at high heating rates. As a result, decomposition reactions that would normally take place at a particular temperature appear to occur at a

higher temperature because the sample temperature lags behind the measured crucible temperature.[9] Arrhenius parameters for higher heating rates have thus been extrapolated from lower heating rate data. Models that incorporate extrapolated Arrhenius parameters suggest that thermal decomposition is delayed to higher temperatures as the rate of heating increases. On the other hand, it has also been suggested that Arrhenius parameters derived from experiments performed at lower heating rates cannot be used to make predictions for higher heating rates.[10] Very few studies have been performed that have successfully collected TGA data on the pyrolysis of pure phenolic resins at high heating rates.[11-13] Of these studies, none has correlated the observed temperature-dependent mass loss with the identities and quantitative yields of specific pyrolysis products.

1.2 THERMAL PROTECTION SYSTEM MATERIALS AND RESINS

A variety of ablative TPSs are needed to shield spacecraft from the wide range of heating environments that spacecraft can encounter as a function of different mission parameters.[14] For example, the Mars Viking lander experienced a relatively mild peak heat flux of ~25 W/cm^2 and the Galileo probe (Jupiter) was subject to a peak heat flux of ~30,000 W/cm^2.[15] To accommodate the wide range of heating environments and other mission critical parameters, new ablative TPS materials are being developed.[16]

Examples of phenolic-based rigid ablative TPSs include PhenCarb 28/15 (Applied Research Associates), BPA-FG (Boeing), and Graded MonA (Lockheed).[17] Additionally, a new type of TPS, Heatshield for Extreme Entry Environment Technology (HEEET) has

been developed, and it incorporates a dual-layer of woven carbon fiber and phenolic based material.[18]

A state-of-the-art TPS is phenolic impregnated carbon ablator (PICA), which was developed at NASA Ames Research Center and which offers low mass per unit volume and high ablation performance.[19] PICA gained heritage during the successful re-entry of the Stardust sample return capsule as well as the recent successful entry, descent, and landing (EDL) of the Mars Science Laboratory (MSL) onto the surface of Mars.[20-23] A similar material, PICA-X, is used on Space-X's commercial crew vehicle.[24] PICA is manufactured by impregnating a carbon fiber preform with a phenolic resole resin. The manufacturing process results in a material with a low density and an ablative resin with a high surface area.

Another heritage material, Avcoat, was the TPS selected for the Apollo space capsules, and a new variant has been selected for NASA's Orion space capsule.[25] Heritage Avcoat consisted of phenolic microballoons, milled E-glass, chopped silica fibers, and epoxy-novolac resin (D.E.N. 438).[26]

Finally, additional polymers are being investigated for enhanced performance properties. Examples include cyanate ester, phthalonitrile, and polyimide.[27] This thesis focuses on the thermal decomposition mechanisms of phenolic and epoxy-novolac resins.

1.3 PREVIOUS WORK

During flight, it is expected that most of the pyrolysis products are produced through the thermal decomposition of the resin in these TPS systems. Therefore, this section of the thesis is a brief review the copious literature on the pyrolysis of epoxy-novolac (D.E.N. 438), and phenolic resole resin systems.

1.3.1 THERMAL DECOMPOSITION OF PHENOLIC RESIN

The work presented in this thesis builds on the substantial literature on the decomposition mechanisms of phenolic resins and carbon/phenolic composites at elevated temperatures. The phenolic polymers that have been studied are generally similar, but there can be important differences in the molecular structure that depend on the details of how the polymer was synthesized and cured. The resulting molecular structure can influence the decomposition mechanisms, including the identity and relative molar yields of pyrolysis products. The final structure of the cured polymer depends on the ratio of formaldehyde to phenol used as reagents, the type of catalyst used during synthesis, the cure time, the cure temperature, and the curing environment. Two types of phenolic resins, resole and novolacs (Fig. 1.2), may be synthesized by the reaction of phenol with formaldehyde. Resole resins are synthesized with an excess of formaldehyde and a basic catalyst. Novolacs are synthesized with an acidic catalyst and formaldehyde-to-phenol mole ratio of less than one, and they require a crosslinking agent (hexamethylenetetramine).[28]

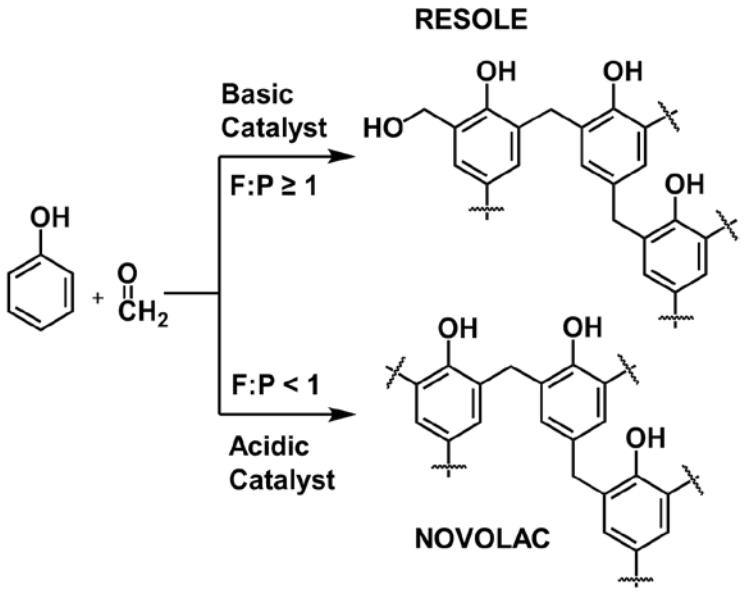

Figure 1.2. General synthesis of resole and novolac phenolic resins.

In general, the structure of a cured phenolic resin consists of a three-dimensional network of phenol molecules joined together by methylene crosslinks. Earlier studies suggest that dibenzyl ether crosslinks are formed in resole resins during the curing stage and that methylol groups may also remain after curing, which may affect the process of thermal degradation.[29-30] Jackson and Conley suggested that oxygen in the polymer structure plays a significant role in the degradation of resole-type resins,[29] in contrast to the conclusions from a study performed by Moterra and Low,[30] who reported that such incorporated oxygen does not play a significant role in the thermal degradation of novolac-type resins. Ouchi and Honda performed a study in which the pyrolysis products of seven different phenolic resins were analyzed by mass spectrometry.[31] The resins were synthesized with varying amounts of substitution by hydroxyl and methyl groups on phenol; their structures prior to synthesis are illustrated in Table 1.1. Ouchi and Honda

reported that there is a direct relationship between the identity of each phenol molecule used to synthesize the resin and the relative molar yields of products that were evolved during pyrolysis. For example, a key result was that the mole ratio of CO to CH_4 increased with increasing hydroxyl substitution in the molecular structure, while this ratio decreased with increasing methyl substitution (see Table 1.1). Thus, the nature of the phenolic resin, resole or novolac, as well as the functional group substitution on the phenol rings in the polymer (resulting either from the synthesis or the curing environment) will likely affect the decomposition mechanisms and the observed relative yields of gaseous pyrolysis products.

Table 1.1. Relationship between phenol precursor structure, formaldehyde:phenol ratio, catalyst, and the relative yields of CO and CH_4 during pyrolysis of the corresponding phenolic resin. Based on the results of Ouchi and Honda.[20]

Precursor	Formaldehyde : Phenol	Catalyst	CO : CH_4
	1	NH_4OH	0.9 : 1.0
	1	HCl	0.6 : 1.0
	2	NH_4OH	0.6 : 1.0
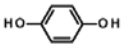	1	NH_4OH	3.0 : 1.0
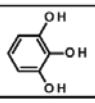	1	NH_4OH	12.0 : 1.0
	1	NH_4OH	1.0 : 2.0
	1	NH_4OH	1.0 : 6.0

Previous work on the pyrolysis mechanisms of phenolic resins has revealed three overlapping stages of pyrolysis.[29,31-33] A schematic representation of the stages of pyrolysis is presented in Fig. 1.3. As the resin is heated from ambient, there is outgassing of the resin as absorbed gases are released (labeled "Stage 0" in Fig. 1.3). The first stage of pyrolysis occurs when the temperature is elevated sufficiently ($T \approx$ 200-550 °C) such that the phenolic resin depolymerizes and produces phenol and its methyl substituted derivatives. In addition to depolymerization, cross-linking of the phenolic backbone takes place between hydroxyl or methylol functional groups, as evidenced by the evolution of H_2O.[29,31] Another product, as shown in the results reported here, is CO, which is produced in relatively low yields in the first stage of pyrolysis. During the second stage of pyrolysis ($T \approx$ 400-800 °C), bonds created from the previous cross-linking events are broken, leading to the evolution of H_2, CO, and CH_4.[29,31-32] H_2 is the dominant product evolved during the third stage of pyrolysis ($T \approx$ 560-1000 °C) as aromatic rings fuse to form a carbonaceous char.[31-32]

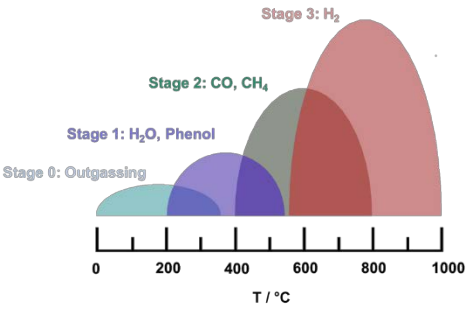

Figure 1.3 Four overlapping, temperature-dependent stages of phenolic pyrolysis, labeled with the corresponding major gas-phase pyrolysis products. Stage 1 (blue) spans an approximate temperature range of 200-550 °C. Stage 2 (green) spans the range 400-800 °C. Stage 3 (red) corresponds to temperatures above 560 °C. Absorbed gases may escape from the material during the earliest stage of heating (Stage 0: Outgassing).

Although the general pyrolysis behavior of phenolic resins has been gleaned from previous studies, these studies disagree on the specific steps involved in the decomposition. The contradictions have been discussed in detail by Trick and Saliba[33] and are summarized here. Experiments performed by Ouchi and Honda[31] and similar work was done later by Jackson and Conley[29] have led to opposing explanations for the early evolution of water (Stage 1, $T \approx$ 200-550 °C). In the mechanism proposed by Ouchi and Honda, a condensation reaction takes place between the phenol groups of the polymer to form a diphenyl ether bond. On the other hand, Jackson and Conley suggest that methylol groups that are attached to phenol undergo a condensation reaction that results in methylene crosslinks. Jackson and Conley further propose that ether crosslinks are not formed at these temperatures. Parker and Winkler[32] propose that H_2O evolves as a consequence of the decomposition of ether linkages but only during the latter stages of pyrolysis ($T \approx$ 700-800 °C). Parker and Winkler also suggest that phenol polymer units that have multiple bonds to adjacent phenol groups are retained in the polymer and that any observed phenol or cresol products are the result of the decomposition of pendant phenol groups.[32] During the cross-linking stage of pyrolysis (Stage 2, $T \approx$ 400-800 °C), Parker and Winkler, as well as Jackson and Conley, suggest that the evolution of CO is a direct consequence of the decomposition of carbonyl crosslinks that have been formed previously. Originally, Ouchi and Honda suggested that CO evolves as a result of the decomposition of ether groups formed from condensation reactions that occur in the first stage of pyrolysis. However, in a later study Ouchi revised the pyrolysis mechanism to include carbonyl functional groups

as a source of CO, following the observation of infrared absorption bands at 1660 cm^{-1} to 1630 cm^{-1}.[34] Ouchi and Honda[31] and Parker and Winkler[32] predicted H_2 as the dominant species evolved toward the end of pyrolysis, with H_2 coming from aromatic rings as they become carbonized. Jackson and Conley,[29] however, did not predict the evolution of H_2 at any point during the process of thermal degradation.

In a more recent qualitative study, Trick and Saliba[33] collected infrared spectra of the material remaining after the pyrolysis of a carbon fiber/phenolic composite, and they drew many of the same conclusions as Ouchi and Honda,[31] Parker and Winkler,[32] and Jackson and Conley,[29] as well as some new conclusions that contradicted the previous studies. For instance, Trick and Saliba[33] proposed a one-step mechanism for the evolution of CH_4, in contradiction to the two-step mechanism that was proposed by Ouchi.[34] Trick and Saliba[33] also suggested that that there is little evidence to support carbonyl formation even though they detected a very weak signal for a carbonyl stretch at 1658 cm^{-1} On the other hand, Jackson and Conley[29] and Ouchi[34] unequivocally suggested the formation of carbonyl functional groups in the decomposing phenolic polymer. The discrepancies in the reported qualitative thermal degradation mechanisms of phenolic resins need to be resolved in order to enhance our basic understanding and validate emerging models designed to predict quantitative yields of pyrolysis products. This resolution and the consequent model validation may come from reliable measurements of the quantitative yields from a material whose thermal degradation is the focus of model simulations.

Quantitative yields have been reported for the pyrolysis of various phenolic-based materials, although questions remain about the accuracy of the results. The majority of

such studies were conducted during the development of the Apollo spacecraft,[31,35-37] and there have also been more recent studies during the last two decades.[38-40] The most common techniques employed in the 1960s were mass spectrometry (MS) as well as gas chromatography (GC). More recent efforts have implemented modern versions of GC and MS, as well as the combination of the two (GC-MS). As mentioned above, Ouchi and Honda performed an experiment in which the thermal decomposition mechanisms of several different phenolic resins were studied (in steps of approximately 100 °C) using mass spectrometry.[31] Although this work was helpful in demonstrating the relationship between the reagents used during synthesis and the relative yields of pyrolysis products, the manner in which the products were collected and analyzed was subject to significant errors. After the resin was pyrolyzed, the gaseous products were collected and stored in a reservoir at relatively high pressure (50 Torr) until pyrolysis was complete, thus providing the opportunity for secondary reactions to occur. In addition, analysis of the pyrolysis products was incomplete. While the permanent gases were analyzed by MS, H_2O and other condensable products were trapped on a cold finger. H_2O was measured by gravimetric methods, and the remaining products were weighed and defined as "lower molecular mass substances," which presumably were a mixture of phenol and substituted phenols. There were potential errors in other studies as well. Friedman performed an experiment in which a phenol-formaldehyde sample was quickly pyrolyzed with a flash lamp, and the decomposition products were subsequently analyzed with the use of a time-of-flight mass spectrometer.[35] Direct temperature measurements of the sample were not made, and the measurements of decomposition products were limited to time intervals of thirty minutes

because of the slow pumping speed of the reaction chamber. Shulman and Lochte performed a pyrolysis experiment on two resole phenolic resins using the MS thermal analysis method (MTA).[36] The MTA method is implemented by heating a sample in a furnace that is located directly beneath an electron beam. As the resin is heated, pyrolysis products are immediately ionized and subsequently analyzed in a time-of-flight mass analyzer. Shulman and Lochte reported day to day variations in sensitivity and instrumental settings, resulting in measurements with limited absolute accuracy. Quantitative analysis using GC as an analytical technique was performed on a novolac resin by Sykes.[37] In order to analyze all of the pyrolysis species evolved from the resin, three different columns were used in separate experiments in order to characterize H_2O, non-condensable gases, and aromatic hydrocarbons, respectively. The use of three GC columns made it difficult to obtain accurate relative yields of products that were analyzed with different columns. In a recent effort to obtain more accurate quantitative data, Wong et al. performed a pyrolysis experiment using a batch reactor.[38] They loaded a phenolic resole sample into a quartz tube, which was then placed inside a ceramic furnace. The sample was pyrolyzed while the furnace was set to a specific temperature and held for one hour to ensure complete degradation of the material. Permanent-gas products from pyrolysis were analyzed by GC, and products that are liquids at room temperature were trapped in a condenser for analysis at a later time. Again, the possibility of secondary reactions exists, and perhaps more importantly, the batch-reactor approach does not lend itself well to non-equilibrium measurements of evolving products in real time. On the other hand, the approach of Wong et al. allows for mass balance, including the determination of

the masses of the gaseous products and the total mass loss of the sample, after the pyrolysis of the sample has been quenched by lowering its temperature.

Several of the more modern studies have combined GC with MS in order to quantify the molar yields of pyrolysis products, but they, too, were incomplete or subject to inaccuracies. Sobera and Hepter[39] used GC-MS to pyrolyze novolac and resole phenolic resins, but their experiments were limited to temperatures of 650 °C, 770 °C, and 900 °C. Although yields of volatile organic pyrolysis products were reported (benzene, phenol, cresol, etc.), Sobera and Hepter did not report yields of permanent gases (H_2, CO, CO_2, etc.) that are known to dominate at the temperatures used in their study. In another recent study, Bennett et al. used a combination of GC, MS, and infrared spectroscopic techniques in order to measure total quantitative yields of pyrolysis products from a phenolic resole resin over a large temperature range (intervals of 100 °C from 100 °C to 800 °C).[40] A pyroprobe (CDS 5200 pyrolyzer) was coupled to a GC-MS system to measure organic products, and yields of permanent gases were measured by coupling the pyroprobe to a Fourier transform infrared (FTIR) spectrometer. Even though both organics and permanent gases were measured, yields of H_2 were not quantified. Ultimately, Bennett et al. reported inconsistencies in the data and suggested that more consistent data would be gathered when one sample is analyzed with two analytical techniques simultaneously. Bennett et al. also suggested that another method, such as GC coupled to thermal conductivity detection, would be needed to detect H_2.

1.3.2 THERMAL DECOMPOSITION OF EPOXY-NOVOLAC D.E.N. 438 RESIN SYSTEM

Epoxy-novolac resins are used in ablative TPSs such as Avcoat. Avcoat was the thermal protection system used by the Apollo space capsules in the 1960's, and a new variant has been selected for the Orion crew capsule.[41] Typically, Avcoat consists of an epoxy-novolac resin system that contains a certain weight percentage of phenolic microballoons with additional silica-based fillers.[26]

Pyrolysis of a large variety of epoxy-novolac resin systems were studied during the 1960s and 1970s. Most of the epoxy-novolac resin systems were cured using an anhydride as a crosslinking agent and a tertiary amine as a catalyst. One such resin system was made by curing D.E.N. 438 (epoxy-novolac resin) with NMA (methyl-5-norbornene-2,3-dicarboxylic anhydride, or nadic methyl anhydride) as the crosslinking agent and BDMA (N,N-dimethylbenzylamine, or benzyldimethylamine). The components of this resin system are illustrated in Fig. 1.4. The mechanism for tertiary amine catalyzed polymerization between anhydrides and epoxide groups is well known.[42] The anhydride ring is opened upon activation by the tertiary amine to form a carboxyl anion and a carbonyl group. The carbonyl group is coupled to the tertiary amine. Finally, carboxyl anion reacts with the epoxide group to form an ester bond. The reaction continues with the displacement of the tertiary amine by an alkoxide ion to form an additional ester bond. The anhydride ring may also be activated by a hydroxy group.[43-44] It has been suggested that residual hydroxyl groups on the phenolic backbone of the epoxy-novolac can initiate polymerization with the anhydride, resulting in an ester bond that is closer to the backbone of the polymer than an ester formed between the anhydride and epoxide.[43]

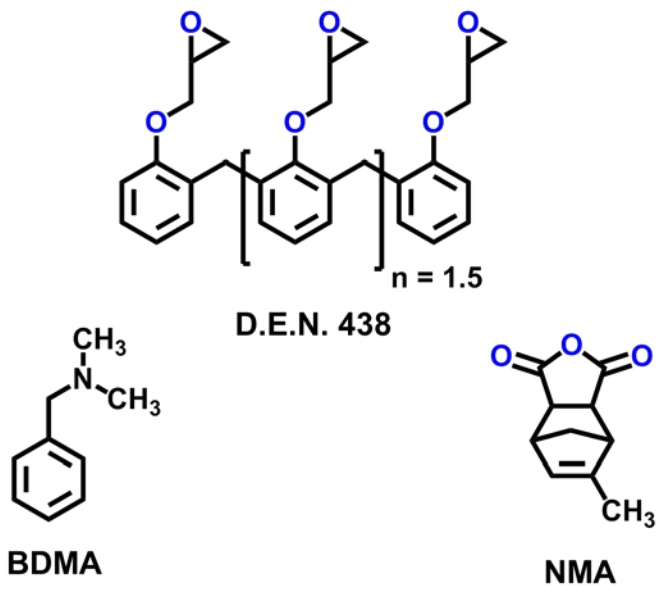

Figure 1.4 Components of epoxy novolac resin system studied in chapter 5.

It has been suggested that residual hydroxyl groups on the phenolic backbone of the novolac polymer, which have not been substituted with an epoxy group, can initiate polymerization with the anhydride. This reaction results in an ester bond that is closer to the backbone of the polymer than an ester formed between the anhydride and the epoxide of the epoxy-novolac resin.[43] Figure 1.5 represents the structure of the crosslink formed between a residual hydroxyl group of an unsubstituted portion of a novolac polymer, an epoxy group from a substituted portion of the novolac polymer, and NMA. The crosslink structure in Fig. 1.5 was first proposed by Fleming and is used as a basis for the discussion in chapter 5 of this thesis.[43]

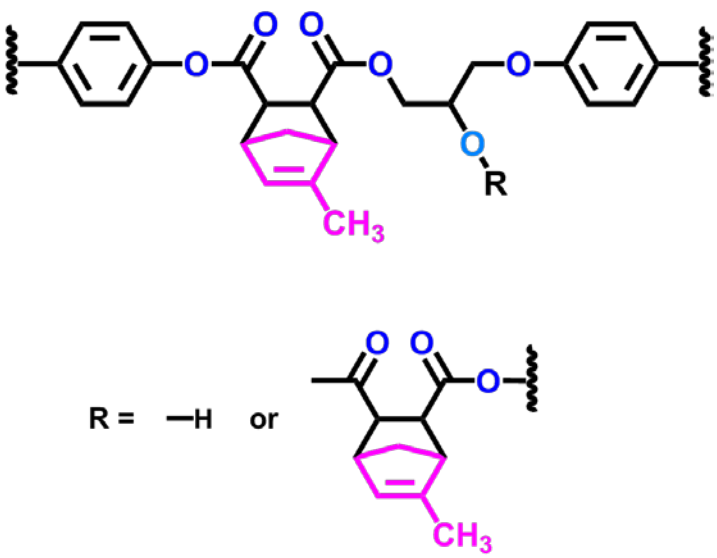

Figure 1.5. Molecular structure of the crosslink proposed by Fleming.[43] The R group attached to the crosslink can be a hydrogen atom or an additional crosslink to a diester group.

Modern thermal degradation studies have been performed on a wide variety of epoxy-novolac resins.[45] However, as previously mentioned, most of the research performed on ablative plastics was performed during the Apollo era.[43, 46-50] Out of all the research performed over the course of the era, only two papers focus on the exact same epoxy-novolac system that is investigated in this thesis (e.g., D.E.N. 438, NMA, BDMA).[43,47] Other studies from this era focus on the thermal decomposition of epoxy-novolac systems made from D.E.N. 438 and NMA but employing a different catalyst (e.g., DMP-30, DB VIII). However, all of the catalysts used in these studies are tertiary amines, and it is unclear if the different varieties of catalysts have an effect on the distribution of molar yields from pyrolysis.

Early attempts at measuring absolute molar yields of pyrolysis products suffered from the same shortcomings as early and even present-day pyrolysis studies on phenolic

resins. For example, molar yields of permanent and condensable pyrolysis gases were measured in separate steps. Condensable gases were measured by collecting condensable species with a cold trap for post-pyrolysis analysis, and permanent gases were fed directly into a mass spectrometer. Additionally, pyrolysis species were collected over a long period of time as the samples were heated in a step-wise fashion.[47,50]

Lee performed one of the first studies aimed at quantifying pyrolysis species from the same epoxy-novolac resin system described in this thesis.[47] Pyrolysis products were collected at 350 °C and 450 °C. The major products of pyrolysis detected at 350 °C were H_2, H_2O, CO_2, and methylcyclopentadiene (MCPD). At 450 °C, these products remained dominant, but the distribution shifted such that CO_2 and MCPD became the most prevalent species. CH_4 was detected in small quantities at these two temperatures, and fragments associated with the breakdown of the novolac backbone of the polymer (e.g., toluene) were also reported in small amounts.

Gac. et al., measured molar yields of the thermal decomposition products the epoxy-novolac system by heating samples in multiple steps over the course of hours.[50] At 300 °C to 450 °C, the major products of pyrolysis were CH_4, H_2O, CO, and CO_2. At higher temperatures (T = 450 °C – 800 °C) the main products of pyrolysis were H_2, CH_4, H_2O, CO, and CO_2. Again, at higher temperatures, the distribution of pyrolysis products changed such that H_2 became the most dominant product of pyrolysis, and CH_4 was measured in greater amounts in this temperature range than at lower temperatures.

Thermal decomposition mechanisms have been proposed in the literature for the epoxy-novolac resin system studied in this thesis. However, most of the proposed

mechanisms only attempt to explain the process by which CO, CO_2, and MCPD are lost during the first steps of thermal decomposition.

TGA of this resin system generally shows mass loss in two stages. The first stage is associated with the loss of the monoacid-monoester species to form the original anhydride, over a temperature range that spans from $T \sim 230$ °C – 350 °C (see Fig. 5.8, red trace).

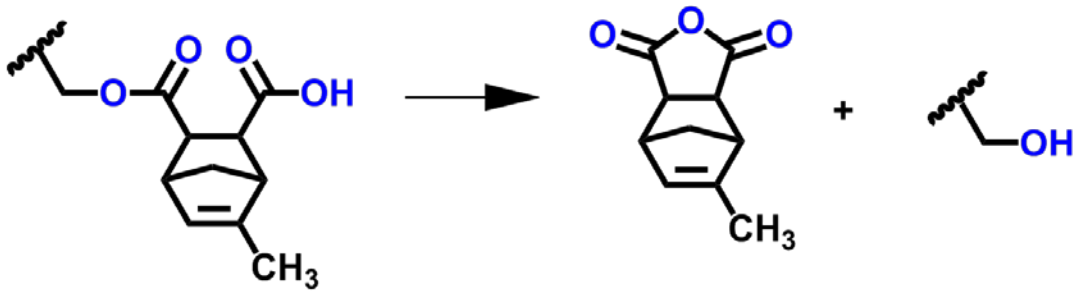

Figure 1.6. Decomposition of a monoacid-monoester species to reform NMA and a primary alcohol.

The second stage ($T > 350$ °C) is associated with the decomposition of the diester. The most common mechanism proposed for the decomposition of the diester involves the loss of MCPD to form an unsaturated polyester followed by decomposition of the unsaturated polyester to form several small molecules (e.g., CO, CO_2, and MCPD). Figures 1.7 and 1.8 were created based on a mechanism discussed by Freeman, and it is representative of mechanisms that have been proposed by others on this resin system.[43, 47-48] The figures omit certain portions of the crosslink by showing R groups where additional carbon-carbon bonds and the aromatic backbone are found (see Fig. 1.5). This simplistic view does not account for contributions that the additional carbon-carbon bonds and

aromatic species may make to the decomposition mechanism. Furthermore, the mechanism does not attempt to explain the appearance of H_2, H_2O, and CH_4 over the course of thermal decomposition.

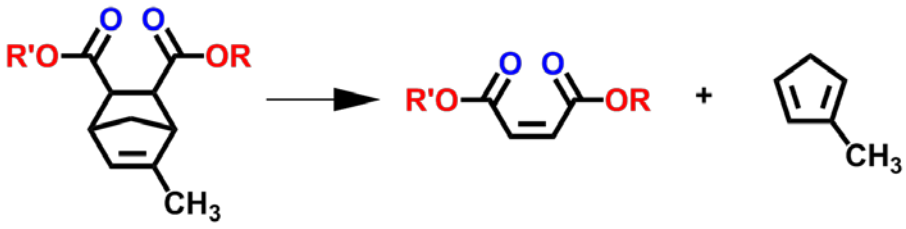

Figure 1.7. Decomposition of diester crosslink to form unsaturated polyester and MCPD.

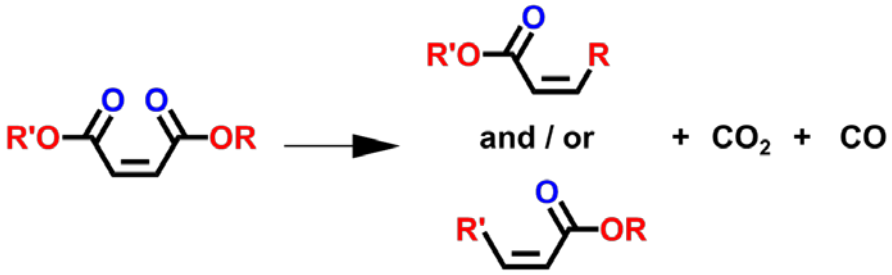

Figure 1.8. Decomposition of unsaturated polyester crosslink to form CO and CO_2.

Shortcomings of each of the previous studies have resulted in uncertain quantitative yields of pyrolysis products. In fact, there has not been a study in which a single technique has been used to measure the quantitative yields of the complete range of pyrolysis products as a function of time over the full range of temperatures for either of the materials in this study. The uncertainties in the measurements are compounded by the unknown differences in the decomposition mechanisms for the different types of phenolic and epoxy-novolac samples in each study, leading to the current situation where there is not a “go-to”

set of data that can be used for the validation of new models aimed at predicting the thermal degradation of thermal protection systems that incorporate phenolic and epoxy-novolac resins.

1.4 THESIS ORGANIZATION

Chapter 1 includes parts of the introduction of published journal articles and one article that is in preparation for future submission. Chapter 2 describes the experimental methods and materials used throughout chapters 3 through 5. Chapters 3 and 4 of this thesis consist of journal articles that have been published in *ACS Applied Materials and Interfaces.* Chapter 5 consists of material that has been prepared in a manuscript format for future submission.

1.5 REFERENCES

1) Anderson, J. D. *Hypersonic and High Temperature Gas Dynamics*. AIAA Education Series; Schetz, J. A., 2nd ed., AIAA: Reston, V.A. **2006**.

2) Chen, Y. K.; Milos, F. S. Ablation and Thermal Response Program for Spacecraft Heatshield Analysis. *J. Spacecr. Rockets* **1999**, *36*, 475-483; DOI: 10.2514/2.3469.

3) Mansour, N. N.; Lachuad, J.; Magin, T. E.; Muelenaere, J.; Chen, Y. K. High-Fidelity Charring Ablator Thermal Response Model. In *42nd AIAA Thermophysics Conference*; Honolulu, Hawaii. June 27-30, **2011**; DOI: 10.2514/6.2011-3124.

4) Omidy, A. D.; Panerai, F.: Lachaud, J. R.; Mansour, N. N.; Martin, A. Effects of Water Phase Change on the Material Response of Low-Density Carbon-Phenolic Ablators. *J. Thermophys. Heat Trans.* **2016**, *30*, 473-478; DOI: 10.2514/1.T4814.

5) Lachaud, J.; Magin, T. E.; Cozmuta, I.; Mansour, N. N. A Short Review of Ablative-Material Response Models and Simulation Tools, In *Proceedings of the 7th Aerothermodynamics Symposium*, European Space Agency, Brugge, Belgium, 9-12 May **2011**; ESA SP, 692.

6) Bahramian, B. R.; Kokabi, M.; Famili, M. H. N.; Beheshty, M. H. Ablation and Thermal Degradation Behavior of a Composite Based on Resole Type Resin: Process Modeling and Experimental. *Polymer* **2006**, *7*, 3661-3673; DOI: 10.1016/j.plymer.2006.03.049.

7) Henderson, J. B.; Tant, M. R.; Moore, G. R. Determination of Kinetic Parameters for the Thermal Decomposition of Phenolic Ablative Materials by a Multiple Heating Rate Method. *Thermochimica Acta*, **1981**, *44*, 253-264 DOI:10.1016/0040-6031(81)85019-8.

8) Trick, K. A.; Saliba, T. E.; Sandhu, S. S. A Kinetic Model of the Pyrolysis of Phenolic Resin in a Carbon/Phenolic Composite. *Carbon* **1997**, *35*, 393-401; DOI: 10.1016/S0008-6223(97)89610-8

9) Wendlandt, W. W. *Thermal Analysis. Chemical Analysis Series, Vol. 19*; Elving, P.J.; Winefordner, J. D., Eds.; 3rd ed., John Wiley and Sons, New York, N.Y. **1984**.

10) Baer, A. D.; Hedges, J. H.; Seader, J. D.; Jayakar, K. M.; Wojcik, L. H. Polymer Pyrolysis over a Wide Range of Heating Rates. *AIAA J.* **1977**, *15*, 1398-1404; DOI: 10.2514/3.7435.

11) Boyle, M. E.; Cozzens, R. F.; McPherson, J. A. The Effect of High Heating Rate on the Pyrolysis of Carbon/Phenolic Composites. NRL Memorandum Report 6343, ADA198052, Naval Research Lab: Washington, D.C., September **1988**.

12) Jackson, W. M.; Conley, R. T. High Temperature Oxidative Degradation of Phenol−Formaldehyde Polycondensates. *J. Appl. Polym. Sci.* **1964**, *8*, 2163−2193; DOI: 10.1002/app.1964.070080516.

13) Stokes, E. H. Kinetics of Pyrolysis Mass Loss from Cured Phenolic Resin. J. *Themophys. Heat Trans.* **1995**, *9*, 352-358; DOI: 10.2514/3.667.

14) Natali, M.; Kenny, J. M.; Torre, L. Science and Technology of Polymeric Ablative Materials for Thermal Protection Systems and Propulsion Devices: A Review. *Prog. Mater. Sci.* **2016**, 84, 192-275

15) Laub, B.; Venkatapathy, E. Thermal Protection System Technology and Facility Needs for Demanding Future Planetary Missions. *International Workshop on Planetary Probe Atmospheric Entry and Descent Trajectory Analysis and Science*. Lisbon, Portugal, 6-9, October 2003.

16) Johnson, S. M., Gasch, M. J., Leiser, D., Stewart, D. Jr., Stackpoole, M., Thornton, J., Espinoza, C. Development of New TPS at NASA Ames Research Center. In *15th AIAA International Space Planes and Hypersonic Systems and Technologies Conference*, Dayton, Ohio, 28 April – 1 May 2008.

17) Feldman, J.; Gasch, M. J.; Poteet., C. C.; Szalai, C. Advanced Rigid Ablative Thermal Protection Systems. *50th AIAA Aerospace Sciences Meeting including the New Horizons Forum and Aerospace Exposition*, Nashville, TN, January 9-12, 2012. DOI: 10.2514/6.2012-472

18) Milos, F. S.; Chen, Y-K.; Mahzari, M. Arcjet Tests and Thermal Response Analysis for Dual-Layer Woven Carbon Phenolic. In *47th AIAA Thermophysics Conference* Denver, Colorado, June 5-9, 2017.

19) Tran, H. K.; Johnson, C. E.; Rasky, D. J.; Hui, F. C. L.; Hsu, M.; Chen, Y. K. Phenolic Impregnated Carbon Ablators (PICA) for Discovery Class Missions. *31st AIAA Thermophysics Conference*, New Orleans, LA, June 17-20, 1996. DOI: 10.2514/6.1996-1911

20) Beck, R. A. S.; Driver, D. M.; Wright, M. J.; Hwang, H. H.; Edquist, K. T; Sepka, S. A. Development of the Mars Science Laboratory Heat Shield Thermal Protection System. *J. Spacecr. Rockets* **2014**, *51*, 1139-1150. DOI: 10.2514/1.A32635

21) Szalai, C.; Slimko, E.; Hoffman, P. Mars Science Laboratory Heat Shield Development, Implementation, and Lessons Learned. *J. Spacecr. Rockets* **2014**, *51*, 1167-1173. DOI: 10.2514/1.A32673

22) Trumble, K. A.; Cozmuta, I.; Sepka, S.; Jenniskens, P.; Winter, M. Postflight Aerothermal Analysis of Stardust Sample Return Capsule. *J. Spacecr. Rockets* **2010**, *47*, 765-774. DOI: 10.2514/1.41514

23) Bose, D.; White, T.; Santos, J. A.; Feldman, J.; Mahzari, M.; Olson, M.; Laub, B. Initial Assessment of Mars Science Laboratory Heat Shield Instrumentation and Flight Data. *51st AIAA Aerospace Sciences Meeting including the New Horizons Forum and Aerospace Exposition*, Grapevine, TX, January 7-10, 2013. DOI: 10.2514/6.201-908

24) Space X website, http://www.spacex.com/news/2013/02/09/spacexs-dragon-spacecraft-successfully-re-enters-orbit (accessed Nov 3, 2014).

25) Titov, E. V.; Kumar, R.; Levin, D. A.; Anderson, B. P. Modeling the Crack Growth in the AVCOAT Heat Shield. *49th AIAA Aerospace Sciences Meeting including the New Horizons Forum and Aerospace Exposition*, Orlando, FL, January 4-7, 2011. DOI: 10.2514-6.2011-137

26) Crouch, R. K.; Walberg, G. D. An Investigation of Ablation Behavior of Avcoat 5026/29M Over a Wide Range of Thermal Environments. NASA TM X-1778; NASA: Washington, D. C., April 1969.

27) Wright, M. J.; Hughes, M.; Calomino, A.; Barnhardt, M. D.; An Overview of Technology Investments in the NASA Entry Systems Modelling Project. In *53rd AIAA Aerospace Sciences Meeting*; AIAA SciTech Forum, January 5-9, 2015.

28) Pilato, L., Resin Chemistry. Phenolic Resins: A Century of Progress. Springer, New York, 2010, pp. 41-45. DOI: 10.1007/978-3-642-04714-5

29) Jackson, W. M.; Conley, R. T. High Temperature Oxidative Degradation of Phenol–Formaldehyde Polycondensates. *J. App. Polym. Sci.* **1964**, *8*, 2163-219. DOI: 10.1002/app.1964.070080516

30) Morterra, C.; Low, M. J. D. IR Studies of Carbons-VII. The Pyrolysis of a Phenol-Formaldehyde Resin. *Carbon* **1985**, *23*, 525-530. DOI: 10.1016/0008-6223(85)90088-0

31) Ouchi, K.; Honda, H. Pyrolysis of Coal 1. Thermal Cracking of Phenol-Formaldehyde Resins Taken as Coal Models. *Fuel* **1959**, *38*, 429-443. DOI: 10.1021/la00063a010

32) Parker, J. A.; Winkler, E.L. The Effects of Molecular Structure on the Thermochemical Properties of Phenolics and Related Polymers. NASA TR R-276, November **1967**.

33) Trick, K. A.; Saliba, T. A. Mechanisms of the Pyrolysis of Phenolic Resin in a Carbon/Phenolic Composite. *Carbon* **1995**, *33*, 1509-1515. DOI: 10.1016/0008-6223(95)00092-R

34) Ouchi, K. Infra-Red Study of Structural Changes During the Pyrolysis of a Phenol-Formaldehyde Resin. *Carbon* **1966**, *4*, 59-66. DOI: 10.1016/0008-6223(66)90009-1

35) Friedman, H. L. Products of Flash Pyrolysis of Phenol-Formaldehyde by Time-of-Flight Mass Spectroscopy. *J. App. Polym. Sci*. **1965**, *9*, 651-662. DOI: 10.1002/app. 1965.070090225

36) Shulman, G. P.; Lochte, H. W. Thermal Degradation of Polymers. II. Mass Spectrometric Thermal Analysis of Phenol-Formaldehyde Polycondensates. *J. App. Polym. Sci.* **1966**, *10*, 619-635. DOI: 10.1002/app.1966.070100407

37) Sykes, G. F. Decomposition Characteristics of a Char-Forming Phenolic Polymer Used For Ablative Composites. NASA TN D-3810, February, **1967**.

38) Wong, H. W.; Peck, J.; Edwards, R.; Reinisch, G.; Lachaud, J.; and Mansour, N. N. Measurement of Pyrolysis Products from Phenolic Polymer Thermal Decomposition. AIAA Science and Technology Forum and Exposition, National Harbor, MD, January 2014. DOI: 10.2514/6.2014-1388

39) Sobera, M.; Hepter, J. Pyrolysis-Gas Chromatography-Mass Spectrometry of Cured Phenolic Resins. *J. Chromat. A* **2003**, *993*, 131-135. DOI: 10.1016/S0021-9673(03)003881-1

40) Bennett, A.; Payne., D. R.; Court., R. W. Pyrolytic and Elemental Analysis of Decomposition Products from a Phenolic Resin. *Macrom. Symp*. **2014**, *339*, 38-47. DOI: 10.1002/masy.201300136

41) Pavlosky, J. E.; Leger, L. G. St., Apollo Experience Report – Thermal Protection Subsystem. NASA TN D-7564. January **1974**.

42) Fischer, R. F.; Polyesters from Epoxides and Anhydrides. *J. Polym. Sci.* **1960**, 44, 155-172.

43) Fleming, G. J. Mechanisms for Initiating Thermal Degradation of Certain Anhydride-Cured Epoxies. *J. Appl. Polym. Sci.* **1966**, 10, 18-13-1830.

44) Tanaka, Y.; Kakiuchi, H. Study of Epoxy Compounds. Part I. Curing Reactions of Epoxy Resin and Acid Anhydride with Amine and Alcohol as Catalyst. J. Appl. Polym. Sci. **1963**, 7, 1063-1081.

45) Levchik. S. V.; Weil. E. D. Thermal decomposition, combustion and flame-retardancy of epoxy resins – a review of the literature. *Polym. Int.* 2004, **53**, 1901-1929.

46) Anderson, H. C. Thermal Degradation of Epoxide Polymers. *J. Appl. Polym. Sci.* **1962**, 6, 484-488.

47) Lee, L.-H. Mechanisms of Thermal Degradation of Phenolic Condensation Polymers. II. Thermal Stability and Degradation Schemes of Epoxy Resins. *J. Appl. Polym Sci. Part A.* **1965**, 3, 859-882.

48) Freeman, E. S.; Becker, A. J. Thermal Degradation of Nadic Methyl Anhydride-Crosslinked Novolac Epoxy Resin. *J. Polym. Sci. Part A.* **1968**, 6, 2829-2851.

49) Taylor, G. C.; Pendleton, E. L. Characterization of an Epoxy-Anhydride Ablative System Using Computer Treatment of Analytical Results. 1969, *J. Macromol. Sci. Part A Chem.* 1969, 3, 453-470.

50) Gac, N. A.; Spokes, G. N.; Benson, S. W. Thermal Degradation of Nadic Methyl Anhydride-Cured Epoxy Novolac. *J. Polym. Sci. Part A.* **1970,** 8, 593-608.

CHAPTER TWO

EXPERIMENTAL METHODS AND MATERIALS

2.1 RESIDUAL GAS ANALYZER

A Stanford Research Systems residual gas analyzer (RGA200) was used as the principle analysis instrument for the studies described in chapter 4 and 5 of this thesis. The detection sensitivity of the RGA is the product of the efficiency of the ionization process in the electron-impact ionizer, the transmission efficiency or throughput in the quadrupole mass filter, and any mass dependent gain in the ion detection system (Fig. 2.1).

Figure 2.1. Basic Assembly of the residual gas analyzer used to measure molar yields of pyrolysis products.

The basic features of the RGA ionizer assembly are the repeller cage, filament, anode grid, and the focus plate (Fig. 2.2). Ionization is accomplished by resistively heating a circular thoriated-iridium filament and holding it at a negative potential relative to ground. Electrons are emitted thermionically from the filament to an anode grid that is held

at a positive potential relative to the filament. Some of the electrons pass through the anode grid and are accelerated back towards the center of the anode grid by the repeller cage. The repeller cage is held at a negative potential to help focus electrons back towards the center of the ionizer. The repeller cage increases the probability that a neutral molecule will collide with an electron and become ionized as it passes through the ionizer assembly. Once an ion is formed, it is extracted by the focus plate, which is held at a negative potential relative to ground. The default settings for the RGA ionizer were used for all the studies in this thesis. The electron energy, defined as the difference in voltage between the ionizer and the anode grid, was kept at 70 eV. A large range of molecules have maximum electron-impact ionization cross sections at or near 70 eV, and most reference mass spectra are collected at this setting. The spectra collected for the studies in this thesis were also collected with the electron energy set at 70 eV.

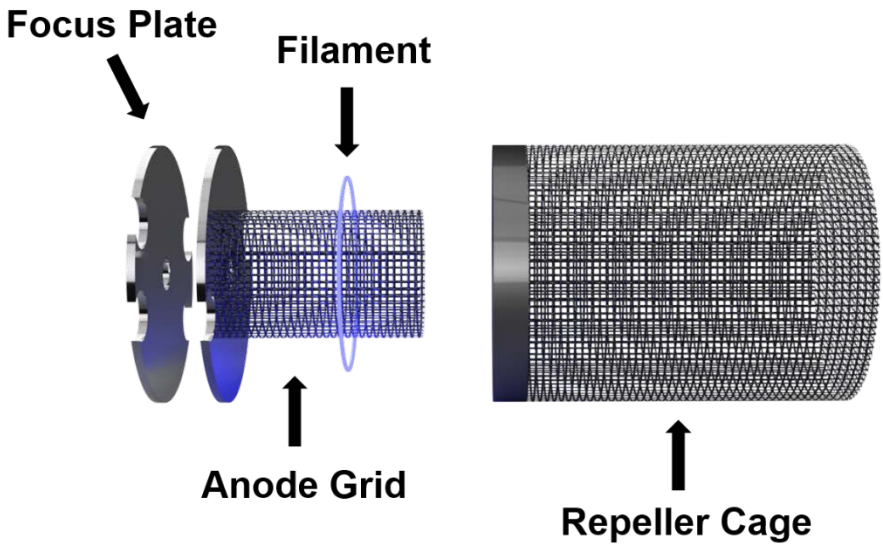

Figure 2.2. Basic ionizer assembly showing the focus plate, filament, anode grid, and repeller cage.

The ion energy was kept at 12 eV, and it is equal to the voltage biasing of the anode grid and the focus plate. The focus plate was kept at -90 V and the emission current of the filament was kept at 3.5 mA.

After ions are directed through the focus plate, they pass through the center of the quadrupole. The quadrupole used in these studies has been given a voltage supply such that its mass range extends from 1 to 200 u. An important characteristic of residual gas analyzers is the throughput or transmission of ions through the quadrupole. In general, the throughput of the filter decreases at higher mass-to-charge ratios (*m/z*). The decrease in transmission efficiency is clearly demonstrated in a study that was published by Ehlers.[51]

The RGA used in these studies was set at the factory to keep the width of the bandpass filter, $\Delta M_{10\%}$, for the entire range of masses, where $\Delta M_{10\%}$ is defined as the full width of the bandpass filter at which the ion current falls to 10% of the maximum value. This condition ensures adequate separation of adjacent masses over the full range, but it also leads to reduced transmission at higher *m/z* values.[52]

After an ion is filtered through the quadrupole, it is guided to the ion detection system through an exit lens. The RGA used in these studies is equipped with a Faraday cup and a multi-channel continuous dynode electron multiplier (CDEM). The Faraday cup is positioned on axis with the quadrupole and exit lens, and the CDEM is positioned off-axis and above the entrance to the Faraday cup (Fig. 2.3). Although the CDEM offers superior sensitivity (particularly with species that have a low *m/z* values), the Faraday cup was chosen as the ion detector due to the lack of mass dependent gain that is characteristic of these devices.[51]

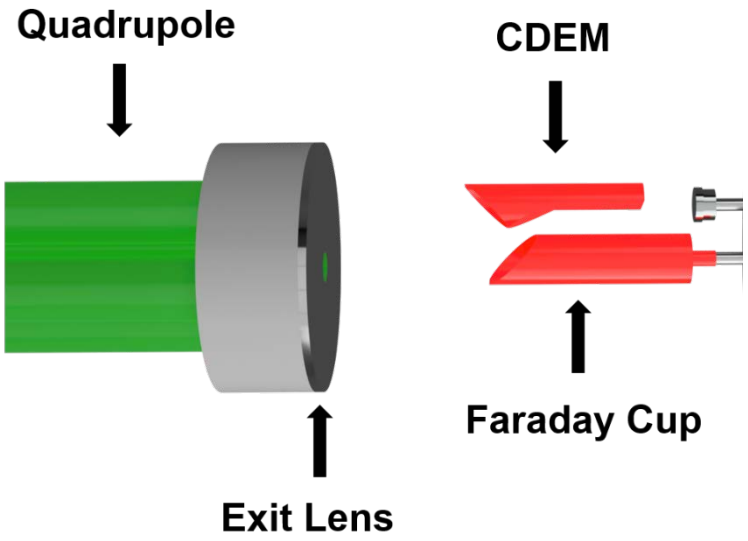

Figure 2.3. Ion detector assembly showing exit lens, Faraday cup, and CDEM.

2.2 LARGE VACUUM APPARATUS

The experiments described in chapter 3 utilized a large vacuum apparatus.[53-55] The apparatus consists of a large vacuum chamber that houses a rotatable mass spectrometer. The mass spectrometer system is equipped with a Brink ionizer (electron-impact ionization), a quadrupole mass filter with 19 mm rods, and a Daly-type ion counting system.[56-57] The mass spectrometer system is housed in a triply differentially pumped vacuum chamber to insure low backgrounds and high sensitivity. The ionizer resides in the innermost region which is maintained at a low base pressure ($< 1 \times 10^{-11}$ Torr). The main chamber of the machine was equipped with two cryogenic pumps (CTI-Cryogenics model Cryo-Torr 10, 3000 L s^{-1}).

2.3 MEDIUM VACUUM APPARATUS

The vacuum apparatus used for the experiments described in chapter 4 of this thesis is illustrated in Fig. 2.4. The main chamber is equipped with a cryogenic pump (CTI Cryogenics Model CT-8F, 1500 L s^{-1}), and a turbomolecular pump (Ebara Model ET1600WS, 1600 L s^{-1}). Pyrolysis of PICA samples took place in a differentially pumped vacuum chamber equipped with a diffusion pump (Edwards model B35031977 2000 L s^{-1}). The pyrolysis chamber was placed opposite of the RGA (SRS RGA200). The RGA was attached to a 2.75" c. f. flange on the main chamber. For this experimental configuration, the RGA was not differentially pumped, and the ionizer extended into the main chamber of the apparatus (see Fig. 2.5). A variable leak valve was fixed to the top of the main vacuum chamber to provide a way to feed calibration gases into the system.

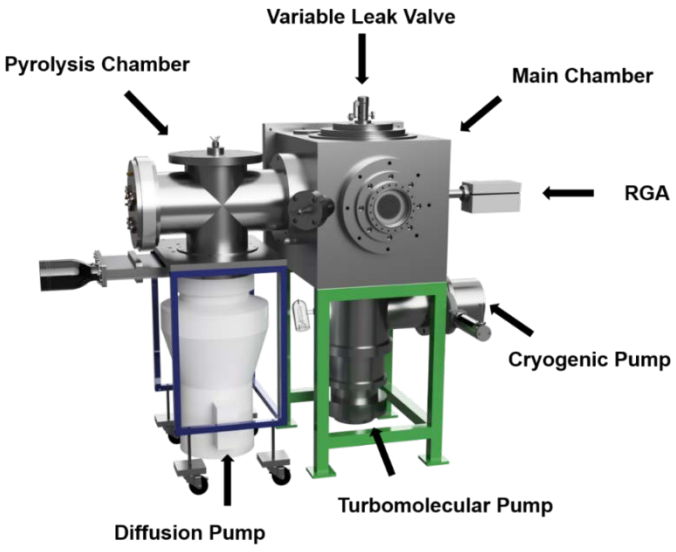

Figure 2.4. Medium vacuum apparatus used to analyze pyrolysis products of PICA. This apparatus was used for the experiments described in chapter 4.

The main chamber and source chamber were typically pumped down to 1 x 10^{-7} and 1 x 10^{-6} Torr, respectively, before the start of an experiment. The main chamber and source chamber can be pumped down to ultimate pressures as low as 1 x 10^{-8} Torr.

Figure 2.5 illustrates the important parameters for the experiments discussed in chapter 4 of this thesis. For this set of experiments, the sample mount (yellow arrow) was placed on a breadboard that was attached to a stainless-steel bar, tapped with ¼-20 holes, which is welded to the inside of the pyrolysis chamber. A copper aperture with a diameter of 1.27 cm was fixed to the front of the pyrolysis chamber. The distance between the aperture and the front face of the sample was kept at 17.8 cm (blue arrow). The distance between the front of the repeller grid and the copper aperture was 30.5 cm (green arrow).

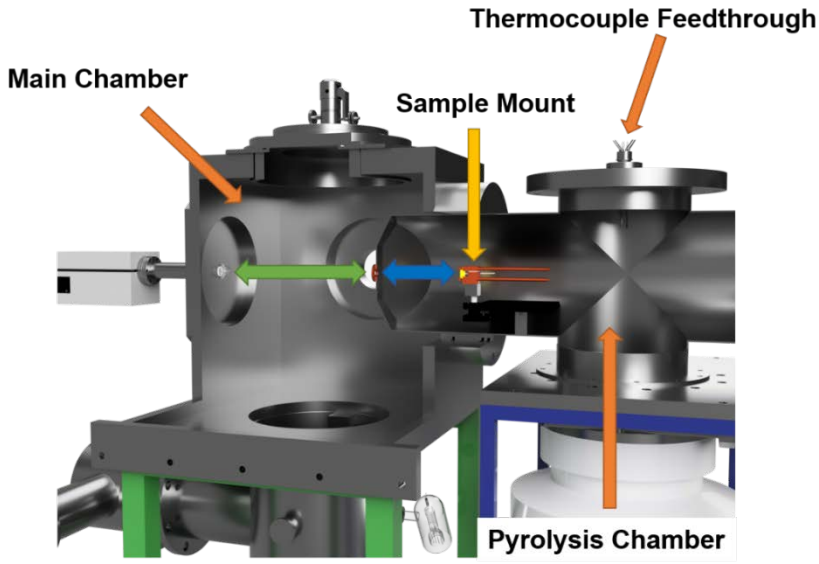

Figure 2.5. Cutaway view of the medium sized vacuum chamber used for the pyrolysis tests described in chapter 4 of this thesis. The arrows show the key dimensions of the experimental configuration.

2.4 THERMOCOUPLES

For the experiments described in chapters 3 and 4, a K-type thermocouple was inserted directly into the sample during each experiment (see Fig. 2.8). Both leads (Alumel and Chromel) extended from the sample and passed through a ceramic thermocouple tube. A thicker gauge size (nominal lead diameter, 0.5 mm) was used to provide good thermal contact between the thermocouple junction and the sample. For the experiments in chapter 5, a K-type thermocouple (nominal lead diameter, 0.255 mm) was spot welded to the inside of a tantalum tube. Temperature measurements for both experiments were recorded using a temperature input device (National Instrument model USB-TCO1) that was interfaced with a LabVIEW program.

Type K thermocouples (obtained from OMEGA engineering) were used because they are inexpensive, they are stable in most environments (excluding reducing environments), and they accurately measure a large range of temperatures (-200 °C to +1350 °C).[58] Caution must be exercised when using type K thermocouples in reducing atmospheres above 800 °C. A significant amount of H_2 is generated during the pyrolysis of phenolic and epoxy-novolac resins. However, the amount of H_2 that comes into contact with the thermocouple leads is low because the testing is done under very low pressure in a vacuum chamber. For the experiments described in chapters 3 and 4, a new thermocouple was used after three to four experiments to mitigate any potential errors in temperature measurement.

2.5 SMALL VACUUM APPARATUS

A small vacuum apparatus was constructed for the experiments described in chapter 5 of this thesis (Fig. 2.6). The small vacuum apparatus is constructed of stainless steel and consists of two chambers. One chamber houses the pyrolysis sample mount and the other chamber is used for differential pumping. The pyrolysis chamber is pumped at a rate of 1400 l s^{-1} (Pfeiffer Model, TMH 1601 P) and the differential chamber is pumped at a rate of 510 l s^{-1} (Pfeiffer Model, TMH 521 P). An SRS RGA200 was used as the detector for the experiments in chapter 5. The RGA was placed behind a small gate valve and pumped at a rate of 220 l s^{-1} with a large ion pump (Varian Model 912-7014). The apparatus is easily configured so that a high-throughput mass spectrometer (Extrel Model HT 500) can take the place of the RGA. The ion pump sits on a table that can translate so that the mass spectrometer is easily aligned to maximize pyrolysis signal. The uppermost table sits on a rail system and is fastened to a threaded rod that translates the table, and ion pump parallel to the back wall of the differential chamber. The bottom table has been fitted with adjustable feet that can translate and tilt the mass spectrometer. A 2.75” conflat-flanged bellows tube was inserted between the differential chamber and the small gate valve to provide flexibility to the system.

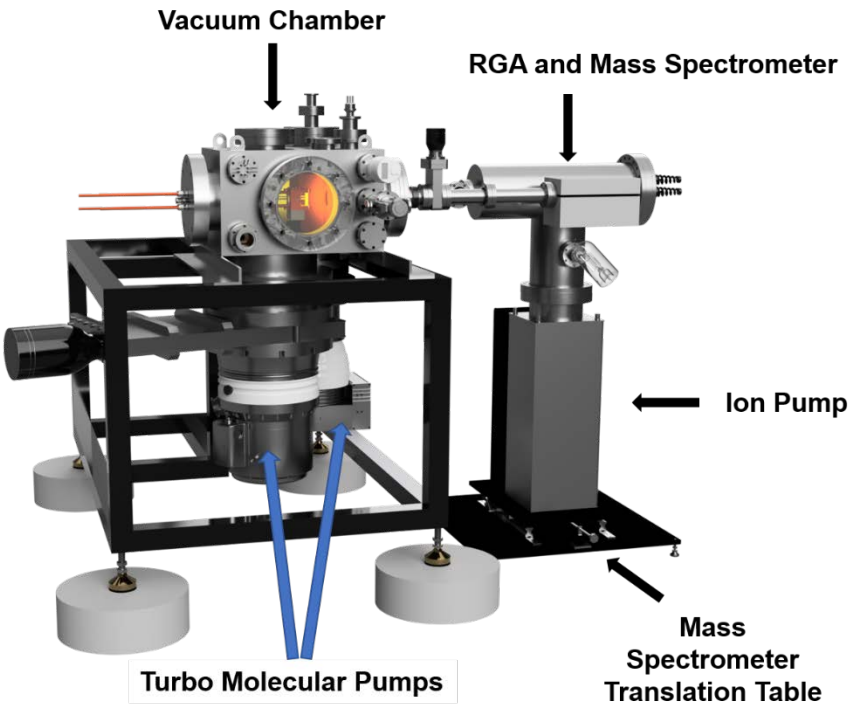

Figure 2.6. Schematic representation of the small vacuum apparatus that was designed to study the pyrolysis process of the D.E.N 438 resin system. The system was equipped with two turbomolecular pumps and large ion pump, and it can be configured to use a mass spectrometer or RGA as a detection system.

In Fig. 2.7, one side of the chamber and has been removed to help illustrate the important parameters for the experiments described in chapter 5. The sample mount sits on two rails in the pyrolysis chamber. One rail runs halfway across the inlet to the turbo molecular pump and is easily translated away from or towards a copper aperture. The second rail is positioned on top of the first rail and allows for translation perpendicular to the copper aperture. The copper aperture is fastened to the wall that separates the pyrolysis chamber and the differential chamber. A copper tube was fashioned into a teardrop shape and welded to a copper plate. The copper plate and copper tube press against the same wall that the copper aperture is attached to. Water circulates through the copper tube, and the

entire assembly serves as a heat sink. The mass spectrometer is housed in a stainless steel conflat tee.

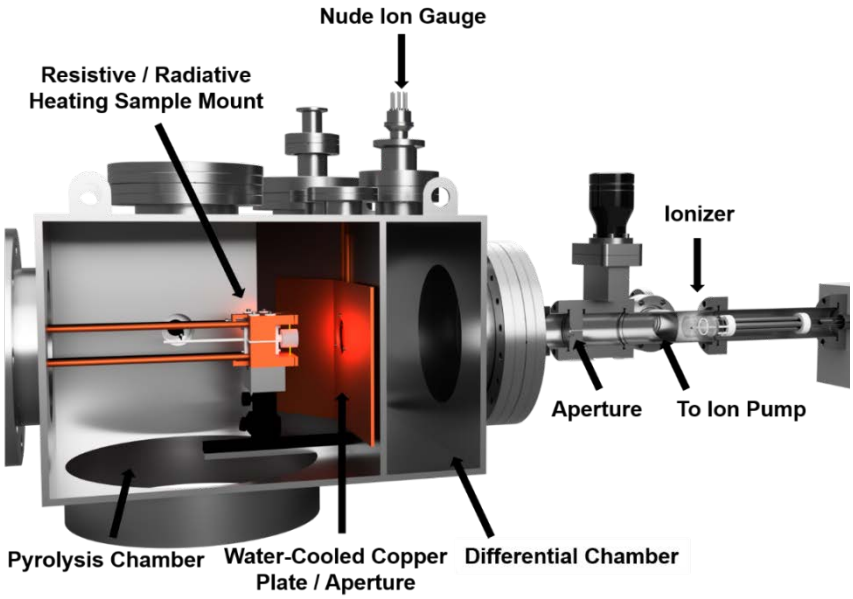

Figure 2.7. Cutaway view of the small vacuum chamber system used to study pyrolysis of the epoxy-novolac system described in chapter 5. The vacuum chamber is equipped with a chamber to house the sample mount and a chamber for differential pumping. The mass spectrometer or RGA are attached to the differential chamber at a 2-3/4" conflat flange.

2.6 SAMPLE HEATING METHODS

Composite and resin samples were heated using a combination of resistive and radiative heating techniques. A LabVIEW program was written to deliver power to the sample or filament in various stages so that the sample is heated linearly. The details of each mount are described in the following sections.

2.6.1 RESISTIVE HEATING SAMPLE MOUNT

In chapters 3 and 4 of this thesis, PICA was heated directly by passing current through each specimen (Joule or resistive heating). The resistive heating sample mount is made of two copper electrodes that are separated by an alumina spacer (Fig. 2.8). Copper tubes are welded to the electrodes to deliver water for cooling and current for heating. The sample is secured to the front face of the sample mount with a pair of sample clamps. During heating, it is expected that large thermal gradients are established between the middle of the sample and the ends of the sample.

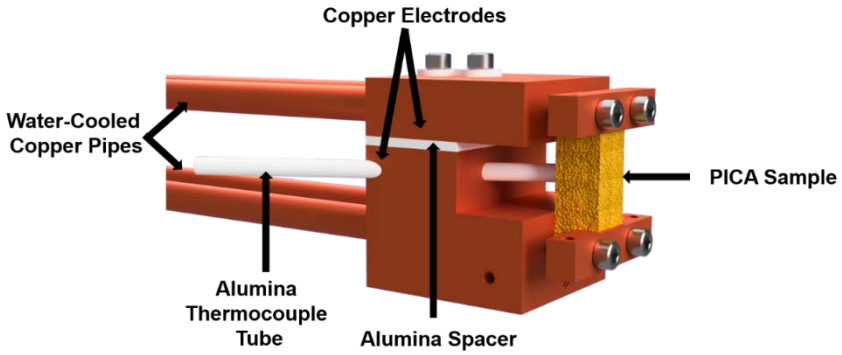

Figure 2.8. Resistive heating sample mount design used to pyrolyze samples of PICA up to 1200 °C in a matter of seconds. The sample mount was used for the pyrolysis studies described in chapters 3 and 4.

It is expected that large thermal gradients are established during heating between the middle of the sample and the ends of the sample. An experiment was devised to measure the difference in heating rate between the middle of the sample and the ends. Three thermocouples were attached to the front face of a PICA sample. One thermocouple was placed in the middle of the sample, and the outermost thermocouples were placed 0.525 cm from the center. The distance between each copper clamp is 1.55 cm. Time and

temperature data were collected, and heating rates were calculated by performing linear regression from 100 °C to the ultimate temperature of each curve. Figure 2.9 shows the results of an experiment at a high heating rate. The nominal heating rate at the center of the sample was 27.3 °C s^{-1}. The heating rates on the edge of the sample were calculated to be 22.4 °C s^{-1} (bottom) and 21.3 °C s^{-1} (top). This procedure was repeated for lower heating rates, and in each case, the rate measured at the edge of the sample was about 20% lower than the rate of heating in the middle of the sample. For additional details see chapter 4.2.3.

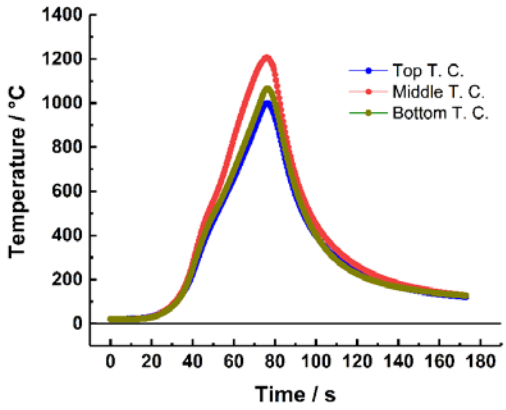

Figure 2.9. Temperature as a function of time measured by three type K thermocouples positioned in the middle and at the edges of a sample of PICA.

Mass loss was determined for each heated sample. A copper clamp system was designed to minimize material loss during handling, as PICA is very brittle (Fig. 2.10). The copper clamps served the purpose of holding the sample to the water-cooled electrodes (with stainless steel screws) and securing the sample when it was not attached to the electrodes. The clamps, screws, and sample were weighed before and after the experiment. The screws that connected the copper clamps were removed after the clamps were secured to the electrodes prior to each experiment and then replaced after the experiment was

finished so that the sample could be handled again without any additional mass loss. This procedure allowed for total mass loss measurements of each sample.

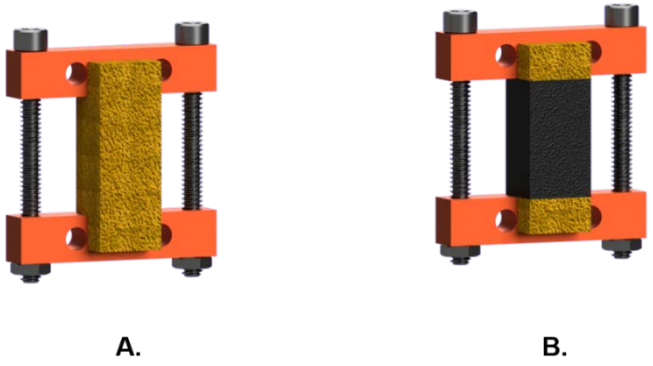

Figure 2.10. Copper clamp design used to minimize sample loss during handling. The figure illustrates what a sample looks like before (A) and after (B) heating.

Figure 2.11 shows a picture of an actual post-test sample. The ends of the sample did not pyrolyze because these regions of the sample were actively cooled by water-cooled electrodes and clamps. To measure the original mass of the charred portion of the sample, the virgin material at the ends was cut away, and the remaining char was weighed. The total mass lost was added to the charred mass to give the initial mass of the pyrolyzed region of the sample. A Mettler Toledo MS104S NewClassic MF balance, with a precision of 0.1 mg, was used to make each mass measurement.

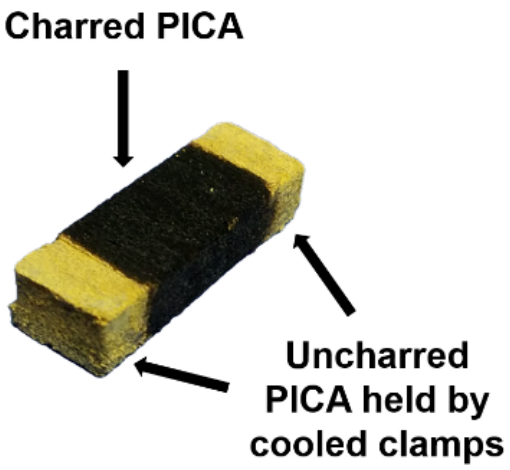

Figure 2.11 Actual post-test sample of PICA. The ends did not char because they were in contact with water-cooled copper electrodes.

2.6.2 RADIATIVE HEATING SAMPLE MOUNT

For the studies described in chapter 5, the samples were heated using a new sample mount (Fig. 2.11). The new sample mount shares many features with the sample mount described in the last section (i.e., water-cooled copper electrodes), but it has new features that give it versatility. A semicircle with a radius of 0.5” was drilled into the bottom center of each electrode to accommodate a 1” diameter quartz nozzle. Additionally, a variety of alumina blocks were designed to fit over the center of the hole to accommodate alumina thermocouple tubes. The new design features adjustable copper clamps that can accept a sample as thick as 0.75”. The thinner portion of each electrode extends 0.75” from the main block, and the distance between the top and bottom of the thinner portion measures 1.25”. The space between each electrode extension was designed so that new methods of heating could be implemented.

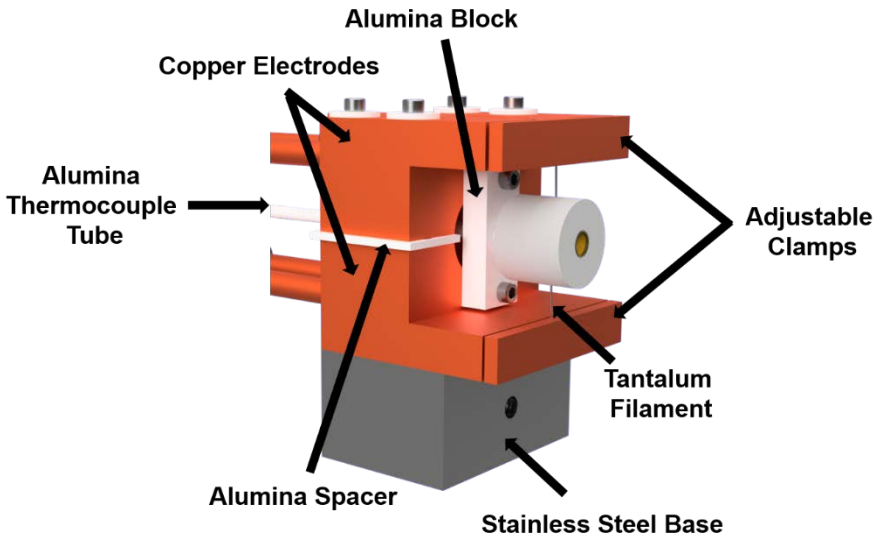

Figure 2.12 The new sample mount shown here is configured to heat samples radiatively.

Figure 2.13 helps to illustrate the heating method employed for the pyrolysis studies described in chapter 5. The motivation for the new heating method was driven by a need to minimize the thermal gradient across the sample during pyrolysis and therefore decrease experimental uncertainty. For this set of experiments, a sample of resin was cured inside of a tube made from tantalum. The tantalum tube was constructed by wrapping a 12 mm wide by 18 mm long section into a tube with a nominal diameter of 5 mm. Half of the tube was then filled with resin and cured with a specified schedule (see section 2.8.2).

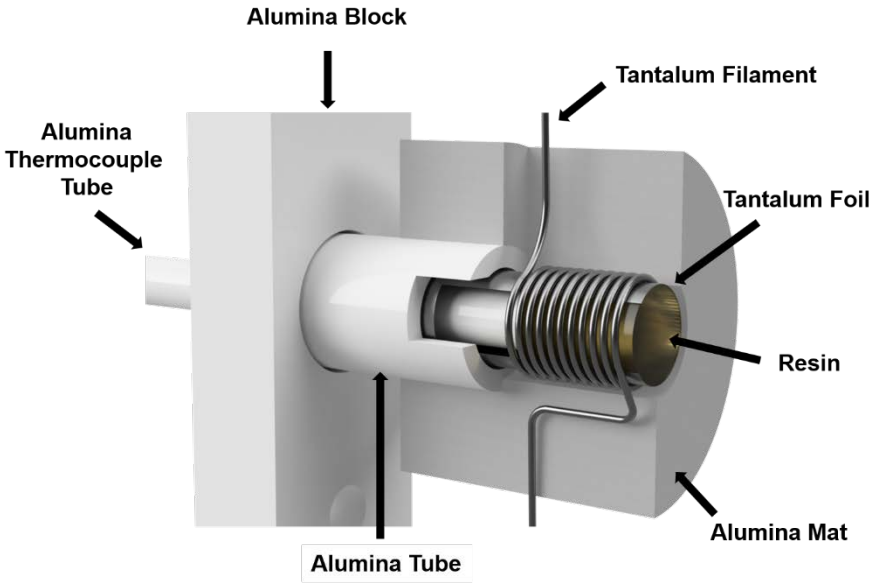

Figure 2.13. Configuration used to heat pure resins and composite materials radiatively. The resin sample and tantalum tube rested on an alumina thermocouple tube. The tantalum tube was surrounded by a tantalum filament which was resistively heated. The filament was surrounded by an alumina mat.

Before each experiment, a fresh type K thermocouple (Ø = 0.255 mm) was prepared by spot welding the Chromel and Alumel leads together. The welded junction had a diameter of roughly twice the diameter of each lead. The thermocouple junction was placed directly behind the sample (Fig. 2.14). The K-type thermocouple was then fed through an alumina thermocouple tube. 1 mm of the back section of the tantalum tube was fit onto the 5 mm diameter thermocouple tube for stability.

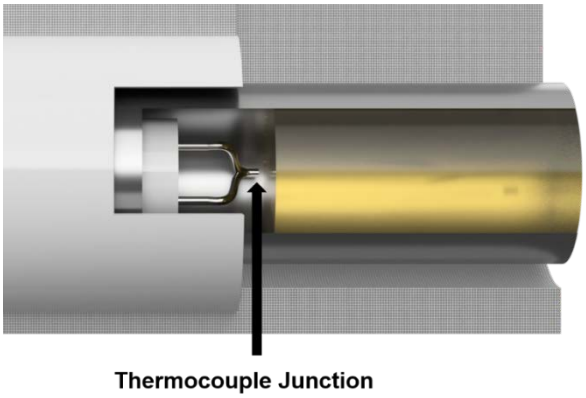

Figure 2.14. This figure shows the placement of the thermocouple junction. The junction was placed directly behind the resin and spot welded to the tantalum foil.

The alumina thermocouple tube was secured inside of a larger alumina tube (O. D. 8.5 mm) that was attached to an alumina block. The alumina block was then fit to the front face of the sample mount with a pair of 4-40 screws. Next, a tantalum coil was made by wrapping a 1.0 mm diameter tantalum wire around a rod so that the inside of the coil measured 8.5 mm in diameter. The coil had a total length of 23 mm, and the spacing between each coil measured 1 to 1.5 mm. The back 6 mm of the coil fit tightly around the large alumina tube.

2.7 DATA ANALYSIS

Mass spectrometers have been used for the quantitative determination of molecular species (e.g., hydrocarbons) since the early 1940's.[59] Modern quantitative mass spectrometry is usually accomplished by passing an analyte mixture through a chromatography column and into a mass spectrometer (e.g., GC-MS, LC-MS). The hyphenated methods are poorly suited to measure pyrolysis products from charring polymers as a function of time. For example, when GC-MS is chosen as the analytical

technique, different classes of capillary columns are necessary in order to analyze groups of compounds (e.g., volatile, non-volatile). This restriction eliminates the ability to measure the full range of pyrolysis products that are produced from thermosetting resins.

Mass spectrometers have been used as a stand-alone technique for the quantitative determination of molecular species (e.g., simple hydrocarbon mixtures) since the early 1940's.[59-60] Quantitative analysis of spectra collected from simple mixtures can be accomplished using several techniques.[61] The first step for both techniques involves collecting a reference library of analyte mass spectra. Spectra of analyte species are collected with the mass spectrometer parameters (e.g., electron energy, ion energy, etc.) fixed at the same settings that are used during experimentation.

In the first technique, a linear combination of reference spectra is fit to an experimental spectrum by adjusting the coefficients until a good fit is achieved. The goodness of fit is monitored by minimizing the residual between the amplitude of the reference spectra and the experimental spectrum. The coefficients that result from the fitting procedure represent relative molar yields of each of the analyte species. When fitting the spectra manually, a best practice is to start fitting the experimental spectrum by adjusting the coefficient in the linear combination that represents the analyte species with the highest mass and sequentially working towards lower masses. The next step is to correct the relative molar yield of each species by applying a detection sensitivity correction factor (see section 4.3.1) This technique is best used when the products of pyrolysis have significant spectral overlap (e.g., methyl substituted derivatives of phenol).

The second technique shares similarities to the first procedure but is better suited to analyze mass spectra that do not have significant spectral overlap. The matrix inversion technique described here is based on a procedure developed by Lilienkamp.[61] In this technique, matrix algebra is used to solve a set of N simultaneous linear equations with N unknowns. The matrix equation for the peak heights of an experimental mass spectrum is represented by:

$$\mathbf{[A][P] = [h]} \quad (1)$$

Where the A matrix is an N x N matrix that is derived from the mass spectrum of each analyte species. The columns of the A matrix represent the peak height of each analyte molecule at specific *m/z*. For instance, the A matrix for a gas mixture made of H_2, CH_4, CO, and CO_2 is represented in Fig. 2.15.

m/z	H_2	CH_4	CO	CO_2
2	1.000	0.000	0.000	0.000
16	0.000	1.000	0.006	0.080
28	0.000	0.000	1.000	0.064
44	0.000	0.000	0.000	1.000

Figure 2.15. 4 x 4 matrix used to solve for the partial pressure of each component in a gaseous mixture of H_2, CH_4, CO, and CO_2. (A 6 x 6 matrix was used to solve for the partial pressures of the six molecules evolved during the pyrolysis of an epoxy-novolac resin system.)

The P matrix is a column matrix that represents the partial pressures of each gas, and the h matrix is a column matrix that represents the peak heights of each analyte molecule. Solving for P gives:

$$\mathbf{[A]^{-1}[h] = [P]} \quad (2)$$

Solving this equation requires that the A matrix is invertible. After solving for the column matrix P, the resulting relative molar yields are corrected by sensitivity correction factors (see section 4.3.2).

2.8 MATERIALS

2.8.1 PHENOLIC IMPREGNATED CARBON ABLATOR (PICA)

PICA samples were obtained from Fiber Materials, Inc. and stored in a desiccator to minimize adsorption of atmospheric water to the surface of the resin, as phenolic resins are hygroscopic. Samples of PICA are easily shaped to any dimension by using a sharp stainless-steel blade. Once the sample is cut to the desired dimensions, great care must be taken to ensure that mass loss is minimized as PICA is a very brittle material. The testing of samples of PICA is described in chapters 3 and 4 of this thesis.

2.8.2 EPOXY-NOVOLAC D.E.N. 438

D.E.N. 438 resin samples were obtained from Olin Epoxy through E. T. Horn. Epoxy-novolac resin samples were prepared by mixing D.E.N. 438 with methyl-5-norbornene-2,3-dicarboxylic anhydride (NMA, 85 phr) as a crosslinking agent, and N,N-dimethylbenzylamine (BDMA, 1.5 phr) as the catalyst. The curing agent and catalyst were purchased from Sigma-Aldrich. The resulting mixture was then heated (54 °C) and degassed in a small vacuum chamber to remove trapped air before curing. Samples of the resulting mixture were heated to 150 °C for 1 minute to decrease viscosity. The warm resin was inserted into 5 mm diameter x 6 mm long tantalum cylinders using a pipette and cured

under atmosphere (Ney Centurion). The cure schedule for this study was chosen to reflect the same conditions that were used by Lee (see Fig. 2.16).[47]

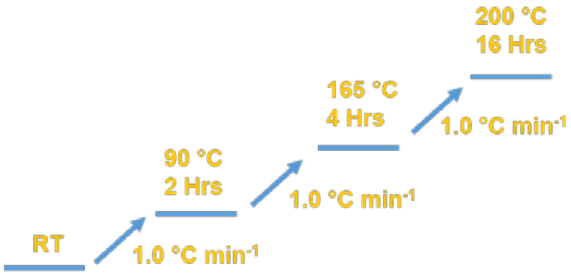

Figure 2.16 Epoxy-novolac samples are cured in three stages. Each stage consists of a temperature ramp (blue arrow) and a temperature soak (horizontal bar).

2.8.3 PHENOLIC MICROBALLOONS COMPOSITE MATERIAL

Composite materials were prepared by adding phenolic microballoons (5.60 wt%) to the epoxy-novolac mixture. Samples of the resulting composite material were then cured under the same conditions as the pure resin (see section 2.8.2). The phenolic microballoons (BJO-0930) were purchased online from U. S. Composites.

2.8.4 METHYLCYCLOPENTADIENE (MCPD)

Methylcyclopentadiene (MCPD) was produced using a procedure described by Darkwa.[62] 100 ml of the dimer is placed in a round bottom flask and maintained at a temperature of 180 °C. The monomer vapor was separated from the dimer with a Vigreux column, and the distillate was collected in an ice-cooled Erlenmeyer flask. The resulting distillate was purified by repeating the procedure twice. The distillate was then stored at -30 °C before testing. The dimer was purchased from Sigma Aldrich.

2.9 REFERENCES

51) Ehlert, T. C. Determination of Transmission Characteristics in Mass Filters *J. Phys. E*., **1969**, 3, 237-239.

52) Lieszkovsky, L.; Filippelli, A. R.; Tilford, C. R.; Metrological Characteristics of a Group of Quadrupole Partial Pressure Analyzers. J. Vac. Sci. Technol. A **1990**, 8, 3838-3854.

53) Zhang, J.; Garton. D. J.; Minton., T. K. Reactive and Inelastic Scattering Dynamics of Hyperthermal Oxygen Atoms on a Saturated Hydrocarbon Surface. *J. Chem. Phys.* **2002**, *117*, 6239-6251. DOI: 10.1063/1.1460858

54) Garton, D. J.; Brunsvold, A. L.; Minton, T. K.; Troya, D.; Maiti, B.; Schatz, G. Experimental and Theoretical Investigations of the Inelastic and Reactive Scattering Dynamics of O (^{3}P) + D_2. *J. Phys. Chem. A* **2006**, *10*, 1327-1341. DOI: 10.1021/jp054053k

55) Lee, Y. T.; McDonald, J. D.; LeBreton, P. R.; Herschbach, D. R. Molecular Beam Reactive Scattering Apparatus with Electron Bombardment Detector. *Rev. Sci. Instrum.* **1969**, *40*, 1402-1408. DOI: 10.1063/1.1683809

56) Brink, G. O.; Electron Bombardment Molecular Beam Detector. *Rev. Sci. Instrum.* **1966**, 37, 857-860.

57) Daly, N. R.; Scintillation Type Mass Spectrometer Ion Detector. *Rev. Sci. Instrum.* **1960**, 31, 264-267.

58) Moore, *J. H. Building Scientific Apparatus A Practical Guide to Design and Construction*, 2nd ed.; Addison-Wesley Redwood City, CA. **1989**.

59) McLafferty, F. W. *Interpretation of Mass Spectra*, 4th ed. Kelly, A., Ed.; University Science Books, Sausalito, CA, **1993**.

60) Skoog, D. A.; Holler, F. J.; Crouch, S. R.; *Principles of Instrumental Analysis*. 6th ed. Kiselica, S. Ed.; Thomson Brooks/Cole, Belmont, CA, **2007**.

61) Lilienkamp, R. H. Methods of Determining Residual Gas Composition from Residual Gas Analyzer Data. In *5th Space Simulation Symposium,* ASTM/IES/AIAA Space Simulation Conference, 14-16 September, 151-164, **1970**.

62) Darkwa, J.; Giolando, D. M.; Murphy, C. J.; Rauchfuss, T. B.; BIS(η^5-Methylcyclopentadienyl) Titanium Pentasulfide, BIS(η^5-Methylcyclopentadienyl)-Divanadium Pentasulfide, and BIS(η^5-Methylcyclopentadienyl) Divanadium Tetrasulfide. Inorg. Synth. **2007**, 27, 51-58.

CHAPTER THREE

PYROLYSIS OF PHENOLIC IMPREGNATED CARBON ABLARTOR (PICA)

Contribution of Authors and Co-Authors

Manuscript: Pyrolysis of Phenolic Carbon Ablator

Author: Brody K. Bessire

Contributions: Collected and analyzed all data. Assisted in writing and editing manuscript.

Co-Author: Sridhar A. Lahankar.

Contributions: Assisted in developing data analysis method.

Co-Author: Timothy K. Minton

Contributions: Assisted with the interpretation of data and edited manuscript.

Manuscript Information Page

Brody K. Bessire, Sridhar A. Lahankar, Timothy K. Minton
ACS Applied Materials and Interfaces

Status of Manuscript:
____ Prepared for submission to a peer-reviewed journal
____ Officially submitted to a peer-review journal
__ Accepted by a peer-reviewed journal
_X_ Published in a peer-reviewed journal

Published by the American Chemical Society
Received: November 8, 2014
Accepted: December 9, 2014

CHAPTER THREE

PYROLYSIS OF PHENOLIC IMPREGNATED CARBON ABLATOR (PICA)

3.1 INTRODUCTION

Thermal protection systems (TPSs) are required to shield spacecraft from the high temperatures generated in the stagnation region during atmospheric entry. TPSs can be designed to act as heat sinks, which use a material with a high heat capacity to absorb energy, or they can be designed to ablate and carry away thermal energy.[63-64] Composite ablative TPS systems are designed such that an organic resin matrix, surrounding a carbon fiber substrate, pyrolyzes to gaseous products and leaves a carbonaceous char behind. The gaseous products eventually make their way into the boundary layer and act as a transpirant, effectively cooling the leading edge of the spacecraft. The remaining char layer continues to absorb heat until it decomposes through sublimation or is removed by spallation.[65]

At present, analysis and design of new ablative heat shields relies on material response models based on 50-year-old methodologies.[66-67] As a consequence, large uncertainties and margins are inherent in the design process, which leads to unnecessarily heavy heat shields and an inability to quantify the reliability of the resultant space hardware.[23] Building models that are based on fundamental understanding of the material behavior and validating them with high fidelity data will enable optimized risk and margin recommendations for a whole generation of future NASA and commercial space missions. The current ablation models assume thermodynamic equilibrium chemistry to estimate the

recession rate, and these models are known to be deficient because they over predicted the recession rate, for example, during the MSL entry into the Martian atmosphere.[68] Clearly, non-equilibrium chemistry is important in such environments; therefore, the new non-equilibrium models that are required must be founded on a fundamental understanding of the relevant non-equilibrium chemical kinetics and dynamics, which may be obtained from *in situ* measurements of dynamic chemical processes in real time. Chemical processes of relevance include the high-temperature decomposition of PICA-class materials and the interactions of decomposition products and boundary layer gases with each other and with the evolving ablator surfaces. Such detailed data will dramatically deepen our understanding of the processes occurring at the interface of a high-temperature hypersonic flow and an ablator, as well as provide a rigorous test of any new model that is developed. The work described herein is the first step in the development of a laboratory approach to understand the non-equilibrium ablation chemistry during atmospheric entry of carbon/phenolic composite TPS materials using advanced techniques that are well established in the field of reaction dynamics but have not previously been applied to the understanding of the chemical processes in an atmospheric entry environment.

Mass spectral measurements taken *in situ* provide an excellent way to obtain accurate and precise data for the whole range of pyrolysis products, and they are well suited for probing the time-dependent decomposition mechanisms of materials under controlled heating conditions. A key objective of the work described herein was, therefore, to develop the methodology to measure relative molar yields of pyrolysis products under conditions where (1) time and temperature are independent variables and (2) there is no interaction of

products with each other, with the hot sample surface, or with any container walls after they leave the decomposing material. A second important objective was to improve our understanding of the decomposition mechanisms of the specific carbon/phenolic composite, PICA, as this material has been chosen for several NASA missions and is an important model material for ongoing theoretical efforts to describe the in-depth temperature response of ablative TPS materials. Our approach was to use a mass spectrometer to detect the pyrolysis products *in situ* as they desorbed from a PICA sample that was heated in high vacuum and to determine relative molar yields of the products by a validated interpretation of the mass spectral data.

3.2 EXPERIMENTAL METHODS

The experiments utilized a crossed molecular beams apparatus with a rotatable mass spectrometer detector.[53-55] For the experiments described here, a heated PICA sample was placed in front of the detector in vacuum, and mass spectra of pyrolysis products were collected as the temperature of the sample was increased. Figure 3.1 shows a diagram of the experimental set-up. A fitting method was developed to derive relative molar product yields from the mass spectral data.

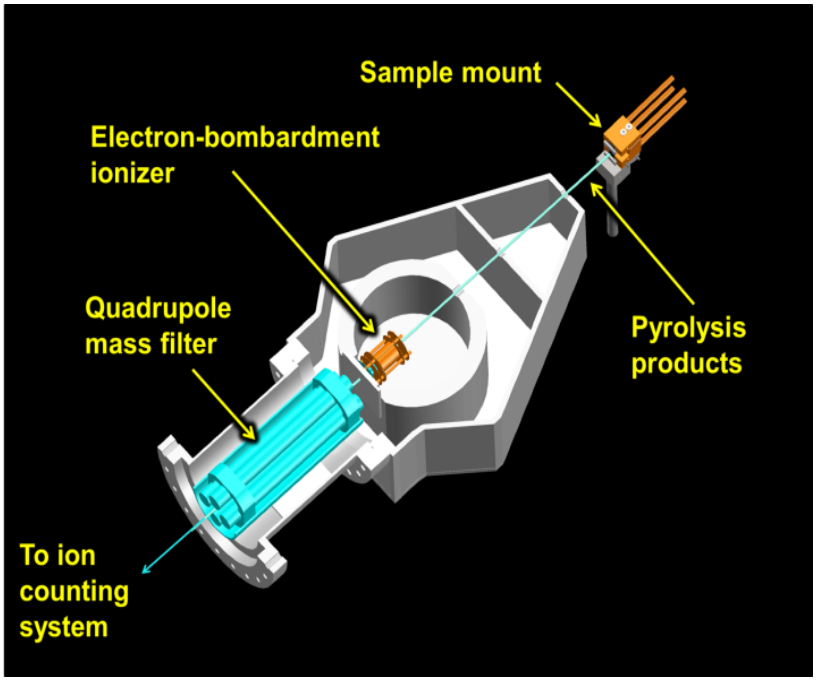

Figure 3.1. Schematic diagram of the experimental set-up, where the resistively heated PICA sample is placed in a separate vacuum chamber in front of a triply differentially pumped mass spectrometer detector with an electron-impact ionizer, a quadrupole mass filter, and a Daly-type ion counter. Volatile products desorb from the sample in all directions, but only those products that exit the surface from a roughly 3 mm x 3 mm square area of the surface pass through the apertures of the detector and reach the ionizer.

The samples were heated by passing current through them. The sample mount (Fig. 3.2) consists of two water-cooled copper blocks that are electrically isolated by a ceramic spacer and connected to a TDK-Lambda GEN 30-25 power supply. Current flowed through copper cooling tubes. Cooling water was circulated through the mount by a pair of chillers, each held at a temperature of 25 °C.

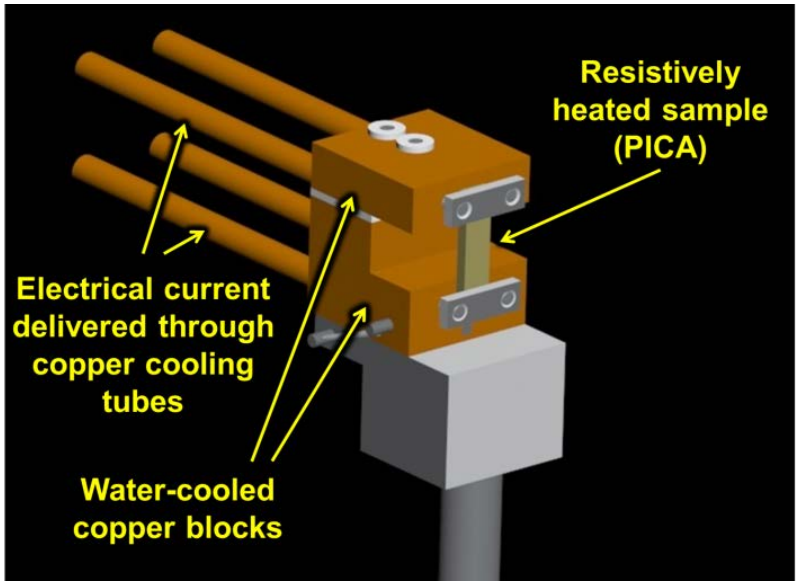

Figure 3.2. Mount used to heat PICA samples. The top and bottom copper blocks act as electrodes and are separated by a ceramic spacer and cooled with water that flows through copper tubes attached to the back. The copper tubes also carry the electrical current used to heat the sample restively.

PICA samples were obtained from Fiber Materials Inc. Each sample in this study was cut to the dimensions of 25 mm long x 6 mm wide x 5 mm thick. A K-type thermocouple was attached to the center of the back side of the PICA sample during each experimental run in order to obtain precise temperature measurements. Before each experimental run, a fresh PICA sample was mounted, and the vacuum chamber was pumped out overnight to a base pressure in the low 10^{-7} Torr range.

The mass spectrometer is triply differentially pumped (Fig. 3.1), to ensure an extremely low pressure ($<10^{-11}$ Torr) in the ionization region and therefore low background and high detection sensitivity. Pyrolysis products emerge continuously from the heated sample and pass through three apertures and then enter the electron-impact (EI) ionizer. Ions are focused into a quadrupole mass filter, and the mass-selected ions are converted

into electrical pulses by a Daly-type ion counter.[55] The values of *m/z* accepted by the quadrupole are varied with time by control electronics, and the ion signal (which is proportional to number density) as a function of time is accumulated with a multichannel scaler. The *m/z* accepted by the mass filter as a function of time allows the data accumulated with the multichannel scaler to be converted into a mass spectrum, which is number density as a function of *m/z* ratio. The products that are not ionized pass through the ionization region and enter a different region of differential pumping, thus ensuring that any products that scatter from surfaces in the detector cannot re-enter the ionizer and have a second chance to be ionized. Details of the mass spectrometer detector have been described previously.[55]

Samples were heated initially from room temperature to 100 °C within a matter of seconds, and then they were heated to nearly 950 °C in roughly 50 °C steps, with a hold time of 15-20 minutes at each temperature step. Mass spectra were collected at specific times after each heating increment. Associated with each heating increment was a pressure jump in the vacuum chamber, as pyrolysis products desorbed quickly from the sample. The high flux of gases desorbing from the sample immediately after each heating increment saturated the detector, so a gate valve that isolates the mass spectrometer detector from the sample chamber was closed during the initial moments of each heating increment and then opened later for data collection. Figure 3.3 shows an example of the partial pressure change in the sample chamber for three pyrolysis products, H_2, CO, and CH_4, after a sample was heated from 686.6 °C to 729.0 °C. Data for this figure were collected with a residual gas analyzer (RGA) in the sample chamber. After the heating current was increased, the

temperature of the sample rose to its final value within seconds, and the partial pressure of pyrolysis gases rose quickly to a maximum and then decayed at a relatively slow rate, on the time scale of minutes. In general, after the pressure in the sample chamber had decreased to an acceptable level (~6 x 10^{-7} Torr), mass spectra were collected repeatedly (with 30 s being required to collect a mass spectrum). After the difference in intensity between two successive spectra had decreased to less than 20%, a set of five mass spectra were collected and summed. Thus, data for a particular temperature were typically collected during a 2.5 min period in the range of 12-15 min after each temperature step. The typical range over which mass spectra were collected after a temperature step is illustrated in Fig. 3.3. The pyrolysis products were thus monitored essentially after a steady state had been reached at a given temperature. Each individual mass spectrum was collected by scanning *m/z* values in steps of 0.045 amu, with a dwell time of 10 ms at each step. The summed spectrum collected at each temperature was used to determine the relative molar yields of pyrolysis products using a procedure, described in the next section, that involved fitting the summed mass spectrum. Similar temperature-dependent mass spectral data were collected for four different samples, and the results were averaged.

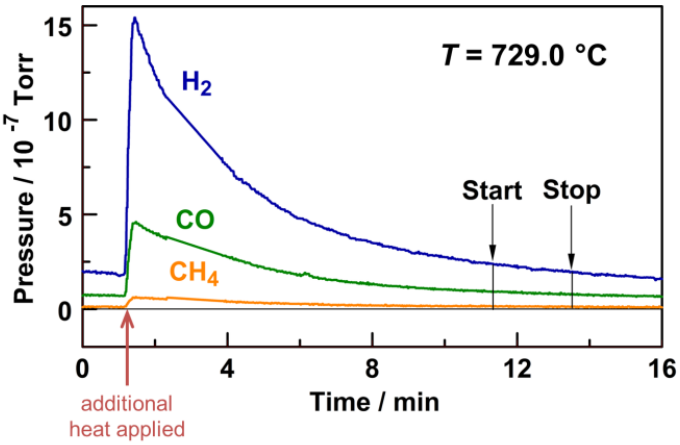

Figure 3.3. Partial pressure of H_2, CO, and CH_4 in the sample chamber as a function of time after a PICA sample was raised (starting at 1.5 minutes from an arbitrary time zero) from 686.6 °C to 729.0 °C, measured with a residual gas analyzer (RGA). Five mass spectra were collected consecutively during the time from "Start" to "Stop", and these mass spectra were summed to give the mass spectrum corresponding to a temperature of 729.0 °C. Hydrogen was clearly detected by the RGA, even though it was not monitored during the collection of mass spectra with the detector depicted in Fig. 3.1.

3.3 RESULTS AND ANALYSIS

3.3.1 ANALYSIS OF MASS SPECTRA

The relative molar yield of each detected species at a given sample temperature was derived from the mass spectrum collected at that temperature. The relative molar yields are equivalent to the relative fluxes of the products that desorb from the sample. All products exit the surface in thermal equilibrium, and their fluxes emanating from a given point on the surface should, therefore, have a cosine angular distribution about the surface normal. When the angular distributions of the products are the same, the relative flux integrated over all exit angles can be obtained from the flux measured at one exit angle.

Thus, all products were collected with the mass spectrometer oriented along the surface normal. Although the EI ionizer makes the mass spectrometer a number density detector, it is a simple matter to convert the measured signals to relative flux.[69]

A list of 34 compounds that might be produced from PICA pyrolysis was generated from observations of pyrolysis products that have been reported in the literature on the pyrolysis of the neat phenolic resins, as well as composite materials made with similar resins. Table 3.1 lists all the compounds that were used to construct the list. All compounds on the list are stable, as it was assumed that any radical species that might have been produced initially had ample time to react (for example, by abstracting a hydrogen atom) and form a stable species while following a tortuous path through the decomposing polymer and incipient char layer. H_2 is undoubtedly among the pyrolysis products, but it was not included in the list of potential products because our mass spectral range at the time the data were collected did not include *m/z* ratios less than 10.

Table 3.1. List of compounds selected as potential pyrolysis products and their respective electron-impact ionization cross sections. Of the 34 compounds listed, only 14 (shown in color and larger font) made a significant contribution to the fit of the experimental mass spectra. The total EI ionization cross sections were taken from several sources[35-37] and scaled to give a set of cross sections that were consistent with those reported in the NIST database.[38] Electron-impact ionization cross sections for 2,2-dimethyl-propanol-1-ol and hexamethylenetetramine were not found in the literature, so the relative molar yields for these species were not corrected for ionization cross section. The lack of correction for ionization cross section would lead to an overestimate of the relative molar yield, but even without correction, the yields of these two species were negligible.

Product Species	Ionization Cross Section / Å^2	Product Species	Ionization Cross Section / Å^2
CH_4	3.52	o-cresol	17.19
H_2O	2.28	p-cresol	18.94
CO	2.52	mesitylene	18.18
CH_2CH_2	5.12	2,6-dimethyl phenol	19.82
CH_3CH_3	6.42	2,4-dimethyl phenol	21.58
CH_3OH	5.11	3,4-dimethyl phenol	23.82
Ar	2.99	2,4,6-trimethyl phenol	24.22
CO_2	3.52	hexamethylenetetramine	-
$CH_3CH_2CH_3$	8.62	2-methylnapthalene	22.12
$(CH_3)_2CHOH$	10.94	2-methyl-1,1'-biphenyl	25.58
benzene	15.03	dibenzofuran	33.05
hexane	16.58	diphenyl methane	34.18
2,2-dimethyl-propanol-1-ol	-	diphenyl ether	34.18
toluene	16.62	anthracene	33.05
phenol	14.55	benzophenone	29.54
o-xylene	15.81	xanthene	33.05
p-xylene	17.04	(4-methylphenyl)-phenyl-methanone	32.56

The calculation of relative molar yields required the knowledge of the EI ionization mass spectra for the compounds on the list in Table 3.1, which were taken from the National Institute of Standards and Technology (NIST) database.[70] The first step in the calculation of the relative molar yield of each molecular species was to fit every peak in its NIST reference mass spectrum with a Gaussian function representative of the mass resolution of our mass spectrometer (~1 u). Next, linear combinations of the Gaussian-fit mass spectra

for individual species were fit to an experimental mass spectrum. Figures 3.4 and 3.5 display representative mass spectra that were collected at relatively low and high temperatures, respectively. The raw data, with background subtracted, are indicated by the green dots, and the fits are indicated by the solid blue lines. Each fit was optimized by minimizing the residuals. Relative molar yields were obtained from the coefficients in the linear combination that gave the best fit to the experimental mass spectrum by weighting each coefficient by the total EI ionization cross section for the respective chemical species and then dividing the result by the square root of the molecular mass of the species to obtain flux.[69] The total EI ionization cross sections were taken from several sources[71-73] and scaled to give a set of cross sections that were consistent with those reported in the NIST database.[74] The values that were used to determine the relative molar yields reported here are listed in Table 3.1.

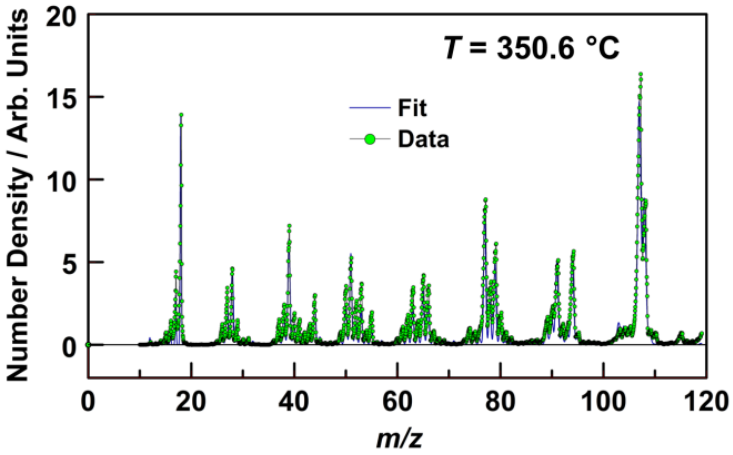

Figure 3.4. Representative mass spectrum and associated fit of pyrolysis products detected with a PICA sample temperature of 350.6 °C. The small peak at *m/z* = 115 suggests that a diphenyl ether group might be evolved at this temperature.

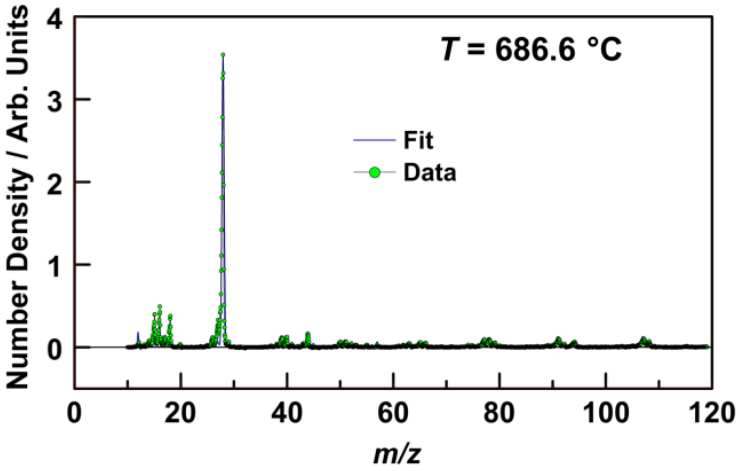

Figure 3.5. Representative mass spectrum and associated fit of pyrolysis products detected with a PICA sample temperature of 686.6 °C. CO and CH_4 dominate the spectrum at this temperature, as crosslinks are broken, and the material is reduced to a char.

There are some key assumptions in the analysis that add much uncertainty to the relative molar yields. Implicit in the analysis that was done is the assumption that the fragmentation patterns of the compounds in the NIST database are identical to those for our mass spectrometer. We have not conducted a systematic study of fragmentation patterns of all the compounds listed in Table 3.1, but we have verified that the fragmentation patterns of phenol and o-cresol measured in our mass spectrometer are similar to those in the NIST database. Another assumption in the analysis is that the transmission probability of ions through the quadrupole mass filter is constant over the *m/z* range in our experiments. The transmission function probably favors higher-mass products in our experiments,[69] in which case the relative molar yields of the higher-mass products that we observed (e.g., phenol and its methylated derivatives) would actually be lower than

what we report. The uncertainties associated with these assumptions are difficult to estimate. Nevertheless, our reported relative molar yields can be considered to be qualitatively, and even semi-quantitatively, correct. Work is underway to determine the transmission function of our mass filter and build our own database of fragmentation patterns for the possible pyrolysis products, in anticipation of future experiments where the temperature-dependent relative molar yields of the products will be measured under non-equilibrium conditions in real time.

3.3.2 RELATIVE MOLAR YIELDS

Of the 34 species chosen as potential gas-phase products for fitting the mass spectra, only 14 species consistently contributed significantly to the fits. A table of the 14 species, with their relative molar yields at each pyrolysis temperature, is presented in Appendix A. Most of the molecules that have been included in the list shown in Table 3.1 were chosen because they have been suggested as decomposition products in prior literature. The four molecules, hexamethylenetetramine, hexane, isopropanol, and methanol, where chosen because they are commonly used as solvents during the synthesis of phenolic resins. The inclusion of these molecules and Ar improved the fit of the mass spectra at low temperatures, but their relative molar yields quickly vanished at temperatures exceeding 200 °C. The appearance of Ar among the desorbed products at low temperatures suggests that it must have been trapped in the polymer, but the source of Ar is unknown, and we can only speculate that an Ar-rich atmosphere might have been used during the processing of the PICA composite. The possible decomposition product, diphenyl ether, has a parent mass (m/z = 170) that is above the mass range used, and we could only obtain good fits to

the mass spectra by considering possible daughter fragments from diphenyl ether. The small peak in the mass spectrum at *m/z* = 115, which corresponds to a daughter fragment of diphenyl ether, supports the assumption that diphenyl ether might be a minor product. But the very low yield of this assumed product and the lack of detection of its parent mass do not give us sufficient confidence to report diphenyl ether as a significant pyrolysis product. Three of the species that were detected, xylene, cresol, and dimethyl phenol, may have different isomeric structures, but the differences in the fragmentation patterns of the isomers of these species are not sufficient to allow their distinction in our mass spectrometer. For example, *o*-xylene and *p*-xylene have maxima in their mass spectra at the same daughter mass of *m/z* = 91. Relative to this largest peak, both isomers have parent and daughter peaks of very similar magnitudes at *m/z* = 106 (parent), 77, 65, and 39. Because of the indistinguishability of the isomers by our mass spectrometer, the molar yields reported for xylene, cresol, and dimethyl phenol include all the isomers of the respective species. Neglecting Ar, diphenyl ether, and the four solvent species mentioned above, and grouping the isomers of detected species, the focus of the results is on eight significant species that were detected during the pyrolysis of PICA: H_2O, CH_4, CO, CO_2, phenol, xylene, cresol, and dimethyl phenol.

Figure 3.6 shows a plot of the relative molar yields of the species mentioned above as a function of pyrolysis temperature. The relative molar yields are plotted as the observed yield relative to the maximum yield (where the observed yields are in arbitrary units) which came from CO at 444.8 °C. The detected lower-mass pyrolysis products were H_2O, CH_4, CO, and CO_2, while the higher-mass (aromatic) products were xylene, phenol, cresol, and

dimethyl phenol. H_2O and CO were the dominant products that were detected over the temperature range in this study, with H_2O being the dominant product below ~400 °C. The yield of CO_2 rises up at 150 °C where it levels off until about 400 °C and then begins to drop, disappearing completely near 650 °C. CH_4 begins to evolve around 300 °C, and its yield reaches a maximum near 450 °C. All the higher-mass products evolve from 300 °C to 450 °C and have maxima in their yields between 350 °C and 400 °C. The higher-mass products have much lower relative molar yields than the lower-mass products.

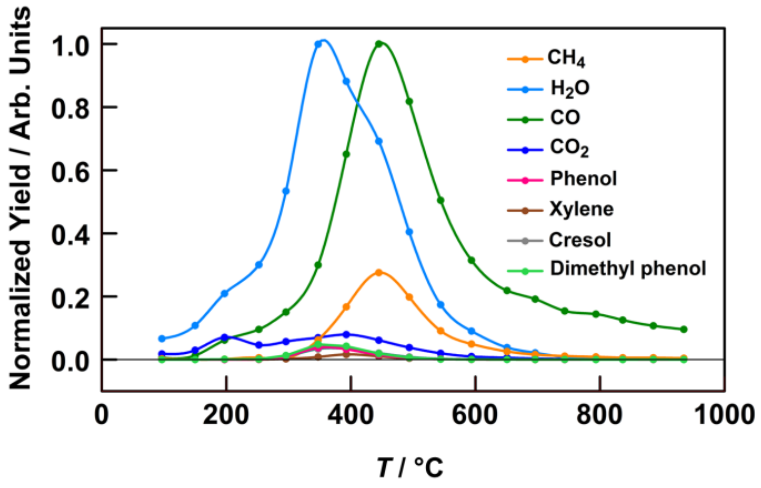

Figure 3.6. Normalized yields of gaseous pyrolysis products as a function of PICA temperature. The yield of each species at each temperature has been normalized to the yield of CO at 444.8 °C.

3.3.3 TEST OF ANALYSIS PROCEDURE WITH A BINARY MIXTURE

The methodology used to derive relative molar yields from the mass spectra was tested with the use of a binary mixture of phenol and *o*-cresol. A vessel containing these two liquids (purchased with a stated purity of 99% from Sigma-Aldrich) with known mole

fractions of 0.54 and 0.46, respectively, was immersed in a temperature-controlled ethanol bath, and the vapor from the mixture at a given temperature was expanded through an effusive nozzle and interrogated with the mass spectrometer detector. Mass spectra of the vapor were collected with the liquid mixture at different temperatures, starting at 20 °C and reduced in 5 °C increments down to 0 °C. A representative mass spectrum collected at 20 °C and the corresponding optimized fit are shown in Fig. 3.7 In general, the mass spectrum is fit well using the procedure discussed above.

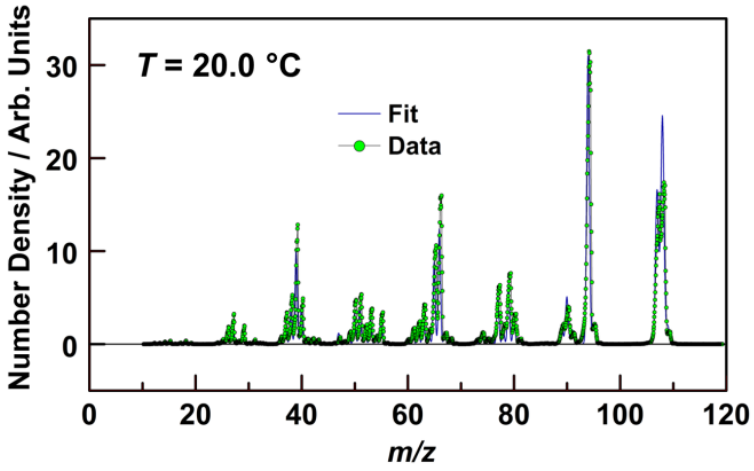

Figure 3.7. Mass spectrum of the vapor from a binary mixture of phenol and o-cresol (with mole fractions of 0.54 and 0.46, respectively) that was held at 20 °C. The raw data are represented by the green dots, and the blue line represents the fit using the procedure described in the text.

The accuracy of the procedure was validated by comparing the known partial pressure ratio in the vapor to the partial pressure ratio derived from the mass spectra. The known partial pressure ratio in the vapor comes from the finding of Rhodes et al. that

phenol and *o*-cresol form an ideal solution.[75] The vapor pressure of the pure substance for each species in the binary mixture was calculated from the integrated Clausius-Clapyeron equation, whose parameters are available in the literature.[76] According to Raoult's Law, the vapor pressure for each pure substance was multiplied by its corresponding mole fraction in the liquid mixture to yield the partial pressure of each constituent at each temperature in the experiment. Figure 3.8 shows a comparison between the calculated partial pressure ratios of phenol to *o*-cresol at different temperatures and the partial pressure ratios that were derived by fitting the mass spectra using the same methodology that was described in section 3.3 (Note that when comparing with partial pressure ratios, which are proportional to number density ratios, the $1/\sqrt{m}$ correction to flux that was mentioned in Section 3.3.1 is not used.) Within experimental error, the ratios derived from the mass spectral fitting methodology agree with the calculated ratios. There appears to be a slight systematic deviation at lower mixture temperatures, where the measured ratio is lower than the calculated ratio. This deviation may be explained by the preferential evaporation of the more volatile phenol during the course of the experiment. The experimental measurement accurately determines the partial pressure ratio of the vapor pressure of this binary solution and is even sensitive enough to detect changes in the composition of the mixture as one component evaporates preferentially over another. Thus, our analysis procedure appears to be a credible approach for determining relative mole fractions from mass spectral data. It should be noted, however, that this validation experiment used two compounds of similar molecular mass and therefore is not sensitive to a systematic error caused by setting the mass-dependent transmission function to a constant value.

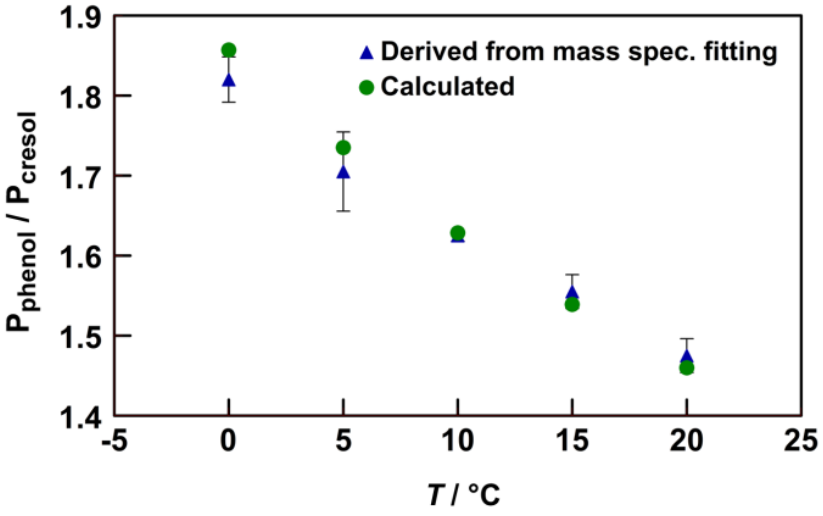

Figure 3.8. Partial pressure ratios in the vapor of a binary mixture of phenol and o-cresol that was held at various temperatures from 0 °C to 20 °C. Blue triangles are the ratios calculated by fitting mass spectra of the vapor collected for each temperature. Data for two identical experiments are averaged. Green dots are partial pressure ratios that are calculated for this ideal mixture. Error bars represent ±1σ, where σ is the standard deviation based on the two experiments.

3.4 DISCUSSION

3.4.1 COMPARISON OF PYROLYSIS YIELDS TO PREVIOUS WORK

Our results are consistent with the general description of three overlapping stages of pyrolysis as represented in Fig. 1.3 of this thesis. Earlier results suggest that H_2O and phenol, as well as phenol's methyl, substituted derivatives, are evolved in the first stage (T ≈ 200-550 °C). We observe H_2O from 100 °C to nearly 700 °C, with the peak yield coming at a temperature of 350 °C (see Fig. 3.6). The evolution of H_2O well below 300 °C is likely to be the result of the outgassing of H_2O that was simply absorbed by PICA, which is

known to be hygroscopic. Note that no attempt was made to de-gas the samples (other than holding them in vacuum overnight) before they were subjected to heat. As the sample temperature approaches 300 °C, the desorption of absorbed H_2O should be complete and additional H_2O would be expected to be produced by condensation reactions. Ouchi and Honda[31] suggested that the evolution of water from a phenolic resin near 350 °C is the result of a condensation reaction that leads to the formation of a diphenyl ether crosslink between phenol groups, as illustrated in Fig. 3.9. FTIR measurements collected by Trick and Saliba[33] on a carbon/phenolic composite corroborate the existence of a diphenyl ether group, as evidenced by an observed absorption at 1264 cm^{-1}. A small peak at *m/z* = 115 in our mass spectral data is also possible evidence that diphenyl ether is an intermediate in the pyrolysis of PICA (Fig. 3.4). The *m/z* = 115 peak, which could be from a daughter fragment of diphenyl ether, begins to evolve at 250 °C, rises to a maximum at 350 °C, and becomes insignificant between 450 °C and 500 °C, which is consistent with the observations made by Ouchi and Honda. However, 2-methyl-naphthalene is another possible minor product that has a daughter fragment at *m/z* = 115, but the structure of this molecule consists of two fused benzene rings and more closely resembles a product that would be expected from the char layer. It is generally accepted that the char layer consists of fused aromatic rings, and volatile products from the char layer are therefore expected to be observed at higher temperatures. Thus, if an unconsidered high-mass species is contributing to the signal at *m/z* = 115, diphenyl ether is the more likely possibility, but it will be necessary to extend the data to higher mass ranges to verify the production of this species.

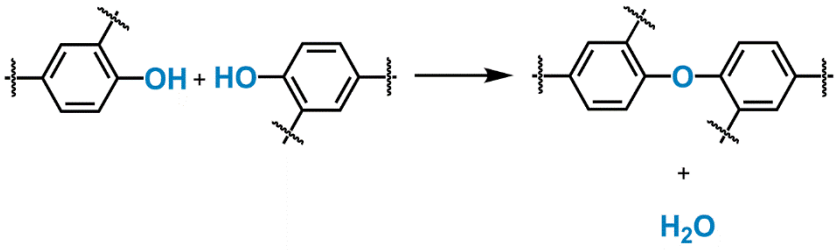

Figure 3.9 Condensation reaction between two adjacent hydroxyl groups to form a diphenyl ether group and H_2O. Based on a mechanism proposed by Ouchi and Honda[31] and Ouchi.[34]

Phenol and its methyl substituted derivatives are also liberated during the first pyrolysis stage ($T \approx$ 200-550 °C). Our results show that higher-mass species, including phenol, cresol, and dimethyl phenol are observed from 250 °C to 450 °C, with a maximum at 350 °C. Parker and Winkler[32] proposed that aromatic groups that are part of the polymer backbone are retained and that only pendant aromatic groups are released as phenol and cresol (they did not discuss dimethyl phenol in this context, but one might imagine that it could also come from the liberation of a pendant group), see fig. 3.10. Our results support this proposed decomposition pathway, as we observe phenol and its methylated derivatives over a narrow temperature range and in relatively small quantities. Xylene is also assigned in the mass spectra and appears in the same temperature range as phenol and its methyl substituted derivatives. The mechanism of xylene production has not been discussed previously, and its origin is unknown. In fact, the assignment of xylene as a product is still ambiguous (*vide infra*). If the assignment is correct, then the shift in maximum yield toward higher temperatures relative to phenol and its derivatives might indicate a transition in the pyrolysis mechanism where the evolution of oxidized aromatic species is giving way to less oxidized aromatic species that are still volatile.

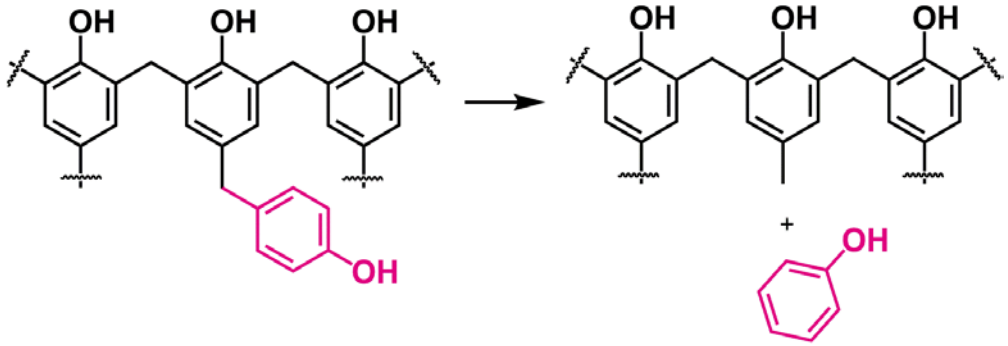

Figure 3.10. Liberation of a pendant group in the form of a phenol molecule. Based on the proposal by Parker and Winkler[32] that phenol (and presumably its substituted derivatives) can only be produced from pendant groups on the polymer backbone.

CO_2 is also observed in the first pyrolysis stage but with relatively low yield (Fig. 3.6). CO_2 reaches a maximum yield at 200 °C and stays relatively constant, with a slight dip at 250 °C, until 400 °C where it begins to drop. Jackson and Conley[29] suggested that CO_2 is evolved from the decomposition of carboxylic acid groups that are formed by the oxidation of methylol groups remaining after the resin has cured. This idea was supported by infrared spectra that revealed the presence of residual methylol functional groups even after curing at 120 °C. Post-curing in air would presumably lead to the oxidation of these methylol groups, and subsequent heating would release CO_2 (Fig. 3.11).

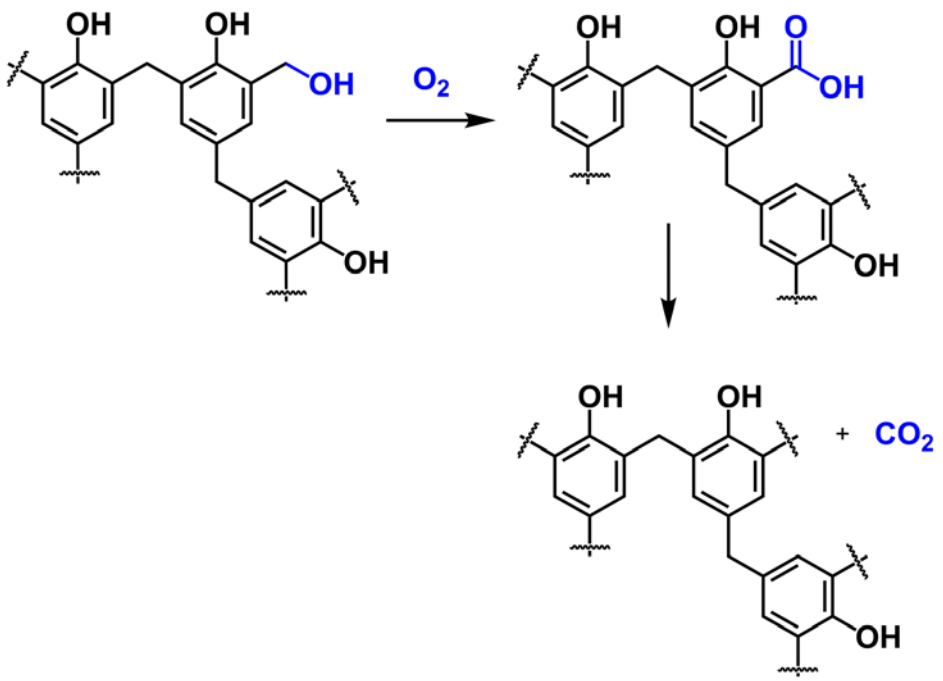

Figure 3.11. Oxidation of a methylol group leads to formation of a carboxylic acid group that subsequently decomposes and releases a CO_2 molecule. Based on a mechanism proposed by Jackson and Conley.[29]

The predominant pyrolysis product that we observed during the second stage of pyrolysis ($T \approx$ 400-800 °C) was CO, which actually evolved over the entire experimental temperature range. Our results indicate that CO has a relatively low yield at temperatures below ~300 °C. Above 300 °C the CO yield rises steeply with temperature to a maximum at 450 °C, after which the yield drops quickly as the temperature increases to 600 °C and then only slowly decreases as the temperature increases further. Mechanisms proposed by Jackson and Conley[29] and by Ouchi[34] suggest that CO is produced as a result of the decomposition of a carbonyl crosslink in the polymer (Fig. 3.12). The FTIR studies of Trick and Saliba[33] showed direct evidence for a carbonyl stretch at 1658 cm^{-1}, but the low intensity of the absorption did not support the decomposition of carbonyl crosslinks as

the main mechanism for the production of CO. The mass fragments collected in our experiment were limited to a range from *m/z* = 10 to 119, which did not enable the unique detection of a high-mass product containing a carbonyl crosslink. We do, however, observe a small peak at *m/z* = 105, which might be evidence for a larger, carbonyl-containing compound, such as benzophenone or 4-(methylphenyl)-phenyl-methanone. The main peak in the mass spectrum of benzophenone appears at *m/z* = 105, and 4-(methylphenyl)-phenyl-methanone has a significant daughter fragment at this value of *m/z*. Benzophenone has a significant peak at *m/z* = 182, and 4-(methylphenyl)-phenyl-methanone has a significant peak at *m/z* = 196. The observation of peaks at either *m/z* = 182 or *m/z* = 196 in conjunction with the observed peak at *m/z* = 105 would give strong evidence for a carbonyl crosslink. Ouchi and Honda[31] also suggested that CO may be released from the decomposition of the diphenyl ether bonds created during the first stage of pyrolysis. The observation of H_2O during Stage 1 of the pyrolysis (see curve for H_2O in Fig. 3.6) and the likely production of diphenyl ether bonds during this process (Fig. 3.9) suggest that ether crosslink species might be involved in the production of CO. Unfortunately, we do not have any direct evidence for either proposed pathway to CO. Such evidence must wait for future experiments which cover a higher mass range of products. Under the assumption that carbonyl crosslinks are the main source of CO, we suppose that these cross links persist in low concentration even at relatively high temperatures, as CO continues to be evolved well above 600 °C. Without proof of carbonyl crosslinks from mass spectra collected with a higher mass range, we have fit the *m/z* = 105 peak in our mass spectra with xylene, as mass spectra of the methyl benzene derivatives

(e.g., xylene) also have peaks at *m/z* = 105. It is unsatisfactory at this point, however, that we cannot propose a chemical mechanism for the production of xylene. Thus, the curve associated with xylene in Fig. 3.6 might actually arise from a daughter of a compound with a carbonyl functional group, which would imply that xylene is not actually a pyrolysis product.

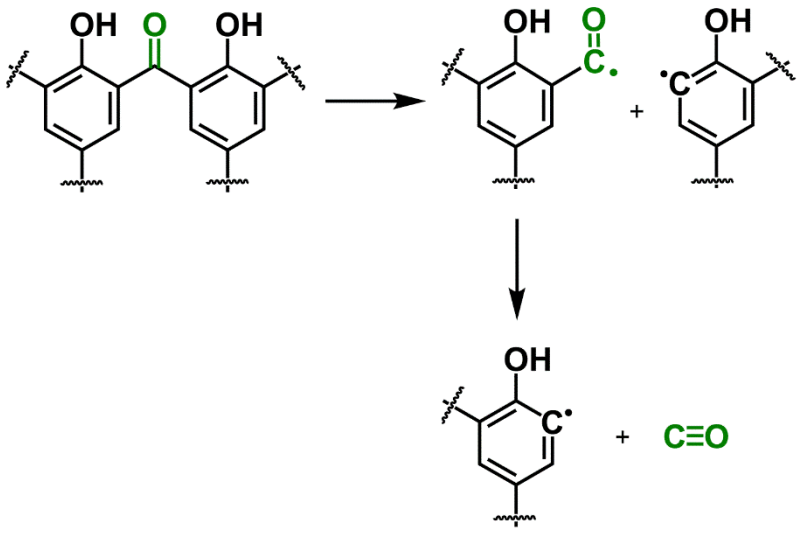

Figure 3.12. Two-step decomposition of a carbonyl crosslink to produce CO. The carbonyl crosslink may be the result of the oxidation of a methyl crosslink during the post-cure of the phenolic resin in air. Based on similar mechanisms proposed by Jackson and Conley[29] and by Ouchi.[34]

CH_4 is another significant product that evolves during the second pyrolysis stage (Fig. 3.6). Ouchi[34] proposed that CH_4 is the product of a two-step decomposition mechanism between methylene crosslinks and H_2, followed by the thermal decomposition of the methyl functional groups that are produced (Fig. 3.13). The first step in the reaction mechanism involves the reaction of hydrogen with the carbon crosslink to form a methyl substituted benzene ring and benzene. H_2 then reacts further with the methyl substituted

aromatic ring to form methane. Alternatively, Trick and Saliba[33] propose that H_2 reacts with a methylene crosslink to form a single bond between the two aromatic groups, resulting in the evolution of methane (Fig. 3.14). In both mechanisms, H_2 would presumably come from the fusing of aromatic rings (Fig. 3.15), although one could imagine similar mechanisms to those shown in Figs. 3.14 and 3.15, where breaking bonds create radical sites which abstract H atoms from nearby C-H moieties and H_2 is not an actual reactant. A variety of substituted aromatic molecules might possibly be evolved in addition to methane in the two-step mechanism proposed by Ouchi. We do observe substituted phenol products in the temperature range 300 – 450 °C. CH_4 is evolved at slightly higher temperatures, which is reasonable if the second step to produce CH_4 (Fig. 3.13) requires more energy. Thus, our data are consistent with the proposed mechanism of Ouchi. We did not have the capability when we conducted our experiments to observe the high-mass polyphenyl products that would support the mechanism proposed by Trick and Saliba.

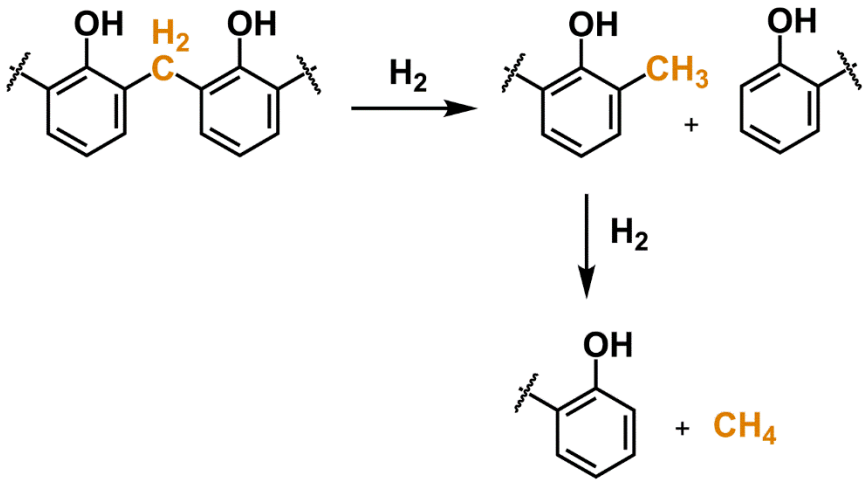

Figure 3.13. Two-step decomposition of a methylene bridge to produce CH_4. Based on a mechanism proposed by Ouchi.[34]

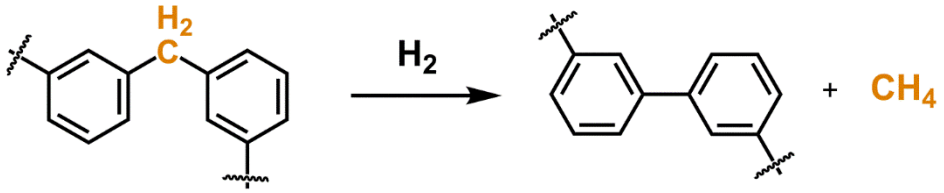

Figure 3.14. One-step decomposition of methylene bridge to produce CH_4. Based on a mechanism proposed by Trick and Saliba.[33]

H_2 is expected to be the dominant pyrolysis gas as temperatures climb above 560 °C into the third stage of pyrolysis.[31-32] Although our mass spectrometer was not set up for detecting H_2 when we performed these experiments, we did detect its presence with a residual gas analyzer that was in the sample chamber. This observation supports the carbonization mechanism proposed by Ouchi and Honda[31] (Fig. 3.15) and is in direct contrast to the mechanism proposed by Jackson and Conley,[29] in which H_2 is not evolved during the entire course of pyrolysis. Parker and Winkler[32] predicted the evolution of water

and hydrogen at temperatures that approach 700 °C to 800 °C. Our quantitative data do not support this mechanism, as we do not observe water above 700 °C. Furthermore, GC studies by Sykes[37] and by Wong et al.[38] both detected H_2 as the dominant product when the pyrolysis temperature of a phenolic resin exceeded 480 °C.

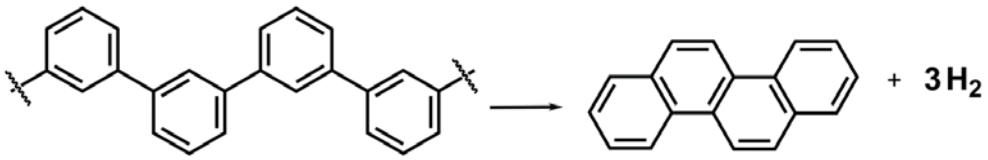

Figure 3.15. An unstable char coalesces to a stable char and H_2 is evolved. Based on a mechanism proposed by Trick and Saliba[33]

3.4.2 QUANTITATIVE YIELDS OF PYROLYSIS PRODUCTS

Quantitative yields of pyrolysis products of phenolic resins as a function of temperature have been measured by Sykes[37] and by Wong et al.[38], who both used GC. GC can provide absolute measurements of the components of a gaseous or liquid mixture, but it has limitations for quantifying pyrolysis products because the products are not measured *in situ*. Instead, they are typically collected over a much longer time period (~1 hr) than the 0.5-10 minute data collection times used in our study, and then they are analyzed later by GC, often with multiple columns because of the broad range of volatilities of the pyrolysis products.

A comparison of our experimental results to the results obtained by Sykes[37] and later by Wong et al.[38] reveals similarities and differences between the relative product yields. First, it should be made clear that Sykes studied a novolac phenolic resin, Wong et al. studied a pure resole phenolic resin, and we studied the carbon/phenolic, PICA. All three

studies reveal similar results with respect to the production of H_2O, which has the highest yield relative to other pyrolysis products during the first stage of pyrolysis. The data collected by Sykes suggested that H_2O desorption reaches a maximum at 450 °C. On the other hand, our data indicate that H_2O desorption has a maximum at 350 °C, which is close to the peak value of 374 °C obtained by Wong et. al.

Sykes and Wong et al. reported a higher yield of CH_4 than CO over the temperature range of pyrolysis, while our results show the opposite trend. Ouchi and Honda[31] found a relationship between the quantity of oxygenated species evolved and the degree of hydroxyl substitution on the phenol molecules used in the synthesis of phenolic resins. Specifically, they discovered that higher degrees of hydroxyl substitution lead to higher yields of H_2O, CO, and CO_2 relative to the yield of CH_4. Ouchi also reported that the peak production of CO and CO_2 shifts to lower temperatures with an increase in hydroxyl substitution. In light of Ouchi's findings, our results suggest that the resin used in the fabrication of PICA might have a higher degree of hydroxyl functional group substitution than what is present in the parent phenol molecule. This result is difficult to confirm from the manufacturer because of the proprietary nature of the material. We also cannot confirm that the phenolic resin used by Sykes and by Wong et al. had a lower degree of hydroxyl group substitution because the details of the polymer were not reported.

Ouchi and Honda[31] also studied the relationship between methyl substitution and CH_4 production, and they found that a higher degree of methyl substitution on the phenol molecule leads to a shift in the peak production of CH_4 to lower temperatures. A similar result was found for the point at which CH_4 was first detected. Ouchi and Honda postulated

that two different reactions account for the production of CH_4. First, any methyl groups that remain in the polymer after it has been synthesized are dissociated during the early stage of pyrolysis. Second, the cleavage of methylene crosslinks and their subsequent reaction with any available hydrogen provides a source of CH_4 at higher temperatures. In the study performed by Ouchi and Honda, the temperature range for the detection of CH_4 from resins synthesized without methyl substituted phenol consistently spanned 300 °C to 850 °C, with peak CH_4 production between 580 °C and 600 °C. CH_4 was detected between 250 °C and 800 °C when they pyrolyzed two separate resins synthesized from *m*-cresol and 3,5-dimethyl phenol. CH_4 was detected with a peak in its production at 500 °C for both resins, suggesting that methyl substitution tends to facilitate the release of CH_4 at lower temperatures. Our results are similar to those that Ouchi and Honda observed with the methyl substituted resins. We observed CH_4 desorption over a range of temperatures that span 300 °C to 750 °C, with a maximum yield at 450 °C. We thus surmise that the phenol resin in PICA has significant methyl functional group substitution.

Sykes[37] reported the detection of higher molecular weight species in the form of phenol and 2,4-dimethyl phenol, with a maximum yield at 500 °C. Wong et al. did not report yields of phenol and its derivatives in their study. Our analysis shows that phenol, cresol, and dimethyl phenol have maximum yields at ~350 °C, which is shifted to lower temperatures relative to the data collected by Sykes. Sykes did not report the observation of xylene or any related derivatives, but Wong et al. reported maximum yields of benzene, toluene, and xylene at 527 °C. We did not observe toluene or benzene but did (possibly) observe xylene with a maximum yield at 400 °C. Our observation of substituted

phenol/benzene derivatives with maximum yields at lower temperatures than those observed by Sykes and Wong et al., respectively, may be explained the higher degree of methyl and hydroxyl group substitution in PICA, as suggested above. Our results indicate that dimethyl phenol and cresol desorb with higher yields than phenol, which is further evidence that the phenol backbone in the resin in PICA has significant methyl substitution.

3.5 CONCLUSION

Relative molar yields of the main pyrolysis products from the carbon/phenolic ablator, PICA, with molecular masses from 10 to 119 amu, have been derived from *in situ* measurements in vacuum, with the use of a differentially-pumped mass spectrometer detector. A fitting procedure for the analysis of mass spectra collected at approximately 50 °C intervals, spanning a temperature range from 100 °C to 935 °C, has been implemented in order to calculate the relative molar yields as a function of temperature. These yields are discussed in light of prior work on the pyrolysis of various phenolic resins and phenolic/carbon composites. A consistent qualitative description of the decomposition pathways that occur in three stages of pyrolysis covering the temperature range from ~200 °C to ~1000 °C has emerged, with light gases being produced in the highest yields at all stages. H_2O is the dominant product in the first stage, with some CO_2 also being formed. CO is the main product during the second stage, and CH_4 is also significant during this stage. H_2 becomes dominant in the third stage, as the production of CO decreases. The heavier products (e.g., phenol, its methylated derivatives, and possibly even heavier species) have relatively low yields and desorb mainly during the second stage. The

quantitative yields are apparently strongly influenced by the exact molecular structure of the phenolic resin. A comparison of our results with those of earlier studies suggests that the phenolic resin used in PICA has significant hydroxyl and methyl substitution on the phenyl rings of the polymer. The relative molar yields and the general mechanistic understanding provided by this work should be directly applicable to developing material response models that target PICA as a focus material. The *in situ* mass spectrometric method that has been described here is well suited for follow-on studies of the decomposition kinetics as a function of temperature under non-equilibrium conditions, with the potential to provide even more detailed data for increasingly sophisticated models that seek to describe the thermal behavior of practical carbon/phenolic heat shields such as PICA in an atmospheric entry environment.

3.6 REFERENCES

23) Bose, D.; White, T.; Santos, J. A.; Feldman, J.; Mahzari, M.; Olson, M.; Laub, B. Initial Assessment of Mars Science Laboratory Heat Shield Instrumentation and Flight Data. *51st AIAA Aerospace Sciences Meeting including the New Horizons Forum and Aerospace Exposition*, Grapevine, TX, January 7-10, 2013. DOI: 10.2514/6.201-908

29) Jackson, W. M.; Conley, R. T. High Temperature Oxidative Degradation of Phenol–Formaldehyde Polycondensates. *J. App. Polym. Sci.* **1964**, *8*, 2163-219. DOI: 10.1002/app.1964.070080516

31) Ouchi, K.; Honda, H. Pyrolysis of Coal 1. Thermal Cracking of Phenol-Formaldehyde Resins Taken as Coal Models. *Fuel* **1959**, *38*, 429-443. DOI: 10.1021/la00063a010

32) Parker, J. A.; Winkler, E.L.. The Effects of Molecular Structure on the Thermochemical Properties of Phenolics and Related Polymers. NASA TR R-276, November **1967**.

33) Trick, K. A.; Saliba, T. A. Mechanisms of the Pyrolysis of Phenolic Resin in a Carbon/Phenolic Composite. *Carbon* **1995**, *33*, 1509-1515. DOI: 10.1016/0008-6223(95)00092-R

34) Ouchi, K. Infra-Red Study of Structural Changes During the Pyrolysis of a Phenol-Formaldehyde Resin. *Carbon* **1966**, *4*, 59-66. DOI: 10.1016/0008-6223(66)90009-1

37) Sykes, G. F. Decomposition Characteristics of a Char-Forming Phenolic Polymer Used For Ablative Composites. NASA TN D-3810, February, **1967**.

38) Wong, H. W.; Peck, J.; Edwards, R.; Reinisch, G.; Lachaud, J.; and Mansour, N. N. Measurement of Pyrolysis Products from Phenolic Polymer Thermal Decomposition. AIAA Science and Technology Forum and Exposition, National Harbor, MD, January, 2014. DOI: 10.2514/6.2014-1388

53) Zhang, J.; Garton. D. J.; Minton., T. K. Reactive and Inelastic Scattering Dynamics of Hyperthermal Oxygen Atoms on a Saturated Hydrocarbon Surface. *J. Chem. Phys.* **2002**, *117*, 6239-6251. DOI: 10.1063/1.1460858

54) Garton, D. J.; Brunsvold, A. L.; Minton, T. K.; Troya, D.; Maiti, B.; Schatz, G. Experimental and Theoretical Investigations of the Inelastic and Reactive Scattering Dynamics of O (^{3}P) + D_2. *J. Phys. Chem. A* **2006**, *10*, 1327-1341. DOI: 10.1021/jp054053k

55) Lee, Y. T.; McDonald, J. D.; LeBreton, P. R.; Herschbach, D. R. Molecular Beam Reactive Scattering Apparatus with Electron Bombardment Detector. *Rev. Sci. Instrum.* **1969**, *40*, 1402-1408. DOI: 10.1063/1.1683809

63) Hankey, W. L., *Re-Entry Aerodynamics*. AIAA Education Series; Przemieniecki, J. S., Ed., Washington, D.C., 1988.

64) Diaconis, N. S.; Fanucci, J. B.; Sutton, G. W. The Heat Protection Potential of Several Ablation Materials for Satellite and Ballistic Re-Entry into the Earth's Atmosphere. *Planet. Space. Sci.* **1961**, *4*, 463-478. DOI: 10.1016/0032-0633(61)90152-0

65) Ungar, E. W. Ablation Thermal Protection Systems Suitability of Ablation Systems to Thermal Protection Depends on Complex Physical and Chemical Processes. *Science* **1967**, *158*, 740-744. DOI: 10.1126/science.158.3802.740

66) April, G. C.; Pike, R. W.; del Valle, E. G. Modeling Reacting Gas Flow in the Char Layer of an Ablator. *AIAA J.* **1971**, *9*, 1113-1119. DOI: 10.2514/3.6330

67) Kendal, R. M.; Bartlett, E. P.; Rindal, R. A.; Moyer, C. B. An Analysis of the Coupled Chemically Reacting Boundary Layer and Charring Ablator: Part 1. *NASA CR-1060* (1968).

68) Lachaud, J.; Cozmuta, I.; Mansour, N. N. Multiscale Approach to Ablation Modeling of Phenolic Impregnated Carbon Ablators. *J. Spacecr. Rockets* **2010**, *47*, 910-921. DOI: 10.2514/1.42681

69) Alexander, W. A.; Wiens, J. P.; Minton, T. K.; Nathanson, G. M. Reactions of Solvated Electrons Initiated by Sodium Atom Ionization at the Vacuum-Liquid Interface. *Science* **2012**, *35*, 1072-1075. DOI: 10.1126/science.1215956

70) Stein, S. E., Mass Spectra. In NIST Chemistry WebBook, NIST Standard Reference Database Number 69, Eds. P.J. Linstrom and W. G. Mallard, National Institute of Standards and Technology, Gaithersburg MD, 20899, http://webbook.nist.gov, (accessed August 2, 2014).

71) Deverse, F. T.; King, A. B. Effect of Molecular Structure on the Ionization Probabilities of Aromatic Molecules. *J. Chem. Phys.* **1964**, *41*, 3833-3838. DOI:10.1063/1.1725822

72) Harrison, A. G.; Jones, E. G.; Gupta, S. K.; Nagy, G. P. Total Cross Sections for Ionization by Electron Impact. *Can. J. Chem.* **1966**, *44*, 1967-1973. DOI: 10.1021/ie50480a054

73) Hudson, J. E.; Hamilton, M. L.; Vallance, C.; Harland, P. W. Absolute Electron Impact Ionization Cross-Sections for the C_1 to C_4 Alcohols. *Phys. Chem. Chem. Phys.* **2003**, *5*, 3162-3168. DOI: 10.1039/b304456d

74) Kim, Y.K., Irikura, K. K., Rudd, M. E., Ali, M. A., Stone, P. M., Chang, J., Coursey, J. S., Dragoset, R. A., Kishore, A. R., Olsen, K. J., Sansonetti, A. M., Wiersma, G. G., Zucker, D. S., and Zucker, M. A. Electron-Impact Ionization Cross Section for Ionization and Excitation Database (version 3.0, 2004). Available: http://physics.nist.gov/ionxsec (accessed August 2, 2014).

75) Rhodes, F. H.; Wells, J. H.; Murray, G. W. Vapor Composition Relationships in the Systems Phenol–Water and Phenol–Cresol. *Ind. Eng. Chem.* **1925**, *17*, 1199-1201. DOI: 10.1021/ie50191a044

76) Biddiscombe, D. P.; Martin, J. F. Vapor Pressures of Phenol and the Cresols. *Trans. Farad. Soc.* **1958**, *54*, 1316-1322. DOI: 10.1039/TF9585401316

CHAPTER FOUR

DECOMPOSITION OF PHENOLIC IMPREGNATED CARBON ABLATOR (PICA) AS A FUNCTION OF TEMPERATURE AND HEATING RATE

Contribution of Authors and Co-Authors

Manuscript: Pyrolysis of Phenolic Carbon Ablator

Author: Brody K. Bessire

Contributions: Collected and analyzed all data. Assisted in writing and editing manuscript.

Co-Author: Timothy K. Minton

Contributions: Assisted with the interpretation of data and edited manuscript.

Manuscript Information Page

Brody K. Bessire, Timothy K. Minton
ACS Applied Materials and Interfaces

Status of Manuscript:
____ Prepared for submission to a peer-reviewed journal
____ Officially submitted to a peer-review journal
___ Accepted by a peer-reviewed journal
_X_ Published in a peer-reviewed journal

Published by the American Chemical Society
Received: March 19, 2017
Published: May 25, 2017

CHAPTER FOUR

DECOMPOSITION OF PHENOLIC IMPREGNATED CARBON ABLATOR AS A FUNCTION OF TEMPERATURE AND HEATING RATE

4.1 INTRODUCTION

As high-speed spacecraft traverse planetary atmospheres, they experience high-temperature effects from radiative and convective heat transfer.[1] The kinetic energy of the gaseous flow around the capsule is converted into internal energy through a strong bow shockwave, resulting in very high temperatures in the shock layer. This heat is transferred to the material on the leading surfaces of the spacecraft, with resulting heat fluxes that can exceed 1 kW cm^{-2}. Thus, thermal protection systems (TPSs) are necessary to shield spacecraft from the high heat loads of atmospheric entry.

Ablative thermal protection systems are one category of TPSs. Ablative TPSs block, absorb, and dissipate heat by taking advantage of the thermal and chemical properties of polymeric composite materials. Heat is blocked by the insulating properties of the polymer, while it is absorbed by endothermic bond-breaking processes and dissipated through radiation or the removal of hot volatile species from the decomposing material. A well-known ablative TPS is phenolic impregnated carbon ablator (PICA).[19] PICA is manufactured by impregnating a carbon fiber preform with a phenolic resole resin having the designation SC-1008. This material offers low mass per unit volume and high ablation performance. PICA gained flight heritage during the successful re-entry of the Stardust

sample return capsule and the more recent successful entry, descent, and landing (EDL) of the Mars Science Laboratory (MSL).[22-23,77] A variant of this material, PICA-X, is currently used on Space-X's Dragon capsule.[24] Additional phenolic-based composite materials have been used[78] or are under development.[79-80]

Although many studies have been conducted on the pyrolysis of phenolic resins and related composite materials, molar yields of volatile pyrolysis products have been reported in only a few studies.[37,40,81-83] One of these studies was part of a previous effort undertaken in our laboratory to develop an experimental methodology by which the pyrolysis products could be measured using *in situ* mass spectrometry.[83] In this previous study, which focused on PICA, relative molar yields of pyrolysis products were derived from mass spectra that spanned the range from 10 u to 119 u. As a consequence of the somewhat limited mass range, the relative molar yield of molecular hydrogen (H_2) was not measured, although it is known to be one of the main products from the pyrolysis of phenolic resin. In addition, the upper limit of 119 u prevented some potential heavy products (e.g., dimethyl phenol, trimethyl phenol, diphenyl ether) from being detected. For the previous study, the data were collected under stepwise heating conditions, with each individual mass spectrum being obtained during quasi-steady-state conditions at a constant temperature after the sample temperature had been incremented about 50 °C. A mass spectral fitting procedure was developed in which a linear combination of reference mass spectra, from the National Institute of Standards and Technology (NIST) database, were fit to each experimental mass spectrum. The coefficients of the linear combination represented uncorrected molar yields

of each of the evolved pyrolysis species. These coefficients were corrected for ionization cross section (from the NIST database), but they did not account for mass-dependent detection sensitivities. The derived molar yields were compared to yields reported in the literature and were found to be in qualitative agreement. Despite the limited mass range and stepwise sample temperature increase, a method was developed which could, in principle, be applied to *in situ* studies of TPS pyrolysis over arbitrarily large mass ranges with variable heating rates. The data that were obtained were used to make inferences about the decomposition mechanisms of PICA in light of earlier data that had been reported on the pyrolysis of phenolic resins.[83] These data did not, however, provide any information on the dependence of the pyrolysis processes on heating rate, nor did they provide independent insight into the decomposition mechanisms or absolute molar and mass yields that could directly inform material response models.

The study reported here is an extension of our previous work and employs a new experimental apparatus to make accurate measurements of absolute yields of pyrolysis products as a function of temperature with heating rates that are relevant to flight conditions. The heating rates were chosen to reflect the in-depth heating rates collected during the entry, descent, and landing (EDL) of MSL.[23,77] Forebody heating rates were ~20 °C s^{-1} at the thermocouple closest to the TPS surface and decreased to ~1 °C s^{-1} at the deepest thermocouple. Although there may be some nonlinearity in the heating rates in particular regions of the heat shield, we chose to use approximately linear heating rates for our experiments. Increased accuracy of the derived molar yields was achieved by carefully

measuring the response of a mass spectrometer detector to a set of compounds that could potentially be released during PICA pyrolysis. In addition, the detected mass range was increased from 1 u to 150 u. As a result, the molar yields of H_2 and several high mass compounds were measured in addition to the compounds that were measured in our previous study. The new data, which provide accurate molar and mass yields as a function of temperature over a broad range of heating rates, permit the calculation of the temperature-dependent mass loss curves. These curves simulate traditional TGA curves but at rates that are not achievable in modern TGA instruments. The absolute product yields depend on heating rate, and the observed dependencies have allowed us to make inferences about the nonequilibrium chemical decomposition mechanisms that must be occurring.

4.2 EXPERIMENTAL METHODS

4.2.1 EXPERIMENTAL CONFIGURATION

The experimental configuration is illustrated in Fig. 4.1. A sample mount, holding a PICA sample (Fig. 4.1 B), was placed in a differentially pumped source chamber that was attached to a larger, "main," vacuum chamber (Fig. 4.1 A). The front face of the sample was situated 17.8 cm behind a 1.27 cm dia. aperture on the front of the source chamber. The source chamber was equipped with an Edwards Model B35031977 (2,000 l s^{-1}) diffusion pump, and the main vacuum chamber was pumped by both a turbomolecular pump (Ebara Model ET1600WS, 1,600 l s^{-1}) and a cryogenic pump (CTI Cryogenics Model CT-8F, 1,500 l s^{-1}). The source and main vacuum chambers were pumped to pressures less

than 1 x 10^{-6} and 5 x 10^{-7} Torr, respectively, before collection of pyrolysis data. During pyrolysis of a sample, the maximum pressures in the source and main chambers did not exceed 1 x 10^{-4} and 8 x 10^{-5} Torr, respectively. The main vacuum chamber housed a Stanford Research Systems residual gas analyzer (RGA 200) that was positioned directly in front of the aperture of the source chamber. The nominal distance from the aperture to the electron-impact ionizer of the RGA was 30.5 cm. The ionizer settings used in this study were: ion energy (12 eV), electron energy (70 eV), focus voltage (-90 V), and emission current (1.0 mA). A Faraday cup was chosen as the ion detector in this study because of its relative stability, lack of mass-dependent discrimination, and ability to operate at higher pressures as compared to electron multipliers.

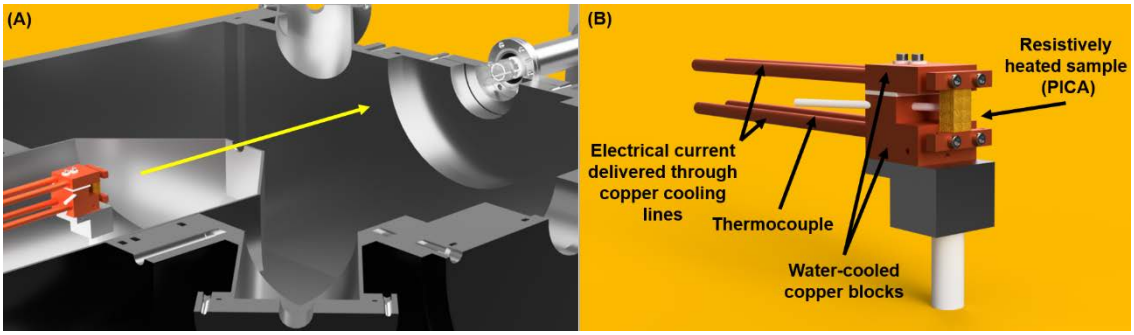

Figure 4.1. (A) Experimental configuration, showing sample mount in differentially pumped source chamber and mass spectrometer (RGA) ionizer in main vacuum chamber. (B) Sample holder for resistive heating of PICA samples.

Each sample of PICA was cut from a billet obtained from Fiber Materials, Inc. such that its dimensions were 2.5 cm long x 0.90 cm wide x 0.70 cm thick, and then the sample was loaded into the sample mount such that one of the 0.90 cm-wide surfaces faced the ionizer of the RGA. The sample mount (Fig. 4.1 B) consists of two water-cooled copper

blocks that are electrically isolated by a ceramic spacer and connected to a power supply. The sample was heated by current that was delivered by a programmable power supply (TDK-Lambda GEN 40-19) to the sample through copper tubes that are attached to water-cooled copper blocks. A chiller circulated 20 °C water through the sample mount to keep it cool during heating. The bottom electrode accommodates a ceramic tube through which a K-type thermocouple was inserted and then pushed into the center of the sample about 3 mm deep from the back side. The use of the ceramic tube allowed the thermocouple to be inserted into the same position of each sample with respect to the copper electrodes, thus allowing sample temperatures to be measured reproducibly.

4.2.2 RGA CALIBRATION

The detection sensitivity of the RGA is the product of the ionization efficiency in the electron-impact ionizer, the transmission efficiency of the quadrupole, and the gain of the ion counting system. The ionization efficiency depends on the nature of the molecular species, and the transmission efficiency of the quadrupole and the gain of the ion counting system depend on the ion *m/z*. These three factors are very difficult to determine with reasonable accuracy. Nevertheless, the large uncertainty in determining the absolute RGA detection sensitivity may be circumvented by calibrating the response of the RGA to a standard reference compound at a known pressure and then using this calibration to determine the detection sensitivity of another analyte compound by comparing the RGA signals of the standard and analyte compounds in a gas mixture of the two with known partial pressures. The initial RGA calibration may be done by introducing a weak beam of pure reference gas into the vacuum chamber, exactly half-way between the ionizer of the

RGA and an accurate pressure gauge, with the flow of reference gas being perpendicular to a plane that contains the ionizer and gauge.

The present study used CO as the standard reference compound. A beam of pure CO gas was introduced, with different flow rates, directly between the ionizer of the RGA and a nude Bayard-Alpert ionization gauge. The ion current registered by the Faraday cup was measured with the RGA tuned to m/z = 28 as a function of pressure measured by the ion gauge (Fig. 4.2). The slope of the resulting curve was 9.08 x 10^{-5} A Torr $^{-1}$, which is the calibration factor for measuring the absolute pressure of CO with the RGA. This calibration factor is expected to remain constant over a large pressure range,[84] including the range of partial pressures from 1.0 x 10^{-7} to 6.0 x 10^{-5} Torr that was relevant for the experiments presented here. The measured calibration factor was set in the RGA software, and this setting was used for all the experiments.

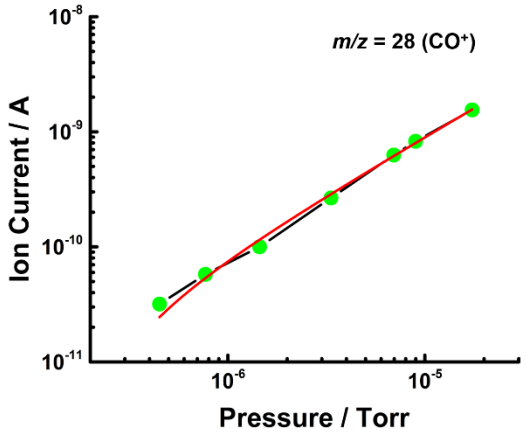

Figure 4.2 Current measured at the Faraday cup of the RGA as a function of CO pressure, with the RGA, tuned to m/z = 28.

Detection sensitivities relative to CO were determined for a variety of compounds that may be liberated from a phenolic resin as it decomposes through pyrolysis. From these relative detection sensitivities, correction factors were derived that allowed the absolute partial pressures of analyte gases to be determined from mass spectra. The correction factors account for the ionization cross section of each compound, the quadrupole mass filter transmission efficiency, and any mass dependent gain in the ion counting system. The relative detection sensitivities and correction factors for the possible pyrolysis compounds were calibrated against CO using the following two methods, depending on whether the gases are permanent or condensable.

4.2.2.1 PERMANENT GASES H_2, CH_4, CO, and CO_2 are permanent gases that are expected to be formed from the pyrolysis of PICA. Each gas, in pure form, was introduced into the main chamber through a variable leak valve that was positioned perpendicular to the RGA and a nude ion gauge. A mass spectrum of each compound was collected with the same RGA settings that were used throughout this study. A mass spectrum of a mixture of these four gases with known molar ratios was then collected. The mass spectrum of the mixture was fit with a linear combination of the mass spectra of the individual compounds. The coefficients used to obtain the optimized fit did not correspond to the known molar composition of the mixture because the simple linear combination of mass spectra does not account for the species-dependent detection sensitivity of the RGA. Therefore, correction factors were applied to the coefficients in order to make them equal to the respective mole fractions based on the known gas composition. This procedure was performed for five pressures from 7.3×10^{-7} Torr to 1.2

x 10^{-5} Torr. The average correction factor for each compound was calculated and is listed in Table 4.1 with $\pm 1\sigma$ errors based on the five measurements.

4.2.2.2 CONDENSABLE GASES All the condensable gases that were detected during the pyrolysis of PICA are listed in Table 4.1. Individual condensable gases from this list were introduced into the main chamber from a heated stainless-steel reservoir through a leak valve, and a mass spectrum of each compound was collected with the same RGA settings that were used throughout the experimental study. After a set of individual mass spectra had been obtained, a gas manifold was constructed to mix CO and a given condensable gas at a known pressure ratio. An individual condensable gas was placed in a reservoir and held at a temperature that produced 1.00 Torr of vapor pressure. The appropriate reservoir temperatures for dimethyl phenol and trimethyl phenol were calculated using Antoine parameters from Terres and Andon.[85-86] Reservoir temperatures for the remaining compounds were derived from the Handbook of Chemistry and Physics.[88] A mass flow controller was used to introduce CO into the manifold, and a thermocouple gauge was placed directly after the mass flow controller to monitor the pressure of CO, which typically fell in the range 1700 – 1900 mTorr, before it was mixed with the vapor of the condensable gas from the reservoir. The vapor/CO mixture, with a known pressure ratio, then entered the main chamber through the leak valve. A mass spectrum of the resulting mixture was collected and fit with a linear combination of the mass spectra of CO and the individual condensable gas. A correction factor was then calculated based on the difference between the known pressure ratio of

the two gases and the coefficients used in the fit of the mass spectrum. The correction factor for each condensable compound is listed in Table 4.1.

Table 4.1. Permanent and condensable gases that were detected from the pyrolysis of PICA. Corresponding correction factors were applied to obtain correct mole fractions from the coefficients of a linear combination of individual mass spectra. Errors represent ±1σ from the mean.

Permanent Gases		Condensable Gases	
Species	Sensitivity C. F.	Species	Sensitivity C. F.
H_2	0.690 ± 0.090	H_2O	1.14
CH_4	1.57 ± 0.14	1-Propanol	0.530
CO	1.00 ± 0.00	2-Propanol	0.810
CO_2	1.01 ± 0.13	Xylene	0.900
		Phenol	1.28
		Cresol	1.40
		Dimethyl Phenol	1.74
		Trimethyl Phenol	2.28
		Benzene	0.870
		Toluene	1.00

4.2.3 COLLECTION OF PYROLYSIS DATA

The resistance of a PICA sample changes as it is heated. Virgin PICA has a relatively high resistance, as a result of the resin content of the material, and as the resin decomposes to char, the sample becomes more conductive. To account for the change in resistance of the PICA samples, a LabVIEW program was used to control the power supply in order to deliver progressively higher currents to the sample. It was found that the delivery of three stages of current was sufficient to achieve fairly linear heating rates of PICA samples over the temperature range from 100 °C to 1200 °C, measured at the center of the sample. Details describing the determination of the heating rates are provided in the appendix B.1.

Heating rate curves for the four heating rates used, 25.0 °C s^{-1} and 12.7 °C s^{-1}, 6.1 °C s^{-1} and 3.1 °C s^{-1}, are also provided in Appendix B (Figs. B.2, B.9, B.16, and B.23).

These four heating rates are nominal rates based on measurements taken with a thermocouple inserted into the center of the sample from the back side, about 3 mm deep. The heating of the sample occurs in a 1.55 cm long section between the two water-cooled electrodes to which the ends of the sample are clamped. Thus, during heating, a symmetric temperature gradient is expected across the sample, with the highest temperature in the middle and decreasing temperatures as the distance from the center increases. In order to investigate effect of the temperature gradient on heating rate away from the center of the sample, thermocouples were placed in the center and at points 0.525 cm from the center, and the heating rates in the center and at the thermocouple positions that were about 2/3 of the distance from the center to the water-cooled clamp was determined. It was found that the heating rate at a sample position 0.525 cm away from the center was approximately 20 percent of the heating rate at the center of the sample. The reduced heating rate on the "wings" of the sample will lead to a final temperature that is lowered by this percentage. The variation in heating rate across the sample is unlikely to affect the effective heating rate in the experiment by as large of a percentage, because the experimental geometry suggests that the pyrolysis products that escape from the center of the sample are most likely to pass through the aperture into the main chamber and be detected before they are pumped away. Therefore, we have chosen to report the heating rates measured at the center of the sample as the "nominal" heating rates, but it should be understood that these rates are maximum values that correspond to the heating rate at the center of the sample. The

data that are collected may reflect processes that occur at heating rates that may be lower by 20 percent (or less) of the nominal rate. Nevertheless, the nominal rates used are sufficiently different that the heating-rate ranges corresponding to the four nominal heating rates should have essentially no overlap.

Figure 4.3 shows an example of a set of mass spectra that were collected at a heating rate of 12.7 °C s^{-1}. Mass spectra were collected in the *m/z* range from 1 to 150 u in 0.1 u increments. The collection of each mass spectrum required 2.8 seconds. The resolution was adjusted to be 1 u, according to the $\Delta M_{10\%}$ definition, throughout the entire spectrum. $\Delta M_{10\%}$ is the width of the bandpass of the filter, defined as the full width at which the signal is 10% of the maximum value. Mass loss was determined for each heated sample, as described in section 2.6.1.

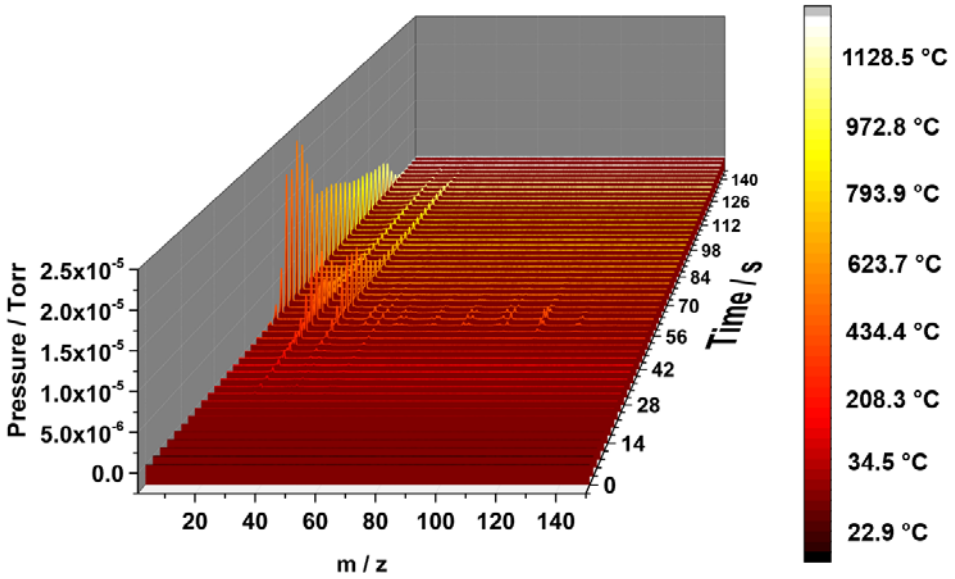

Figure 4.3. Mass spectra of PICA pyrolysis products as a function of time, with a nominal heating rate of 12.7° C s^{-1}.

4.3 RESULTS AND ANALYSIS

4.3.1 ANALYSIS OF MASS SPECTRA

The 14 compounds that constitute all significant pyrolysis products of PICA are listed in Table 4.1. This list of compounds was chosen based on observations from the literature and past results,[37,40,81-82] as well as significant experience gained from the collection of mass spectra of PICA pyrolysis products during the course of our experiments. In our previous study,[83] we used 8 compounds (CH_4, H_2O, CO, CO_2, xylene, phenol, cresol, dimethyl phenol) to fit the mass spectral data that were collected in the *m/z* range from 10 u to 119 u. The isomers of xylene, cresol, and dimethyl phenol were not distinguished because the isomers of each respective compound have similar mass spectra. For the analysis of the new mass spectral data collected over the range 1-150 u, we added six compounds: H_2, 1-propanol, 2-propanol, benzene, toluene, trimethyl phenol. H_2 and trimethyl phenol appeared in the new mass spectra because of the extended mass spectral range. The other four added compounds had relatively low yields, but scrutiny of the mass spectra showed that they were indeed observed consistently, and the inclusion of these compounds in the analysis provided better fits to the mass spectra. Benzene and toluene have been reported as pyrolysis products from resole resin and PICA,[81-82] and the presence of propanol among the pyrolysis products is not surprising because it is a well-known solvent for the resole phenolic resin used in PICA (SC-1008). All compounds used in the analysis are stable, as it was assumed that any volatile radical species that might have been produced would react to form stable products before exiting the decomposing material.

Relative molar yields as a function of temperature were derived from mass spectra that were collected at 2.8 second intervals during heating at a programmed rate. The calculation of the relative molar yields of the pyrolysis products began with the mass spectra of the pure compounds in Table 4.1, which were measured with the same resolution and ionizer settings used during the pyrolysis runs. Each mass spectrum of a pure compound was normalized such that the maximum value of the most abundant peak was set equal to 1.0. Next, linear combinations of the mass spectra of each of the 14 pure compounds were fit to an experimental mass spectrum. Figure 4.4 displays a representative mass spectrum that was collected at a relatively low temperature of 368.3 °C. The raw data, with background subtracted, are indicated by the orange dots, and the fits are indicated by the solid blue line. Each fit was optimized by minimizing the residuals. Partial pressures of each compound were obtained by weighting the coefficients of the best-fit linear combination by their respective correction factors (Table 4.1). The partial pressure recorded by the RGA is proportional to the number density of molecules that reach the electron-impact ionizer. Note that the RGA sampled the density of pyrolysis products that had a residence time of tens of milliseconds in the main chamber, so it sampled an approximately steady-state gas as opposed to a stream of products that made a single pass through the electron-impact ionizer of the RGA. Thus, the measured partial pressure, P_i, of a particular pyrolysis product is proportional to its integrated flux from the sample and can be thought of as the relative molar yield of that product (n_i^r).

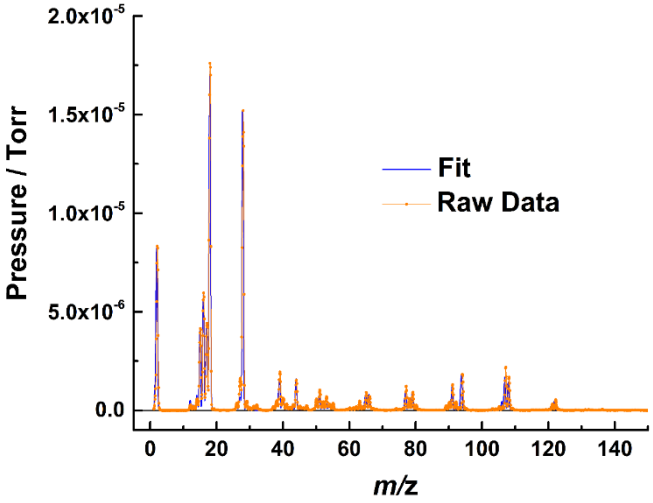

Figure 4.4. Fit of representative mass spectrum collected with a nominal temperature of 368.3 °C during heating at 25.0 °C s^{-1}.

4.3.2 CALCULATION OF ABSOLUTE MOLAR YIELDS, MASS YIELDS, AND SIMULATED TGA CURVES

The absolute molar yield of each product may be determined from the relative molar yields and total mass loss of the sample. First, the absolute mass loss at temperature, *T*, must be determined. The relative mass loss, $m^r(T)$, at a given temperature may be obtained by

$$m^r(T) = \sum_i n_i^r(T) \bullet MW_i \qquad (1)$$

where n_i^r is the relative molar yield of product *i*, and MW_i is the molecular weight of product *i*. The total relative mass loss, m_{total}^r, integrated over all temperatures is thus

$$m_{total}^r = \sum_i m^r(T) \qquad (2)$$

The fraction of the total mass loss (*TML*), $f_m(T)$, at a given temperature is

(3) $$f_m(T) = \frac{m^r(T)}{m^r_{total}}$$

Therefore, the absolute mass loss at temperature, *T*, may be determined as follows:

(4) $$m(T) = TML \bullet f_m(T)$$

The absolute mass loss at temperature, *T*, may be used to find the constant factor, $\chi(T)$, which relates the relative molar yield to the absolute molar yield

(5) $$n_i(T) = \chi(T)\, n_i^r(T)$$

where

(6) $$\chi(T) = \frac{m(T)}{\sum_i n_i^r(T) \bullet MW_i}$$

From the absolute molar yield of a particular product at temperature, *T*, it is a simple matter to calculate the mass yield of that product from its molecular weight:

(7) $$m_i(T) = n_i(T) \bullet MW_i$$

The fraction of the total mass loss at temperature, *T*, may be used to calculate a simulated TGA curve in terms of weight percentage remaining as a function of temperature. The weight percentage remaining at a particular temperature is given by:

$$\text{(8)} \qquad \text{weight percentage remaining} = \frac{100}{M_0} \bullet \left[M_0 - TML \bullet \sum_{j=T_0}^{T} f_m(T_j) \right]$$

It is important to note that the value of each function of *T* in the equations above is determined from an area of the relevant distribution that is calculated from the trapezoid rule. The temperature, *T*, assigned to this area is the median temperature during the 2.8 s required to collect an entire mass spectrum. Therefore, the temperature resolution decreases with increasing heating rate. In addition, it should be noted that the rate of temperature change between each mass spectrum is not exactly constant – i.e., there is some deviation from linearity in the heating rate, as seen, for example, in Fig. B.1. The calculations of area used the actual temperature change during the 2.8 s measurement time rather than a temperature change based on the nominal heating rate that is reported.

The analysis of the mass spectra that were collected as a function of temperature at four different heating rates led to temperature-dependent absolute molar yields and mass yields of 14 pyrolysis products (Figs. 4.5 and 4.6, respectively), in addition to simulated TGA curves (Fig. 4.7). These data are presented in more detail in Appendix B, where the data are plotted on different scales for clarity, and uncertainties, based on standard deviations in the results of multiple pyrolysis runs, are represented by error bars on the plots. In addition, numerical values associated with all the plots are tabulated. Figure 4.5 shows that the light products, H_2, CH_4, H_2O, CO, and CO_2, dominate the pyrolysis products of PICA. Heavier products, including benzene, xylene, and phenol and its derivatives are also clearly observed, but these heavier products have much lower molar yields and tend to evolve in a similar temperature range of 200-600 °C. The light products may also be

liberated in this temperature range, and they are, by far, the main products above 600 °C. As seen in Fig. 4.6, both light and heavy products carry substantial mass away from the material, with the contribution of H_2 being modest, as a result of its light mass, even though it has the highest molar yield. The simulated TGA curves in Fig. 4.7 show that most of the mass loss occurs in the temperature range of 300-550 °C.

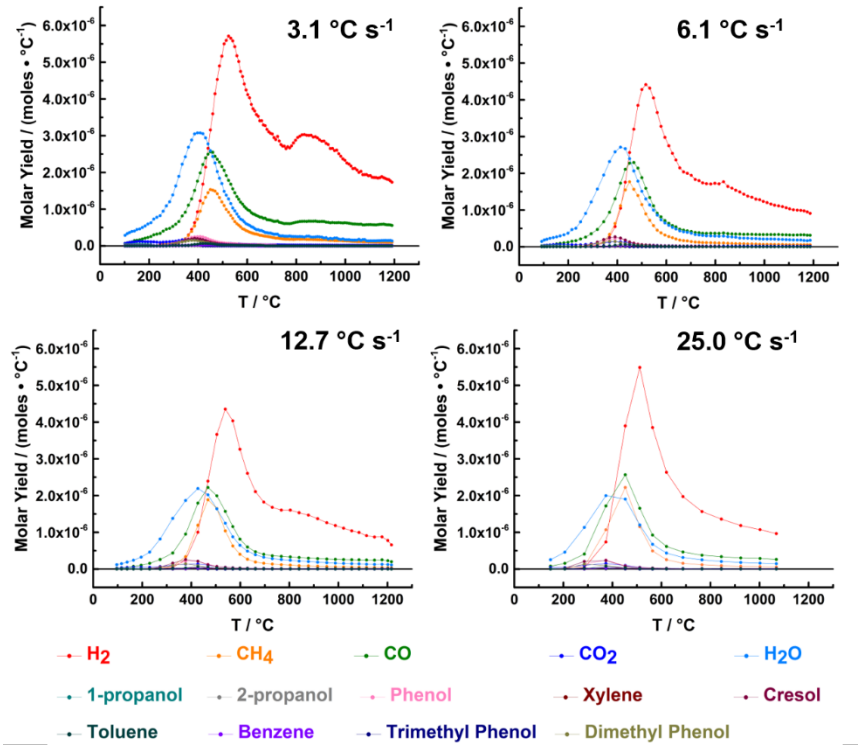

Figure 4.5 Molar yields as a function of temperature for the four nominal heating rates used.

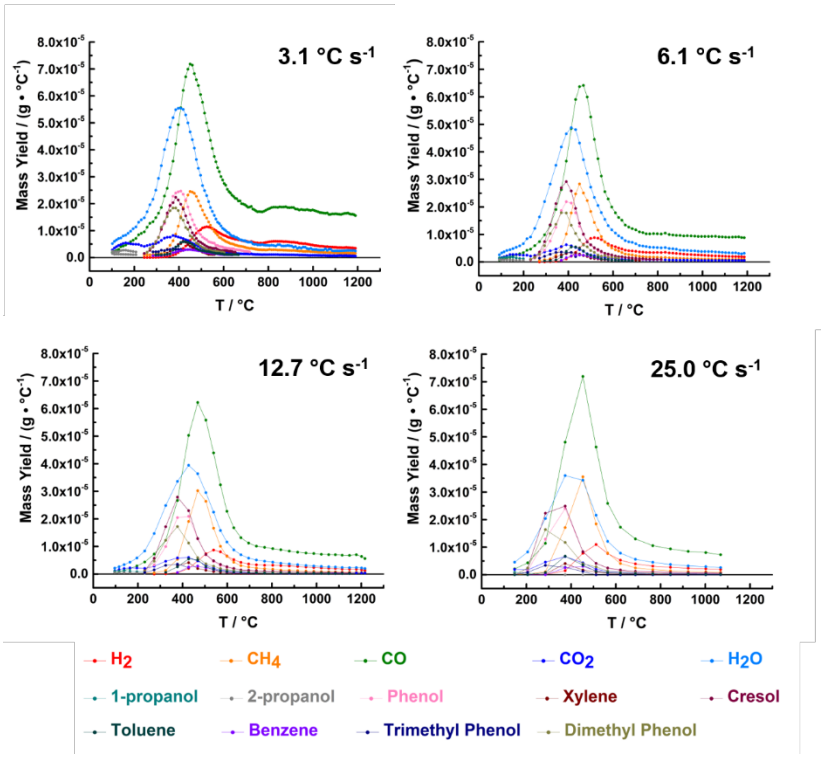

Figure 4.6 Mass yields as a function of temperature for the four nominal heating rates used.

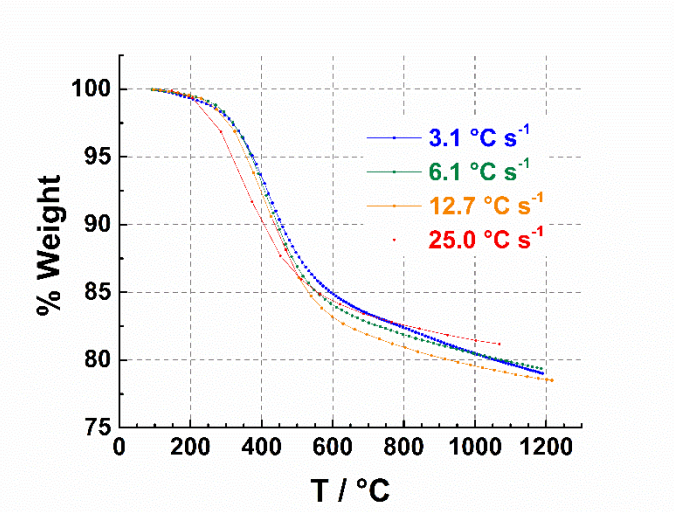

Figure 4.7 Simulated thermogravimetric analysis (TGA) curves corresponding to the four nominal heating rates used.

Because most of the mass loss occurs before the ultimate experimental temperature is reached, the errors in absolute molar and mass yields that might be caused by the non-uniform heating rate of the sample are minimal. Such errors could come from the uncertainty in total mass loss introduced in Equation (4). For a given final temperature in the center of the sample (typically 1200 °C), the final temperatures of the wings of the sample will be lower. Thus, the total mass loss of the sample is less than it would be if the final temperature were uniform at 1200 °C. Nevertheless, visual inspection of the samples showed that they charred up to where they were in contact with the water-cooled clamp and even slightly underneath it. Thus, the outermost edges of the sample must have reached temperatures of ~600 °C or more. In addition, we know from our thermocouple measurements that the temperature of the middle 2/3 of the sample must have reached 950 °C or higher. Given that the vast majority of the mass loss occurs below 600 °C, we estimate that the error in the total mass loss from the experiments is within 10 percent, and perhaps significantly lower if most of the detected products come from the center region of the sample. As the error results in a measured total mass loss (TML) value that is too low, the calculated absolute molar and mass yields in Figs. 4.5 and 4.6 should be considered to be lower limits. It should be noted, however, that the uncertainty in the reproducibility of the molar and mass yields and the simulated TGA curves (represented by the error bars given in appendix B) are larger than or comparable to the expected error caused by the non-uniform heating rate of the samples.

4.4 DISCUSSION

4.4.1 MASS LOSS (THERMOGRAVIMETRIC ANALYSIS)

As indicated in Fig. 4.7, the total mass loss is nearly constant across all heating rates, with the percentage mass loss falling in the range of 18-22 percent. This mass-loss fraction is similar to what has been measured at much lower heating rates.[19] Fig. 4.8 shows the relationship between the simulated TGA curve and the mass yields of individual products, with a heating rate of 3.1 °C s^{-1}. The smooth TGA curve belies the complex, temperature-dependent processes that result in the mass loss of PICA. In the range of 400-450 °C, where the rate of mass loss is greatest, the relative yields of the various products change dramatically. The mass yield of H_2O is at its peak at 400 °C, and the mass yield of CO is nearly the same, but still increasing. There is a significant mass yield from phenol and its derivatives at 400 °C that dies away quickly above 400 °C and gives way to CH_4 and, to some extent H_2, at 450 °C. CO dominates the mass loss at 450 °C, although H_2O is still significant. Rapidly changing relative mass yields suggest that the underlying mechanisms leading to mass loss are also changing quickly with temperature in this range.

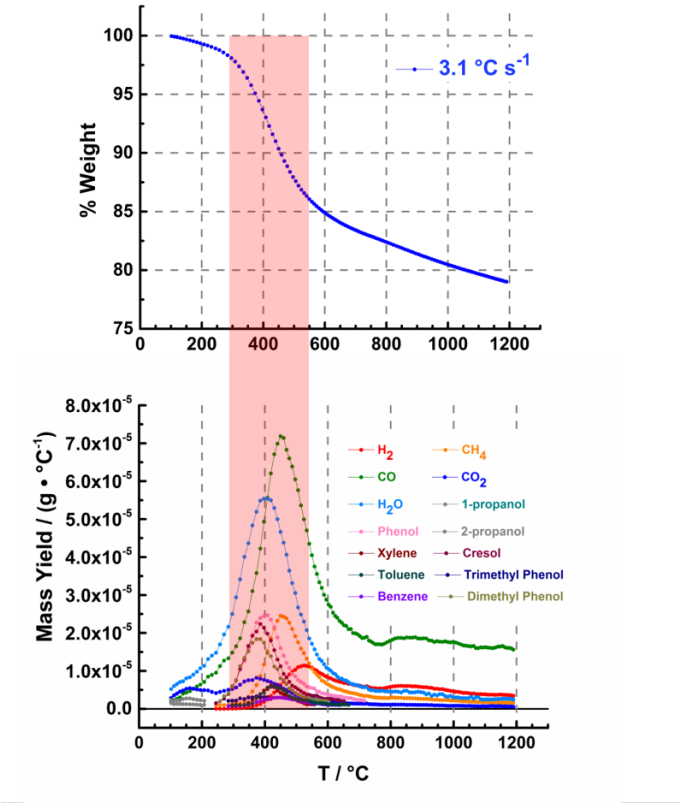

Figure 4.8. Simulated TGA curve and mass yields as a function of temperature, corresponding to a heating rate 3.1 °C s^{-1}.

Indications of changing decomposition mechanisms with heating rate have been seen in some of the many earlier TGA studies of phenolic resins and phenolic-based composite materials.[10,13,88-93] The majority of the previous studies have focused on the pyrolysis of samples in inert environments with heating rates that are much lower than those used in our experiments or experienced by a TPS during flight conditions. A typical TGA uses heating rates of <1 °C s^{-1} and a purge gas of He, N_2, or Ar to prevent oxidation of the sample. However, it has been shown that the rate of decomposition may depend on the heating rate and on the purge gas. For example, decomposition rates are higher with He

than with N_2 and Ar, as a result of the higher thermal conductivity of He.[9] In vacuum, TGA curves are generally shifted to lower temperatures with respect to studies performed under inert atmospheric conditions.[9] Thus, the ambient environment must be taken into account when interpreting TGA curves, as differences in TGA curves might not indicate differences in chemical decomposition mechanisms. The effect of heating rate on TGA curves of the phenolic resin is seen in the unique study of the SC-1008 resin by Stokes,[13] which employed a broad range of heating rates from 0.25 °C min^{-1} to 2500 °C min^{-1} under the same environmental conditions (Ar purge). This study showed that at lower heating rates of 0.25 – 300 °C min^{-1} (0.0042 – 5 °C s^{-1}), the point at which 50 percent of the total mass loss occurred shifted to higher temperatures with increasing heating rate. However, at higher heating rates in the range of 300 – 2500 °C min^{-1} (5 – 42 °C s^{-1}), the point at which 50 percent of total mass loss occurred shifted to lower temperatures with increasing heating rate. The results of Stokes are consistent with a much earlier study by Jackson and Conley,[12] who pyrolyzed a resole resin under a He atmosphere and found that the midpoint of mass loss shifted to a lower temperature when the heating rate changed from 0.5 °C s^{-1} to 300 °C s^{-1}. The observed reversal in the rate of mass loss at high heating rates is an indication that the mechanisms of thermal decomposition may change with heating rate.

4.4.2 RATE-DEPENDENT QUANTITATIVE YIELDS OF PYROLYSIS PRODUCTS

The data herein provide the first report of the molar (and mass) yields of a phenolic-based material as a function of temperature and heating rate. In addition, the heating rates used are representative of TPS materials in an atmospheric-entry environment. As mentioned above, some TGA data show the dependence of total mass loss on heating

rate,[12-13] but while the heating rates may be relevant to flight conditions, the decomposition mechanisms cannot be inferred from these data. Other pyrolysis studies have provided chemical insight through spectroscopic measurements of the partially charred material[12,30,34,78,94] or through the analysis of the gaseous products under quasi-steady-state heating conditions,[81-83] but these studies have not examined the dependence of the decomposition mechanisms on the heating rate, which is necessary to reveal the extent to which reaction kinetics must be considered in the decomposition of a phenolic-based material. Our new data, in combination with earlier studies of phenolic resin and PICA pyrolysis, allow inferences to be made about the decomposition mechanisms under flight-relevant conditions that go beyond the insight that is available from earlier studies.

Most of the previous studies on the pyrolysis of phenolic resin and phenolic-based composites were summarized in our recent paper,[83] although a new study which reported the molar yields of PICA pyrolysis products has appeared since then.[81] These studies have described phenolic pyrolysis in terms of three stages of decomposition, corresponding to increasing temperatures and overlapping temperature ranges. In stage 1, H_2O, phenol, and derivatives of phenol, are the main gaseous pyrolysis products. In stage 2, CO and CH_4 are the main products. In stage, 3, H_2 is the dominant product. These trends are evident in our earlier work[83] and in the experiments of Wong et al.,[81-82] where the pyrolysis products of PICA were collected in steps for relatively long periods at a constant temperature. The molar yields in Fig. 4.5 also display the same trends, although these data clearly show that the molar yields change as a function of heating rate, indicating that the decomposition processes are kinetically controlled at the heating rates used. This conclusion is consistent

with the TGA results from Stokes,[13] but the determination of molar yields at different heating rates provides additional insight into the underlying mechanisms that lead to the observed mass-loss behavior.

The different kinetics are manifested in the products that are liberated from the material above ~200 °C, where outgassing is no longer expected to be important. Inspection of the curves in Fig. 4.5 shows that the molar yields of H_2O and CO decrease with increasing heating rate, whereas the molar yield of CH_4 increases. The molar yields of phenol and its derivatives increase slightly with heating rate and, notably, these products tend to evolve at lower temperatures when the heating rate increases. The molar yield of H_2 exhibits complex behavior, as the shape of the curve of H_2 molar yield as a function of temperature is bimodal at lower heating rates, with the second peak, above 800 °C, diminishing as the heating rate increases. When the molar-yield curves in Fig. 4.5 are integrated, quantitative trends may be seen in the ratios of various product yields. Figure 4.9A shows the ratio of the total molar yield of C atoms to O atoms as a function of heating rate. It is clear that the yield of carbon-containing species compared to oxygen-containing species increases with heating rate, indicating that a higher fraction of oxygen is liberated from the surface at lower heating rates. This trend suggests that the charring material may retain more oxygen at higher heating rates. As seen in Fig. 4.9B, the molar yield of the volatile organic compounds (VOCs: benzene, toluene, xylene, phenol, cresol, dimethyl phenol, trimethyl phenol) relative to the light products (H_2, H_2O, CH_4, CO, CO_2) increases with heating rate. In a study of phenolic resin pyrolysis during stepwise heating with vastly different heating rates than the current study, Bennet[40] also observed a higher yield of

VOCs and a lower yield of light products on going from a very low to a very high heating rate. The increasing fraction of VOCs compared to the light products, which carry most of the oxygen atoms away from the material, is another indication of the greater retention of oxygen at higher heating rates. Not only does the relative yield of VOCs increase with heating rate, but the evolution of VOCs shifts to lower temperatures as the heating rate increases (Fig. 4.6), which is consistent with a shift in the TGA curve to lower temperatures with higher heating rates (Fig. 4.7). In addition, the molar yield of H_2O decreases with heating rate while that of CH_4 increases. As discussed below, these trends are related to the increased yield of VOCs when the heating rate is increased from 3.1 to 12.7 °C s^{-1}. However, at the highest heating rate (25 °C s^{-1}), the fast charring of the material and the retention of oxygen might qualitatively alter the decomposition kinetics. An indication of this qualitative change may be seen in the ratio of the H_2O molar yield to that of phenol and its derivatives. Figure 4.9C shows that this ratio decreases with heating rate until the highest heating rate is reached, at which point, the trend reverses. The molar yield of H_2O monotonically decreases with heating rate across the whole range, so the observed increase in the H_2O to phenol and derivatives ratio at the highest heating rate comes from a qualitative change in the molar yield of phenol and its derivatives at this heating rate, where the yield of these products decreases rather sharply. Corresponding to this pronounced decrease in the yield of phenol and its derivatives is a significant increase in H_2 yield (Fig. 4.5). Furthermore, at the highest heating rate, the total mass loss is somewhat less than what is observed at the lower three heating rates. These observations suggest that a high heating rate may lead to rapid charring of the material that preferentially traps oxygenated

species (precursors to H_2O) over species that can leave as phenol and its derivatives (or other VOCs). A higher yield of H_2 at the highest heating rate presumably comes at the expense of hydrocarbon species, which decompose to hydrogen and non-volatile carbon (or oxygen-rich carbon) moieties before they have a chance to be liberated as intact hydrocarbon molecules, thus resulting in a lower total mass loss.

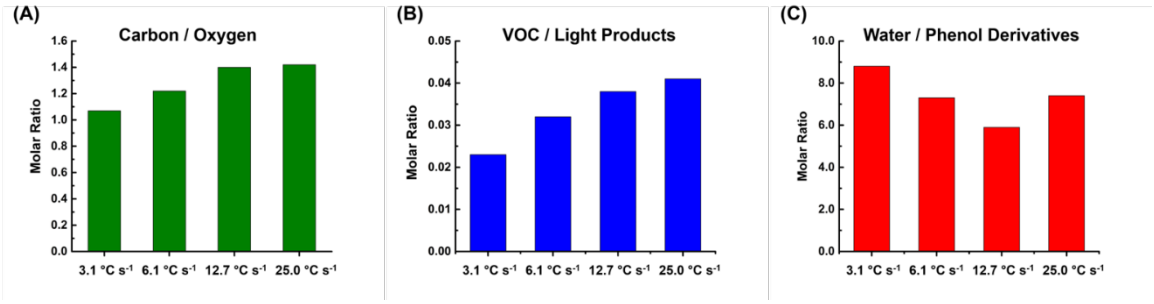

Figure 4.9. (A) Ratio of integrated molar yield of C to integrated molar yield of O. (B) Ratio of integrated molar yield of volatile organic carbons (VOCs: benzene, toluene, xylene, phenol, cresol, dimethyl phenol, trimethyl phenol) to integrated yield of light products (H_2, H_2O, CH_4, CO, CO_2). (C) Ratio of integrated yield of H_2O to integrated yield of phenol and its derivatives.

The initial steps in the decomposition of phenolic resin involve condensation reactions that form ether and carbon-carbon bonds and liberate H_2O. Condensation reactions that lead to the formation of a diphenyl ether moiety have been suggested previously.[31,78,83] As seen in Fig. 4.5, H_2O is evolved primarily in the temperature range 200-600 °C, with the maximum yield occurring at 400 °C. Infrared studies of partially charred phenolic resin show an increase in both carbon-carbon and ether bond formation when the material is heated to temperatures between 250 °C and 400 °C.[30,34,94] Figure 4.10 illustrates two categories of condensation reactions that are probably responsible for the formation of H_2O.[34] As described previously; ether bonds can be formed by

intermolecular dehydration to form a diphenyl ether cross-link. In addition, ether bonds may be formed by intramolecular dehydration to form a xanthene functional group. As the temperature is increased further, it is likely that the diphenyl ether cross-link would react further to a dibenzofuran structure and release H_2. In addition to ether bonds, two types of carbon-carbon cross-linking bonds can form. The reaction of a phenol hydroxyl group and an aromatic carbon atom may form an aryl-aryl bond. The hydroxyl group can also react with a methylene bridge group to form an alkyl-aryl bond. Thus, because of the initial stages of decomposition, the resin releases H_2O and forms a highly cross-linked network made up of additional ether groups and carbon-carbon bonds.

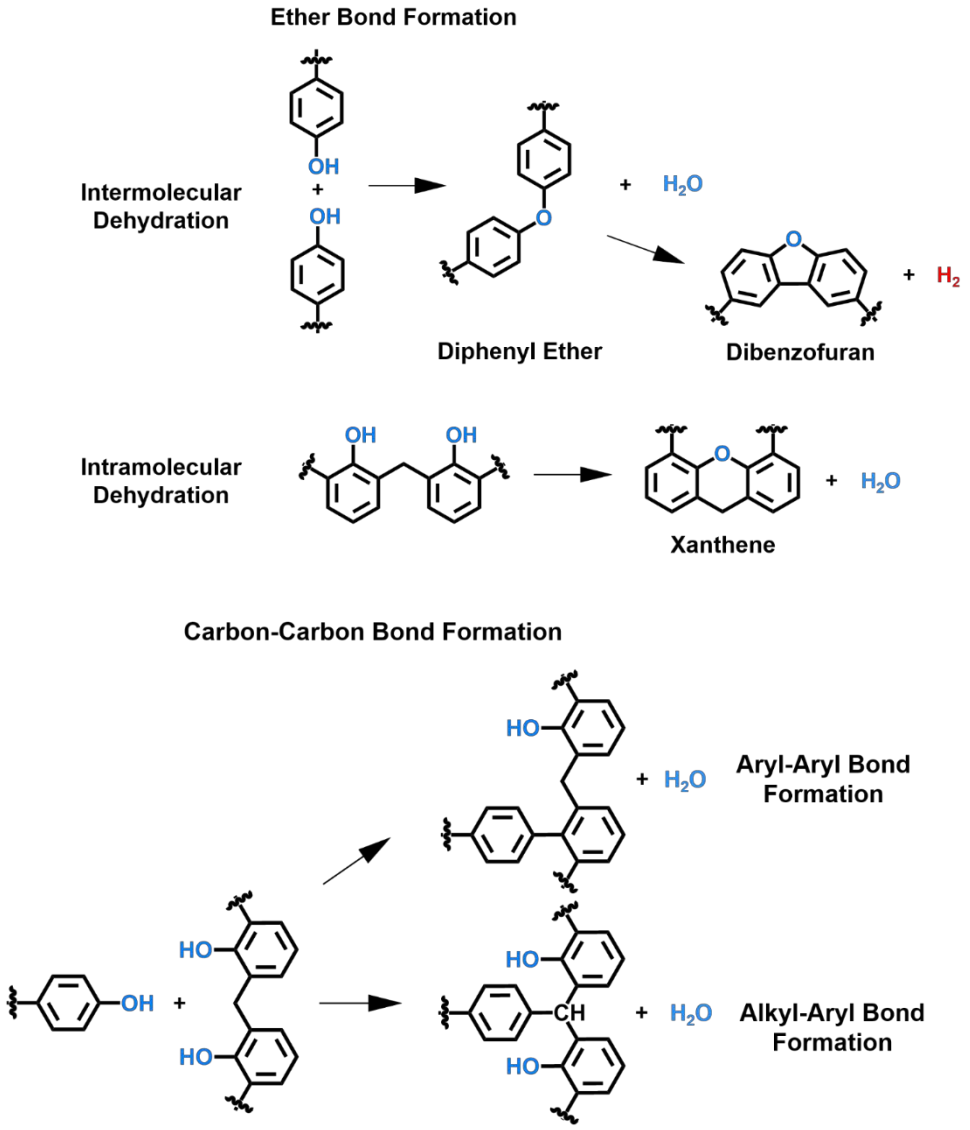

Figure 4.10. Condensation reactions leading to cross-linking through ether bond formation and carbon-carbon bond formation.

Phenol and its derivatives evolve over a relatively narrow range of temperatures (250 – 550 °C), and the temperature of maximum yield for these species is nearly identical to that of H_2O. The evolution of phenol and its derivatives has been explained as the release of pendant aromatic groups,[93] but these species more likely originate from the scission of the methylene bridges between phenol groups. Indeed, infrared studies have shown a

decrease in the absorption band corresponding to the scissor bending mode in methylene bridge units as the temperature of the decomposing resin increases up to 400 °C.[30,34,94] Figure 4.11 illustrates the breakdown of a methylene bridge, which may lead to phenol or substituted phenol depending on the structure of the polymer backbone near the methylene bridge. Specifically, this figure illustrates a case where *o*-cresol is liberated, and a methyl functional group is on the phenol ring that remains in the resin.

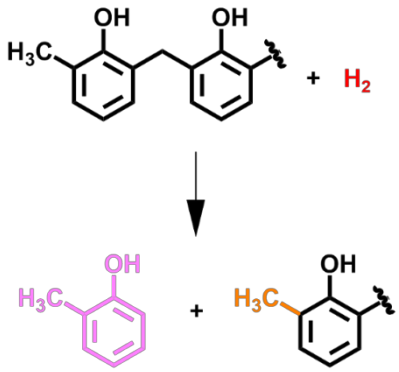

Figure 4.11 Example of methylene bridge scission, where volatile *o*-cresol is formed, and a methylated phenol group remains in the resin.

The observed heating-rate-dependent changes in the yields of H_2O and phenol and its derivatives may be interpreted in terms of a competition between condensation reactions and methylene bridge scission. As seen in Fig. 4.5, the yield of H_2O decreases as the heating rate increases. In addition, as mentioned above, the ratio of molar yields of H_2O to phenol and its derivatives decreases as the heating rate increases from 3.1 to 12.7 °C (Fig. 4.9 C). It is thus apparent that the yield of phenol and its derivatives increases with heating rate as the yield of H_2O decreases. These phenomena suggest that methylene scission competes more effectively with condensation reactions at higher heating rates. Furthermore, the evolution of phenol and its derivatives shifts to lower temperatures as the

heating rate increases (Fig. 4.6), also suggesting that methylene scission becomes more facile at higher heating rates. The breakdown of the polymer backbone and disappearance of aromatic hydrocarbons will take away sites for cross-linking, resulting in reduced H_2O production. Phenol and its derivatives are much heavier than H_2O, so the increased probability of their evolution at the expense of H_2O at higher heating rates shifts the TGA curve to lower temperatures (Fig. 4.7). The explanation of the relationship between the yields of H_2O and phenol and its derivatives in terms of a competition between condensation and methylene scission reactions depends on these two basic processes occurring on time scales to which the data are sensitive. Given the heating rates of 3.1 – 25 °C s^{-1} and the fact that 2.8 seconds are required to collect each mass spectrum, the reaction time scales must be on the order of seconds to minutes in order for differences in heating rate dependencies to be observed. Although the reaction rates of condensation and methylene scission reactions in a pyrolyzing phenolic resin are not known, the condensation reactions during the curing of polyimides are known to take place on the time scale of minutes.[95-96] Reactive hydroxyl groups that participate in the condensation reaction of polyimides are already in close proximity to their bonding counterparts and are not expected to be hindered by steric effects, yet the reaction takes place on a relatively long time scale. Therefore, it is reasonable to assume that the condensation reactions that occur in the early stages of the pyrolysis of PICA, which may need to overcome steric effects within or between phenol polymer chains, occur on a time scale of minutes or longer.

H_2O may oxidize methylol groups to form carboxylic acid or aldehyde functional groups. Methylol groups may persist after the phenolic resin is cured, with the concentration of these groups depending on the curing conditions.[12, 97-98] Using infrared detection techniques, Jackson and Conley revealed the formation of carboxylic acid and benzophenone functional groups after curing a resole resin for 3 hours at 120 °C.[12] These functional groups were detected in the post-cured resin even though curing was performed under high vacuum. This study also established that the presence of H_2O during the curing process promoted carbonyl formation, perhaps through the oxidation of residual methylol groups as shown in Fig. 4.12. H_2O formed by condensation reactions during pyrolysis would thus presumably react to produce carboxylic acid and aldehyde groups. These aldehyde groups could then react with adjacent benzene rings to form the benzophenone structure, as illustrated in Fig. 4.12. One would expect carbonyl formation to be reduced in probability by the breakdown of the methylene bridge and the removal of aromatic hydrocarbons, and this supposition is supported by the heating-rate-dependent rate results for the CO and CO_2 products, as discussed below.

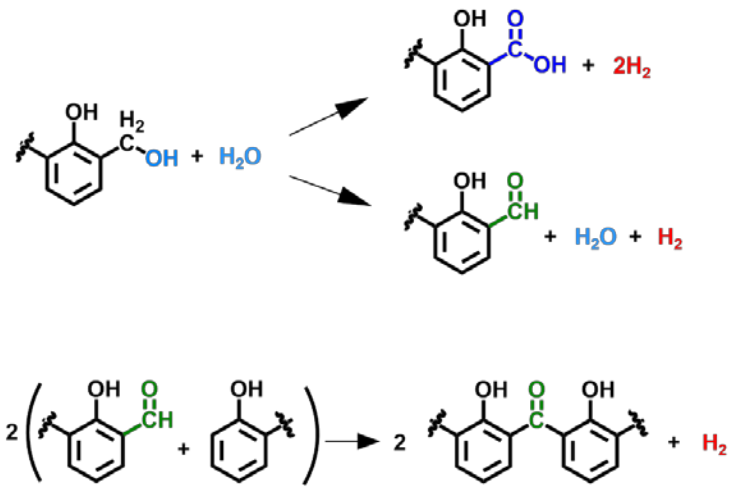

Figure 4.12. Oxidation of methylol groups and subsequent formation of a benzophenone structure.

The formation of carboxylic acids, aldehydes, and ketones is most likely responsible for the observation of CO and CO_2 during phenolic decomposition at relatively low temperatures. At very low temperatures (<200 °C), CO and CO_2 may come from the decomposition of carboxylic acid and aldehyde groups that remain in the resin after curing (Fig. 4.13). As H_2O is formed through condensation reactions, the production rate of carboxylic acids and aldehydes would be expected to increase through reaction with methylol groups (Fig. 4.12) and therefore increase the production rate of CO_2 and CO. The temperature-dependent behavior of the CO_2 molar yield suggests a two-stage process that is consistent with the speculation above. As the temperature increases from 100 °C, the CO_2 yield rises, reaches a maximum between 150 and 200 °C, and decreases slightly before rising more substantially to a peak near 400 °C before decaying (see Figs. 4.5 and 4.6). The initial maximum in the yield of CO_2 occurs before any significant production of H_2O, and the second maximum in the CO_2 yield occurs almost simultaneously with the

maximum in the H_2O yield. Thus, it is conceivable that the initial formation of CO_2 is the result of the decomposition of carboxylic acid in the pristine resin while the subsequent formation of CO_2 comes from the decomposition of similar groups that have been formed by reactions with H_2O produced through condensation reactions as the resin starts to decompose. Support for this idea comes from the fact that we observe that the CO_2 yield decreases when the heating rate is increased from 3.1 °C s^{-1} to 12.7 °C s^{-1}, which would be expected because an increased heating rate reduces the probability of H_2O-producing condensation reactions. The molar yield of CO does not show the same bimodal temperature dependence as CO_2. The CO yield rises substantially from the lowest temperature and reaches a maximum near 450 °C – i.e., at a higher temperature than the maximum in the H_2O yield. Clearly, there are mechanisms that lead to CO production that are distinct from those that lead to CO_2 production, but the formation of CO at low temperatures (<400 °C) may also originate from leftover and newly formed aldehyde groups. A two-step decomposition mechanism leading to CO from a benzophenone group has also been proposed.[13,31,83]

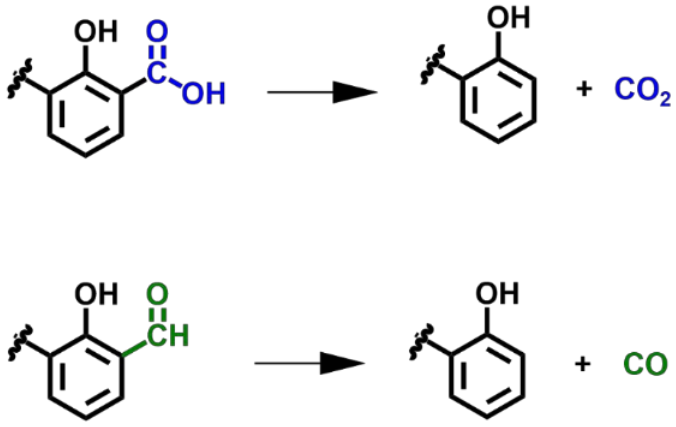

Figure 4.13. Possible formation mechanisms of CO_2 and CO through the decomposition of carboxylic acid and aldehyde functional groups, respectively.

The high yields of CO and CH_4 that peak above 400 °C are most probably tied to the competitive processes that involve cross-linking reactions and methylene bridge scission. The molar yields of CO and CH_4 peak at the same temperature (near 450 °C). Figure 4.14 shows the ratio of the total molar yield of CO to CH_4 for each of the four heating rates used. This figure shows that as the heating rate is increased the relative yield of CO compared to CH_4 decreases. This behavior may be interpreted in terms of the presumed mechanisms for CO and CH_4 formation. The evolution of CO in the temperature range of about 400 to 700 °C most likely originates from the thermal decomposition of ketone (dibenzophenone) and ether (diphenyl ether) functional groups, as illustrated in Fig. 4.15. It is well known that poly (phenylene oxides) break down at T ≈ 500 °C, and when they are substituted with methyl functional groups, they break down at lower temperatures (T ≈ 450 °C).[99] Ether groups in the form of xanthene and dibenzofuran structures (Fig. 4.10) likely survive to higher temperatures, as these molecules are stable up to temperatures of 700 - 800 °C.[100-101] Thus, the formation of high yields of CO is dependent on prior

reactions that liberated water and produced the CO precursor products either directly (Fig. 4.10) or indirectly (Fig. 4.12). The findings from studies using IR spectroscopy and solid-state NMR have suggested that most of the CH_4 produced during pyrolysis of phenolic resins originates from the breakdown of the methylene backbone of the polymer, as illustrated in Fig. 4.11.[30,97,102] The loss of phenol or one of its derivatives presumably leaves a methyl substituted aromatic group attached to the bulk of the resin, and this methyl group may be liberated as a CH_4 molecule. Our data suggest that this decomposition process is likely because the rise in molar yield of CH_4 is immediately preceded by an increase in the yields of phenol and its derivatives at slightly lower temperatures. In addition, the decrease in the total yield of CO relative to CH_4 with increasing heating rate appears to be correlated with the decrease in the total yield of H_2O relative to phenol and its derivatives with heating rate. Therefore, the relative CO and CH_4 yields seem to be rooted in the competition between condensation and methylene bridge scission reactions at lower temperatures. It is possible that CH_4 might be formed from a one-step decomposition of the methylene bridge to produce a diphenyl group.[78,83] It is also possible that some of the evolved CH_4 originates from methyl groups that are not associated with the backbone of the polymer, as it has been shown that increasing methyl substitution on the phenol precursor molecule increases the molar yield of CH_4 during pyrolysis.[31] However, the strong correlation between the evolution of CH_4 and phenol and its derivatives suggests that these additional pathways to CH_4 are relatively improbable.

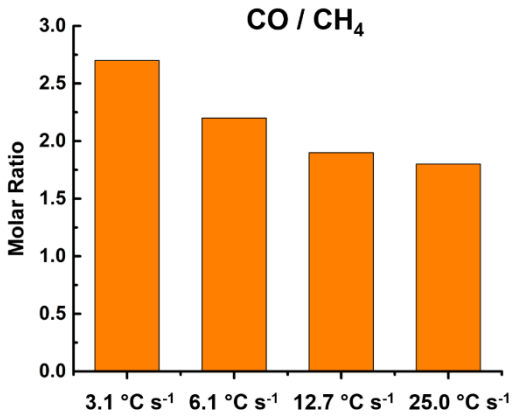

Figure 4.14. Ratio of integrated molar yield of CO to integrated molar yield of CH_4.

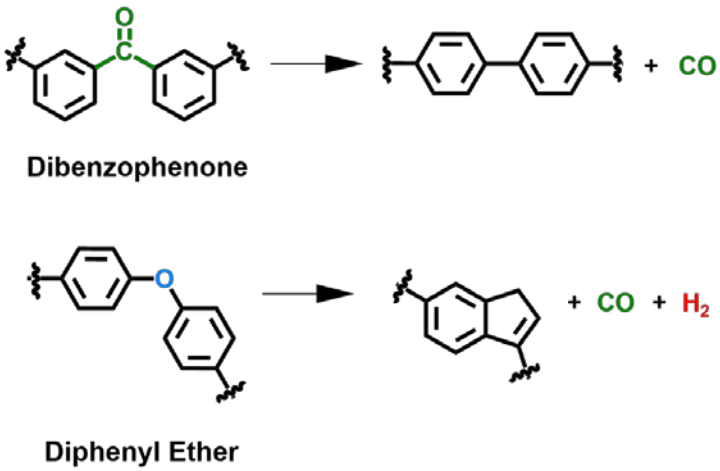

Figure 4.15. Formation of CO through the decomposition of ketone (dibenzophenone) and ether (diphenyl ether) functional groups.

Benzene and its derivatives, toluene, and xylene, are minor products that are liberated over a narrow range of temperatures from 325 to 550 °C (Fig. 4.16), and their peak yields occur at higher temperatures than those of phenol and its derivatives. Parker and Winkler suggested that benzene and its derivatives arise from terminal aromatic groups that are attached to the main chain of the pristine polymer, based on the justification that the carbon-

carbon bonds attaching the terminal groups to the backbone are thermodynamically the least stable in the polymer system.[93] This suggestion can explain the low yields of benzene and its derivatives because the number of terminal aromatic groups is significantly lower than the number of aromatic groups associated with the backbone of the polymer. However, as noted above, the scission of methylene bridges would also lead to the formation of terminal aromatic groups (Fig. 4.11), thus creating an additional source of benzene and its derivatives that was not present in the pristine resin. The fact that benzene and its derivatives evolve at approximately the same temperature as CH_4 (Fig. 4.16), which follows methylene bridge scission, supports the idea that benzene and its derivatives come from terminal aromatic groups. Benzene and its derivatives have very low yields; thus, terminal aromatic groups may be more likely to be liberated as phenol and its derivatives or perhaps pathways that lead to benzene and its derivatives are more likely to lead to their incorporation into incipient char in the range of temperatures where they are produced. The relatively high char yield of the phenolic resin is consistent with the latter.

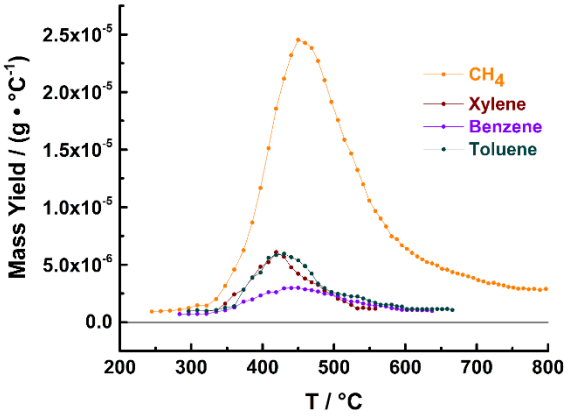

Figure 4.16. Mass yields of CH_4, xylene, toluene, and benzene, with a heating rate of 3.1 °C s^{-1}.

As the decomposition of phenolic resin progresses, H_2 becomes the dominant product as the temperature rises above 500 °C. H_2 may be formed by a ring closure mechanism in a diphenyl ether moiety to form a dibenzofuran-like product, as shown in Fig. 4.10. In this reaction, two hydrogen atoms are stripped from two separate carbon atoms that are in the ortho position with respect to the ether crosslink. This mechanism has been proposed by Ehlers and Patel to explain the appearance of H_2 after the initial steps of decomposition for PPO (poly(p-phenylene oxide)), PPE (polyphenyl ether), and PEEK (polyether ether ketone).[99,103] The dibenzofuran structure is relatively stable and may persist in the charring material up to a temperature of ~800 °C. The main source of H_2 is the stepwise fusing of phenyl rings to create domains of graphitic carbon (Fig. 4.17).[78,83] First, a polyphenyl polymer coalesces to a polyaromatic hydrocarbon (PAH). Talyzin et al. showed that molecules as large as coronene fuse together to form larger PAHs at temperatures in the range 530 – 550 °C.[104] It is assumed that as the temperature increases smaller PAHs

consolidate into higher mass PAHs as illustrated in the second reaction step in Fig. 4.17. This process likely continues until the material is completely carbonized.

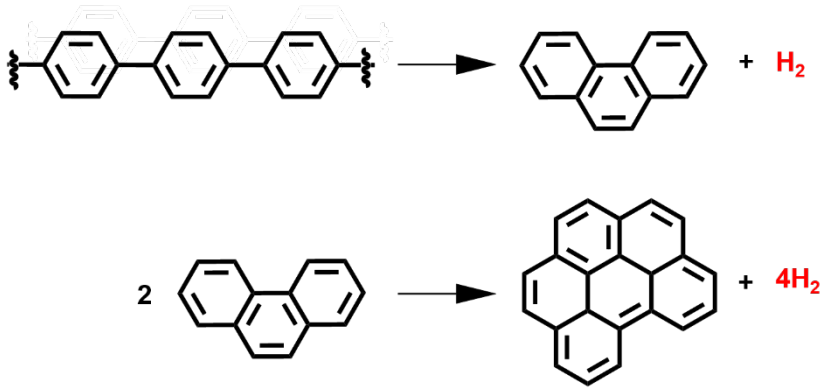

Figure 4.17. Formation of H_2 through the fusing of phenyl rings to create domains of graphitic carbon.

A remarkable observation is the appearance of a "bump" in the temperature dependent molar yield curves for H_2, CH_4, H_2O, and CO at temperatures above 800 °C (Fig. 4.5). This feature is quite pronounced at the lowest heating rate of 3.1 °C s^{-1} and gradually disappears as the heating rate increases to 25 °C s^{-1}. This observation is a manifestation of the competing cross-linking and methylene bridge scission reactions that take place at much lower temperatures (~400 °C). Elemental analysis of pyrolyzed phenolic SC-1008 resin reveals a significant oxygen content in the material that remains even at temperatures as high as 800 °C.[37,40,105] This oxygen content may be in the form of ether groups, such as dibenzofuran and xanthene, which are stable up to this temperature. Ouchi pyrolyzed a resole resin at a rate of 2 °C min^{-1} in vacuum and collected infrared spectra of the solid material at varying stages of decomposition.[34] His measurements suggest that xanthene, dibenzofuran, and diphenyl ether form over a temperature range of

400-500 °C and decrease in intensity as the temperature increases to 700 °C. These compounds have also been observed as pyrolysis products in GC/MS experiments.[40, 106] In addition, TPD and XPS studies of oxidized carbon nanotubes performed under high vacuum reveal that these structures do not decompose until 700-800 °C.[100-101] Stable ethers would be expected to be formed with higher probability at low heating rates, when condensation/crosslinking reactions compete more effectively with the breakdown of the polymer backbone through methylene bridge scission. These ether structures eventually decompose at high temperatures above 800 °C and release the light gases, H_2, CH_4, H_2O, and CO, which would lead to a relatively sudden increase in the yields of these products (Fig. 4.18). At high heating rates, the breakdown of the polymer backbone becomes more probable, and the extent of stable ether formation is diminished, resulting in a lower residual ether content in the material at high temperatures. Thus, there is no sudden increase in the production of light gases above 800 °C, although there is still a change in slope in the molar yield curves, suggesting that the stable ether content is not negligible even at high heating rates.

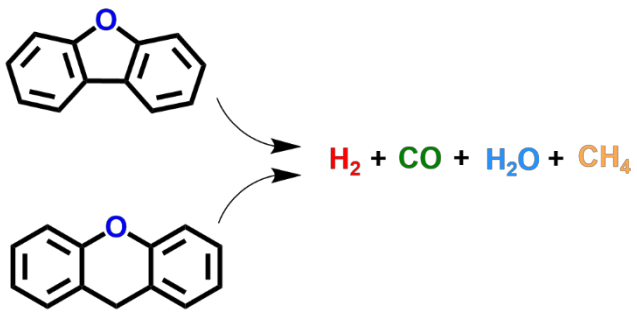

Figure 4.18. Schematic illustration suggesting that stable dibenzofuran and xanthene structures may persist to high temperatures and then decompose above 800 °C.

We conducted additional experiments to investigate the persistence of oxygen and hydrogen in the charring material at high temperatures. Two pristine samples of PICA were first pyrolyzed at higher and lower heating rates of 24.9 and 2.8 °C s^{-1}, respectively, to a temperature above 1100 °C, and the heat to the samples was turned off, and they were allowed to cool to ambient temperature. Then, each sample was reheated slowly. The sample that had been pyrolyzed at the higher rate was reheated at 4.5 °C s^{-1}, and the sample that had been pyrolyzed at the lower rate was reheated at 3.3 °C s^{-1}. The second heating of the samples allowed them to reach temperatures near 1000 °C, with one sample reaching about 1050 °C while the other sample reached only about 900 °C. Figure 4.19 shows the relative molar yields of H_2, CH_4, H_2O, and CO during each heating run for each sample. These products were monitored by continuously collecting mass spectra over the rage *m/z* = 1 – 30. Although the second heating of the two samples resulted in somewhat different maximum temperatures, it is still clear that the higher heating rate produces a char that contains more oxygen and hydrogen than the char produced at the lower heating rate. Indeed, this result is consistent with our observation that the ratio of the total molar yield of C atoms to O atoms decreases with heating rate (Fig. 4.9 A). Furthermore, the elemental analysis performed by Bennet et al. suggests that the weight percent of oxygen remaining in the char increases by as much as 11 percent as the heating rate increases.[40]

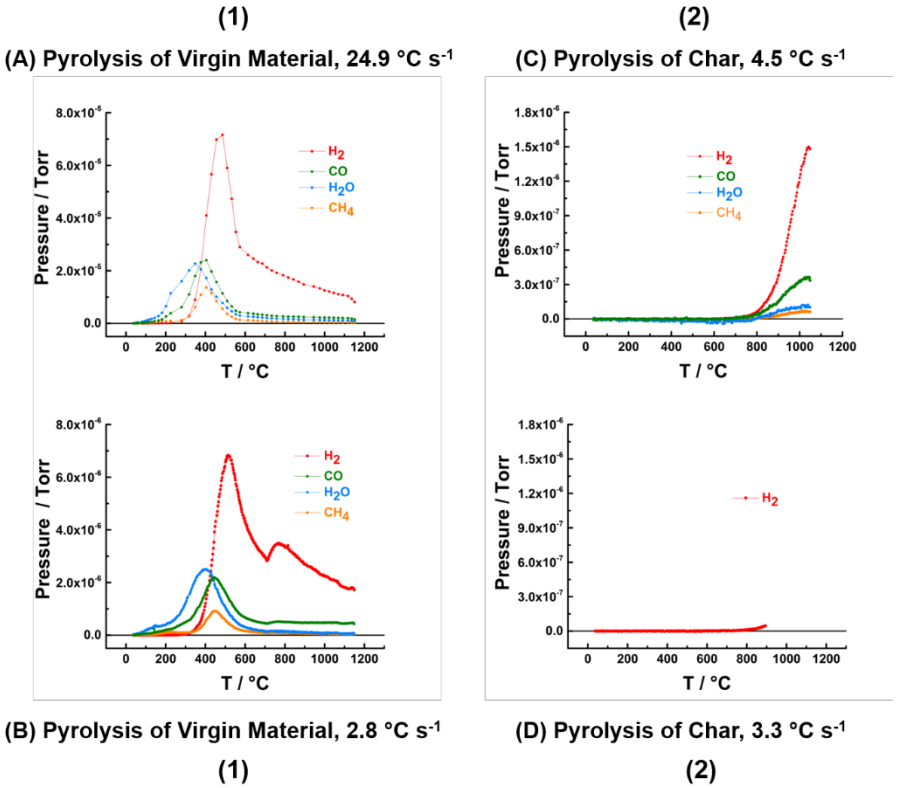

Figure 4.19. (1) Relative molar yields of light products detected during pyrolysis of the virgin material, with heating rates of (A) 24.9 °C s^{-1} and (B) 2.8 °C s^{-1}. (2) Relative molar yields of light products detected during pyrolysis of the char, heating rates of (C) 4.5 °C s^{-1} and (D) 3.3 °C s^{-1}.

The presence of higher oxygen content in the char that is produced at a higher heating rate appears to be at odds with the conclusion that ether formation is enhanced at lower heating rates (at temperatures around 400 °C). However, the form in which oxygen is retained in the char must affect the ease with which it is liberated. At low heating rates, oxygen is most likely bound preferentially in the char in the form of ether functional groups. These ether groups appear to be able to break down relatively easily when the temperature rises above 800 °C, leaving a char that does not release additional oxygen when it is reheated. On the other hand, when the heating rate is high the material is

expected to form fewer ether groups, yet the oxygen content remains relatively high and this oxygen can be released when the material is reheated at a low heating rate. Perhaps oxygen-containing domains are physically trapped in the charring material at high heating rates and may not be able to decompose by the time the sample temperature has reached its maximum (~1200 °C in the case of the experiments reported here). In any case, reheating the material at low rates is able to release much of the retained oxygen (and hydrogen). The processes by which H_2, CH_4, H_2O, and CO are liberated upon reheating cannot readily be understood. The lack of any observable volatile products at temperatures below 800 °C during reheating suggests that oxygen and hydrogen are not bound in relatively pristine domains but must be retained (or trapped) in fairly stable forms.

It is expected that chars containing oxygen functional groups will have lower thermal conductivities than pure carbon and that the nature of the chemical structures involving oxygen will have a quantitative effect on the extent of reduction in thermal conductivity. A study by Zhang et al. revealed that the thermal conductivity of graphene sheets is substantially reduced even a with a small amount of substitution of hydroxide, epoxide, and ether groups.[107] The reduction in thermal conductivity was the greatest upon ether substitution. Zhao et al. were in basic agreement, but they attributed the reduction in thermal conductivity to carbonyl functional groups.[108] Thus, material response models for phenolic-based heat shields should consider not only the heating-rate dependence on molar yields but also the likely connection between thermal conductivity and the heating-rate-dependent oxygen content of the charring material.

4.5 CONCLUSION

Temperature-dependent molar yields of the 14 main pyrolysis products of PICA have been derived from *in situ* mass spectrometric measurements at four nominal heating rates, 3.1, 6.1, 12.7, and 25 °C s^{-1}, over the temperature range 100 – 1200 °C. Mass yields and simulated TGA curves have been derived from the molar yield data and measurements of the mass loss. The temperature dependencies of the molar yields change with heating rate, suggesting that pyrolysis of PICA is a nonequilibrium process and that the relative importance of competing mechanisms depends on heating rate. It is suggested that the thermal degradation of the phenolic resin of PICA is dominated by two major decomposition processes that occur at relatively low temperatures in the range of approximately 300 to 500 °C. One process comprises cross-linking reactions that release H_2O while forming ether and carbon-carbon bonds. The second process is scission of methylene bridges, which leads directly to liberation of phenol and its derivatives. Both processes undoubtedly occur at all heating rates, but the relative importance of the latter increases with increasing heating rate. The breakdown of the polymer backbone and disappearance of aromatic hydrocarbons removes sites for crosslinking, resulting in reduced H_2O production. The preferred release of higher mass products through methylene bridge scission with higher heating rates explains the observations from previous TGA studies that the midpoint in overall mass loss shifts to lower temperatures at higher heating rates. The yield of CO decreases in response to lower yields of H_2O as well as the diminished formation of ether bonds at higher heating rates. In contrast, CH_4 yields increase at higher heating rates in response to the increased decomposition of the backbone

of the polymer. Enhanced formation of ether groups at lower heating rates leads to stable dibenzofuran and xanthene ether structures that survive to high temperatures and then decompose rapidly as the temperature rises above 800 °C. Higher heating rates lead to greater ultimate oxygen retention in the charred material, even though ether formation is suppressed at higher heating rates. The chemical nature of the high oxygen content resulting from high heating rates is unknown. Oxygen content in the charring material is expected to lower its thermal conductivity. The molar yields as a function of temperature and heating rate and the mechanistic information that may be inferred from them should be useful for nonequilibrium models whose aim is to describe the material response of PICA and other phenolic-based thermal protection systems.

4.6 REFERENCES

1) Anderson, J. D. *Hypersonic and High Temperature Gas Dynamics*. AIAA Education Series; Schetz, J. A., 2nd ed., AIAA: Reston, V.A. **2006**.

9) Wendlandt, W. W. *Thermal Analysis*. *Chemical Analysis Series, Vol. 19*; Elving, P.J.; Winefordner, J. D., Eds.; 3rd ed., John Wiley and Sons, New York, N.Y. **1984**.

10) Baer, A. D.; Hedges, J. H.; Seader, J. D.; Jayakar, K. M.; Wojcik, L. H. Polymer Pyrolysis over a Wide Range of Heating Rates. *AIAA J.* **1977**, *15*, 1398-1404; DOI: 10.2514/3.7435.

12) Jackson, W. M.; Conley, R. T. High Temperature Oxidative Degradation of Phenol−Formaldehyde Polycondensates. *J. Appl. Polym. Sci.* **1964**, *8*, 2163−2193; DOI: 10.1002/app.1964.070080516.

13) Stokes, E. H. Kinetics of Pyrolysis Mass Loss from Cured Phenolic Resin. J. *Themophys. Heat Trans.* **1995**, *9*, 352-358; DOI: 10.2514/3.667.

19) Tran, H. K.; Johnson, C. E.; Rasky, D. J.; Hui, F. C. L.; Hsu, M.; Chen, Y. K. Phenolic Impregnated Carbon Ablators (PICA) for Discovery Class Missions. *31st AIAA*

Thermophysics Conference, New Orleans, LA, June 17-20, 1996. DOI: 10.2514/6.1996-1911

22) Trumble, K. A.; Cozmuta, I.; Sepka, S.; Jenniskens, P.; Winter, M. Postflight Aerothermal Analysis of Stardust Sample Return Capsule. *J. Spacecr. Rockets* **2010**, *47*, 765-774. DOI: 10.2514/1.41514

23) Bose, D.; White, T.; Santos, J. A.; Feldman, J.; Mahzari, M.; Olson, M.; Laub, B. Initial Assessment of Mars Science Laboratory Heat Shield Instrumentation and Flight Data. *51st AIAA Aerospace Sciences Meeting including the New Horizons Forum and Aerospace Exposition*, Grapevine, TX, January 7-10, 2013. DOI: 10.2514/6.201-908

24) Space X website, http://www.spacex.com/news/2013/02/09/spacexs-dragon-spacecraft-successfully-re-enters-orbit (accessed Nov 3, 2014).

30) Morterra, C.; Low, M. J. D. IR Studies of Carbons-VII. The Pyrolysis of a Phenol-Formaldehyde Resin. *Carbon* **1985**, *23*, 525-530. DOI: 10.1016/0008-6223(85)90088-0

31) Ouchi, K.; Honda, H. Pyrolysis of Coal 1. Thermal Cracking of Phenol-Formaldehyde Resins Taken as Coal Models. *Fuel* **1959**, *38*, 429-443. DOI: 10.1021/la00063a010

34) Ouchi, K. Infra-Red Study of Structural Changes During the Pyrolysis of a Phenol-Formaldehyde Resin. *Carbon* **1966**, *4*, 59-66. DOI: 10.1016/0008-6223(66)90009-1

37) Sykes, G. F. Decomposition Characteristics of a Char-Forming Phenolic Polymer Used For Ablative Composites. NASA TN D-3810, February, **1967**.

40) Bennett, A.; Payne., D. R.; Court., R. W. Pyrolytic and Elemental Analysis of Decomposition Products from a Phenolic Resin. *Macrom. Symp*. **2014**, *339*, 38-47. DOI: 10.1002/masy.201300136

77) Mahzari, M.; Braun, R. D.; White, T. R.; Bose, D. Inverse Estimation of the Mars Science Laboratory Entry Aeroheating and Heatshield Response. *J. Spacecr. Rockets* **2015**, *52*, 1203-1216; DOI: 10.2514/1.A33053.

78) Sawant, S. S.; Harpale, A.; Jambunathan, R.; Chew, H. B.; Levin, D. A. High Fidelity and Multi-scale Thermal Response Modelling of an Avcoat-like TPS. In *55th AIAA Aerospace Sciences Meeting* Grapvine, TX, Jan 9-13, 2017 DOI: 10.2514/6.2017-0438

79) Cheng, H.; Xue, H.; Hong, C.; Zhang, H. Preparation, Mechanical, Thermal and Ablative Properties of Lightweight Needled Carbon Fibre Felt/Phenolic Resin Aerogel Composite With a Bird's Nest Structure. *Comp. Sci. and Tech.* **2017**, 140, 63-72; DOI: 10.2514/6.2017-0438

80) Cheng, H,; Hong, C.; Zhang, X.; Xue, H.; Meng, S.; Han, J. Super Flame-Retardant Lightweight Rime-Like Carbon-Phenolic Nanofoam Sci. Rep. **2016**, 6, 33480 DOI: 10.1038/srep33480

81) Wong, H. W.; Peck, J.; Assif, J.; Panerai, F.; Lachaud, J.; Mansour, N. N.; Detailed Analysis of Species Production from the Pyrolysis of the Phenolic Impregnated Carbon Ablator. *J. Anal. Appl. Polym. Sci.* **2016**, *122*, 258-267; DOI: 10.1016/j.jaap.2016.09.016

82) Wong, H. W.; Peck, Bonomi, R. E.; J.; Assif, J.; Panerai, F.; Reinisch, G.; Lachaud, J.; Mansour, N. N.; Quantitative Determination of Species Production from Phenol-Formaldehyde Resin Pyrolysis. *Polym. Deg. Stab.* **2015**, *122*, 122-131; DOI: 10.1016/j.polymdegradstab.2014.12.020.

83) Bessire, B. K.; Lahankar, S. A.; Minton, T. K. Pyrolysis of Phenolic Impregnated Carbon Ablator (PICA). *ACS Appl. Mater. Interfaces.* **2015**, *7*, 1383-1395; DOI: 10.1021/am507816f.

84) Basford, J. A.; Boeckmann, M. D.; Ellefson, R. E.; Filipelli, A. R.; Holkeboer, D. H.; Lieszkovszky, L.; Stupak, C. M. Recommended Practice for the Calibration of Mass Spectrometers for Partial Pressure Analysis. *J. Vac. Sci. Technol. A.* **1993**, *11*, A22-A40; DOI: 10.1116/1.4755937.

85) Terres, E.; Gebert, F.; Hulsemann, H.; Petereit, H.; Toepsch, H.; Ruppert, W., *Zur Kenntnis der physikalisch-chemischen Grundlagen der Gewinnung und Zerlegung der Phenolfraktionen von Steinkohlenteer und Braunkohlenschwelteer. IV. Mitteilung Die Dampfdrucke von Phenol und Phenolderivaten. Brennst. Chem.* **1955**, *36*, 272-274.

86) Andon, R. J. L.; Biddiscombe, D. P.; Cox, J. D.; Handley, R.; Harrop, D.; Herington, E. F. G.; Martin, J. F. Thermodynamic Properties of Organic Oxygen Compounds. Part I. Preparation and Physical Properties of Pure Phenol, Cresols, and Xylenols. *J. Chem. Soc.* **1960**, 5246-5254 DOI: 10.1039/JR9600005246.

87) CRC Handbook of Chemistry and Physics, 71st ed. Lide, D.R., Ed.; CRC Press: Boca Raton, Fl, **1991**: Chapter 6, pp. 50-63.

88) Tate, J.S.; Gaikwad, S.; Theodoropoulou, N.; Trevino, E.; Koo, J. H. Carbon/Phenolic Nanocomposites as Advanced Thermal Protection Material in Aerospace Applications. *J. Composites.* **2013**, 403656; DOI: 10.1155/2013/403656.

89) Chang, C.; Tackett, J. R. Characterization of Phenolic Resins with Thermogravimetry-Mass Spectrometry. *Thermochim. Acta* **1991**, *192*, 181-190; DOI: 10.1016/0040-6031(91)87160-X.

90) Farmer, R. W. Phenolic Resin Char-Formation During Hyperthermal Ablation. *Thermochimica Acta* **1972**, *4*, 223-238; DOI: 10.1016/0040-6031(72)87007-2.

91) Goldstein, H. E. Pyrolysis Kinetics of Nylon 6-6, Phenolic Resin, and Their Composites. *J. Macromolec. Sci.: Part A – Chemistry* **1969**, *3:4*, 649-673; DOI: 10.1080/10601326908053834.

92) Friedman, H. L., Kinetics of Thermal Degradation of Char-Forming Plastics from Thermogravimetry. Application to a Phenolic Plastic. *J. Polym. Sci.* **1964**, *6*, 183-195; DOI: 10.1002/polc.5070060121.

93) Parker, J. A.; Winkler, E. L. The Effects of Molecular Structure on the Thermochemical Properties of Phenolics and Related Polymers. NASA TR R-276; NASA: Washington, D.C., November **1967**.

94) Costa, L.; Montelera, R.; Camino, G.; Weil, E. D.; Pearce, E. M. Structure-Charring Relationship in Phenol-Formaldehyde Type Resins. *J. Polym. Degrad. Stab.* **1997**, *56*, 23-35 DOI: 10.1016/S0141-3910(39)00171-1.

95) Pyun, E.; Mathisen, R. J.; Sung, C. S. P.; Kinetics and Mechanisms for Thermal Imidization of Polyamic Acid Studied by Ultraviolet-Visible Spectroscopy. *Macromolec.* **1988**, *22*, 1174-1183; DOI: 10.1021/ma00193a031.

96) Kruez, J. A.; Endrey, A. L.; Gay, F. P.; Sroog, C. E.; Studies of Thermal Cyclizations of Polyamic Acids and Tertiary Amine Salts. *J. Poly. Sci. Part A-1* **1966**, *4*, 2607-2616; DOI: 10.1002/pol.1966.150041023.

97) Fyfe, C.A.; Rudin, A.; Tchir, W. Application of High-Resolution ^{13}C NMR Spectroscopy Using Magic Angle Spinning Techniques to the Direct Investigation of Solid Cured Phenolic Resins. *J. Macromol.* **1980**, *13*, 1320-1322; **DOI:** 10.1021/ma60077a059.

98) Fyfe, C. A.; McKinnon, M. S.; Rudin, A.; Tchir, W. J. Investigation of the Mechanism of the Thermal Decomposition of Cured Phenolic Resins by High-Resolution ^{13}C CP/MAS Solid-State NMR Spectroscopy. *J. Macromolec.* **1983**, *16*, 1216-1219; DOI: 10.1021/ma00241a033.

99) Ehlers, G. F. L.; Fisch, K. R.; Powell, W. R. Thermal Degradation of Polymers with Phenylene Units in the Chain. I. Polyphenylenes and Poly(phenylene oxides). *J. Poly. Sci.* **1969**, *7*, 2931-2953; DOI: 10.1002/pol.1969.150071015.

100) Kundu, S.; Wang, Y.; Xia, W.; Muhler, M. Thermal Stability and Reducibility of Oxygen-Containing Functional Groups on Multiwalled Carbon Nanotube Surfaces: A Quantitative High-Resolution XPS and TPD/TPR Study. *J. Phys. Chem. C.* **2008**, *112*, 16869-16878; DOI: 10.1021/jp804413a.

101) Kuznetsova, A.; Popova, I.; Yates, J. T. Jr.; Bronikowski, M. J.; Huffman, C. B.; Liu, J.; Smalley, R. E.; Hwu, H. H.; Chen, J. G. Oxygen-Containing Functional Groups on Single-Wall Carbon Nanotubes: NEXAFS and Vibrational Spectroscopic Studies. *J. Am. Chem. Soc.* **2001**, *123*, 10699-10704; DOI: 10.1021/ja011021b.

102) Yamashita, Y.; Ouchi, K. A Study on Carbonization of Phenol-Formaldehyde Resin Labelled with Deuterium and ^{13}C. *Carbon* **1981**, *19*, 89-94; DOI: 10.1002/pol.1969.150071015.

103) Patel, P.; Hull, R. T.; McCabe, R. W.; Flath, D.; Grasmeder, J.; Percy, M. Mechanism of Thermal Decomposition of Poly (Ether Ether Ketone)) (PEEK) From a Review of Decomposition Studies. *J. Polym. Degrad. Stab.* **2010**, *95*, 709-718; DOI: 10.1016/j.polymdegradstab.2010.01.024.

104) Talyzin, A. V.; Luzan, S. M.; Leifer, K.; Akhtar, S.; Fetzer, J.; Cataldo, F.; Tysbin, Y. O.; Tai, C. W.; Dzwilewski, A; Moons, E. Coronene Fusion by Heat Treatment: Road to Nanographenes. *J. Phys. Chem. C.* **2011**, *115*, 13207-; DOI: 10.1021/jp2028627.

105) Lochte, H. W.; Strauss, E. L.; Conley, R. T. The Thermo-Oxidative Degradation of Phenol-Formaldehyde Polycondensates: Thermogravimetric and Elemental Composition Studies of Char Formation. *J. Appl. Polym. Sci.* **1965**, *9*, 2799-2810; DOI: 10.1002/app.1965.070090814.

106) Sobera, M.; Hepter, J. Pyrolysis-Gas Chromatography-Mass Spectrometry of Cured Phenolic Resins. *J. Chromat. A* **2003**, *993*, 131-135; DOI: 10.1016/S0021-9673(03)003881-1.

107) Zhang, H.; Fonseca, A. F.; Cho, K. Tailoring Thermal Transport Property of Graphene through Oxygen Functionalization. *J. Phys. Chem. C.* **2014**, *118*, 1436-1442; DOI: 10.1021/jp4096369.

108) Zhao, W.; Wang, Y.; Wu, Z.; Wang, W.; Bi, K.; Liang, Z.; Yang, J.; Chen, Y.; Xu, Z.; Ni, Z. Defect-Engineered Heat Transport in Graphene: A Route to High Efficient Thermal Rectification. *Scientific Reports* **2015**, *5*, 11962; DOI: 10.1038/srep11962.

CHAPTER FIVE

PYROLYSIS OF EPOXY-NOVOLAC MATERIALS AS A FUNCTION OF TIME AND TEMPERATURE

Contribution of Authors and Co-Authors

Manuscript in Chapter 5: Pyrolysis of an Epoxy-Novolac Materials as a Function of Time and Temperature

Author: Brody K. Bessire

Contributions: Collected and analyzed data. Assisted in writing and editing manuscript.

Co-Author: Timothy K. Minton

Contributions: Assisted with data interpretation and edited manuscript.

Manuscript Information Page

Brody K. Bessire and Timothy K. Minton
The Journal of Analytical and Applied Pyrolysis

Status of Manuscript:
_X__ Prepared for submission to a peer-reviewed journal
____ Officially submitted to a peer-review journal
____ Accepted by a peer-reviewed journal
____ Published in a peer-reviewed journal

Manuscript is in preparation for submission to the Journal of Analytical and Applied Pyrolysis.

CHAPTER FIVE

PYROLYSIS OF EPOXY-NOVOLAC MATRERIALS AS A FUNCTION OF TIME AND TEMPERATURE

5.1 INTRODUCTION

Epoxy-novolac resins are important constituents in heritage thermal protection system (TPS) materials such as Avcoat.[41] Most pyrolysis experiments on epoxy-novolac ablative materials were performed during the 1960s and 1970s. This chapter describes experiments that are aimed at further understanding the thermal decomposition mechanism of a specific epoxy-novolac system (e.g., D.E.N. 438, NMA, and BDMA). During this era, molar yields from the pyrolysis processes of the epoxy-novolac system were performed using mass spectrometric techniques.[43,47-50,108] However, the studies suffered from some of the same shortcomings as the pyrolysis studies for phenolic based materials (see chapter 1.1). Thermal decomposition mechanisms have been proposed for this resin system, but they fail to explain the production of several small molecules (e.g., H_2, CH_4, and H_2O). Additionally, previous studies were not able to measure the full range of pyrolysis products as a function of heating rate.

Therefore, this chapter leverages the experience gained during the pyrolysis experiments described in chapters 3 and 4 of this thesis. The pyrolysis of an epoxy-novolac resin system is described here, along with a composite material made from the epoxy-novolac system and 5.60 wt% microballoons. A new method for heating samples was developed with the goal of minimizing uncertainties caused by thermal gradients. A new

vacuum apparatus was developed for these studies and is described in detail in chapter 2.5. Additionally, a change in the analysis method was implemented, because the epoxy-novolac systems that have a small number of pyrolysis species (see section 2.7)

5.2 EXPERIMENTAL METHODS

5.2.1 MATERIALS

The synthesis of epoxy-novolac samples and composite materials studied in chapter 5 of this thesis are described in detail in chapter 2.8.2-2.8.4. The preparation of methylcyclopentadiene (MCPD) is described in chapter 2.8.5.

5.2.2 EXPERIMENTAL CONFIGURATION

A new vacuum apparatus was constructed to perform pyrolysis measurements on epoxy-novolac samples. The basic set-up of the vacuum apparatus is described in chapter 2.5 of this thesis. Figure 5.1 helps to illustrate the experimental configuration of the apparatus during testing of the epoxy-novolac and composite resin samples.

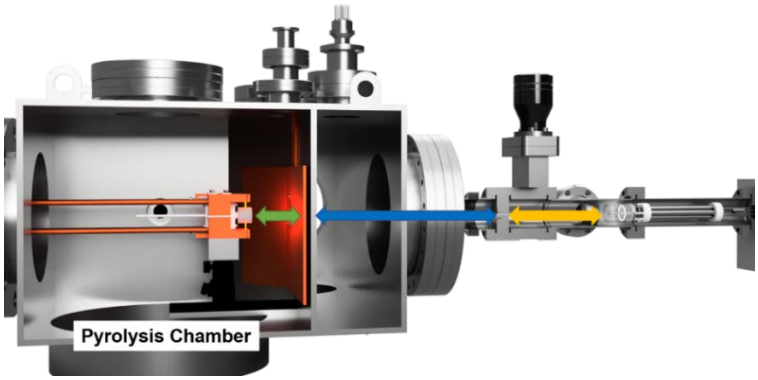

Figure 5.1. Cutaway figure of the small vacuum apparatus illustrating the critical dimensions of the experimental configuration.

The sample mount was secured in the pyrolysis chamber so that the distance between the front face of the sample and the front of the copper aperture (green arrow) was 31.8 mm. The sample mount is described in detail in chapter 2.6.2. Before the start of each experiment, the pyrolysis chamber and differential chamber were pumped down to 9 x 10^{-7} and 2 x 10^{-7} Torr, respectively. Both chambers are pumped by turbomolecular pumps (see chapter 2.5). The distance between the copper aperture and the second aperture (blue arrow) was 279 mm. Finally, the distance between the second aperture and the front of the repeller cage of the RGA (yellow arrow) measured 127 mm. The RGA was pumped by a large ion pump (Varian model RVA-220-TR-O, 200 l s^{-1}) and the base pressure near the ionizer was kept below 1 x 10^{-8} Torr. The first copper aperture measured 3.18 mm in diameter and the second aperture measured 4.00 mm in diameter. The RGA was kept at the following settings: emission current (1.0 mA), focus voltage (-90 V), electron energy (70 eV), and ion energy (12 eV). The RGA is equipped with a Faraday cup, and it was used as the detector for the experiments described in this chapter of the thesis. The pyrolysis studies in this chapter utilized a new heating technique that was developed to decrease the thermal gradient across the sample during testing. The new heating method is described in detail in chapter 2.6.2 of this thesis.

5.2.3. DETECTION SENSITIVITY CORRECTION FACTOR CALIBRATION

The detection sensitivity of the mass spectrometer is the product of the ionization efficiency in the ionizer, the transmission efficiency of ions through the quadrupole mass filter, and any ion mass dependent gain in the ion detector. To adjust the offset that results from these factors, a method was developed to derive sensitivity correction factors. The

method begins by calibrating the RGA against a standard compound such as carbon monoxide. The next step is to introduce a mixture of the standard and an analyte compound at a known pressure ratio into the mass spectrometer. If the pressure ratio measured by the mass spectrometer is different than the true pressure ratio, a detection sensitivity correction factor is calculated so that when it is multiplied against the measured pressure ratio, the true pressure is realized.

The pyrolysis of the epoxy-novolac is expected to produce four permanent gases (e.g., H_2, CH_4, CO, CO_2). A mixture of these gases was introduced into the vacuum apparatus through a mass flow controller and a copper tube. The flow rate of the gas mixture was controlled by a mass flow controller (Sierra Instruments MicroTrak 101). A mass spectrum of the mixture was measured at six different flow rates (e.g., 4.0, 3.0, 2.0, 1.0, 0.5, and 0.1 sccm). A system of linear equations was solved (see chapter 2.7) to determine the mole fraction of each of the compounds in the mixture. The measured mole fraction did not match the known mole fraction because it did not account for the species-dependent detection sensitivity of the RGA. Detection sensitivity correction factors were calculated for each flow rate measurement so that the measured mole fraction of each compound matched the known mole fraction within 1%. The average detection sensitivity correction factor was calculated and is listed in Table 5.1 with ± 1σ errors based on the six measurements.

Additional experiments were designed to calculate detection sensitivity correction factors for condensable gases (e.g., MCPD and H_2O). H_2O was placed in a stainless-steel container, and then the container was attached to a gas manifold. The container was held

at a temperature (-17 °C) that produced 1.00 Torr of vapor pressure. CO was mixed into the gas manifold at a known pressure, and a mass spectrum of the mixture was measured with the RGA. The detection sensitivity correction factor for MCPD was measured using a variation of the previously described method. Vapor pressure data are not available in the literature for MCPD. Therefore, the method for measuring detection sensitivity correction factors was changed slightly. MCPD was placed in a stainless-steel container and held at -20 °C. The container was maintained at this temperature to keep the vapor pressure low and to keep MCPD from re-forming a dimer. MCPD vapor was introduced into the gas manifold through a needle valve, and the pressure was measured with a thermocouple gauge (678 mTorr). CO was introduced to the gas manifold at a pressure of 1990 mTorr, and the resulting mixture was measured by the RGA. Correction factors for condensable gases were calculated based on the difference between the known pressure ratio and the results from the fit of the mass spectrum for each compound. Detection sensitivity correction factors for MCPD and H_2O are listed in Table 5.1.

Table 5.1. Permanent and condensable gases that were detected from the pyrolysis of PICA. Corresponding correction factors were applied to obtain correct mole fractions from the coefficients of a linear combination of individual mass spectra. Errors represent ±1σ from the mean.

Permanent Gases		Condensable Gases	
Species	Sensitivity C. F.	Species	Sensitivity C. F.
H_2	0.980 ± 0.060	H_2O	0.907
CH_4	1.47 ± 0.02	MCPD	0.590
CO	1.00 ± 0.00		
CO_2	1.12 ± 0.07		

5.2.4 COLLECTION OF PYROLYSIS DATA

Samples of the epoxy-novolac and composite materials were heated using a sample mount design that is described in detail in chapter 2.6.2 of this thesis. Samples of epoxy-novolac and the composite material were cured inside of a tantalum tube (see sections 2.8.2-2.8.3). The tantalum tube and sample are radiatively heated by Joule heating a tantalum coil that floats just above the sample tube. It is assumed that the sample tube will experience temperature gradients along the length of the tube for two reasons. First, it is expected that small temperature gradients result from the open spacing between each of the coil loops. Each loop is separated by 1.0 to 1.5 mm of open space. Additionally, the coil is heated resistively, and consequently, the middle loops of the coil are hotter than the coils on the edge of the sample tube. To minimize thermal gradient effects from the coil and increase heating efficiency an alumina mat was wrapped around the outside of the coil. The nominal thickness of the alumina mat was 5 mm. Temperature measurements were recorded with the use of a data acquisition device (National Instruments USB-TC01) that was incorporated into a LabVIEW heating program and a K-type thermocouple. For these experiments, the LabVIEW program was used to control a power supply (TDK-Lambda GEN 60-55) to deliver current in multiple stages. Nominal linear heating curves were measured when current was delivered equally over three stages. 18 amps and approximately 108 Watts were needed to heat samples from ambient to 1,000 °C.

Figure 5.2 shows a waterfall plot of a set of mass spectra that were collected at a nominal heating rate of 8.2 °C s^{-1}. Each mass spectrum was collected over a 1.9 second interval of time, and the resolution of the entire spectrum was maintained at 1 u according

to the $\Delta M_{10\%}$ definition. Initial investigations of the pyrolysis of the epoxy-novolac resin revealed that the major products of pyrolysis for this resin were less than 80 u. Higher *m/z* values of 91, 94, and 108 were observed at temperatures near 550 °C. It is believed that the signals for these peaks likely originate from fragments of the novolac backbone (e.g., phenol and cresol).[47] However, it was difficult to distinguish these three signals from the background, and the peaks were not always observable from one experiment to the next. For this reason, mass spectra were collected in the *m/z* range of 1.0 to 85 u in 0.1 u increments.

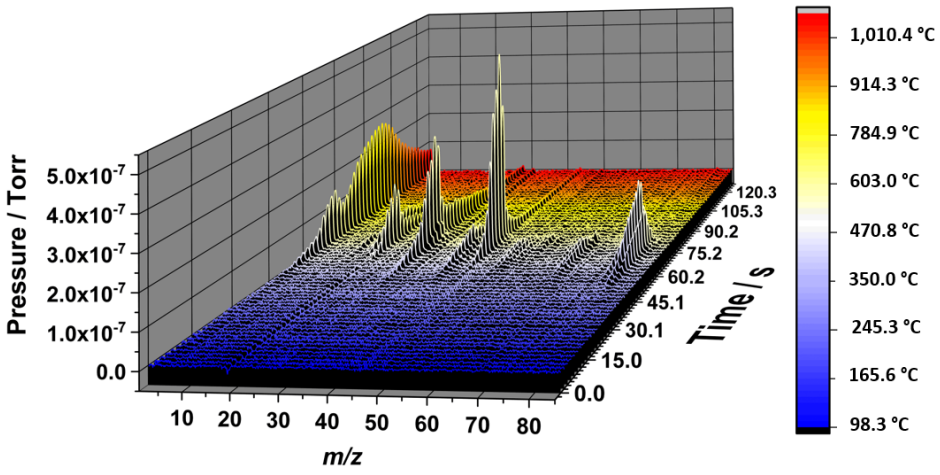

Figure 5.2. Mass spectra of the pyrolysis products collected from heating D.E.N. 438 (crosslinked with NMA) as a function of time. The nominal heating rate was 8.2 °C s^{-1}.

Total mass loss measurements of the epoxy-novolac resin are needed to calculate molar yields, mass yields, and TGA curves. First, a tantalum tube was weighed before filling it with resin, and then the resin was cured in the tantalum tube. After curing was

complete, the resin and tantalum tube were weighed once more to determine the initial mass of the resin. After pyrolysis was complete, the mass of the charred resin was measured without the tantalum tube to determine the overall mass loss.

5.2.5 COLLECTION OF TRADITIONAL TGA

Traditional thermogravimetric measurements were performed using a TA Discovery Series TGA. The same parameters were used for all the experiments mentioned in this section. For these experiments, flat samples were placed in a platinum pan. Pyrolysis was performed in a nitrogen atmosphere at a flow rate of 200 ml min^{-1}. Temperature measurements were made every 0.5 seconds, and the heating rate was set at 10 °C min^{-1}.

5.3 RESULTS AND ANALYSIS

5.3.1 ANALYSIS OF MASS SPECTRA

Table 5.1 lists 6 six compounds that constitute the major products of pyrolysis for D.E.N. 438 crosslinked with NMA. The list was compiled from observations made in the literature.[43, 47-50] The compounds listed in Table 5.1 represent neutral molecules, as it was assumed that any radical products would react to form stable species before they desorb from the material.

For this study, relative molar yields of pyrolysis products were calculated using the matrix inversion technique (see chapter 2.7). Experimental mass spectra were collected at 1.9 second intervals, at a specified heating rate, and over a range of *m/z* values that spanned 1.0 to 85 u. Mass spectra of each of the compounds in Table 5.1 were collected by passing a pure beam of gas through the RGA at the same mass spectrometer settings that were used

during pyrolysis experiments. Each of the reference mass spectra was normalized to the most abundant *m/z* value for a given compound. An invertible 6 x 6 matrix was constructed out of the reference mass spectra so that the columns of the matrix include the major *m/z* values of each species (e.g., *m/z* = 2, 16, 18, 28, 44, 79). Some of the species in Table 5.1 have significant overlap in their spectral signal at *m/z* = 18 and m/z = 28. To correct for this overlap, the relative ion abundance of daughter fragments from CH_4, H_2O, CO, and CO_2, at *m/z* = 18 and *m/z* = 28, were included in the reference matrix. The inverse of the matrix is multiplied by a 6 x 1 column matrix of experimentally measured *m/z* values and the resulting values are corrected for the detection sensitivity of the mass spectrometer using the values in Table 5.1. This process yields the partial pressures of each of the compounds that are present during pyrolysis at a certain temperature and time during the experiment. The measured partial pressure, P_i, of a pyrolysis product, is proportional to the integrated flux from the sample and can be thought of as the relative molar yield (n_i^r) of that product.[110]

5.3.2 CALCULATION OF ABSOLUTE MOLAR YIELDS, MASS YIELDS, SIMULATED TGA CURVES, AND TRADITIONAL TGA MEASUREMENTS

Absolute molar yields, mass yields, and simulated TGA curves are calculated using the formalism described in chapter 4.3.2 of this thesis. Temperature-dependent absolute molar yields of six compounds from the pyrolysis of D.E.N. 438 and the composite material are shown in Figs. 5.3 and 5.4, at nominal heating rates of 8.5 °C s^{-1} and 8.6 °C s^{-1}, respectively. It should be noted that these heating rates should be considered virtually identical due to the uncertainty in temperature measurement between experiments (see

plots and tables in Appendix C). Additional plots of temperature-dependent molar yields and heating curves are available in Appendix C. The plots in Appendix C show error bars for temperature and molar yields that are based on the standard deviation of four pyrolysis experiments. The heating profiles for these experiments show a departure from linearity. It is believed that at least some of the nonlinearity is the result of the nature of the indirect measurements of the sample temperature. Temperature measurements were made by a K-type thermocouple that was placed directly behind the sample and spot welded to the inside of the tantalum tube. At ~400 °C, the resin begins to decompose, and significant amounts of pyrolysis gases are evolved which cool the tube and lower the measured temperature. Nevertheless, the heating profiles are nearly linear, and it is believed that this slight departure from linearity has a small effect on the calculation of molar yields, mass yields, and simulated TGA.

Figures 5.3 and 5.4 show that the initial evolution of MCPD begins at lower temperatures (T ~ 300 °C) relative to the initial evolution of CO_2, CO, and H_2O (T_i ~ 400 °C). The peak evolution of CH_4 is delayed to higher temperatures (T ~ 500 °C) relative to CO_2, CO, and H_2O (T ~ 500 °C) and the evolution of H_2 peaks at even higher temperatures (T ~ 800 °C). The molar yield traces in Figs. 5.3 and 5.4 show sudden spikes and dips (e.g., MCPD, CO, and H_2). After testing was complete, the tantalum foil that surrounded the sample was removed, and the post-test sample was inspected under an optical microscope. Inspection of both materials (pure resin and composite) revealed relatively large voids, cracks, and pores. These features are believed to form when pockets of pyrolysis gases build up and explode from within the bulk of the resin. In addition to the

non-homogenous nature of the material, the buildup and release of pockets of pressure are believed to be the most likely the source for the apparent fluctuations in molar yield traces. This phenomenon is also considered the main source of uncertainty in the experiments as expressed by the error bars in Figs. 5.3 and 5.4.

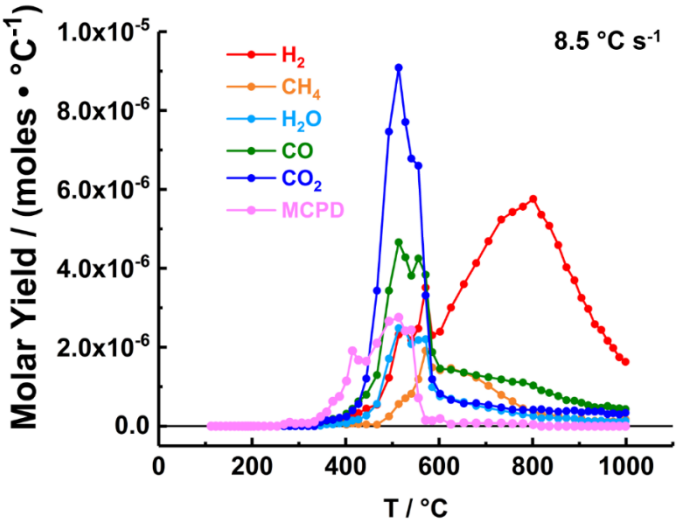

Figure 5.3. Molar yields of the six pyrolysis products measured during the pyrolysis of D.E.N. 438 at a nominal heating rate of 8.5 °C s^{-1}.

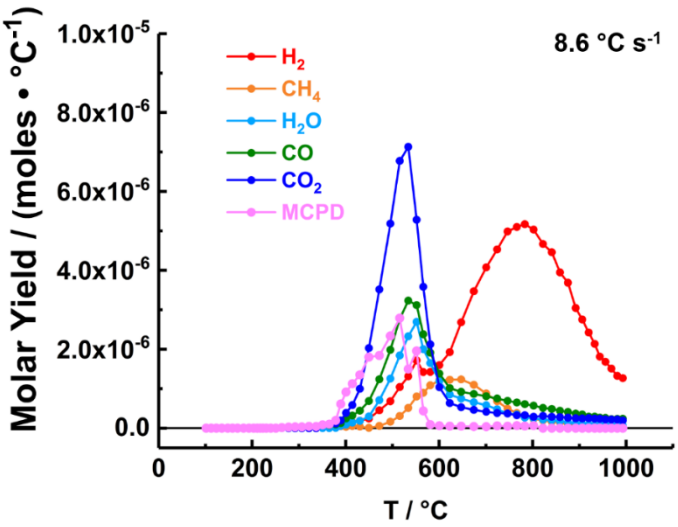

Figure 5.4. Molar yields of the six pyrolysis products measured during the pyrolysis of the composite material at a nominal heating rate of 8.6 °C s^{-1}.

Figures 5.5 and 5.6 show the temperature-dependent mass yields of the epoxy novolac and the composite material. Most of the mass loss occurs over a temperature range of 300 – 600 °C.

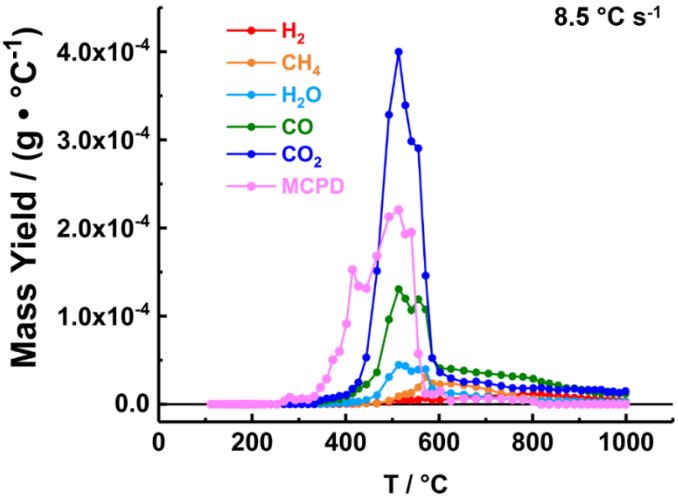

Figure 5.5. Mass yields of the six pyrolysis products measured during the pyrolysis of D.E.N. 438 at a nominal heating rate of 8.5 °C s^{-1}.

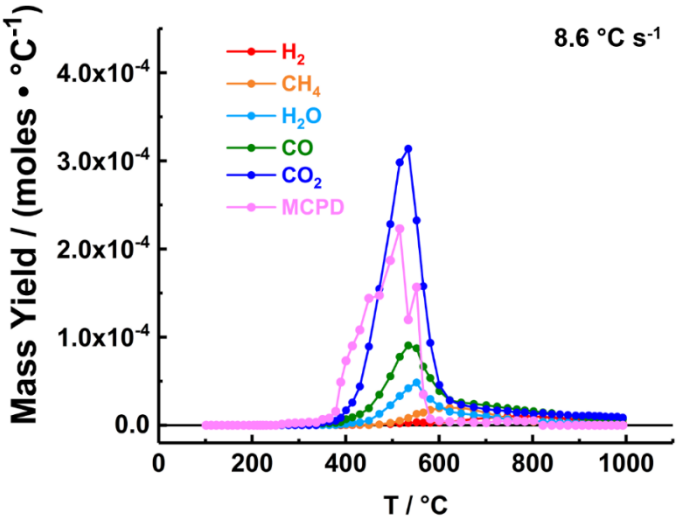

Figure 5.6. Mass yields of hydrogen, methane, carbon monoxide, and water, measured during the pyrolysis of PICA with a nominal heating rate of 25.0 °C s^{-1}.

Figure 5.7 shows simulated TGA curves of D.E.N. 438 (blue trace) and D.E.N. combined with 5.60 wt % phenolic microballoons (green trace) at nominal heating rates of 8.5 °C s^{-1} and 8.6 °C s^{-1}, respectively. Traditional TGA measurements were collected to benchmark the thermal degradation characteristics of the resin sample of this study against previous studies.[47] Figure 5.8 shows traditional TGA curves of the composite material (green trace), D.E.N. 438 (red trace), and precured D.E.N. 438 (blue trace) collected at a heating rate of 10 °C min^{-1}. A traditional TGA measurement was also performed on phenolic microballoons under the same conditions (orange trace). A single experiment was performed on each of the materials in Fig. 5.8.

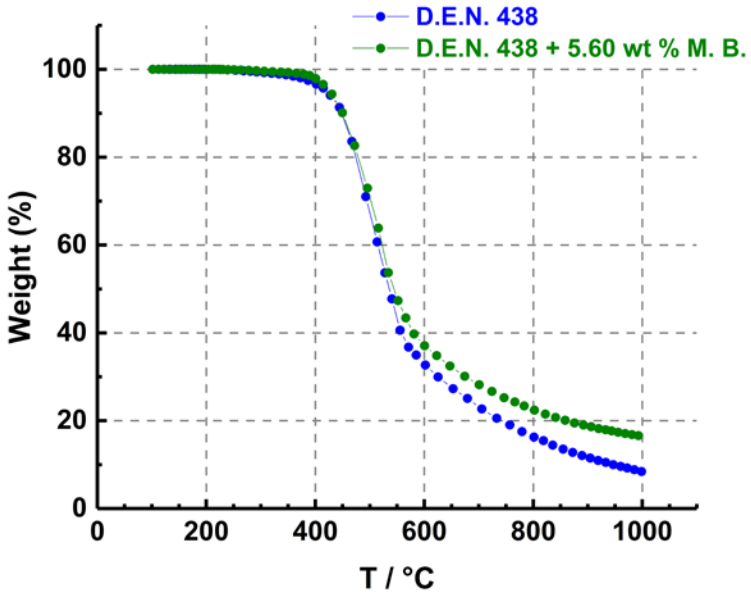

Figure 5.7. Simulated TGA curves of D.E.N. 438 (blue trace) and the composite material (green trace) at heating rates of 8.5 °C s^{-1} and 8.6 °C s^{-1}, respectively.

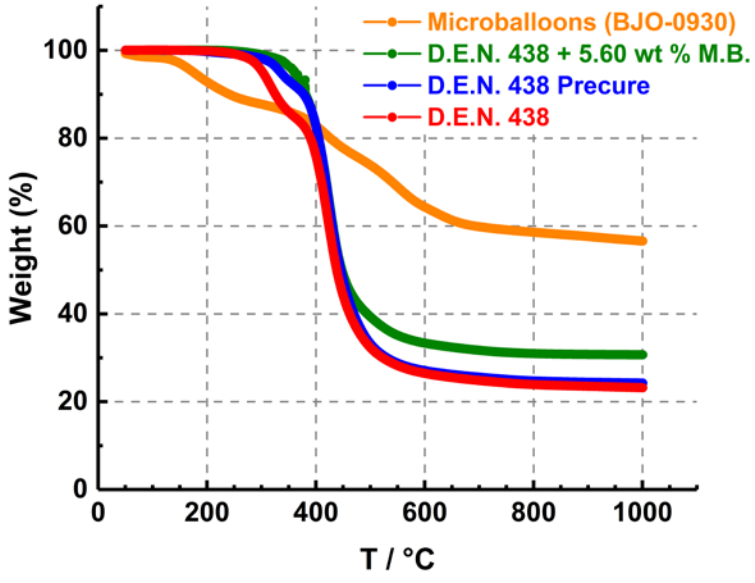

Figure 5.8. Traditional TGA curves of the D.E.N. 438 resin system (red and blue traces), the composite material (green trace), and phenolic microballoons (orange trace).

5.4 DISCUSSION

5.4.1 MASS LOSS (THERMOGRAVIMETRIC ANALYSIS)

Figure 5.9 shows the mass yield plot of D.E.N. 438 positioned underneath its corresponding simulated TGA curve. D.E.N. 438 loses almost 60% of its mass between 350 °C and 600 °C (region shaded in red). Most of the mass loss in this region is attributed to the evolution of MCPD, CO_2, CO, and H_2O to a lesser extent. The results show that thermal decomposition begins with the evolution of MCPD ($T \sim 350$ °C) followed by lighter molecules (CO_2, CO, and H_2O) that reach peak production near 500 °C. The evolution of CH_4 is delayed relative to the rest of the pyrolysis products ($T \sim 500$ °C), and its overall contribution to mass loss is relatively small. The contribution to mass loss from H_2 is almost negligible even though the material produces an abundance of H_2 in terms of molar yield. Additionally, there are non-negligible contributions to mass loss from permanent gases above 600 °C (region shaded in yellow). Mass yields for the composite material show qualitatively similar trends (Fig. 5.6).

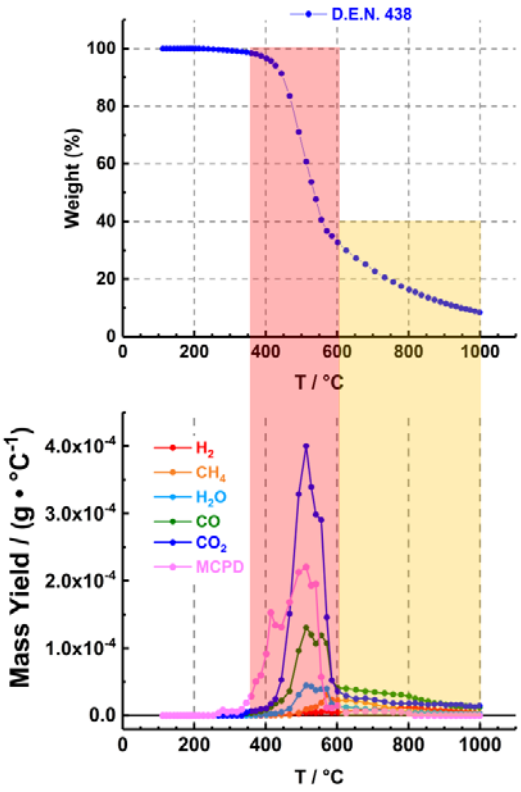

Figure 5.9. Simulated TGA curve of D.E.N. 438 compared with mass yields. The TGA curve and mass yields were calculated from data that were collected at a nominal heating rate of 8.5 °C s^{-1}.

Traditional TGA measurements (Fig. 5.9) were collected to benchmark the thermal response of the resin in this study against the thermal response of previous studies that used the exact same resin system (e.g., D.E.N. 438, NMA, BDMA). Lee performed TGA of this resin system in a vacuum (0.2 Torr), at a heating rate of 10 °C min^{-1}, from ambient to 660 °C.[47] Lee's results show three distinct stages of mass loss. The first region of mass loss (T ~ 240 °C - 380 °C) has been attributed to the loss of monoester monoacid species (see Fig. 5.8, red trace) in the form of an anhydride and accounts for the first 20% of the overall mass loss.[43,47] Traditional TGA of the resin used for pyrolysis testing (Fig. 5.8, blue trace)

shows 10% mass loss from $T \sim 300$ °C - 350 °C. The lack of mass loss in this range of temperature can be attributed to the precure treatment of the resin before testing. Before resin samples were inserted into tantalum tubes, they were preheated to 150 °C for 2-3 minutes. This procedure was implemented to lower the viscosity of the resin so that it could be inserted into the tantalum tube. It is postulated that monoacid-monoester species form additional crosslinks or are lost as pyrolysis products during the precure. The red trace in Fig. 5.8 was collected on a sample of resin that did not undergo the precure treatment, and it shows the same low temperature trend observed by Lee. A traditional TGA measurement was also collected on the composite material (Fig. 5.8, green trace). The TGA curve for the composite material shows that mass loss begins at slightly higher temperatures relative to the precured resin and almost no contribution to mass loss from the monoester-monoacid species. It is hypothesized that the lack of mass loss in the composite material at this low temperature region results from the formation of additional ester bonds between residual monoester-monoacid species of the epoxy-novolac and hydroxyl functional groups of the phenolic microballoons.

Figure 5.7 shows simulated TGA curves for pyrolysis studies of D.E.N. 438 and D.E.N. 438 combined with 5.60 wt % microballoons. This figure shows that the overall mass loss for each material was 91.6 wt % and 83.4 wt %, respectively. Traditional TGA measurements show that the overall mass loss for D.E.N. 438 and the composite material were measured at 78.0 wt % and 69.8 wt %, respectively (Fig. 5.8). Clearly, the total mass loss for the pyrolysis experiments was about 10% greater than the experiments carried out using traditional techniques, which use a much lower heating rate. However, the magnitude

of the difference between the total mass loss of the pure epoxy-novolac and the composite material were identical for both techniques (8.2%). It is likely that the extra mass loss measured for the high heating rate experiments (8 °C s^{-1}) is the result of small particle ejection from the surface of the material. As previously mentioned, inspection of the post-test materials revealed relatively large pores. It is postulated that pockets of pyrolysis gas build up and explode when the resin is subjected to high rates of heating.

The data show that the char yield for the composite material was higher than the char yield of the pure resin. This result is not surprising because the composite material is manufactured by replacing a small portion of D.E.N. 438 with phenolic microballoons and it is well known that phenolic resins lose approximately half of their mass when pyrolyzed at temperatures that approach or exceed 1,000 °C.[12,81] If the overall mass loss for the composite material can be predicted by a simple rule of mixtures

$$W_T = W_{\mu.b.} X_{\mu.b.} + W_{E.N.} X_{E.N.} \quad (1)$$

where $W_{\mu.b.}$ and $W_{E.N.}$ represent the expected overall mass losses from phenolic microballoons and epoxy-novolac, respectively, and $X_{\mu.b.}$ and $X_{E.N.}$ represent the original mass fractions of the microballoons and epoxy novolac, respectively. Using 5.60 wt % for $W_{\mu.b.}$ and 94.4 wt % for $W_{E.N.}$, along with the expected char yield from the microballoons and epoxy-novolac (see Fig. 5.8), an overall mass loss of 76.1 wt % is predicted. However, the green trace in Fig. 5.8 shows that the composite material experiences a mass loss of 69.8 wt %. It is hypothesized that hydroxyl functional groups from the phenolic microballoons react with residual monoester-monoacid species or epoxy groups to form extra carbon-oxygen bonds that enhance the char yield of the composite material. It

should be noted that the simulated TGA curves in Fig. 5.7 are shifted to higher temperatures relative to the traditional TGA curves in Fig. 5.8 by ~50 °C. This apparent shift of the simulated TGA curve to higher temperatures may be the result of temperature gradients that are established across the tantalum tube. The thermocouple junction was spot welded at the interface between resin sample and the tantalum tube (see Fig. 2.14). It is likely that the tantalum foil heats up faster than the resin sample and as a result, the measured temperature is higher than the true temperature of the resin sample, especially at high rates of heating. It should also be noted that the endothermic decomposition process cooled the tantalum tube at lower temperatures. This effect is observed in the heating profile plots in appendix C.

Finally, there is a notable difference between the slopes of the simulated TGA and traditional TGA curves at $T \sim 500 - 550$ °C. The slower rate of mass loss in this region of temperature for the simulated TGA curve can be explained by a lack of signal from the novolac backbone. During the initial phases of testing, *m/z* values of 91, 94, and 108 were detected in this temperature range, but the signal was not always observable from one experiment to the next. An increase in detection sensitivity towards these heavy molecules would almost certainly increase the rate of mass loss in the simulated TGA curve in this temperature range, and the resulting TGA curve would more closely resemble the shape of the traditional TGA curve.

5.4.2 QUANTITATIVE MOLAR YIELDS AND THERMAL DECOMPOSITION MECHANISM

Figure 5.10 shows integrated molar yield ratios of CH_4, H_2O, CO, and CO_2, to MCPD. The plot was made by integrating the total molar yields of H_2O, CO, CO_2, and

MCPD, from Fig. 5.3, over a temperature range that spans 300 °C to 600 °C. Total molar yields of CH_4 were integrated from 500 °C to 800 °C. MCPD provides a good reference when inferring the thermal decomposition mechanism of the crosslink from these ratios because each crosslink that results from a reaction of NMA yields exactly one molecule of MCPD.

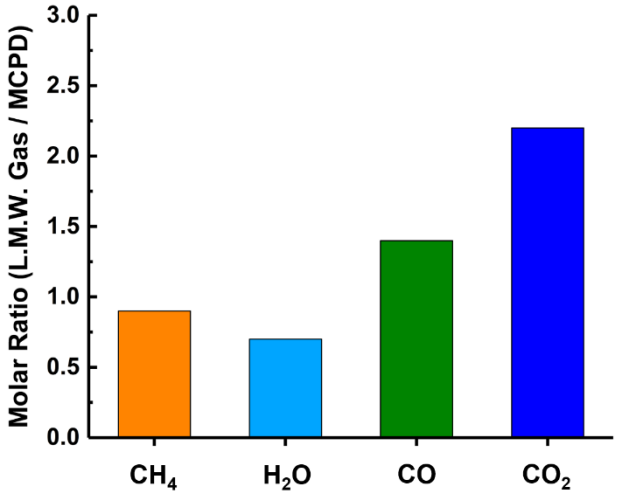

Figure 5.10. Molar yields ratios of the four pyrolysis products shown to MCPD, obtained with a nominal heating rate of 8.5 °C s^{-1}.

Past studies of the pyrolysis of D.E.N. 438 cured with NMA suggest that the decomposition of the resin occurs in two steps.[43,47-48] The two-step mechanism accepted throughout the literature is inferred from the observation that MCPD and CO_2, are the main products of pyrolysis. Our results are consistent with this observation, but our data suggest that there are additional steps in the thermal decomposition mechanism of this resin system. The following discussion proposes that two additional steps are necessary to describe the

entire decomposition process. Each step is based on the total integrated molar yield ratios from Fig. 5.10 and observations in the literature on the pyrolysis of similar materials. Each of the steps is bound by regions of temperature that overlap.

Figure 5.3 illustrates that in the first stage of pyrolysis (T ~ 350 °C – 550 °C) MCPD is evolved from the diester cross-link. The evolution of MCPD leaves an unsaturated carbon-carbon bond in between two carbonyl functional groups of a crosslink that resembles a short-chain unsaturated polyester. This mechanism was first proposed by Lee based on the appearance of a peak at m/z = 80 (molecular ion of MCPD) at temperatures of 350 °C and 450 °C.[47]

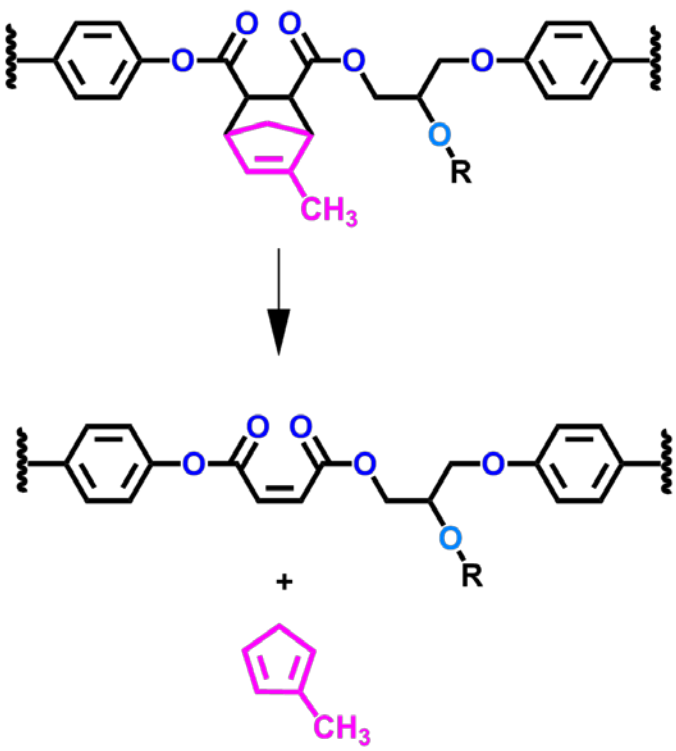

Figure 5.11. Loss of MCPD leads to formation of unsaturated diester crosslink.

The second stage of thermal decomposition ($T \sim 400$ °C – 600 °C) consists of the breakdown of the unsaturated diester crosslink in several steps to form small molecules (see Figs. 5.12 and 5.13). Our data show that H_2O is evolved in greatest quantity from 400 °C to 600 °C and in smaller quantities from 600 °C to 1000 °C. Figure 5.12 illustrates that H_2O is likely lost through a beta-hydrogen elimination reaction over the lower range of temperatures (400 °C – 600 °C). This figure shows that the dehydration reaction yields an additional unsaturated carbon-carbon bond on the unsaturated diester crosslink. This reaction assumes that the R group in Fig. 5.11 is a hydrogen atom. But Fig. 5.11 shows that the molar yield ratio of H_2O to MCPD is 0.7. Therefore, some of the R groups are likely to be additional diester cross-links (see Fig. 1.5). It is believed that this group forms in somewhat significant amounts during the curing of the resin system and is attributed to the decrease in the molar yield ratio of H_2O to MCPD over the same range of temperatures.

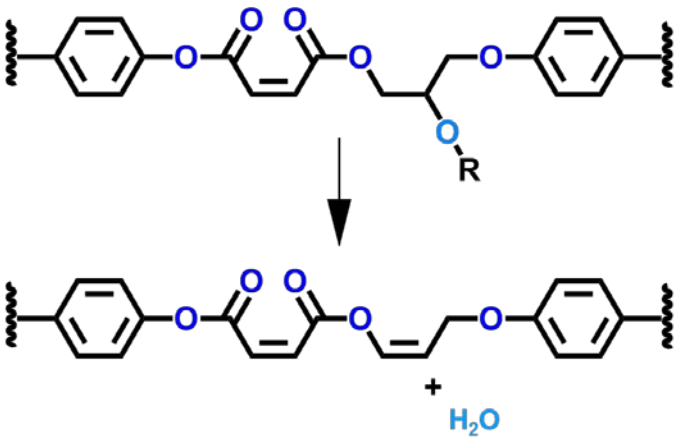

Figure 5.12. Loss of H_2O leads to formation of an additional unsaturated carbon-carbon bond in the diester crosslink.

Our data show that CO_2 and CO are evolved in significant amounts from 400 °C to 600 °C and in reduced quantities from 600 °C to 1000 °C. Figure 5.13 illustrates the

decomposition of the unsaturated diester into two separate oxygen containing heterocyclic rings attached to the benzene backbone of the novolac resin. This process likely begins with the cleavage of the unsaturated carbon-carbon bond between the two ester groups of the polymer crosslink via a beta hydrogen elimination reaction to yield an alkyne substituted ester and a carboxylic acid (see Fig. 5.14). These types of elimination reactions are well known for polyesters that have a hydrogen atom available at the beta position. [111-113]

The unsaturated carboxylic acid functional group (right side of Fig. 5.13) may decompose through an additional beta hydrogen elimination reaction to yield CO_2 and a terminal alkyne. The terminal alkyne is likely to form a cyclic ether as illustrated on the right side of reaction (A) in Fig. 5.13. In fact, the formation of cyclic ethers from the thermal decomposition of aliphatic esters were suggested by Goldfarb and McGuchan.[113] It is assumed that the cyclic ether decomposes at relatively low temperatures to form a molecule of CO and a vinyl group (Fig. 5.13, reaction (B)) as indicated by the molar yield distribution of CO in Fig. 5.3 from 400 °C to 600 °C. The vinyl group is most likely incorporated into the char.

Presumably, the alkyne substituted ester group can decompose into acetylene and CO_2, but this reaction is unlikely, as our mass spectra did not show a signal at $m/z = 26$. Likewise, ethene and CO_2 or ethane and CO_2 may form through H_2 addition reactions, but the lack of signal at $m/z = 27$ and $m/z = 30$ is an indication that these reactions are not occurring. Therefore, it is postulated here that the alkyne substituted ester bond forms a methyl substituted five-membered lactone ring (reaction (A), left side of Fig. 5.13). This

reaction would require the consumption of H_2. Figure 5.3 shows that the production of H_2 begins to rise at $T \sim 400$ °C and then levels off from $T \sim 500$ °C – 600 °C. The plateau in H_2 production supports the proposed mechanism in Fig. 5.13.

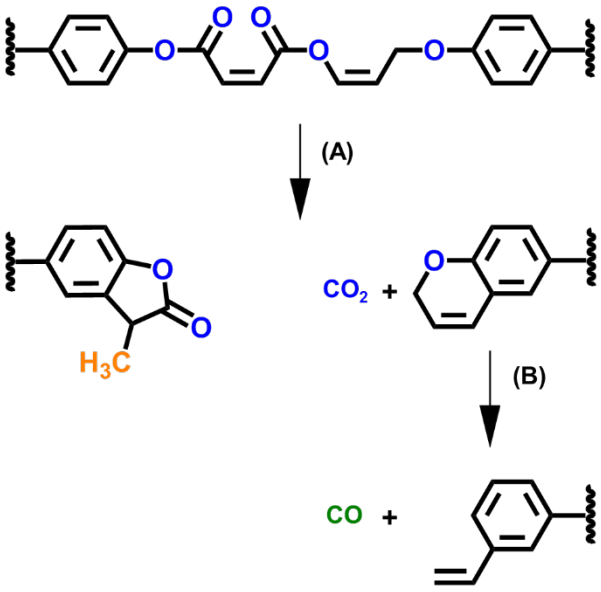

Figure 5.13. Diester decomposes via β-hydrogen elimination to form (A) heterocyclic rings and CO_2, and (B) the heterocyclic ether product decomposes to form CO.

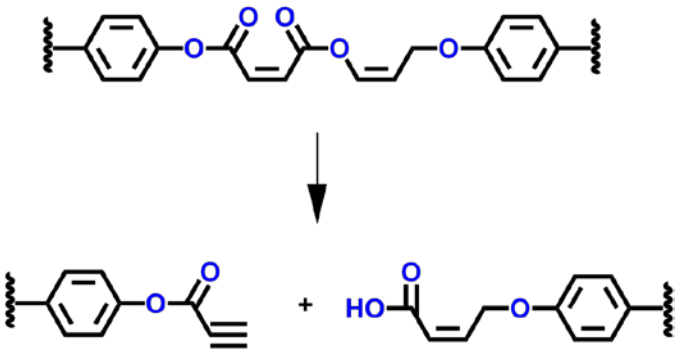

Figure 5.14 Cleavage of diester bond through beta hydrogen elimination to yield an alkyne substituted ester and a carboxylic acid.

Figure 5.3 shows that H_2, CH_4, CO, and CO_2 are evolved in significant quantities in the third stage of thermal decomposition ($T \sim$ 500 °C – 800 °C). Bailey and Bird observed that five and six membered lactone rings are thermally stable up to 590 °C.[114] Therefore, the five-membered lactone ring formed in the second stage of pyrolysis is assumed to break down at somewhat higher temperatures to yield CO_2 or CH_4. Figure 5.3 shows that the peak production of CH_4 is offset to higher temperatures relative to the peak production of CO_2. Gac measured the evolution of CH_4 in this temperature range ($T \sim$ 500 °C – 800 °C) via mass spectrometry, but a mechanism to explain the evolution of CH_4 has not been suggested in the literature.[50] Figure 5.15 shows the lactone ring breaking down according to two schemes. In scheme A the lactone ring decomposes to evolve a molecule of CO_2, and a vinyl substituted aromatic ring or the methyl group on the lactone ring is evolved, and the lactone ring stays intact. It is assumed that the vinyl substituted aromatic ring and the lactone ring are incorporated into the char. In scheme B the lactone ring breaks down to form a molecule of CH_4 and a molecule of CO_2. It is possible that a combination of the two schemes is responsible for the production of CH_4 and CO_2 with one or more of the schemes being dominant at lower temperatures. For instance, the reaction in scheme B and the first reaction in scheme A may be more probable at low temperatures than the second reaction in scheme A. Figure 5.10 shows that molar yield ratios for CO_2 to MCPD and CO to MCPD are 2.2 and 1.4, respectively. The mechanism suggests that roughly two molecules of CO_2 and 1 molecule of CO should be evolved from the cross-link over the course of stage two and three. Extra CO_2 and CO are likely produced during the thermal decomposition of the phenolic backbone.[110] The mechanism suggests that 1 molecule of

CH_4 should be produced for every cross-link in the resin, and Fig. 5.10 shows that the ratio of CH_4 to MCPD is 0.9.

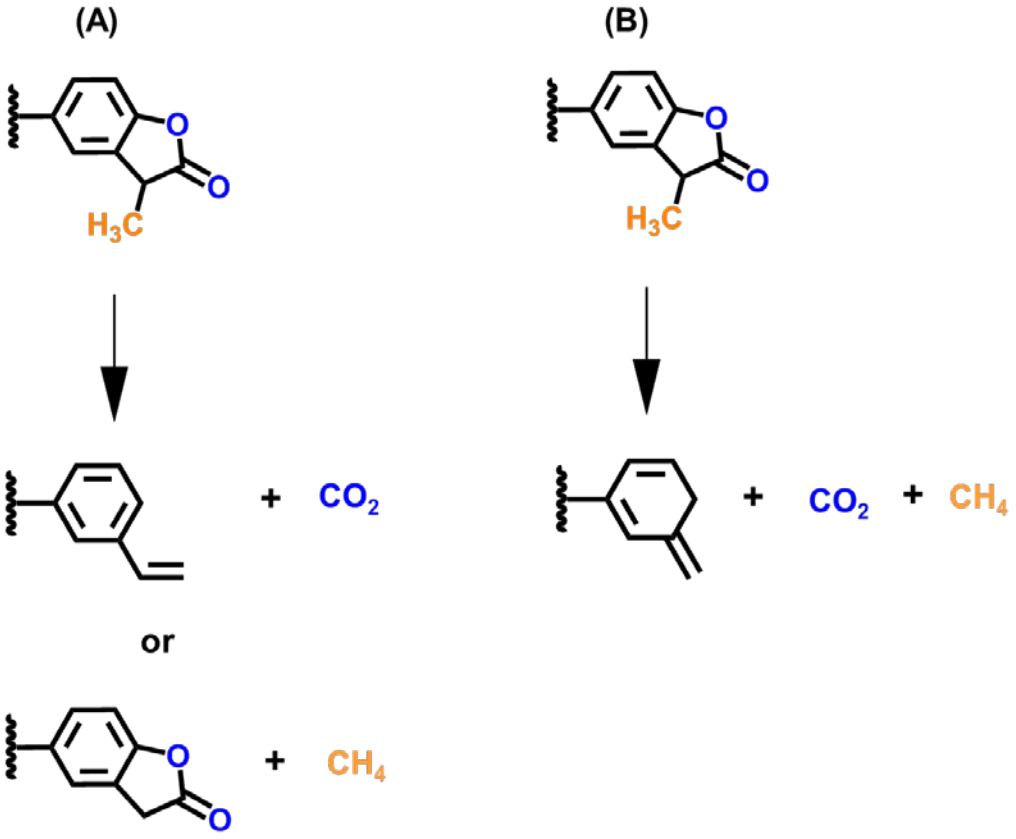

Figure 5.15. (A) Heterocyclic ring breaks down to form either CO_2 and vinyl substituted aromatic ring or loses CH_4 functional group. (B) Heterocyclic ring breaks down to form both CO_2 and CH_4 and aromatic hydrocarbon is formed. Aromatic molecules coalesce into growing domains of PAH's. Both mechanisms require the consumption of H_2.

The fourth stage of pyrolysis is marked by the production of H_2 at high temperature. The rate of H_2 production increases from 600 °C until 800 °C where it turns over and begins to decrease. The evolution of H_2 at these high temperatures is the result of the formation of growing domains of PAH's.[83,110] CO is evolved in significant quantities in this stage along with smaller quantities of H_2O and CO_2. The production of CO can be attributed to the

pyrolysis of dibenzofuran and xanthene molecules that were incorporated into the char at lower temperatures. These molecules are known to resist thermal decomposition up to 800 °C. The existence of these molecules is likely, as evidenced by peaks at *m/z* = 168 and 181 observed by Achar.[109] It should be noted that contributions to the total molar yield from the catalyst are likely to be negligible, as the amount of catalyst in the system is small compared to the rest of the resin system.

5.4.3 RATE-DEPENDENT MOLAR YIELDS OF PYROLYSIS PRODUCTS

An experiment was performed to determine if the epoxy-novolac resin exhibited the same rate dependent phenomena as observed during the pyrolysis testing of PICA. In chapter 4 it was demonstrated that PICA retains more oxygen in the char at higher rates of heating. This was evidenced by the release of small molecules (e.g., H_2, H_2O, CO, and CH_4) from a charred specimen subjected to pyrolysis at a slow rate of heating after the char had been produced by pyrolysis of the virgin material at a high heating rate. Another charred sample was tested in a similar manner but was produced from heating a virgin sample at slower rates. The resulting char only produced small quantities of H_2.

A similar experiment was performed by heating the virgin resin at 8 °C s^{-1} and re-heating the resulting char at a low heating rate (Fig. 5.16, (A)). Similarly, the virgin material was heated at 4 °C $s^{-1,}$ and the resulting char was re-heated at a low heating rate (Fig. 5.16, (B)). Figure 5.16 clearly shows that the pyrolysis of this epoxy-novolac resin system does not show the same heating rate dependent behavior as the phenolic resin in PICA.

Perhaps this result is not surprising considering the extent of crosslinking for the resin system. According to Fleming, the highest percentage of crosslinking is obtained when the epoxy-novolac resin is cured using 85 parts crosslinking agents to 100 parts epoxy-novolac (ratio used in this study).[43] This may mean that the epoxy-novolac resin does not have a chance to form additional crosslinks at lower temperatures in the form of ester bonds due to steric effects. It is also possible that the precure drives the formation of diester bonds to completion throughout the resin system, eliminating the possibility of competing reactions.

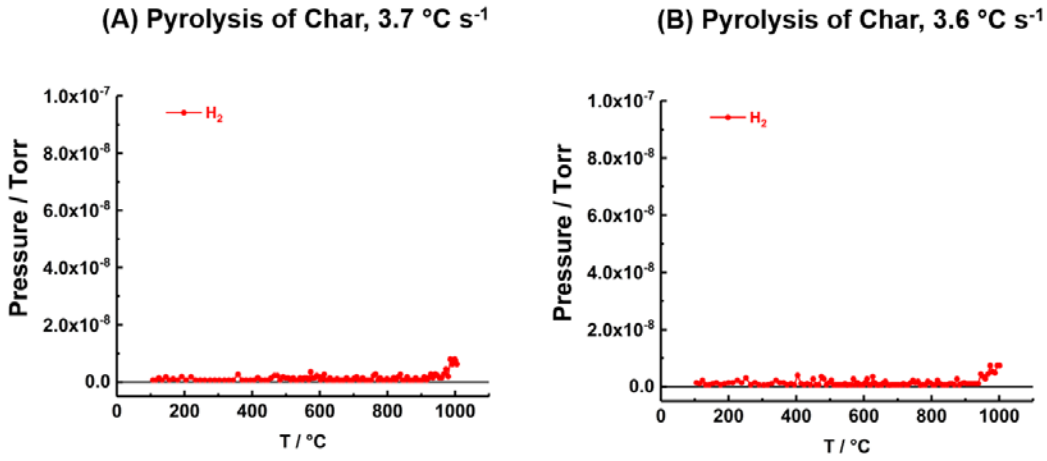

Figure 5.16 Pyrolysis of char samples that resulted from heating virgin samples of D.E.N. 438 at (A) 4 °C s^{-1} and (B) 8 °C s^{-1}.

5.5 CONCLUSION

Temperature-dependent molar yields of the 6 main pyrolysis products of D.E.N. 438 have been derived from *in situ* mass spectrometric measurements for two materials, at a

nominal heating rate of 8.0 °C s^{-1}, over the temperature range of 100 to 1,000 °C. Mass yields and simulated TGA curves have been derived from the molar yield data and measurements of the mass loss. Molar yields and simulated TGA data are available in appendix C for use in material response models. It is suggested that the thermal degradation of the epoxy-novolac resin system takes place in four temperature-dependent stages. The first step involves the loss of MCPD at low temperatures to produce an unsaturated polyester. The second step involves the dehydration reactions and the breakdown of the unsaturated polyester to form H_2O, CO, CO_2, and oxygen containing heterocyclic rings. In the third step, one of the heterocyclic rings breaks down to form combinations of CO_2 and CH_4. At the highest temperatures, domains of PAHs are formed as evidenced by the formation of H_2.

Simulated TGA curves show qualitative differences and quantitative similarities when compared to traditional TGA measurements on the same systems. Addition of 5.60 wt% phenolic microballoons results in a greater percentage of mass retention. The retention of mass is greater than predicted from a simple rule of mixtures. This effect is attributed to the formation of additional oxygen bonds (e.g., ester and ether bonds) between monoester-monoacid species, residual epoxy groups, and hydroxy groups on the phenolic microballoons.

The epoxy-novolac resin system does not show the same heating rate dependent phenomena as phenolic composite samples. The chars, resulting from heating the virgin resin at slow and fast heating rates, show only small amounts of H_2 production. The lack

of heating-rate dependent phenomena is attributed to the high degree of crosslinking that was imposed by the curing agents and method.

5.6 REFERENCES

12) Jackson, W. M.; Conley, R. T. High Temperature Oxidative Degradation of Phenol−Formaldehyde Polycondensates. *J. Appl. Polym. Sci.* **1964**, *8*, 2163−2193; DOI: 10.1002/app.1964.070080516.

41) Pavlosky, J. E.; Leger, L. G. St., Apollo Experience Report – Thermal Protection Subsystem. NASA TN D-7564. January **1974**.

43) Fleming, G. J. Mechanisms for Initiating Thermal Degradation of Certain Anhydride-Cured Epoxies. *J. Appl. Polym. Sci.* **1966**, 10, 18-13-1830.

47) Lee, L.-H. Mechanisms of Thermal Degradation of Phenolic Condensation Polymers. II. Thermal Stability and Degradation Schemes of Epoxy Resins. *J. Appl. Polym Sci. Part A.* **1965**, 3, 859-882.

48) Freeman, E. S.; Becker, A. J. Thermal Degradation of Nadic Methyl Anhydride-Crosslinked Novolac Epoxy Resin. *J. Polym. Sci. Part A.* **1968**, 6, 2829-2851.

49) Taylor, G. C.; Pendleton, E. L. Characterization of an Epoxy-Anhydride Ablative System Using Computer Treatment of Analytical Results. 1969, *J. Macromol. Sci. Part A Chem.* 1969, 3, 453-470.

50) Gac, N. A.; Spokes, G. N.; Benson, S. W. Thermal Degradation of Nadic Methyl Anhydride-Cured Epoxy Novolac. *J. Polym. Sci. Part A.* **1970,** 8, 593-608.

81) Wong, H. W.; Peck, J.; Assif, J.; Panerai, F.; Lachaud, J.; Mansour, N. N.; Detailed Analysis of Species Production from the Pyrolysis of the Phenolic Impregnated Carbon Ablator. *J. Anal. Appl. Polym. Sci.* **2016**, *122*, 258-267; DOI: 10.1016/j.jaap.2016.09.016

83) Bessire, B. K.; Lahankar, S. A.; Minton, T. K. Pyrolysis of Phenolic Impregnated Carbon Ablator (PICA). *ACS Appl. Mater. Interfaces.* **2015**, *7*, 1383-1395; DOI: 10.1021/am507816f.

109) Achar, B. N.; Fohlen, G. M.; HSU, M. S.; Parker, J. A. Mass Spectroscopy of Epoxylated Novolac Resin Cured with Phthalocyanine Tetraamines. *J. Polym. Sci.* **1984**, 22, 1471-1479.

110) Bessire, B. K.; Minton, T. K. Decomposition of Phenolic Impregnated Carbon Ablator (PICA) as a Function of Temperature and Heating Rate. ACS Appl. Mater. Interfaces **2017**, 9, 21422-21437

111) Ravey, M, Pryolysis of Unsaturated Polyester Resin Quantitative Aspects. *J. Polym. Sci.* **1983**, 21, 1-15.

112) DePuy, C. H.; King, R. W. Pyrolytic Cis Eliminations. Chem. Rev. **1960**, 60, 431-457.

113) Goldfarb, I. J.; McCuchan, R. Thermal Degradation of Polyesters. I Aliphatic Polymers. October **1968**, T. R. AFML-TR-68-182.

114) Bailey, W. J.; Bird, C. N. Pyrolysis of Esters. 27. Pyrolysis of Lactones. *J. Org. Chem.* **1977**, 42, 3895-3899.

CHAPTER SIX

CONCLUSION

6.1 SUMMARY

The experiments described in this thesis were designed to accomplish two primary goals. The first goal was to develop a methodology that would provide a technique to measure the molar yields of pyrolysis products as a function of time and temperature. An additional goal of the research was to gain new insight into the decomposition mechanisms of ablative composite materials and resins. To this end, mass spectrometric techniques were developed that allow for the *in situ* measurement of pyrolysis products from ablative composite materials and resins.

The methodologies described in this thesis provide a way to measure molar yields and mass yields as a function of time and temperature. This data can be used to simulate TGA curves which are useful when comparing data from the methodologies described in this thesis to traditional techniques. Two heating methods were developed to heat samples directly using Joule heating or indirectly using a radiative technique. Samples of PICA are easily heated from ambient to 1200 °C in a matter of seconds using the resistive heating method. However, significant thermal gradients are established across the sample over the course of the experiment which may add to uncertainties in the measurement of molar yields as well as the mechanisms that are deduced from this data. A new sample mount was designed with the intent of minimizing uncertainties from thermal gradient effects. The sample mount uses a resistively heated tantalum coil, wrapped with an alumina mat,

to radiatively heat the sample in a matter of seconds. It is postulated that the combination of the alumina mat and the tantalum coil reduces the lateral thermal gradient across the sample, but a radial gradient is still present.

The thermal decomposition of phenolic impregnated carbon ablator (PICA) has been investigated with the objective of measuring molar yields of pyrolysis products at heating rates that are relevant to flight conditions. These yields are discussed in light of prior work on the pyrolysis of various phenolic resins and phenolic/carbon composites. A consistent qualitative description of the decomposition pathways that occur in three stages of pyrolysis covering the temperature range from ~200 °C to ~1000 °C has emerged, with light gases being produced in the highest yields at all stages. H_2O is the dominant product in the first stage, with some CO_2 also being formed. CO is the main product during the second stage, and CH_4 is also significant during this stage. H_2 becomes dominant in the third stage, as the production of CO decreases. The heavier products (e.g., phenol, its methylated derivatives, and possibly even heavier species) have relatively low yields and desorb mainly during the second stage.

PICA has been pyrolyzed at heating rates of 3.1, 6.1, 12.7 and 25 °C s^{-1} that spanned a temperature range of 100 °C to1200 °C. The relative molar yields of 14 pyrolysis gases were obtained in conjunction with mass loss measurements. These measurements allowed for the calculation of absolute molar yields and mass yields as a function of heating rate, as well as the simulation of TGA curves.

The thermal decomposition of an epoxy-novolac resin system (e.g., D.E.N. 438, NMA, and BDMA) and a composite material have been discussed. A radiative heating

method was described that minimizes experimental uncertainties that may emerge from thermal gradients that are established across the samples as they experience high rates of heating. The molar yields and mass yields of the six dominant pyrolysis products have been measured at a heating rate of 8 °C s^{-1}. The total mass loss was measured for each experiment and was found to be greater than expected when compared to the total mass loss measured using a commercial TGA instrument. The additional mass loss was attributed, in part, to the thermal decomposition mechanism of the sample and the rate of heating. As the sample rapidly warms up, pockets of pyrolysis gas build up inside at the same temperature ($T \sim 500$ °C). During this process particles of the resin are blown away and add to the overall mass loss. Simulated TGA curves were derived from pyrolysis data but have a different shape when compared to traditional TGA measurements. This difference is attributed to the lack of signal from the novolac backbone that would be expected at temperatures that range from $T \sim 500$ °C to 550 °C.

A new thermal decomposition mechanism is proposed for the epoxy-novolac resin system and is driven by new observations made from the absolute molar yields measured during pyrolysis. The major products of pyrolysis come from the decomposition of the crosslink formed between the epoxy-novolac backbone and the anhydride. It is proposed that the thermal decomposition mechanism takes place in four temperature dependent stages that overlap. The first step is the loss of MCPD from the anhydride crosslink to form an unsaturated diester ($T \sim 350$ °C – 550 °C). In the second region of mass loss, the unsaturated diester begins to decompose through a series of steps that lead to thermally stable oxygen bearing heterocyclic molecules ($T \sim 400$ °C – 600 °C). The third region is

marked by the production of CH_4 ($T \sim 500$ °C to 800 °C). It is proposed that methyl groups are formed at low temperature during the formation of the thermally stable heterocyclic rings. The CH_4 is lost at high temperature when the heterocyclic rings break down to form additional small molecules (e.g., CO) and aromatic structures that are incorporated into the char. The fourth and final region is marked by the production of copious amounts of H_2, as the resin char coalesces into domains of PAHs ($T \sim 600 – 1000$ °C).

The thermal decomposition studies of phenolic based PICA materials and the epoxy-novolac resin give evidence that the pyrolysis process is dependent on heating rate. Pyrolysis studies of PICA show that the molar yields from pyrolysis do depend on the heating rate. This has been attributed to competition between mechanisms that compete at low temperature. The first reaction involves the condensation of hydroxyl functional groups to form carbon-carbon bonds or ether functional groups. The second reaction involves the breakdown of the methylene bridge between phenol monomers to yield phenol and its derivatives. The second decomposition reaction dominates at higher heating rates.

Inspection of post-test samples of the epoxy-novolac resin revealed relatively large pores that were ostensibly formed after pockets of pyrolysis gas erupted from within the resin. The formation of these pores were not observed in post-test samples from TGA experiments (heating rate = 10 °C min^{-1}). Therefore, it is postulated that the mechanism responsible for the release of gases from the resin is time-dependent. However, the mechanism that is responsible for this process is not known.

REFERENCES CITED

1) Anderson, J. D. *Hypersonic and High Temperature Gas Dynamics*. AIAA Education Series; Schetz, J. A., 2nd ed., AIAA: Reston, V.A. **2006**.

2) Chen, Y. K.; Milos, F. S. Ablation and Thermal Response Program for Spacecraft Heatshield Analysis. *J. Spacecr. Rockets* **1999**, *36*, 475-483; DOI: 10.2514/2.3469.

3) Mansour, N. N.; Lachuad, J.; Magin, T. E.; Muelenaere, J.; Chen, Y. K. High-Fidelity Charring Ablator Thermal Response Model. In *42nd AIAA Thermophysics Conference*; Honolulu, Hawaii. June 27-30, **2011**; DOI: 10.2514/6.2011-3124.

4) Omidy, A. D.; Panerai, F.: Lachaud, J. R.; Mansour, N. N.; Martin, A. Effects of Water Phase Change on the Material Response of Low-Density Carbon-Phenolic Ablators. *J. Thermophys. Heat Trans.* **2016**, *30*, 473-478; DOI: 10.2514/1.T4814.

5) Lachaud, J.; Magin, T. E.; Cozmuta, I.; Mansour, N. N. A Short Review of Ablative-Material Response Models and Simulation Tools, In *Proceedings of the 7th Aerothermodynamics Symposium*, European Space Agency, Brugge, Belgium, 9-12 May **2011**; ESA SP, 692.

6) Bahramian, B. R.; Kokabi, M.; Famili, M. H. N.; Beheshty, M. H. Ablation and Thermal Degradation Behavior of a Composite Based on Resole Type Resin: Process Modeling and Experimental. *Polymer* **2006**, *7*, 3661-3673; DOI: 10.1016/j.plymer.2006.03.049.

7) Henderson, J. B.; Tant, M. R.; Moore, G. R. Determination of Kinetic Parameters for the Thermal Decomposition of Phenolic Ablative Materials by a Multiple Heating Rate Method. *Thermochimica Acta*, **1981**, *44*, 253-264 DOI:10.1016/0040-6031(81)85019-8.

8) Trick, K. A.; Saliba, T. E.; Sandhu, S. S. A Kinetic Model of the Pyrolysis of Phenolic Resin in a Carbon/Phenolic Composite. *Carbon* **1997**, *35*, 393-401; DOI: 10.1016/S0008-6223(97)89610-8

9) Wendlandt, W. W. *Thermal Analysis*. *Chemical Analysis Series, Vol. 19*; Elving, P.J.; Winefordner, J. D., Eds.; 3rd ed., John Wiley and Sons, New York, N.Y. **1984**.

10) Baer, A. D.; Hedges, J. H.; Seader, J. D.; Jayakar, K. M.; Wojcik, L. H. Polymer Pyrolysis over a Wide Range of Heating Rates. *AIAA J.* **1977**, *15*, 1398-1404; DOI: 10.2514/3.7435.

11) Boyle, M. E.; Cozzens, R. F.; McPherson, J. A. The Effect of High Heating Rate on the Pyrolysis of Carbon/Phenolic Composites. NRL Memorandum Report 6343, ADA198052, Naval Research Lab: Washington, D.C., September **1988**.

12) Jackson, W. M.; Conley, R. T. High Temperature Oxidative Degradation of Phenol−Formaldehyde Polycondensates. *J. Appl. Polym. Sci.* **1964**, *8*, 2163−2193; DOI: 10.1002/app.1964.070080516.

13) Stokes, E. H. Kinetics of Pyrolysis Mass Loss from Cured Phenolic Resin. J. *Themophys. Heat Trans.* **1995**, *9*, 352-358; DOI: 10.2514/3.667.

14) Natali, M.; Kenny, J. M.; Torre, L. Science and Technology of Polymeric Ablative Materials for Thermal Protection Systems and Propulsion Devices: A Review. *Prog. Mater. Sci.* **2016**, 84, 192-275

15) Laub, B.; Venkatapathy, E. Thermal Protection System Technology and Facility Needs for Demanding Future Planetary Missions. *International Workshop on Planetary Probe Atmospheric Entry and Descent Trajectory Analysis and Science*. Lisbon, Portugal, 6-9, October 2003.

16) Johnson, S. M., Gasch, M. J., Leiser, D., Stewart, D. Jr., Stackpoole, M., Thornton, J., Espinoza, C. Development of New TPS at NASA Ames Research Center. In *15th AIAA International Space Planes and Hypersonic Systems and Technologies Conference*, Dayton, Ohio, 28 April – 1 May, 2008.

17) Feldman, J.; Gasch, M. J.; Poteet., C. C.; Szalai, C. Advanced Rigid Ablative Thermal Protection Systems. *50th AIAA Aerospace Sciences Meeting including the New Horizons Forum and Aerospace Exposition*, Nashville, TN, January 9-12, 2012. DOI: 10.2514/6.2012-472

18) Milos, F. S.; Chen, Y-K.; Mahzari, M. Arcjet Tests and Thermal Response Analysis for Dual-Layer Woven Carbon Phenolic. In *47th AIAA Thermophysics Conference* Denver, Colorado, June 5-9, 2017.

19) Tran, H. K.; Johnson, C. E.; Rasky, D. J.; Hui, F. C. L.; Hsu, M.; Chen, Y. K. Phenolic Impregnated Carbon Ablators (PICA) for Discovery Class Missions. *31st AIAA Thermophysics Conference*, New Orleans, LA, June 17-20, 1996. DOI: 10.2514/6.1996-1911

20) Beck, R. A. S.; Driver, D. M.; Wright, M. J.; Hwang, H. H.; Edquist, K. T; Sepka, S. A. Development of the Mars Science Laboratory Heat Shield Thermal Protection System. *J. Spacecr. Rockets* **2014**, *51*, 1139-1150. DOI: 10.2514/1.A32635

21) Szalai, C.; Slimko, E.; Hoffman, P. Mars Science Laboratory Heat Shield Development, Implementation, and Lessons Learned. *J. Spacecr. Rockets* **2014**, *51*, 1167-1173. DOI: 10.2514/1.A32673

22) Trumble, K. A.; Cozmuta, I.; Sepka, S.; Jenniskens, P.; Winter, M. Postflight Aerothermal Analysis of Stardust Sample Return Capsule. *J. Spacecr. Rockets* **2010**, *47*, 765-774. DOI: 10.2514/1.41514

23) Bose, D.; White, T.; Santos, J. A.; Feldman, J.; Mahzari, M.; Olson, M.; Laub, B. Initial Assessment of Mars Science Laboratory Heat Shield Instrumentation and Flight Data. *51st AIAA Aerospace Sciences Meeting including the New Horizons Forum and Aerospace Exposition*, Grapevine, TX, January 7-10, 2013. DOI: 10.2514/6.201-908

24) Space X website, http://www.spacex.com/news/2013/02/09/spacexs-dragon-spacecraft-successfully-re-enters-orbit (accessed Nov 3, 2014).

25) Titov, E. V.; Kumar, R.; Levin, D. A.; Anderson, B. P. Modeling the Crack Growth in the AVCOAT Heat Shield. *49th AIAA Aerospace Sciences Meeting including the New Horizons Forum and Aerospace Exposition*, Orlando, FL, January 4-7, 2011. DOI: 10.2514-6.2011-137

26) Crouch, R. K.; Walberg, G. D. An Investigation of Ablation Behavior of Avcoat 5026/29M Over a Wide Range of Thermal Environments. NASA TM X-1778; NASA: Washington, D. C., April 1969.

27) Wright, M. J.; Hughes, M.; Calomino, A.; Barnhardt, M. D.; An Overview of Technology Investments in the NASA Entry Systems Modelling Project. In *53rd AIAA Aerospace Sciences Meeting*; AIAA SciTech Forum, January 5-9, 2015.

28) Pilato, L., Resin Chemistry. Phenolic Resins: A Century of Progress. Springer, New York, 2010, pp. 41-45. DOI: 10.1007/978-3-642-04714-5

29) Jackson, W. M.; Conley, R. T. High Temperature Oxidative Degradation of Phenol–Formaldehyde Polycondensates. *J. App. Polym. Sci.* **1964**, *8*, 2163-219. DOI: 10.1002/app.1964.070080516

30) Morterra, C.; Low, M. J. D. IR Studies of Carbons-VII. The Pyrolysis of a Phenol-Formaldehyde Resin. *Carbon* **1985**, *23*, 525-530. DOI: 10.1016/0008-6223(85)90088-0

31) Ouchi, K.; Honda, H. Pyrolysis of Coal 1. Thermal Cracking of Phenol-Formaldehyde Resins Taken as Coal Models. *Fuel* **1959**, *38*, 429-443. DOI: 10.1021/la00063a010

32) Parker, J. A.; Winkler, E.L.. The Effects of Molecular Structure on the Thermochemical Properties of Phenolics and Related Polymers. NASA TR R-276, November **1967**.

33) Trick, K. A.; Saliba, T. A. Mechanisms of the Pyrolysis of Phenolic Resin in a Carbon/Phenolic Composite. *Carbon* **1995**, *33*, 1509-1515. DOI: 10.1016/0008-6223(95)00092-R

34) Ouchi, K. Infra-Red Study of Structural Changes During the Pyrolysis of a Phenol-Formaldehyde Resin. *Carbon* **1966**, *4*, 59-66. DOI: 10.1016/0008-6223(66)90009-1

35) Friedman, H. L. Products of Flash Pyrolysis of Phenol-Formaldehyde by Time-of-Flight Mass Spectroscopy. *J. App. Polym. Sci*. **1965**, *9*, 651-662. DOI: 10.1002/app. 1965.070090225

36) Shulman, G. P.; Lochte, H. W. Thermal Degradation of Polymers. II. Mass Spectrometric Thermal Analysis of Phenol-Formaldehyde Polycondensates. *J. App. Polym. Sci.* **1966**, *10*, 619-635. DOI: 10.1002/app.1966.070100407

37) Sykes, G. F. Decomposition Characteristics of a Char-Forming Phenolic Polymer Used For Ablative Composites. NASA TN D-3810, February, **1967**.

38) Wong, H. W.; Peck, J.; Edwards, R.; Reinisch, G.; Lachaud, J.; and Mansour, N. N. Measurement of Pyrolysis Products from Phenolic Polymer Thermal Decomposition. AIAA Science and Technology Forum and Exposition, National Harbor, MD, January, 2014. DOI: 10.2514/6.2014-1388

39) Sobera, M.; Hepter, J. Pyrolysis-Gas Chromatography-Mass Spectrometry of Cured Phenolic Resins. *J. Chromat. A* **2003**, *993*, 131-135. DOI: 10.1016/S0021-9673(03)003881-1

40) Bennett, A.; Payne., D. R.; Court., R. W. Pyrolytic and Elemental Analysis of Decomposition Products from a Phenolic Resin. *Macrom. Symp*. **2014**, *339*, 38-47. DOI: 10.1002/masy.201300136

41) Pavlosky, J. E.; Leger, L. G. St., Apollo Experience Report – Thermal Protection Subsystem. NASA TN D-7564. January **1974**.

42) Fischer, R. F.; Polyesters from Epoxides and Anhydrides. *J. Polym. Sci.* **1960**, 44, 155-172.

43) Fleming, G. J. Mechanisms for Initiating Thermal Degradation of Certain Anhydride-Cured Epoxies. *J. Appl. Polym. Sci.* **1966**, 10, 18-13-1830.

44) Tanaka, Y.; Kakiuchi, H. Study of Epoxy Compounds. Part I. Curing Reactions of Epoxy Resin and Acid Anhydride with Amine and Alcohol as Catalyst. J. Appl. Polym. Sci. **1963**, 7, 1063-1081.

45) Levchik. S. V.; Weil. E. D. Thermal decomposition, combustion and flame-retardancy of epoxy resins – a review of the literature. *Polym. Int.* 2004, **53**, 1901-1929.

46) Anderson, H. C. Thermal Degradation of Epoxide Polymers. *J. Appl. Polym. Sci.* **1962**, 6, 484-488.

47) Lee, L.-H. Mechanisms of Thermal Degradation of Phenolic Condensation Polymers. II. Thermal Stability and Degradation Schemes of Epoxy Resins. *J. Appl. Polym Sci. Part A.* **1965**, 3, 859-882.

48) Freeman, E. S.; Becker, A. J. Thermal Degradation of Nadic Methyl Anhydride-Crosslinked Novolac Epoxy Resin. *J. Polym. Sci. Part A.* **1968**, 6, 2829-2851.

49) Taylor, G. C.; Pendleton, E. L. Characterization of an Epoxy-Anhydride Ablative System Using Computer Treatment of Analytical Results. 1969, *J. Macromol. Sci. Part A Chem.* 1969, 3, 453-470.

50) Gac, N. A.; Spokes, G. N.; Benson, S. W. Thermal Degradation of Nadic Methyl Anhydride-Cured Epoxy Novolac. *J. Polym. Sci. Part A.* **1970,** 8, 593-608.

51) Ehlert, T. C. Determination of Transmission Characteristics in Mass Filters *J. Phys. E*., **1969**, 3, 237-239.

52) Lieszkovsky, L.; Filippelli, A. R.; Tilford, C. R.; Metrological Characteristics of a Group of Quadrupole Partial Pressure Analyzers. J. Vac. Sci. Technol. A **1990**, 8, 3838-3854.

53) Zhang, J.; Garton. D. J.; Minton., T. K. Reactive and Inelastic Scattering Dynamics of Hyperthermal Oxygen Atoms on a Saturated Hydrocarbon Surface. *J. Chem. Phys*. **2002**, *117*, 6239-6251. DOI: 10.1063/1.1460858

54) Garton, D. J.; Brunsvold, A. L.; Minton, T. K.; Troya, D.; Maiti, B.; Schatz, G. Experimental and Theoretical Investigations of the Inelastic and Reactive Scattering Dynamics of O (^{3}P) + D_2. *J. Phys. Chem. A* **2006**, *10*, 1327-1341. DOI: 10.1021/jp054053k

55) Lee, Y. T.; McDonald, J. D.; LeBreton, P. R.; Herschbach, D. R. Molecular Beam Reactive Scattering Apparatus with Electron Bombardment Detector. *Rev. Sci. Instrum.* **1969**, *40*, 1402-1408. DOI: 10.1063/1.1683809

56) Brink, G. O.; Electron Bombardment Molecular Beam Detector. *Rev. Sci. Instrum.* **1966**, 37, 857-860.

57) Daly, N. R.; Scintillation Type Mass Spectrometer Ion Detector. *Rev. Sci. Instrum.* **1960**, 31, 264-267.

58) Moore, *J. H. Building Scientific Apparatus A Practical Guide to Design and Construction*, 2nd ed.; Addison-Wesley Redwood City, CA. **1989**.

59) McLafferty, F. W. *Interpretation of Mass Spectra*, 4th ed. Kelly, A., Ed.; University Science Books, Sausalito, CA, **1993**.

60) Skoog, D. A.; Holler, F. J.; Crouch, S. R.; *Principles of Instrumental Analysis*. 6th ed. Kiselica, S. Ed.; Thomson Brooks/Cole, Belmont, CA, **2007**.

61) Lilienkamp, R. H. Methods of Determining Residual Gas Composition from Residual Gas Analyzer Data. In *5th Space Simulation Symposium*, ASTM/IES/AIAA Space Simulation Conference, 14-16 September, 151-164, **1970**.

62) Darkwa, J.; Giolando, D. M.; Murphy, C. J.; Rauchfuss, T. B.; BIS(η^5-Methylcyclopentadienyl) Titanium Pentasulfide, BIS(η^5-Methylcyclopentadienyl)-Divanadium Pentasulfide, and BIS(η^5-Methylcyclopentadienyl) Divanadium Tetrasulfide. Inorg. Synth. **2007**, 27, 51-58.

63) Hankey, W. L., *Re-Entry Aerodynamics*. AIAA Education Series; Przemieniecki, J. S., Ed., Washington, D.C., 1988.

64) Diaconis, N. S.; Fanucci, J. B.; Sutton, G. W. The Heat Protection Potential of Several Ablation Materials for Satellite and Ballistic Re-Entry into the Earth's Atmosphere. *Planet. Space. Sci.* **1961**, *4*, 463-478. DOI: 10.1016/0032-0633(61)90152-0

65) Ungar, E. W. Ablation Thermal Protection Systems Suitability of Ablation Systems to Thermal Protection Depends on Complex Physical and Chemical Processes. *Science* **1967**, *158*, 740-744. DOI: 10.1126/science.158.3802.740

66) April, G. C.; Pike, R. W.; del Valle, E. G. Modeling Reacting Gas Flow in the Char Layer of an Ablator. *AIAA J.* **1971**, *9*, 1113-1119. DOI: 10.2514/3.6330

67) Kendal, R. M.; Bartlett, E. P.; Rindal, R. A.; Moyer, C. B. An Analysis of the Coupled Chemically Reacting Boundary Layer and Charring Ablator: Part 1. *NASA CR-1060* (1968).

68) Lachaud, J.; Cozmuta, I.; Mansour, N. N. Multiscale Approach to Ablation Modeling of Phenolic Impregnated Carbon Ablators. *J. Spacecr. Rockets* **2010**, *47*, 910-921. DOI: 10.2514/1.42681

69) Alexander, W. A.; Wiens, J. P.; Minton, T. K.; Nathanson, G. M. Reactions of Solvated Electrons Initiated by Sodium Atom Ionization at the Vacuum-Liquid Interface. *Science* **2012**, *35*, 1072-1075. DOI: 10.1126/science.1215956

70) Stein, S. E., Mass Spectra. In NIST Chemistry WebBook, NIST Standard Reference Database Number 69, Eds. P.J. Linstrom and W. G. Mallard, National Institute of

Standards and Technology, Gaithersburg MD, 20899, http://webbook.nist.gov, (accessed August 2, 2014).

71) Deverse, F. T.; King, A. B. Effect of Molecular Structure on the Ionization Probabilities of Aromatic Molecules. *J. Chem. Phys.* **1964**, *41*, 3833-3838. DOI:10.1063/1.1725822

72) Harrison, A. G.; Jones, E. G.; Gupta, S. K.; Nagy, G. P. Total Cross Sections for Ionization by Electron Impact. *Can. J. Chem.* **1966**, *44*, 1967-1973. DOI: 10.1021/ie50480a054

73) Hudson, J. E.; Hamilton, M. L.; Vallance, C.; Harland, P. W. Absolute Electron Impact Ionization Cross-Sections for the C_1 to C_4 Alcohols. *Phys. Chem. Chem. Phys.* **2003**, *5*, 3162-3168. DOI: 10.1039/b304456d

74) Kim, Y.K., Irikura, K. K., Rudd, M. E., Ali, M. A., Stone, P. M., Chang, J., Coursey, J. S., Dragoset, R. A., Kishore, A. R., Olsen, K. J., Sansonetti, A. M., Wiersma, G. G., Zucker, D. S., and Zucker, M. A. Electron-Impact Ionization Cross Section for Ionization and Excitation Database (version 3.0, 2004). Available: http://physics.nist.gov/ionxsec (accessed August 2, 2014).

75) Rhodes, F. H.; Wells, J. H.; Murray, G. W. Vapor Composition Relationships in the Systems Phenol–Water and Phenol–Cresol. *Ind. Eng. Chem.* **1925**, *17*, 1199-1201. DOI: 10.1021/ie50191a044

76) Biddiscombe, D. P.; Martin, J. F. Vapor Pressures of Phenol and the Cresols. *Trans. Farad. Soc*. **1958**, *54*, 1316-1322. DOI: 10.1039/TF9585401316

77) Mahzari, M.; Braun, R. D.; White, T. R.; Bose, D. Inverse Estimation of the Mars Science Laboratory Entry Aeroheating and Heatshield Response. *J. Spacecr. Rockets* **2015**, *52*, 1203-1216; DOI: 10.2514/1.A33053.

78) Sawant, S. S.; Harpale, A.; Jambunathan, R.; Chew, H. B.; Levin, D. A. High Fidelity and Multi-scale Thermal Response Modelling of an Avcoat-like TPS. In *55th AIAA Aerospace Sciences Meeting* Grapvine, TX, Jan 9-13, 2017 DOI: 10.2514/6.2017-0438

79) Cheng, H.; Xue, H.; Hong, C.; Zhang, H. Preparation, Mechanical, Thermal and Ablative Properties of Lightweight Needled Carbon Fibre Felt/Phenolic Resin Aerogel Composite With a Bird's Nest Structure. *Comp. Sci. and Tech.* **2017**, 140, 63-72; DOI: 10.2514/6.2017-0438

80) Cheng, H,; Hong, C.; Zhang, X.; Xue, H.; Meng, S.; Han, J. Super Flame-Retardant Lightweight Rime-Like Carbon-Phenolic Nanofoam Sci. Rep. **2016**, 6, 33480 DOI: 10.1038/srep33480

81) Wong, H. W.; Peck, J.; Assif, J.; Panerai, F.; Lachaud, J.; Mansour, N. N.; Detailed Analysis of Species Production from the Pyrolysis of the Phenolic Impregnated Carbon Ablator. *J. Anal. Appl. Polym. Sci.* **2016**, *122*, 258-267; DOI: 10.1016/j.jaap.2016.09.016

82) Wong, H. W.; Peck, Bonomi, R. E.; J.; Assif, J.; Panerai, F.; Reinisch, G.; Lachaud, J.; Mansour, N. N.; Quantitative Determination of Species Production from Phenol-Formaldehyde Resin Pyrolysis. *Polym. Deg. Stab.* **2015**, *122*, 122-131; DOI: 10.1016/j.polymdegradstab.2014.12.020.

83) Bessire, B. K.; Lahankar, S. A.; Minton, T. K. Pyrolysis of Phenolic Impregnated Carbon Ablator (PICA). *ACS Appl. Mater. Interfaces.* **2015**, *7*, 1383-1395; DOI: 10.1021/am507816f.

84) Basford, J. A.; Boeckmann, M. D.; Ellefson, R. E.; Filipelli, A. R.; Holkeboer, D. H.; Lieszkovszky, L.; Stupak, C. M. Recommended Practice for the Calibration of Mass Spectrometers for Partial Pressure Analysis. *J. Vac. Sci. Technol. A.* **1993**, *11*, A22-A40; DOI: 10.1116/1.4755937.

85) Terres, E.; Gebert, F.; Hulsemann, H.; Petereit, H.; Toepsch, H.; Ruppert, W., *Zur Kenntnis der physikalisch-chemischen Grundlagen der Gewinnung und Zerlegung der Phenolfraktionen von Steinkohlenteer und Braunkohlenschwelteer. IV. Mitteilung Die Dampfdrucke von Phenol und Phenolderivaten. Brennst. Chem.* **1955**, *36*, 272-274.

86) Andon, R. J. L.; Biddiscombe, D. P.; Cox, J. D.; Handley, R.; Harrop, D.; Herington, E. F. G.; Martin, J. F. Thermodynamic Properties of Organic Oxygen Compounds. Part I. Preparation and Physical Properties of Pure Phenol, Cresols, and Xylenols. *J. Chem. Soc*. **1960**, 5246-5254 DOI: 10.1039/JR9600005246.

87) CRC Handbook of Chemistry and Physics, 71st ed. Lide, D.R., Ed.; CRC Press: Boca Raton, Fl, **1991**: Chapter 6, pp. 50-63.

88) Tate, J.S.; Gaikwad, S.; Theodoropoulou, N.; Trevino, E.; Koo, J. H. Carbon/Phenolic Nanocomposites as Advanced Thermal Protection Material in Aerospace Applications. *J. Composites.* **2013**, 403656; DOI: 10.1155/2013/403656.

89) Chang, C.; Tackett, J. R. Characterization of Phenolic Resins with Thermogravimetry-Mass Spectrometry. *Thermochim. Acta* **1991**, *192*, 181-190; DOI: 10.1016/0040-6031(91)87160-X.

90) Farmer, R. W. Phenolic Resin Char-Formation During Hyperthermal Ablation. *Thermochimica Acta* **1972**, *4*, 223-238; DOI: 10.1016/0040-6031(72)87007-2.

91) Goldstein, H. E. Pyrolysis Kinetics of Nylon 6-6, Phenolic Resin, and Their Composites. *J. Macromolec. Sci.: Part A – Chemistry* **1969**, *3:4*, 649-673; DOI: 10.1080/10601326908053834.

92) Friedman, H. L., Kinetics of Thermal Degradation of Char-Forming Plastics from Thermogravimetry. Application to a Phenolic Plastic. *J. Polym. Sci.* **1964**, *6*, 183-195; DOI: 10.1002/polc.5070060121.

93) Parker, J. A.; Winkler, E. L. The Effects of Molecular Structure on the Thermochemical Properties of Phenolics and Related Polymers. NASA TR R-276; NASA: Washington, D.C., November **1967**.

94) Costa, L.; Montelera, R.; Camino, G.; Weil, E. D.; Pearce, E. M. Structure-Charring Relationship in Phenol-Formaldehyde Type Resins. *J. Polym. Degrad. Stab.* **1997**, *56*, 23-35 DOI: 10.1016/S0141-3910(39)00171-1.

95) Pyun, E.; Mathisen, R. J.; Sung, C. S. P.; Kinetics and Mechanisms for Thermal Imidization of Polyamic Acid Studied by Ultraviolet-Visible Spectroscopy. *Macromolec.* **1988**, *22*, 1174-1183; DOI: 10.1021/ma00193a031.

96) Kruez, J. A.; Endrey, A. L.; Gay, F. P.; Sroog, C. E.; Studies of Thermal Cyclizations of Polyamic Acids and Tertiary Amine Salts. *J. Poly. Sci. Part A-1* **1966**, *4*, 2607-2616; DOI: 10.1002/pol.1966.150041023.

97) Fyfe, C.A.; Rudin, A.; Tchir, W. Application of High-Resolution ^{13}C NMR Spectroscopy Using Magic Angle Spinning Techniques to the Direct Investigation of Solid Cured Phenolic Resins. *J. Macromol.* **1980**, *13*, 1320-1322; **DOI:** 10.1021/ma60077a059.

98) Fyfe, C. A.; McKinnon, M. S.; Rudin, A.; Tchir, W. J. Investigation of the Mechanism of the Thermal Decomposition of Cured Phenolic Resins by High-Resolution ^{13}C CP/MAS Solid-State NMR Spectroscopy. *J. Macromolec.* **1983**, *16*, 1216-1219; DOI: 10.1021/ma00241a033.

99) Ehlers, G. F. L.; Fisch, K. R.; Powell, W. R. Thermal Degradation of Polymers with Phenylene Units in the Chain. I. Polyphenylenes and Poly(phenylene oxides). *J. Poly. Sci.* **1969**, *7*, 2931-2953; DOI: 10.1002/pol.1969.150071015.

100) Kundu, S.; Wang, Y.; Xia, W.; Muhler, M. Thermal Stability and Reducibility of Oxygen-Containing Functional Groups on Multiwalled Carbon Nanotube Surfaces: A Quantitative High-Resolution XPS and TPD/TPR Study. *J. Phys. Chem. C.* **2008**, *112*, 16869-16878; DOI: 10.1021/jp804413a.

101) Kuznetsova, A.; Popova, I.; Yates, J. T. Jr.; Bronikowski, M. J.; Huffman, C. B.; Liu, J.; Smalley, R. E.; Hwu, H. H.; Chen, J. G. Oxygen-Containing Functional Groups on Single-Wall Carbon Nanotubes: NEXAFS and Vibrational Spectroscopic Studies. *J. Am. Chem. Soc.* **2001**, *123*, 10699-10704; DOI: 10.1021/ja011021b.

102) Yamashita, Y.; Ouchi, K. A Study on Carbonization of Phenol-Formaldehyde Resin Labelled with Deuterium and ^{13}C. *Carbon* **1981**, *19*, 89-94; DOI: 10.1002/pol.1969.150071015.

103) Patel, P.; Hull, R. T.; McCabe, R. W.; Flath, D.; Grasmeder, J.; Percy, M. Mechanism of Thermal Decomposition of Poly (Ether Ether Ketone)) (PEEK) From a

Review of Decomposition Studies. *J. Polym. Degrad. Stab.* **2010**, *95*, 709-718; DOI: 10.1016/j.polymdegradstab.2010.01.024.

104) Talyzin, A. V.; Luzan, S. M.; Leifer, K.; Akhtar, S.; Fetzer, J.; Cataldo, F.; Tysbin, Y. O.; Tai, C. W.; Dzwilewski, A; Moons, E. Coronene Fusion by Heat Treatment: Road to Nanographenes. *J. Phys. Chem. C.* **2011**, *115*, 13207-; DOI: 10.1021/jp2028627.

105) Lochte, H. W.; Strauss, E. L.; Conley, R. T. The Thermo-Oxidative Degradation of Phenol-Formaldehyde Polycondensates: Thermogravimetric and Elemental Composition Studies of Char Formation. *J. Appl. Polym. Sci.* **1965**, *9*, 2799-2810; DOI: 10.1002/app.1965.070090814.

106) Sobera, M.; Hepter, J. Pyrolysis-Gas Chromatography-Mass Spectrometry of Cured Phenolic Resins. *J. Chromat. A* **2003**, *993*, 131-135; DOI: 10.1016/S0021-9673(03)003881-1.

107) Zhang, H.; Fonseca, A. F.; Cho, K. Tailoring Thermal Transport Property of Graphene through Oxygen Functionalization. *J. Phys. Chem. C.* **2014**, *118*, 1436-1442; DOI: 10.1021/jp4096369.

108) (54) Zhao, W.; Wang, Y.; Wu, Z.; Wang, W.; Bi, K.; Liang, Z.; Yang, J.; Chen, Y.; Xu, Z.; Ni, Z. Defect-Engineered Heat Transport in Graphene: A Route to High Efficient Thermal Rectification. *Scientific Reports* **2015**, *5*, 11962; DOI: 10.1038/srep11962.

109) Achar, B. N.; Fohlen, G. M.; HSU, M. S.; Parker, J. A. Mass Spectroscopy of Epoxylated Novolac Resin Cured with Phthalocyanine Tetraamines. *J. Polym. Sci.* **1984**, 22, 1471-1479.

110) Bessire, B. K.; Minton, T. K. Decomposition of Phenolic Impregnated Carbon Ablator (PICA) as a Function of Temperature and Heating Rate. ACS Appl. Mater. Interfaces **2017**, 9, 21422-21437

111) Ravey, M, Pryolysis of Unsaturated Polyester Resin Quantitative Aspects. *J. Polym. Sci.* **1983**, 21, 1-15.

112) DePuy, C. H.; King, R. W. Pyrolytic Cis Eliminations. Chem. Rev. **1960**, 60, 431-457.

113) Goldfarb, I. J.; McCuchan, R. Thermal Degradation of Polyesters. I Aliphatic Polymers. October **1968**, T. R. AFML-TR-68-182.

114) Bailey, W. J.; Bird, C. N. Pyrolysis of Esters. 27. Pyrolysis of Lactones. *J. Org. Chem.* **1977**, 42, 3895-3899.

APPENDICES

APPENDIX A

DATA TABLE FOR PICA

Table A.T.1. Relative molar yields of pyrolysis products collected during quasi-steady state conditions.

T / °C	CH_4	H_2O	CO	CH_3OH	argon	CO_2	isopropanol	hexane	phenol	xylene	cresol	dimethyl phenol	hexamethylenetetramine	diphenyl ether
96.6	1.79E-02	4.85E-01	5.35E-02	5.77E-02	3.99E-02	1.34E-01	3.28E-02	1.87E-02	1.47E-05	8.16E-05	2.39E-05	2.20E-05	4.44E-04	1.87E-05
150.0	1.60E-05	5.63E-01	8.48E-02	2.35E-02	2.70E-02	1.54E-01	1.37E-02	9.55E-03	1.13E-05	6.49E-05	2.00E-05	1.66E-05	3.31E-04	1.41E-05
196.9	3.56E-03	5.23E-01	1.98E-01	2.15E-02	8.68E-06	1.50E-01	7.22E-03	4.32E-03	6.86E-06	2.07E-04	1.65E-04	9.64E-06	1.52E-04	8.17E-06
252.2	1.43E-02	5.81E-01	2.42E-01	4.35E-03	1.26E-06	9.19E-02	2.25E-03	1.59E-03	3.25E-03	6.74E-04	2.33E-03	1.58E-06	3.58E-06	1.34E-06
295.7	1.21E-02	5.54E-01	2.38E-01	5.98E-03	3.77E-06	6.98E-02	1.13E-03	6.03E-04	1.01E-02	2.57E-03	9.63E-03	2.26E-03	5.99E-05	1.91E-03
347.5	3.18E-02	5.40E-01	2.06E-01	3.26E-03	2.12E-06	3.60E-02	4.97E-04	2.53E-04	1.74E-02	4.44E-03	1.92E-02	5.16E-03	9.90E-04	4.37E-03
392.6	6.19E-02	3.98E-01	3.49E-01	2.44E-03	1.55E-06	3.62E-02	4.52E-04	2.18E-04	1.57E-02	7.23E-03	1.56E-02	4.55E-03	1.12E-03	3.86E-03
444.9	1.12E-01	2.80E-01	5.34E-01	1.58E-03	1.70E-06	2.44E-02	4.06E-04	1.86E-04	8.51E-03	4.21E-03	6.29E-03	2.70E-03	6.69E-04	2.29E-03
493.8	1.10E-01	2.23E-01	6.39E-01	2.69E-03	3.92E-06	2.12E-02	7.14E-04	3.16E-04	4.50E-03	2.02E-03	2.91E-03	1.66E-03	5.74E-04	1.41E-03
544.2	9.31E-02	1.77E-01	7.20E-01	2.61E-03	7.72E-06	1.94E-02	1.29E-03	4.67E-04	2.72E-03	1.74E-03	1.83E-03	1.51E-03	7.20E-04	1.28E-03
593.7	8.62E-02	1.51E-01	7.69E-01	4.76E-06	1.29E-05	1.80E-02	7.54E-04	5.11E-04	1.73E-03	8.87E-04	1.21E-03	5.29E-04	2.87E-04	4.48E-04
650.5	7.07E-02	1.01E-01	8.41E-01	6.98E-06	1.90E-05	1.58E-02	1.28E-03	6.71E-04	1.54E-03	6.78E-04	1.03E-03	3.75E-04	4.21E-04	3.17E-04
695.9	5.43E-02	6.81E-02	9.01E-01	7.44E-06	2.30E-05	1.12E-02	6.04E-04	5.53E-04	1.64E-03	6.50E-04	1.29E-03	5.24E-04	6.12E-04	4.44E-04
743.8	5.11E-02	3.71E-02	9.39E-01	1.05E-05	2.52E-05	9.52E-03	7.85E-04	6.77E-04	1.71E-03	6.83E-04	8.67E-04	6.85E-04	6.72E-04	5.80E-04
794.3	4.26E-02	3.73E-02	9.46E-01	1.10E-05	3.01E-05	5.54E-03	8.54E-04	7.29E-04	1.33E-03	7.97E-04	9.14E-04	7.56E-04	7.95E-04	6.40E-04
837.4	3.75E-02	3.08E-02	9.68E-01	1.49E-05	3.06E-05	4.81E-03	9.90E-04	8.50E-04	1.57E-03	2.65E-04	4.78E-04	8.53E-04	7.87E-04	7.22E-04
885.8	3.96E-02	3.44E-02	9.32E-01	1.35E-05	4.14E-05	5.33E-03	1.15E-03	9.85E-04	1.60E-03	2.75E-04	6.34E-04	9.10E-04	1.16E-03	7.71E-04
935.0	3.55E-02	7.34E-03	1.00E+00	2.18E-05	4.19E-05	4.39E-03	3.02E-04	6.10E-04	8.99E-04	1.94E-04	9.06E-05	5.66E-04	1.22E-03	4.79E-04

APPENDIX B

DATA TABLES AND FIGURES FOR PICA

B.1. DETERMINATION OF HEATING RATE

A representative heating curve is illustrated in Figure B.1. The resistance of the sample is initially very high, and the sample temperature increases slowly (blue part of the curve in Fig. B.1). Near 100 °C, the sample temperature begins to increase approximately linearly, with a heating rate of 3.1 °C s^{-1}, until it reaches the maximum temperature for the experiment, typically around 1200 °C (red part of the curve in Fig. B.1). After the maximum temperature is achieved, the current is decreased from its maximum value to zero within a few seconds, and the temperature decreases quickly as a consequence (green part of the curve in Figure B.1). The heating rate for each pyrolysis run was calculated over the roughly linear section of the curve. The heating profile shows a "bump" at lower temperatures, in the vicinity of 200 °C, which stems from the inability of the heating program to overcome the large change in sample conductivity in this temperature range during the heating ramp. This small deviation from linearity (as evidenced by a correlation coefficient above 0.99) is not expected to have any measurable effect on the results. Average heating rates of PICA were calculated from the linear portion of the heating profile for each pyrolysis run. Heating rates of 25.0 °C s^{-1} and 12.7 °C s^{-1} were calculated from the average of five runs. Heating rates of 6.1 °C s^{-1} and 3.1 °C s^{-1} were calculated from the average of three runs.

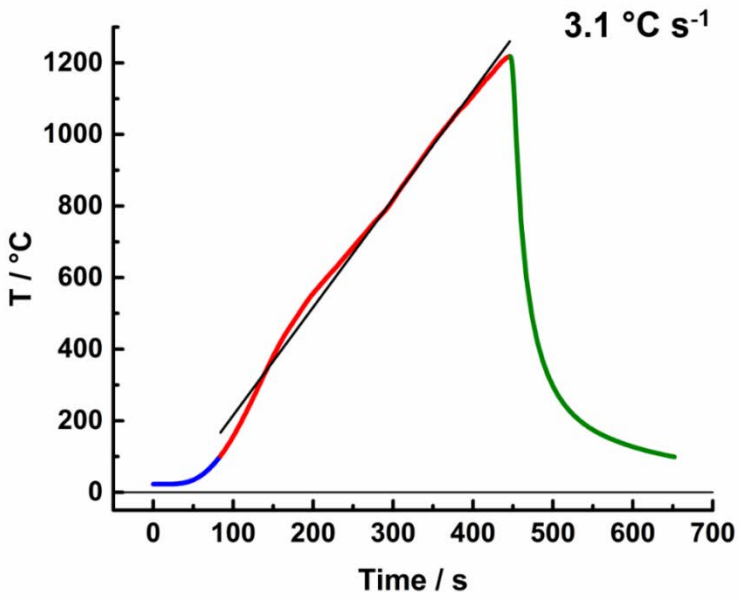

Figure B.1. Representative heating profile, with a nominal heating rate of 3.1 °C s^{-1}.

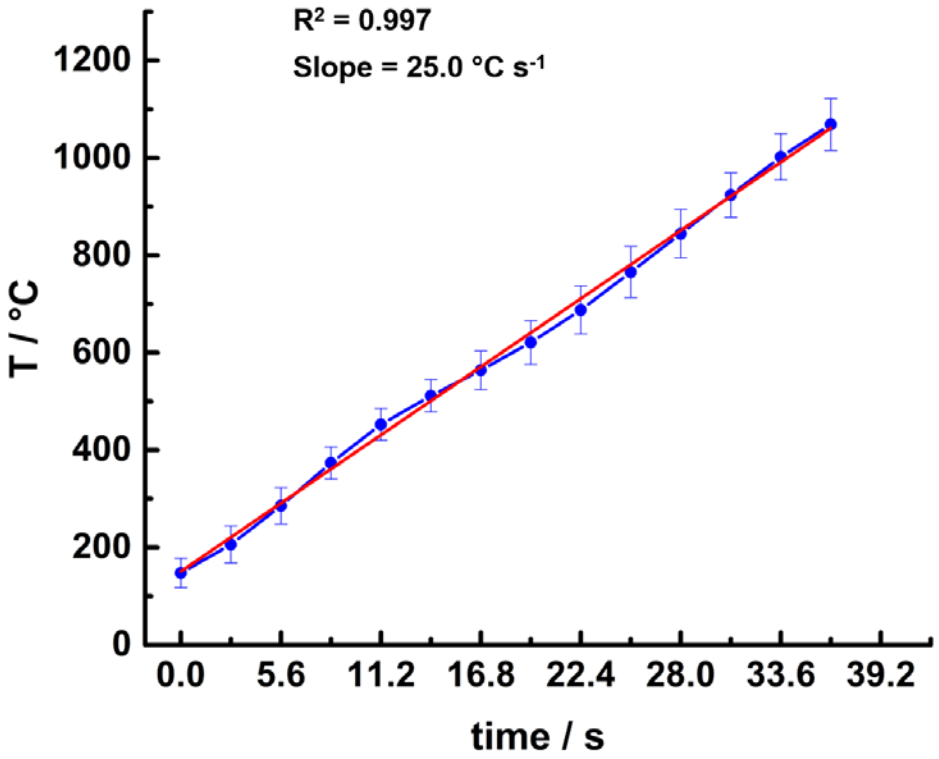

Figure B.2. Heating profile for PICA, with a nominal heating rate of 25.0 °C s^{-1}.

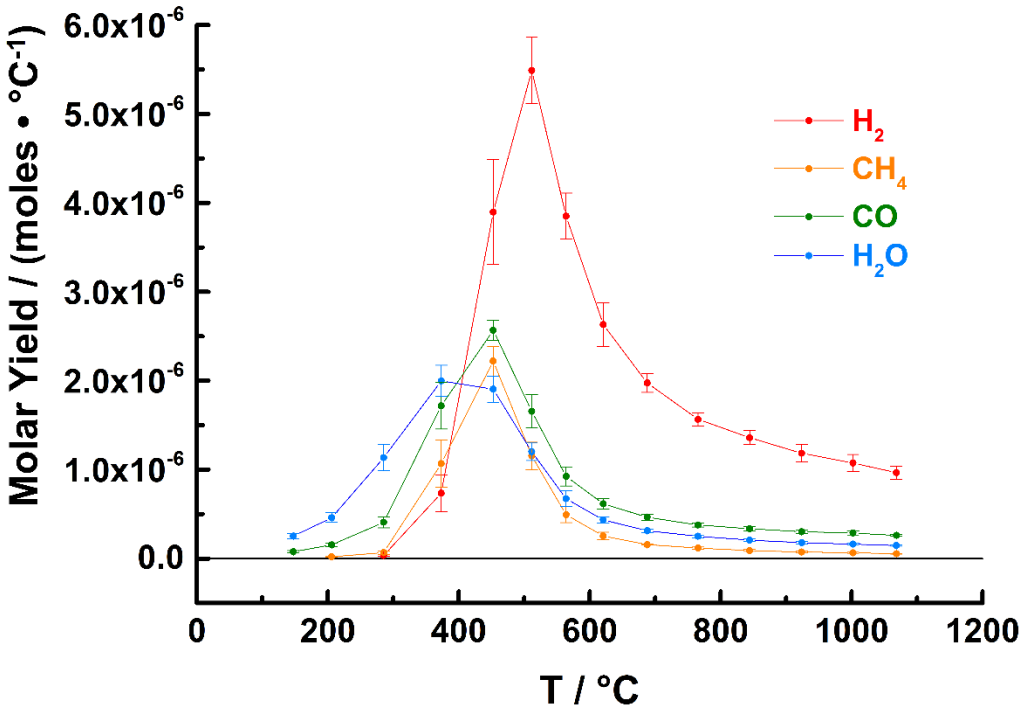

Figure B.3. Molar yields of H_2, CH_4, CO, and H_2O, measured during the pyrolysis of PICA with a nominal heating rate of 25.0 °C s^{-1}.

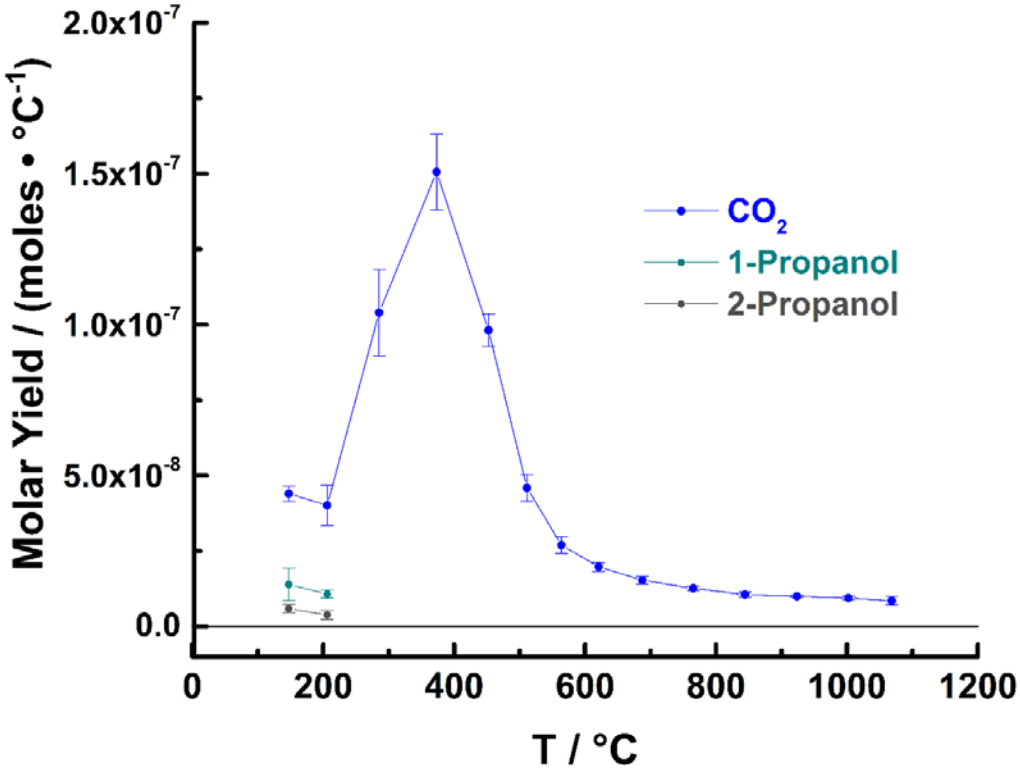

Figure B.4. Molar yields of CO_2, 1-propanol, and 2-propanol, measured during the pyrolysis of PICA with a nominal heating rate of 25.0 °C s^{-1}.

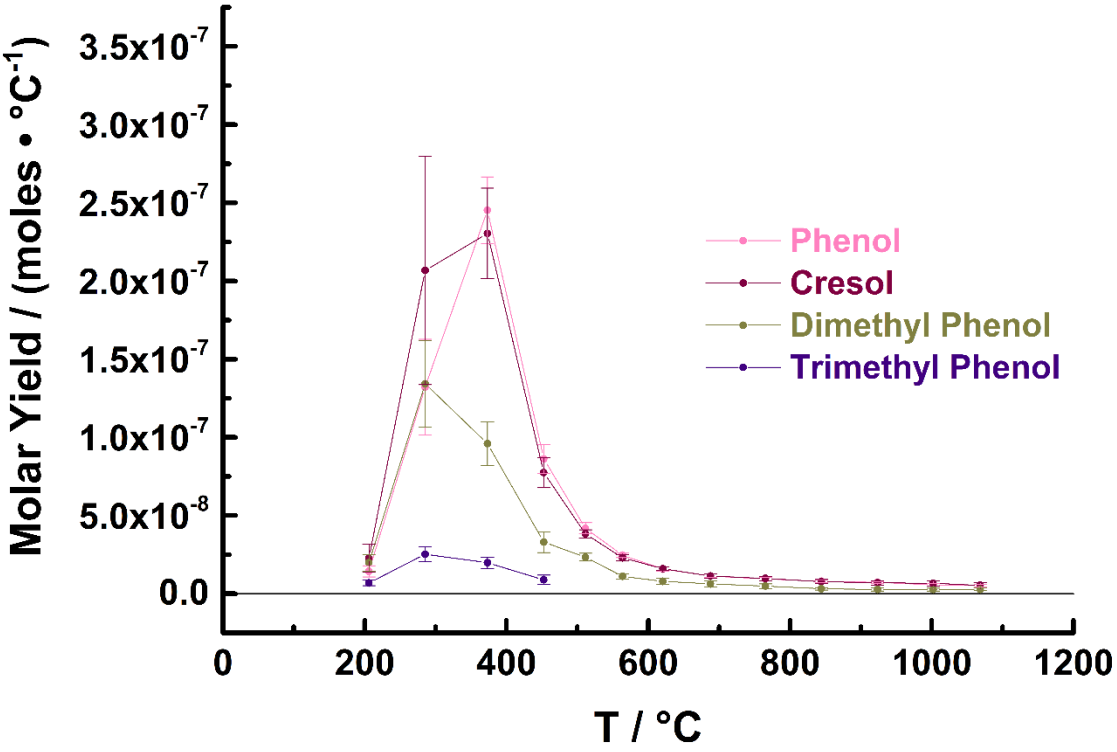

Figure B.5. Molar yields of phenol and its derivatives, measured during the pyrolysis of PICA with a nominal heating rate of 25.0 °C s^{-1}.

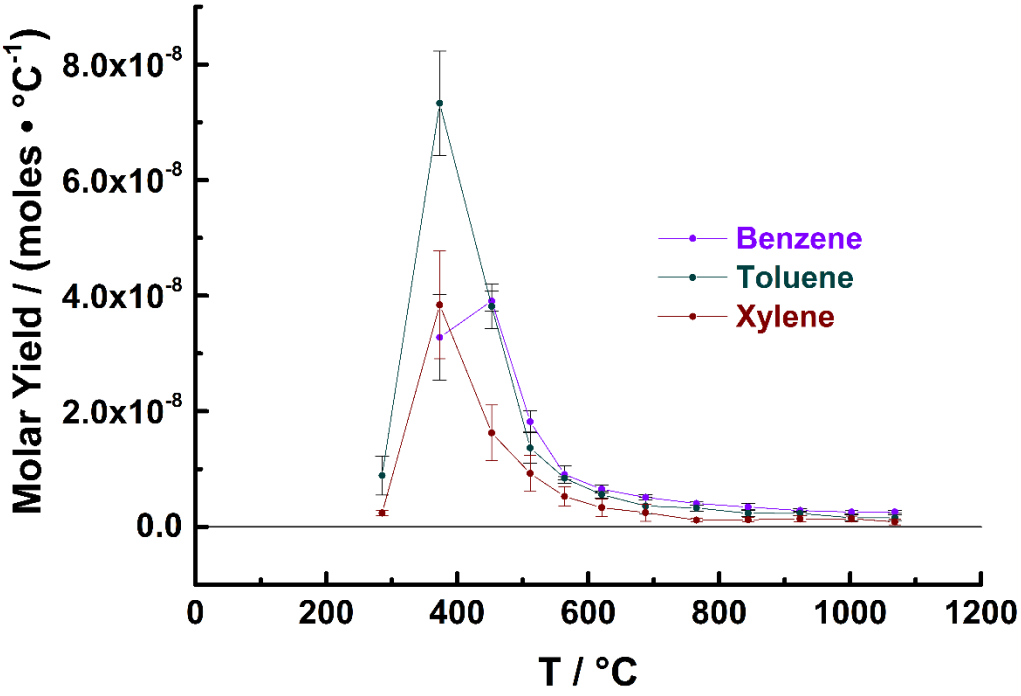

Figure B.6. Molar yields of benzene and its derivatives, measured during the pyrolysis of PICA with a nominal heating rate of 25.0 °C s^{-1}.

Table B.T.1. Molar yields of pyrolysis products, measured during the pyrolysis of PICA with a nominal heating rate of 25.0 °C s^{-1}.

		H_2		CH_4		CO		CO_2		Phenol		H_2O		1-Propanol	
T / °C	± °C	moles ·°C^{-1}	SD (1σ)	moles ·°C^{-1}	SD (1σ)	moles ·°C^{-1}	SD (1σ)	moles ·°C^{-1}	SD (1σ)	moles ·°C^{-1}	SD (1σ)	moles ·°C^{-1}	SD (1σ)	moles ·°C^{-1}	SD (1σ)
147.5	30.0					7.6E-08	1.4E-08	4.4E-08	2.5E-09			2.5E-07	2.9E-08	1.4E-08	5.3E-09
206.1	38.0			2.0E-08	1.3E-09	1.5E-07	1.9E-08	4.0E-08	6.6E-09	1.4E-08	3.6E-09	4.6E-07	5.4E-08	1.1E-08	1.3E-09
285.4	37.6	3.5E-08	9.5E-09	6.8E-08	2.0E-08	4.1E-07	6.2E-08	1.0E-07	1.4E-08	1.3E-07	3.1E-08	1.1E-06	1.5E-07		
373.3	32.7	7.4E-07	2.0E-07	1.1E-06	2.6E-07	1.7E-06	2.6E-07	1.5E-07	1.3E-08	2.5E-07	2.1E-08	2.0E-06	1.8E-07		
452.6	32.5	3.9E-06	5.9E-07	2.2E-06	1.7E-07	2.6E-06	1.1E-07	9.8E-08	5.3E-09	8.6E-08	9.2E-09	1.9E-06	1.5E-07		
511.5	33.3	5.5E-06	3.7E-07	1.2E-06	1.6E-07	1.7E-06	1.9E-07	4.6E-08	4.4E-09	4.2E-08	3.5E-09	1.2E-06	9.8E-08		
563.8	39.4	3.9E-06	2.6E-07	4.9E-07	8.9E-08	9.2E-07	1.1E-07	2.7E-08	2.8E-09	2.5E-08	1.5E-09	6.7E-07	8.7E-08		
620.8	44.6	2.6E-06	2.5E-07	2.6E-07	4.1E-08	6.2E-07	6.0E-08	2.0E-08	1.4E-09	1.6E-08	1.6E-09	4.4E-07	3.4E-08		
687.6	49.1	2.0E-06	1.1E-07	1.6E-07	5.3E-09	4.6E-07	3.7E-08	1.5E-08	1.3E-09	1.1E-08	1.1E-09	3.1E-07	2.0E-08		
765.4	52.7	1.6E-06	7.5E-08	1.2E-07	1.1E-08	3.8E-07	2.2E-08	1.3E-08	7.0E-10	9.5E-09	1.1E-09	2.5E-07	1.5E-08		
844.3	49.7	1.4E-06	7.7E-08	9.1E-08	9.9E-09	3.4E-07	2.3E-08	1.1E-08	8.2E-10	7.9E-09	6.6E-10	2.1E-07	1.4E-08		
923.7	45.4	1.2E-06	9.9E-08	7.4E-08	9.2E-09	3.0E-07	2.3E-08	1.0E-08	3.5E-10	7.2E-09	4.8E-10	1.8E-07	1.3E-08		
1002.1	47.2	1.1E-06	9.6E-08	6.6E-08	6.0E-09	2.9E-07	2.2E-08	9.4E-09	5.7E-10	5.7E-09	9.6E-10	1.6E-07	1.1E-08		
1068.5	53.3	9.7E-07	7.5E-08	5.4E-08	3.4E-09	2.6E-07	1.2E-08	8.5E-09	1.4E-09	5.2E-09	9.1E-10	1.5E-07	6.1E-09		
		2-Propanol		Xylene		Cresol		Dimethyl Phenol		Trimethyl Phenol		Benzene		Toluene	
T / °C	± °C	moles ·°C^{-1}	SD (1σ)	moles ·°C^{-1}	SD (1σ)	moles ·°C^{-1}	SD (1σ)	moles ·°C^{-1}	SD (1σ)	moles ·°C^{-1}	SD (1σ)	moles ·°C^{-1}	SD (1σ)	moles ·°C^{-1}	SD (1σ)
147.5	30.0	5.9E-09	1.3E-09												
206.1	38.0	3.8E-09	1.5E-09			2.3E-08	8.8E-09	2.0E-08	5.4E-09	6.9E-09	1.8E-09				
285.4	37.6			2.4E-09	4.5E-10	2.1E-07	7.3E-08	1.3E-07	2.8E-08	2.5E-08	4.9E-09			8.9E-09	3.4E-09
373.3	32.7			3.8E-08	9.3E-09	2.3E-07	2.9E-08	9.6E-08	1.4E-08	2.0E-08	3.5E-09	3.3E-08	7.4E-09	7.3E-08	9.0E-09
452.6	32.5			1.6E-08	4.8E-09	7.7E-08	9.6E-09	3.3E-08	6.6E-09	8.9E-09	3.0E-09	3.9E-08	1.7E-09	3.8E-08	3.9E-09
511.5	33.3			9.2E-09	3.1E-09	3.8E-08	2.6E-09	2.3E-08	2.5E-09			1.8E-08	1.8E-09	1.4E-08	2.7E-09
563.8	39.4			5.3E-09	1.7E-09	2.3E-08	2.1E-09	1.1E-08	1.8E-09			9.1E-09	1.5E-09	8.4E-09	2.5E-10
620.8	44.6			3.3E-09	1.5E-09	1.6E-08	1.3E-09	8.0E-09	2.0E-09			6.5E-09	6.7E-10	5.6E-09	5.9E-10
687.6	49.1			2.5E-09	1.5E-09	1.1E-08	1.5E-09	6.3E-09	1.9E-09			5.1E-09	4.6E-10	3.6E-09	1.4E-09
765.4	52.7			1.2E-09	2.8E-10	9.8E-09	1.5E-09	4.9E-09	1.4E-09			4.1E-09	3.6E-10	3.3E-09	5.4E-10
844.3	49.7			1.2E-09	3.5E-10	7.7E-09	1.3E-09	3.2E-09	8.1E-10			3.4E-09	6.5E-10	2.4E-09	5.9E-10
923.7	45.4			1.4E-09	4.9E-10	7.0E-09	1.3E-09	2.7E-09	9.0E-10			2.8E-09	3.2E-10	2.3E-09	4.0E-10
1002.1	47.2			1.4E-09	4.8E-10	6.7E-09	1.6E-09	2.7E-09	8.8E-10			2.6E-09	3.4E-10	1.6E-09	5.5E-10
1068.5	53.3			8.8E-10	5.1E-10	5.4E-09	1.6E-09	2.8E-09	9.0E-10			2.6E-09	2.3E-10	1.6E-09	4.8E-10

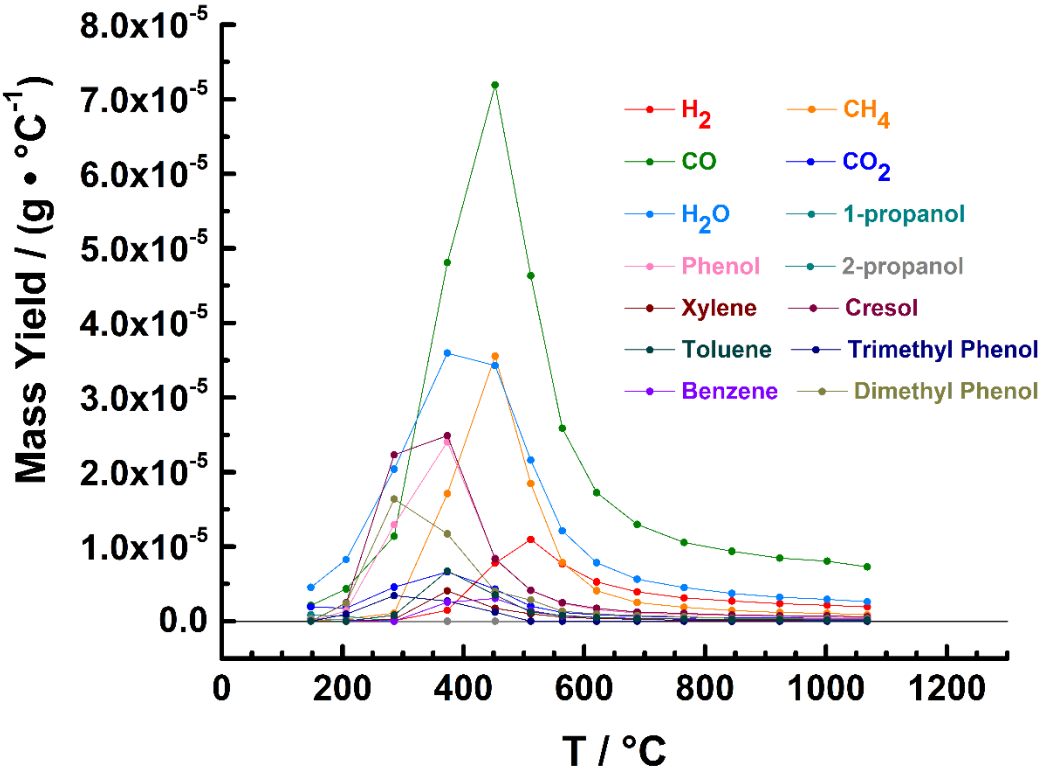

Figure B.7. Mass yields of pyrolysis products as a function of nominal heating rate of PICA, measured during the pyrolysis of PICA with a nominal heating rate of 25.0 °C s^{-1}.

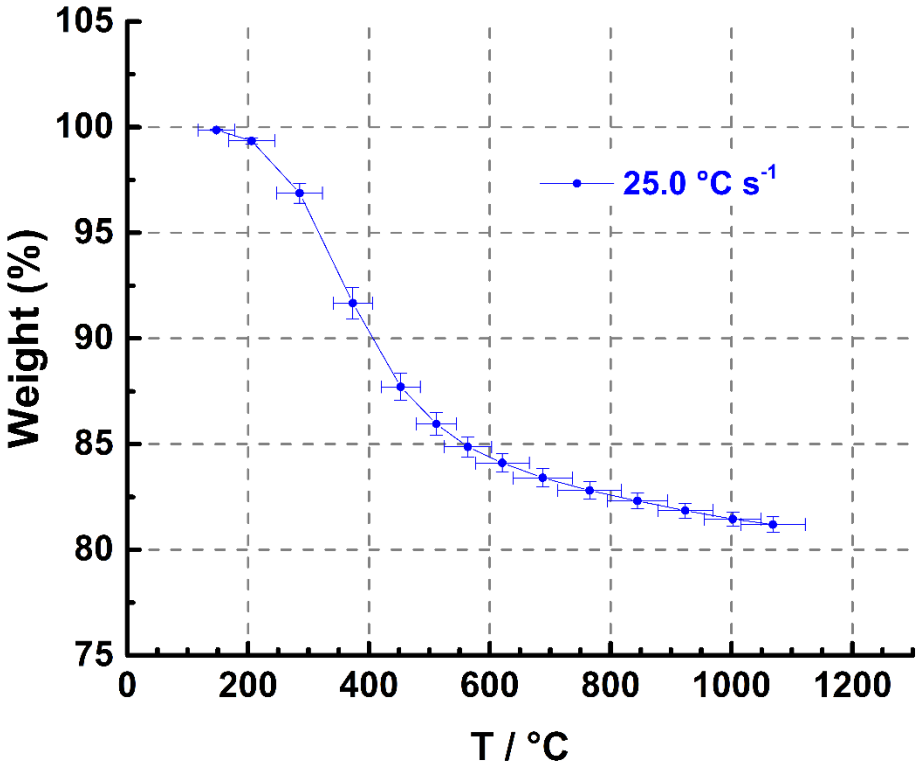

Figure B.8. Simulated thermogravimetric analysis (TGA) curve of PICA, with a nominal heating rate of 25.0 °C s^{-1}.

Table B.T.2. TGA data collected with a nominal heating rate of 25.0 °C s^{-1}.

T / °C	± °C	Weight (%)	± Weight (%)
147.5	30.0	99.9	0.0
206.1	38.0	99.3	0.1
285.4	37.6	96.9	0.5
373.3	32.7	91.7	0.8
452.6	32.5	87.7	0.6
511.5	33.3	85.9	0.5
563.8	39.4	84.9	0.5
620.8	44.6	84.1	0.4
687.6	49.1	83.4	0.4
765.4	52.7	82.8	0.4
844.3	49.7	82.3	0.4
923.7	45.4	81.9	0.3
1002.1	47.2	81.5	0.3
1068.5	53.3	81.2	0.4
	SD (1σ)		SD (1σ)

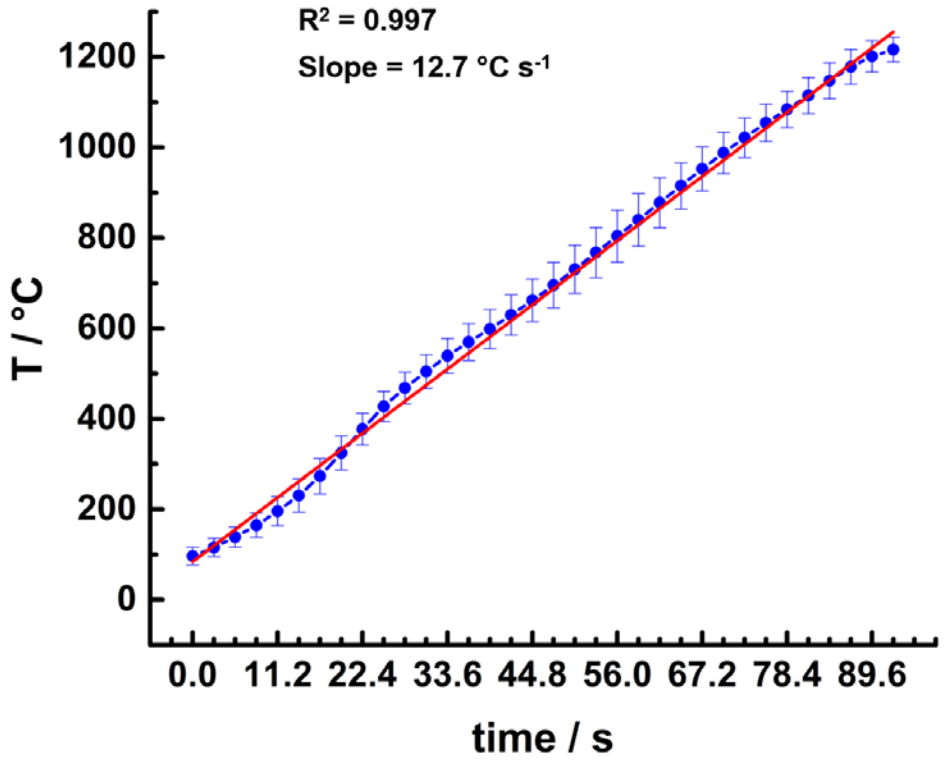

Figure B.9. Heating profile for PICA, with a nominal heating rate of 12.7 °C s^{-1}.

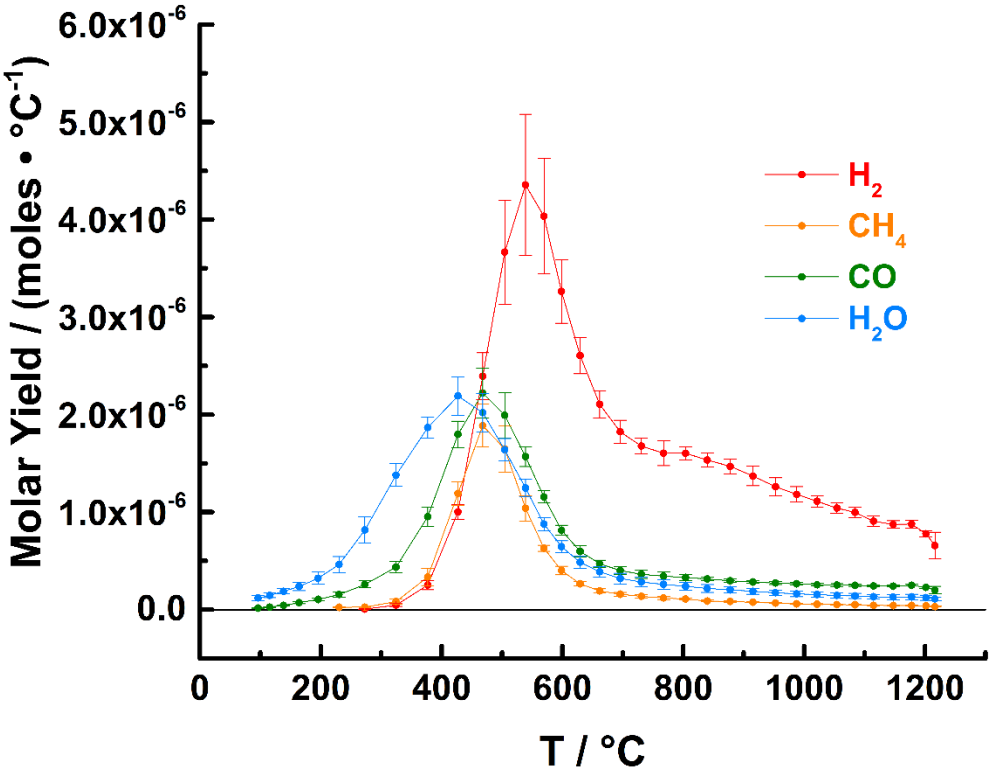

Figure B.10. Molar yields of H_2, CH_4, CO, and H_2O, measured during the pyrolysis of PICA with a nominal heating rate of 12.7 °C s^{-1}.

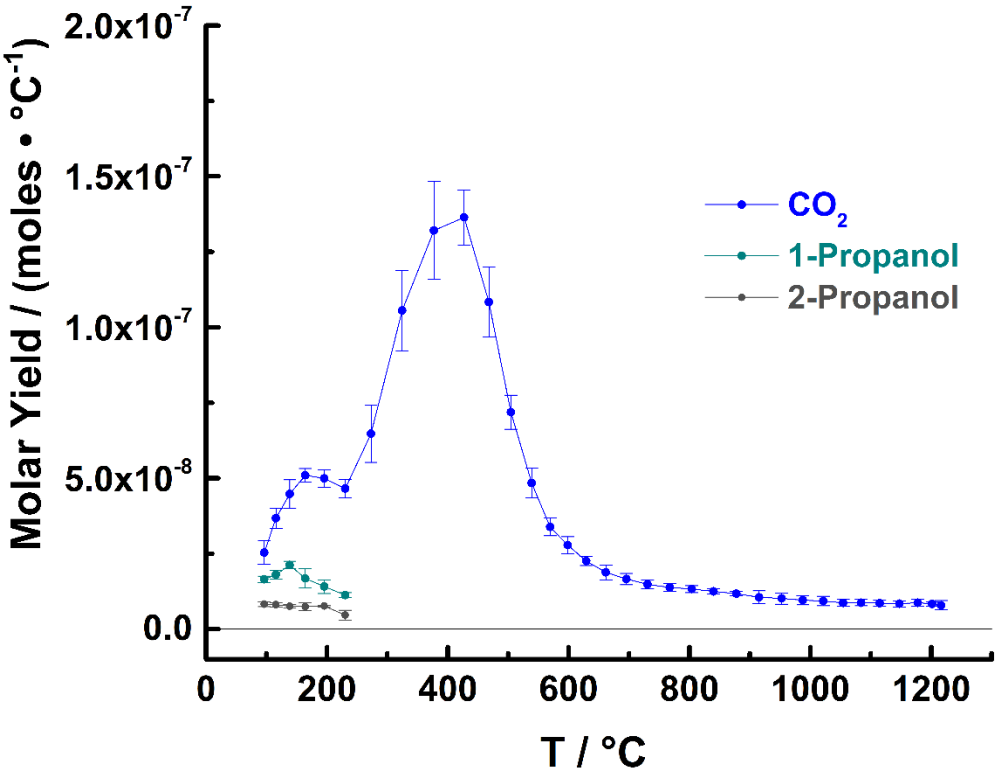

Figure B.11. Molar yields of CO_2, 1-propanol, and 2-propanol, measured during the pyrolysis of PICA with a nominal heating rate of 12.7 °C s^{-1}.

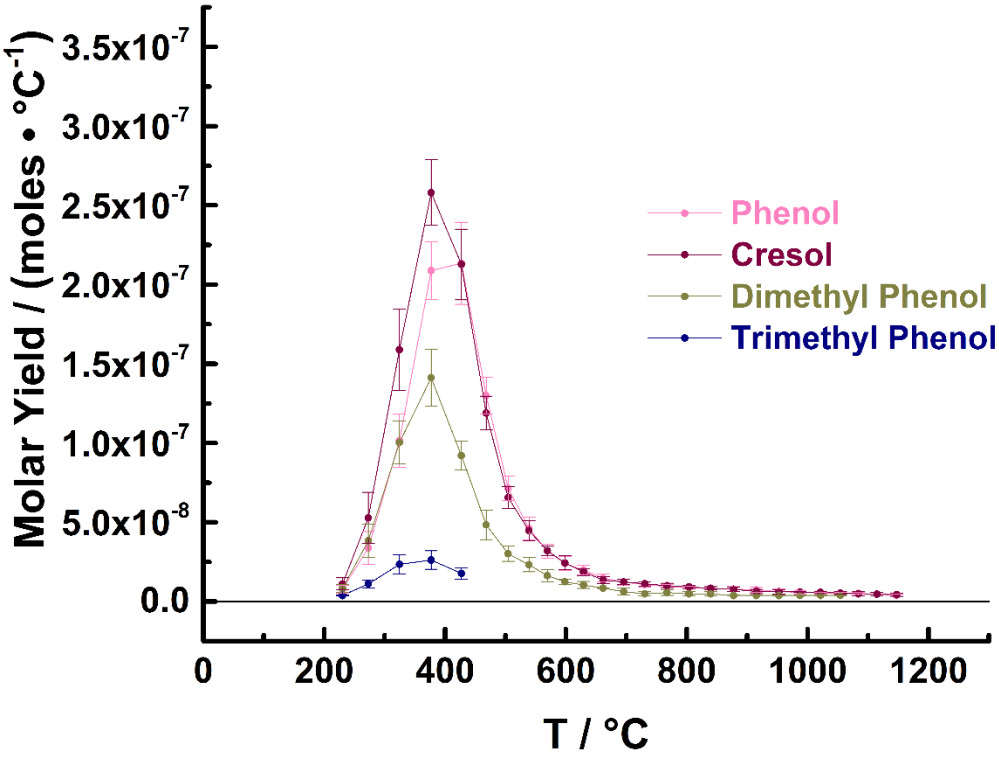

Figure B.12. Molar yields of phenol and its derivatives, measured during the pyrolysis of PICA with a nominal heating rate of 12.7 °C s^{-1}.

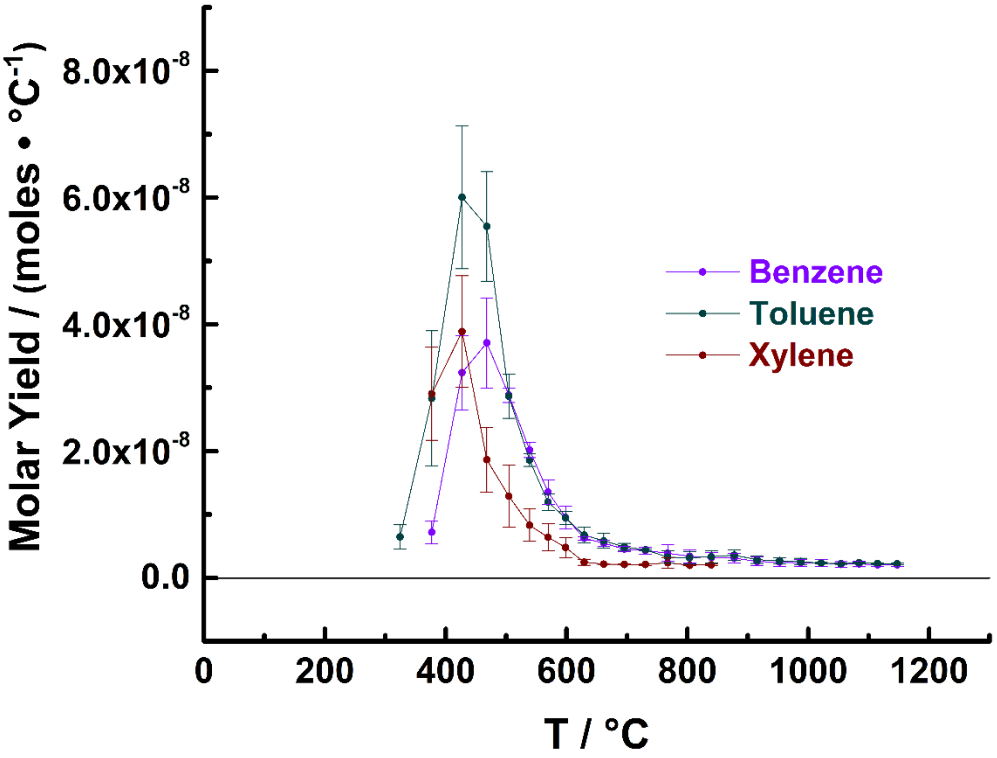

Figure B.13. Molar yields of benzene and its derivatives, measured during the pyrolysis of PICA with a nominal heating rate of 12.7 °C s^{-1}.

Table B.T.3. Molar yields of pyrolysis products, measured during the pyrolysis of PICA with a nominal heating rate of 12.7 °C s^{-1}.

		H_2		CH_4		CO		CO_2		Phenol		H_2O		1-Propanol	
T / °C	± °C	moles ·°C^{-1}	SD (1σ)	moles ·°C^{-1}	SD (1σ)	moles ·°C^{-1}	SD (1σ)	moles ·°C^{-1}	SD (1σ)	moles ·°C^{-1}	SD (1σ)	moles ·°C^{-1}	SD (1σ)	moles ·°C^{-1}	SD (1σ)
96.4	19.2					1.8E-08	2.1E-09	2.5E-08	3.8E-09			1.2E-07	2.6E-08	1.7E-08	1.1E-09
115.5	20.3					2.7E-08	3.9E-09	3.7E-08	3.3E-09			1.5E-07	2.4E-08	1.8E-08	1.5E-09
138.5	22.7					4.4E-08	5.8E-09	4.5E-08	4.7E-09			1.9E-07	2.8E-08	2.1E-08	1.3E-09
164.2	27.0					7.2E-08	1.1E-08	5.1E-08	2.3E-09			2.4E-07	4.2E-08	1.7E-08	3.2E-09
195.6	32.3					1.0E-07	1.2E-08	5.0E-08	2.8E-09			3.2E-07	6.2E-08	1.4E-08	2.3E-09
230.2	36.6			2.5E-08	2.8E-09	1.6E-07	2.4E-08	4.7E-08	3.1E-09	7.8E-09	2.5E-09	4.6E-07	8.2E-08	1.1E-08	8.4E-10
273.0	39.1	5.7E-09	1.6E-09	2.6E-08	2.9E-09	2.6E-07	3.5E-08	6.5E-08	9.6E-09	3.4E-08	1.0E-08	8.2E-07	1.4E-07		
324.5	37.6	4.7E-08	1.3E-08	8.2E-08	2.6E-08	4.4E-07	5.8E-08	1.1E-07	1.3E-08	1.0E-07	1.7E-08	1.4E-06	1.2E-07		
377.0	34.8	2.5E-07	4.7E-08	3.4E-07	8.9E-08	9.5E-07	1.0E-07	1.3E-07	1.6E-08	2.1E-07	1.8E-08	1.9E-06	1.1E-07		
427.1	33.5	1.0E-06	7.4E-08	1.2E-06	1.2E-07	1.8E-06	1.4E-07	1.4E-07	9.1E-09	2.1E-07	2.6E-08	2.2E-06	2.0E-07		
467.9	35.0	2.4E-06	2.4E-07	1.9E-06	2.2E-07	2.2E-06	2.6E-07	1.1E-07	1.2E-08	1.3E-07	1.2E-08	2.0E-06	1.9E-07		
504.5	37.4	3.7E-06	5.4E-07	1.6E-06	2.4E-07	2.0E-06	2.3E-07	7.2E-08	5.7E-09	7.1E-08	7.9E-09	1.6E-06	1.2E-07		
539.0	38.9	4.4E-06	7.2E-07	1.0E-06	1.3E-07	1.6E-06	1.0E-07	4.8E-08	4.9E-09	4.6E-08	7.1E-09	1.2E-06	9.0E-08		
569.4	40.8	4.0E-06	5.9E-07	6.3E-07	3.1E-08	1.2E-06	6.2E-08	3.4E-08	2.9E-09	3.2E-08	4.4E-09	8.8E-07	6.7E-08		
598.5	43.1	3.3E-06	3.2E-07	4.0E-07	4.4E-08	8.1E-07	5.3E-08	2.8E-08	2.8E-09	2.4E-08	4.5E-09	6.5E-07	6.0E-08		
629.3	44.8	2.6E-06	1.9E-07	2.7E-07	2.2E-08	6.0E-07	5.7E-08	2.3E-08	1.5E-09	2.0E-08	3.1E-09	4.9E-07	6.2E-08		
661.7	47.2	2.1E-06	1.4E-07	1.9E-07	2.2E-08	4.7E-07	3.6E-08	1.9E-08	2.5E-09	1.5E-08	2.4E-09	3.9E-07	5.4E-08		
695.6	50.2	1.8E-06	1.2E-07	1.6E-07	1.8E-08	4.0E-07	3.8E-08	1.7E-08	1.9E-09	1.2E-08	2.0E-09	3.2E-07	5.3E-08		
730.5	53.4	1.7E-06	8.2E-08	1.4E-07	1.9E-08	3.6E-07	4.2E-08	1.5E-08	1.4E-09	1.1E-08	1.8E-09	2.8E-07	5.1E-08		
767.5	55.4	1.6E-06	1.3E-07	1.2E-07	1.8E-08	3.5E-07	4.2E-08	1.4E-08	1.3E-09	9.6E-09	1.2E-09	2.6E-07	5.1E-08		
803.8	57.1	1.6E-06	6.7E-08	1.1E-07	1.1E-08	3.3E-07	3.0E-08	1.3E-08	1.2E-09	8.8E-09	9.5E-10	2.4E-07	4.1E-08		
839.6	58.2	1.5E-06	7.0E-08	8.9E-08	7.6E-09	3.1E-07	1.7E-08	1.3E-08	8.6E-10	8.0E-09	1.4E-09	2.2E-07	4.1E-08		
877.8	54.9	1.5E-06	7.6E-08	8.4E-08	6.9E-09	3.0E-07	1.6E-08	1.2E-08	7.3E-10	7.9E-09	1.5E-09	2.0E-07	3.3E-08		
915.2	51.4	1.4E-06	1.0E-07	7.6E-08	4.2E-09	2.8E-07	1.3E-08	1.1E-08	2.1E-09	7.4E-09	1.7E-09	1.9E-07	2.9E-08		
952.6	48.4	1.3E-06	9.2E-08	6.7E-08	3.9E-09	2.7E-07	1.4E-08	1.0E-08	1.9E-09	6.3E-09	1.6E-09	1.7E-07	2.8E-08		
987.7	45.8	1.2E-06	7.9E-08	6.0E-08	4.8E-09	2.7E-07	1.6E-08	9.6E-09	1.5E-09	6.0E-09	1.2E-09	1.6E-07	2.8E-08		
1021.4	44.1	1.1E-06	5.7E-08	5.6E-08	4.7E-09	2.6E-07	1.4E-08	9.3E-09	1.6E-09	5.4E-09	4.4E-10	1.5E-07	2.5E-08		
1054.3	41.2	1.0E-06	5.1E-08	5.1E-08	3.4E-09	2.5E-07	1.5E-08	8.7E-09	1.1E-09	4.9E-09	1.1E-09	1.5E-07	2.7E-08		
1084.1	40.0	1.0E-06	5.2E-08	4.9E-08	3.8E-09	2.5E-07	1.2E-08	8.8E-09	1.0E-09	5.1E-09	4.8E-10	1.4E-07	2.7E-08		
1114.8	39.8	9.1E-07	5.1E-08	4.4E-08	3.7E-09	2.4E-07	1.1E-08	8.6E-09	1.0E-09	4.7E-09	1.0E-09	1.3E-07	2.5E-08		
1147.5	39.5	8.7E-07	3.9E-08	4.3E-08	2.6E-09	2.4E-07	1.0E-08	8.4E-09	1.0E-09	4.0E-09	7.1E-10	1.3E-07	2.4E-08		
1178.0	38.8	8.8E-07	3.8E-08	4.3E-08	2.5E-09	2.5E-07	9.1E-09	8.8E-09	1.1E-09			1.3E-07	2.8E-08		
1201.5	34.8	7.8E-07	3.3E-08	3.8E-08	2.5E-09	2.3E-07	9.6E-09	8.3E-09	7.0E-10			1.2E-07	2.7E-08		
1216.4	27.8	6.6E-07	1.4E-07	3.2E-08	5.9E-09	2.0E-07	3.8E-08	7.9E-09	1.6E-09			1.1E-07	2.0E-08		

		2-Propanol		Xylene		Cresol		Dimethyl Phenol		Trimethyl Phenol		Benzene		Toluene	
T / °C	± °C	moles ·°C^{-1}	SD (1σ)	moles ·°C^{-1}	SD (1σ)	moles ·°C^{-1}	SD (1σ)	moles ·°C^{-1}	SD (1σ)	moles ·°C^{-1}	SD (1σ)	moles ·°C^{-1}	SD (1σ)	moles ·°C^{-1}	SD (1σ)
96.4	19.2	8.3E-09	8.1E-10												
115.5	20.3	8.1E-09	7.3E-10												
138.5	22.7	7.6E-09	6.3E-10												
164.2	27.0	7.5E-09	1.3E-09												
195.6	32.3	7.7E-09	2.7E-10												
230.2	36.6	4.7E-09	1.6E-09			1.1E-08	3.8E-09	8.3E-09	2.3E-09	3.8E-09	1.1E-10				
273.0	39.1					5.3E-08	1.6E-08	3.8E-08	1.1E-08	1.1E-08	2.6E-09				
324.5	37.6					1.6E-07	2.6E-08	1.0E-07	1.4E-08	2.3E-08	6.1E-09			6.5E-09	1.9E-09
377.0	34.8			2.9E-08	7.3E-09	2.6E-07	2.1E-08	1.4E-07	1.8E-08	2.6E-08	5.8E-09	7.2E-09	1.8E-09	2.8E-08	1.1E-08
427.1	33.5			3.9E-08	8.8E-09	2.1E-07	2.2E-08	9.2E-08	9.1E-09	1.8E-08	3.6E-09	3.2E-08	5.9E-09	6.0E-08	1.1E-08
467.9	35.0			1.9E-08	5.1E-09	1.2E-07	1.1E-08	4.8E-08	9.3E-09			3.7E-08	7.1E-09	5.5E-08	8.6E-09
504.5	37.4			1.3E-08	4.9E-09	6.6E-08	6.8E-09	3.0E-08	4.8E-09			2.9E-08	1.2E-09	2.9E-08	3.5E-09
539.0	38.9			8.3E-09	2.5E-09	4.5E-08	6.5E-09	2.3E-08	4.4E-09			2.0E-08	1.2E-09	1.9E-08	9.7E-10
569.4	40.8			6.4E-09	2.1E-09	3.2E-08	3.1E-09	1.6E-08	3.9E-09			1.4E-08	1.9E-09	1.2E-08	1.3E-09
598.5	43.1			4.8E-09	1.6E-09	2.4E-08	4.4E-09	1.2E-08	1.8E-09			9.6E-09	1.8E-09	9.4E-09	1.1E-09
629.3	44.8			2.5E-09	4.8E-10	1.9E-08	2.2E-09	1.0E-08	2.2E-09			6.2E-09	2.8E-10	6.8E-09	1.3E-09
661.7	47.2			2.2E-09	2.3E-11	1.4E-08	2.1E-09	8.3E-09	9.0E-11			5.5E-09	4.5E-10	5.8E-09	1.2E-09
695.6	50.2			2.1E-09	7.1E-11	1.2E-08	1.5E-09	6.2E-09	2.2E-09			4.5E-09	4.3E-10	4.9E-09	5.5E-10
730.5	53.4			2.1E-09	1.5E-10	1.1E-08	1.4E-09	4.9E-09	1.4E-09			4.3E-09	5.2E-10	4.4E-09	1.3E-10
767.5	55.4			2.4E-09	8.3E-10	1.0E-08	1.5E-09	5.7E-09	1.8E-09			3.9E-09	1.3E-09	3.3E-09	9.8E-10
803.8	57.1			2.0E-09	8.3E-11	9.2E-09	1.2E-09	4.8E-09	1.4E-09			3.4E-09	1.1E-09	3.2E-09	9.5E-10
839.6	58.2			2.1E-09	1.7E-10	8.4E-09	9.6E-10	4.8E-09	1.4E-09			3.2E-09	8.0E-10	3.3E-09	9.6E-10
877.8	54.9					7.7E-09	1.2E-09	3.9E-09	6.8E-11			3.1E-09	8.0E-10	3.6E-09	8.2E-10
915.2	51.4					6.4E-09	1.3E-09	3.9E-09	8.3E-11			2.6E-09	7.0E-10	2.9E-09	6.0E-10
952.6	48.4					6.3E-09	1.4E-09	3.9E-09	1.1E-10			2.5E-09	7.3E-10	2.7E-09	4.6E-10
987.7	45.8					6.0E-09	4.3E-10	3.9E-09	9.7E-11			2.4E-09	5.5E-10	2.6E-09	5.2E-10
1021.4	44.1					5.8E-09	8.2E-10	3.9E-09	1.2E-10			2.4E-09	5.7E-10	2.3E-09	1.4E-10
1054.3	41.2					5.5E-09	8.7E-10	3.8E-09	1.1E-10			2.1E-09	4.2E-10	2.2E-09	1.2E-10
1084.1	40.0					4.8E-09	1.2E-09					2.2E-09	4.4E-10	2.4E-09	1.7E-10
1114.8	39.8					4.6E-09	1.1E-09					2.1E-09	2.7E-10	2.2E-09	1.1E-10
1147.5	39.5					4.4E-09	1.1E-09					2.1E-09	2.5E-10	2.2E-09	1.3E-10
1178.0	38.8														
1201.5	34.8														
1216.4	27.8														

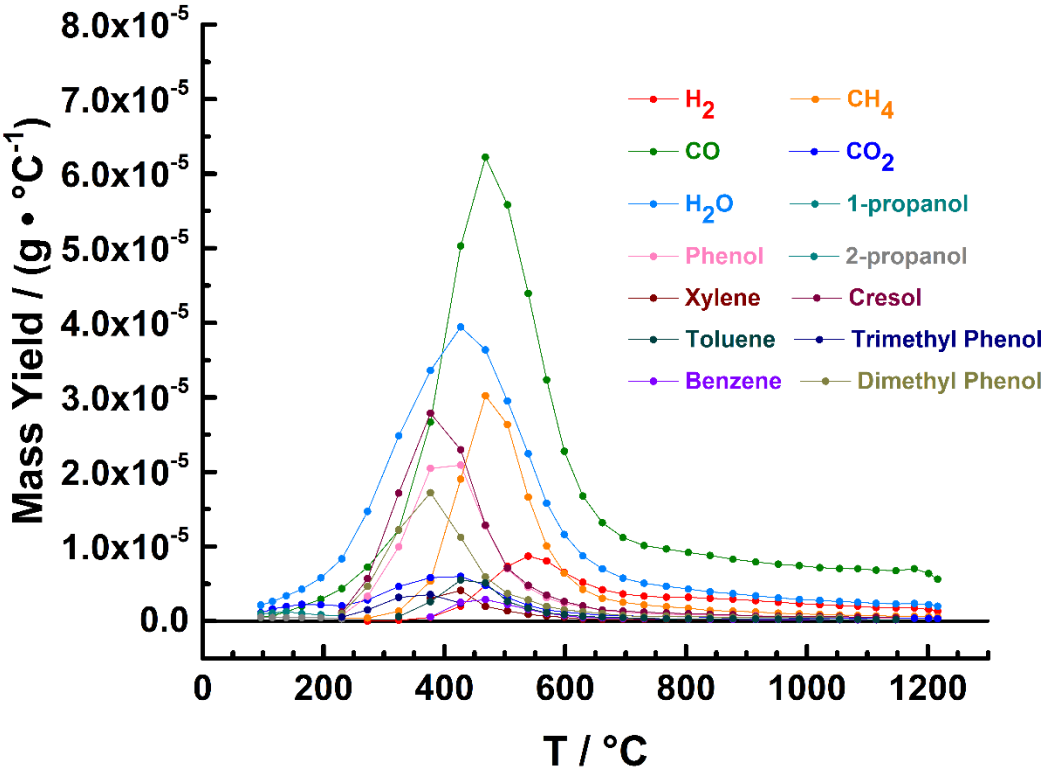

Figure B.14. Mass yields of pyrolysis products as a function of nominal heating rate of PICA, measured during the pyrolysis of PICA with a nominal heating rate of 12.7 °C s^{-1}.

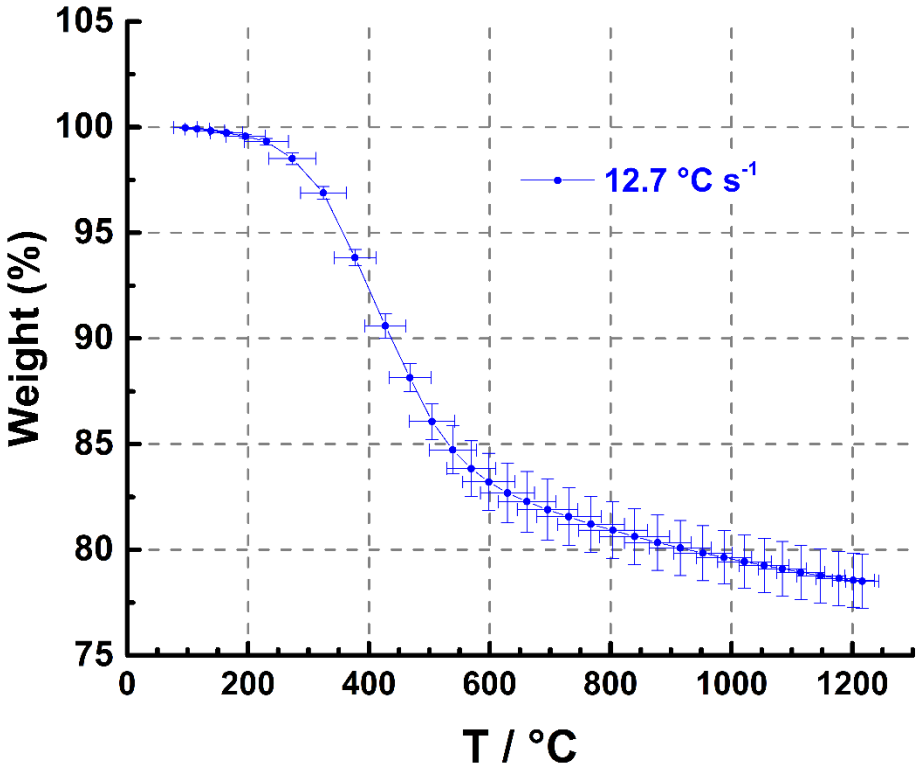

Figure B.15. Simulated thermogravimetric analysis (TGA) curve of PICA with a nominal heating rate of 12.7 °C s^{-1}.

Table B.T.4. TGA data collected with a nominal heating rate of 12.7°C s^{-1}.

T / °C	± °C	% Weight	± % Weight
96.4	19.2	100.0	0.0
115.5	20.3	99.9	0.0
138.5	22.7	99.8	0.0
164.2	27.0	99.7	0.1
195.6	32.3	99.6	0.1
230.2	36.6	99.3	0.2
273.0	39.1	98.5	0.3
324.5	37.6	96.9	0.3
377.0	34.8	93.8	0.4
427.1	33.5	90.6	0.6
467.9	35.0	88.1	0.7
504.5	37.4	86.1	0.8
539.0	38.9	84.7	1.1
569.4	40.8	83.8	1.3
598.5	43.1	83.2	1.4
629.3	44.8	82.7	1.4
661.7	47.2	82.3	1.4
695.6	50.2	81.9	1.4
730.5	53.4	81.6	1.4
767.5	55.4	81.2	1.3
803.8	57.1	80.9	1.3
839.6	58.2	80.6	1.3
877.8	54.9	80.3	1.3
915.2	51.4	80.1	1.3
952.6	48.4	79.8	1.3
987.7	45.8	79.6	1.3
1021.4	44.1	79.4	1.3
1054.3	41.2	79.3	1.3
1084.1	40.0	79.1	1.3
1114.8	39.8	78.9	1.3
1147.5	39.5	78.8	1.3
1178.0	38.8	78.6	1.3
1201.5	34.8	78.6	1.3
1216.4	27.8	78.5	1.3
	SD (1σ)		SD (1σ)

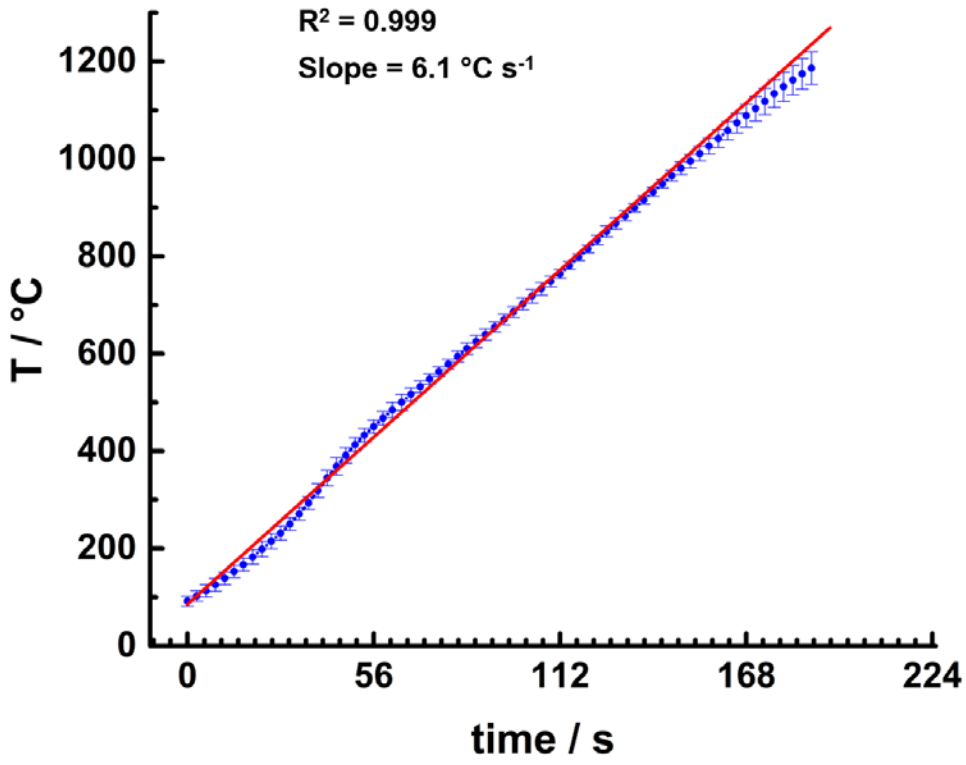

Figure B.16. Heating profile for PICA, with a nominal heating rate of 6.1 °C s^{-1}.

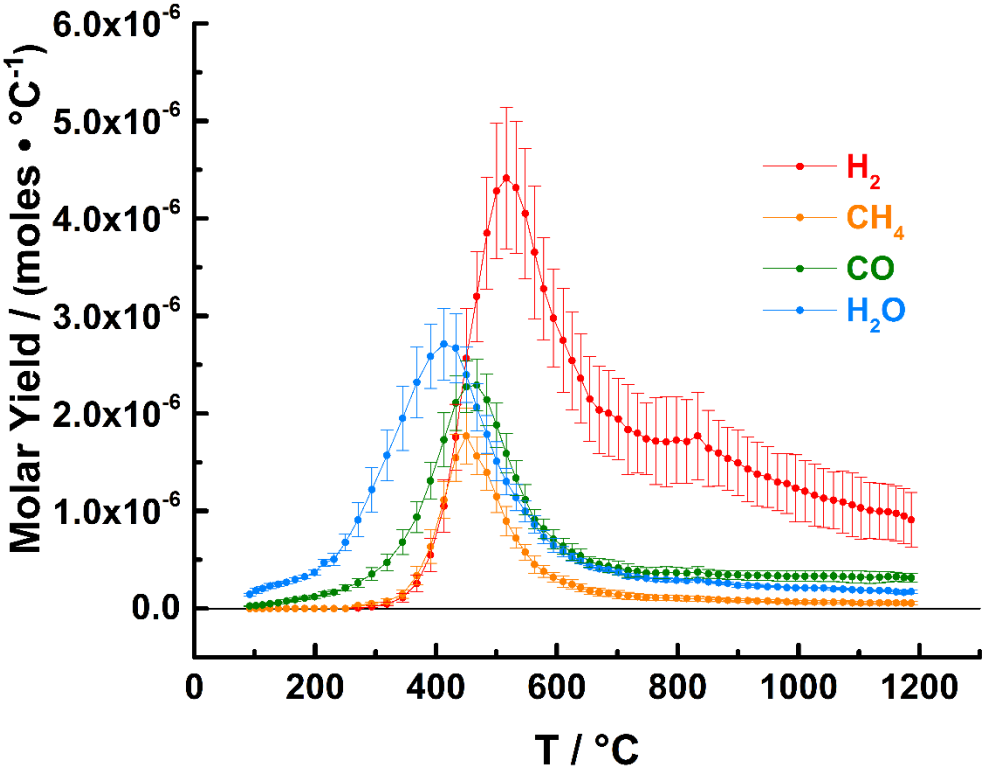

Figure B.17. Molar yields of H_2, CH_4, CO, and H_2O, measured during the pyrolysis of PICA with a nominal heating rate of 6.1 °C s^{-1}.

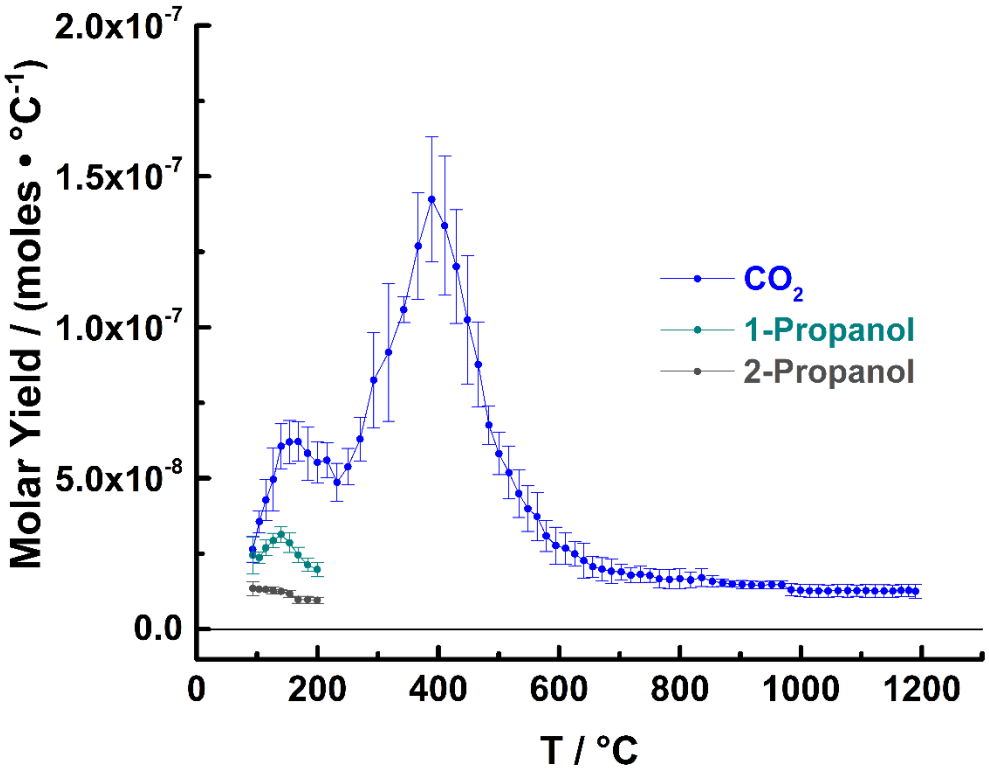

Figure B.18. Molar yields of CO_2, 1-propanol, and 2-propanol, measured during the pyrolysis of PICA, with at a nominal heating rate of 6.1 °C s^{-1}.

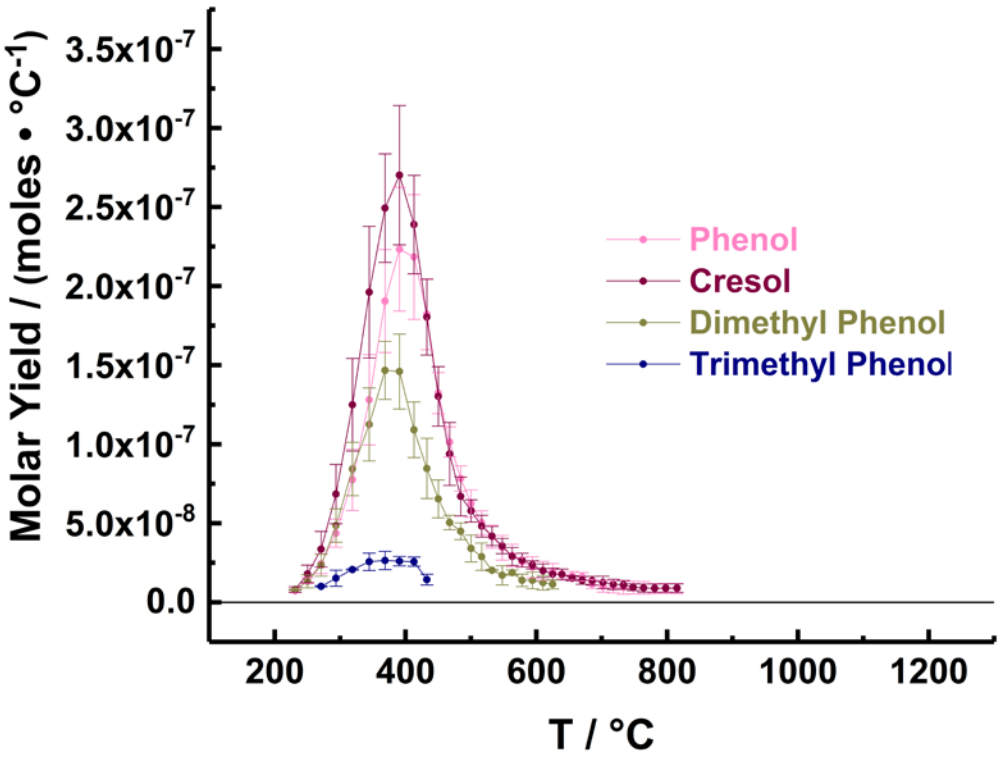

Figure B.19. Molar yields of phenol and its derivatives, measured during the pyrolysis of PICA with a nominal heating rate of 6.1 °C s^{-1}.

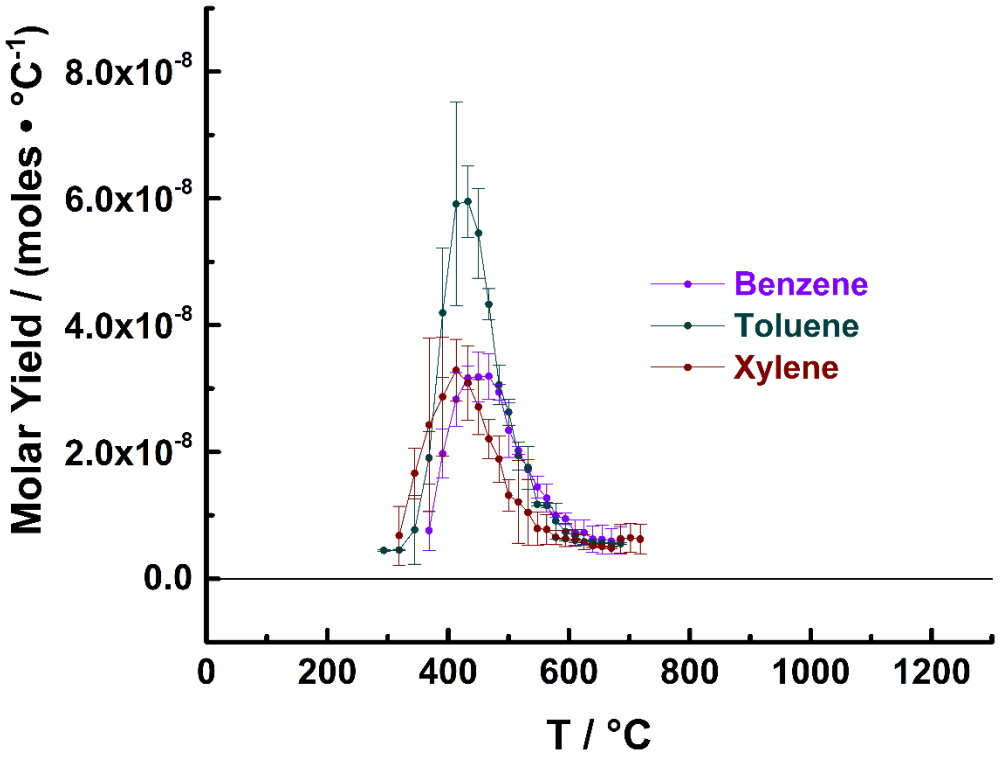

Figure B.20. Molar yields of benzene and derivatives, measured during the pyrolysis of PICA with a nominal heating rate of 6.1 °C s^{-1}.

Table B.T.5. Molar yields of pyrolysis products, measured during the pyrolysis of PICA with a nominal heating rate of 6.1 °C s^{-1}.

		H_2		CH_4		CO		CO_2		Phenol		H_2O		1-Propanol	
T / °C	± °C	moles ·°C^{-1}	SD (1σ)	moles ·°C^{-1}	SD (1σ)	moles ·°C^{-1}	SD (1σ)	moles ·°C^{-1}	SD (1σ)	moles ·°C^{-1}	SD (1σ)	moles ·°C^{-1}	SD (1σ)	moles ·°C^{-1}	SD (1σ)
91.9	12.4					2.5E-08	5.4E-09	2.6E-08	4.2E-09			1.4E-07	1.4E-08	2.4E-08	6.1E-09
102.3	13.3					2.9E-08	9.4E-09	3.6E-08	3.6E-09			1.8E-07	2.5E-08	2.4E-08	2.0E-09
113.0	14.9					3.7E-08	8.0E-09	4.3E-08	6.9E-09			2.1E-07	2.1E-08	2.7E-08	2.5E-09
125.3	15.6					5.0E-08	7.9E-09	5.0E-08	1.0E-08			2.3E-07	2.7E-08	2.9E-08	2.4E-09
139.0	15.8					5.8E-08	1.0E-08	6.1E-08	7.4E-09			2.5E-07	1.8E-08	3.1E-08	2.6E-09
152.6	14.4					7.8E-08	1.4E-08	6.2E-08	7.1E-09			2.7E-07	1.3E-08	2.9E-08	3.2E-09
166.9	13.0					9.3E-08	1.5E-08	6.2E-08	6.6E-09			3.0E-07	1.6E-08	2.5E-08	2.6E-09
182.5	13.0					1.1E-07	1.6E-08	5.8E-08	8.8E-09			3.3E-07	1.7E-08	2.1E-08	2.1E-09
198.8	12.8					1.2E-07	1.6E-08	5.5E-08	6.8E-09			3.7E-07	2.5E-08	2.0E-08	2.4E-09
214.8	13.9					1.5E-07	2.1E-08	5.6E-08	5.7E-09			4.7E-07	3.5E-08		
231.2	16.1					1.7E-07	2.1E-08	4.9E-08	6.3E-09	7.3E-09	1.2E-09	5.0E-07	6.1E-08		
250.2	18.1					2.1E-07	3.0E-08	5.4E-08	6.0E-09	1.4E-08	1.8E-09	6.8E-07	8.8E-08		
270.9	16.2	6.3E-09	1.3E-09	3.4E-08	5.8E-09	2.6E-07	4.5E-08	6.3E-08	7.3E-09	2.4E-08	6.3E-09	9.1E-07	1.7E-07		
293.7	14.3	1.9E-08	7.0E-09	5.1E-08	1.4E-08	3.5E-07	6.6E-08	8.3E-08	1.6E-08	4.4E-08	8.9E-09	1.2E-06	2.3E-07		
318.9	14.2	4.6E-08	1.8E-08	7.4E-08	2.4E-08	4.7E-07	8.6E-08	9.2E-08	2.3E-08	7.7E-08	1.9E-08	1.6E-06	2.6E-07		
344.6	13.9	1.1E-07	4.3E-08	1.5E-07	4.2E-08	6.8E-07	1.3E-07	1.1E-07	4.2E-09	1.3E-07	2.9E-08	2.0E-06	3.3E-07		
368.6	14.2	2.6E-07	8.9E-08	3.4E-07	9.6E-08	9.4E-07	1.6E-07	1.3E-07	1.8E-08	1.9E-07	3.3E-08	2.3E-06	3.6E-07		
390.9	15.8	5.5E-07	1.7E-07	6.3E-07	1.7E-07	1.3E-06	1.9E-07	1.4E-07	2.1E-08	2.2E-07	3.9E-08	2.6E-06	3.3E-07		
413.0	16.8	1.0E-06	2.7E-07	1.1E-06	1.9E-07	1.7E-06	2.8E-07	1.3E-07	2.3E-08	2.2E-07	3.9E-08	2.7E-06	3.7E-07		
432.7	13.8	1.8E-06	3.4E-07	1.5E-06	2.4E-07	2.1E-06	2.8E-07	1.2E-07	1.9E-08	1.8E-07	2.2E-08	2.7E-06	3.5E-07		
450.1	11.8	2.6E-06	5.1E-07	1.8E-06	2.9E-07	2.3E-06	2.7E-07	1.0E-07	2.1E-08	1.3E-07	1.3E-08	2.4E-06	2.9E-07		
467.4	11.0	3.2E-06	4.6E-07	1.6E-06	1.9E-07	2.3E-06	2.7E-07	8.8E-08	1.4E-08	1.0E-07	9.5E-09	2.1E-06	2.4E-07		
484.3	10.0	3.9E-06	5.7E-07	1.4E-06	1.8E-07	2.1E-06	2.6E-07	6.8E-08	6.3E-09	7.8E-08	8.1E-09	1.8E-06	1.9E-07		
500.2	10.3	4.3E-06	7.0E-07	1.1E-06	1.6E-07	1.9E-06	2.3E-07	5.8E-08	7.0E-09	6.2E-08	8.6E-09	1.5E-06	2.0E-07		
516.4	11.5	4.4E-06	7.2E-07	9.0E-07	1.5E-07	1.6E-06	2.0E-07	5.2E-08	8.7E-09	5.0E-08	7.5E-09	1.3E-06	1.4E-07		
532.3	12.0	4.3E-06	6.8E-07	7.2E-07	1.0E-07	1.3E-06	1.8E-07	4.5E-08	7.9E-09	4.2E-08	7.2E-09	1.1E-06	1.4E-07		
547.9	12.6	4.1E-06	6.7E-07	5.8E-07	7.9E-08	1.1E-06	1.6E-07	4.0E-08	7.6E-09	3.5E-08	7.8E-09	1.0E-06	1.1E-07		
563.2	11.7	3.7E-06	6.8E-07	4.5E-07	8.9E-08	9.1E-07	9.8E-08	3.7E-08	8.0E-09	3.0E-08	7.0E-09	8.6E-07	8.8E-08		
578.1	10.5	3.3E-06	5.2E-07	3.8E-07	6.0E-08	8.2E-07	1.0E-07	3.1E-08	5.1E-09	2.5E-08	3.1E-09	7.3E-07	6.6E-08		
594.2	10.9	3.0E-06	5.0E-07	3.2E-07	4.9E-08	7.1E-07	9.9E-08	2.8E-08	6.1E-09	2.2E-08	6.7E-09	6.5E-07	6.9E-08		
610.2	11.0	2.8E-06	5.3E-07	2.8E-07	5.5E-08	6.4E-07	8.3E-08	2.7E-08	5.2E-09	2.0E-08	5.9E-09	5.8E-07	5.1E-08		
625.1	12.2	2.5E-06	5.0E-07	2.5E-07	4.8E-08	5.8E-07	8.5E-08	2.5E-08	4.0E-09	1.9E-08	5.1E-09	5.3E-07	4.4E-08		
639.4	13.4	2.4E-06	4.6E-07	2.1E-07	4.2E-08	5.4E-07	7.4E-08	2.3E-08	5.8E-09	1.8E-08	2.9E-09	4.8E-07	2.5E-08		
654.7	12.9	2.1E-06	4.4E-07	1.8E-07	3.2E-08	4.8E-07	5.3E-08	2.1E-08	3.5E-09	1.7E-08	2.8E-09	4.3E-07	1.3E-08		
		H_2		CH_4		CO		CO_2		Phenol		H_2O		1-Propanol	
T / °C	± °C	moles ·°C^{-1}	SD (1σ)	moles ·°C^{-1}	SD (1σ)	moles ·°C^{-1}	SD (1σ)	moles ·°C^{-1}	SD (1σ)	moles ·°C^{-1}	SD (1σ)	moles ·°C^{-1}	SD (1σ)	moles ·°C^{-1}	SD (1σ)
670.2	11.0	2.0E-06	4.5E-07	1.7E-07	3.7E-08	4.5E-07	6.0E-08	2.0E-08	3.8E-09	1.6E-08	2.7E-09	4.1E-07	2.1E-08		
685.6	8.8	2.0E-06	4.4E-07	1.6E-07	3.5E-08	4.3E-07	6.7E-08	1.9E-08	4.0E-09	1.2E-08	2.9E-09	4.0E-07	2.1E-08		
701.9	7.9	1.9E-06	4.2E-07	1.4E-07	4.4E-08	4.2E-07	7.0E-08	1.9E-08	2.7E-09	1.0E-08	3.6E-09	3.7E-07	2.2E-08		
717.9	6.8	1.8E-06	4.6E-07	1.3E-07	3.9E-08	3.9E-07	6.9E-08	1.8E-08	2.4E-09	9.8E-09	3.8E-09	3.3E-07	2.5E-08		
733.3	7.6	1.8E-06	4.1E-07	1.2E-07	3.4E-08	3.8E-07	5.5E-08	1.8E-08	2.8E-09	9.5E-09	4.4E-09	3.2E-07	1.6E-08		
748.1	9.7	1.7E-06	3.7E-07	1.1E-07	2.8E-08	3.6E-07	5.4E-08	1.8E-08	2.2E-09	9.3E-09	4.0E-09	3.1E-07	4.6E-09		
763.9	11.4	1.7E-06	4.4E-07	1.1E-07	2.9E-08	3.6E-07	5.9E-08	1.7E-08	3.0E-09	9.2E-09	3.9E-09	3.0E-07	1.6E-08		
781.1	11.8	1.7E-06	4.6E-07	1.1E-07	3.0E-08	3.7E-07	6.0E-08	1.7E-08	3.2E-09	8.7E-09	3.2E-09	3.0E-07	2.1E-08		
798.0	10.2	1.7E-06	4.4E-07	1.1E-07	2.7E-08	3.7E-07	5.6E-08	1.7E-08	3.3E-09	8.8E-09	3.2E-09	2.9E-07	1.6E-08		
815.1	8.7	1.7E-06	4.3E-07	1.0E-07	2.8E-08	3.6E-07	5.4E-08	1.6E-08	2.7E-09	8.7E-09	3.2E-09	2.9E-07	1.1E-08		
833.1	8.7	1.8E-06	4.5E-07	1.0E-07	2.5E-08	3.7E-07	5.4E-08	1.7E-08	3.0E-09			2.9E-07	5.1E-09		
851.0	9.2	1.6E-06	3.9E-07	9.3E-08	2.3E-08	3.6E-07	4.5E-08	1.6E-08	1.9E-09			2.7E-07	4.6E-09		
867.4	9.1	1.6E-06	3.4E-07	9.1E-08	1.9E-08	3.5E-07	4.2E-08	1.5E-08	1.2E-09			2.7E-07	7.7E-09		
882.9	11.0	1.5E-06	3.2E-07	8.5E-08	1.5E-08	3.5E-07	4.4E-08	1.5E-08	1.1E-09			2.6E-07	1.4E-08		
899.6	13.5	1.5E-06	3.4E-07	8.5E-08	1.6E-08	3.4E-07	4.2E-08	1.5E-08	1.3E-09			2.4E-07	1.8E-08		
916.1	13.9	1.4E-06	3.3E-07	8.2E-08	1.7E-08	3.4E-07	4.6E-08	1.5E-08	1.3E-09			2.4E-07	2.0E-08		
932.0	14.6	1.4E-06	3.3E-07	7.8E-08	1.4E-08	3.4E-07	4.7E-08	1.5E-08	1.2E-09			2.3E-07	1.5E-08		
948.8	16.3	1.3E-06	3.1E-07	7.8E-08	1.4E-08	3.4E-07	4.7E-08	1.5E-08	1.3E-09			2.2E-07	8.8E-09		
965.4	18.1	1.3E-06	2.9E-07	7.4E-08	1.7E-08	3.3E-07	5.1E-08	1.5E-08	1.3E-09			2.2E-07	6.9E-09		
980.9	18.5	1.3E-06	3.1E-07	7.0E-08	1.3E-08	3.3E-07	5.3E-08	1.3E-08	2.0E-09			2.2E-07	1.1E-09		
995.3	20.4	1.2E-06	3.4E-07	6.6E-08	1.6E-08	3.3E-07	5.2E-08	1.3E-08	2.1E-09			2.1E-07	3.9E-09		
1010.9	23.5	1.2E-06	3.1E-07	6.7E-08	1.6E-08	3.3E-07	5.4E-08	1.3E-08	2.1E-09			2.1E-07	2.7E-09		
1026.3	25.1	1.2E-06	3.2E-07	6.6E-08	1.7E-08	3.3E-07	5.4E-08	1.3E-08	2.1E-09			2.1E-07	2.5E-09		
1041.6	27.0	1.1E-06	3.0E-07	6.4E-08	1.7E-08	3.3E-07	5.6E-08	1.3E-08	2.0E-09			2.1E-07	2.8E-09		
1057.8	28.7	1.1E-06	2.9E-07	6.4E-08	1.8E-08	3.3E-07	5.6E-08	1.3E-08	2.0E-09			2.0E-07	1.1E-08		
1073.7	30.0	1.1E-06	3.2E-07	6.4E-08	1.8E-08	3.3E-07	5.9E-08	1.3E-08	2.1E-09			2.0E-07	9.6E-09		
1088.8	30.1	1.1E-06	3.3E-07	5.9E-08	1.5E-08	3.3E-07	6.4E-08	1.3E-08	1.9E-09			1.9E-07	4.6E-09		
1103.0	31.2	1.0E-06	3.2E-07	5.7E-08	1.8E-08	3.2E-07	6.3E-08	1.3E-08	2.2E-09			1.9E-07	1.6E-09		
1118.2	33.6	1.0E-06	2.8E-07	5.8E-08	1.5E-08	3.2E-07	6.2E-08	1.3E-08	2.0E-09			1.9E-07	7.1E-09		
1133.9	34.8	1.0E-06	2.9E-07	5.8E-08	1.6E-08	3.2E-07	5.8E-08	1.3E-08	2.1E-09			1.8E-07	7.6E-09		
1148.3	35.1	9.9E-07	2.9E-07	5.6E-08	1.7E-08	3.3E-07	5.4E-08	1.3E-08	2.0E-09			1.8E-07	8.7E-09		
1161.7	34.0	9.8E-07	2.8E-07	5.7E-08	1.7E-08	3.3E-07	4.7E-08	1.3E-08	2.1E-09			1.7E-07	1.9E-08		
1174.6	30.7	9.5E-07	2.8E-07	5.7E-08	1.8E-08	3.2E-07	4.8E-08	1.3E-08	2.1E-09			1.7E-07	2.0E-08		
1186.5	27.3	9.1E-07	2.8E-07	5.5E-08	1.7E-08	3.1E-07	4.6E-08	1.3E-08	2.3E-09			1.7E-07	1.9E-08		

Table B.T.5. - continued

		2-Propanol		Xylene		Cresol		Dimethyl Phenol		Trimethyl Phenol		Benzene		Toluene	
T / °C	± °C	moles ·°C^{-1}	SD (1σ)	moles ·°C^{-1}	SD (1σ)	moles ·°C^{-1}	SD (1σ)	moles ·°C^{-1}	SD (1σ)	moles ·°C^{-1}	SD (1σ)	moles ·°C^{-1}	SD (1σ)	moles ·°C^{-1}	SD (1σ)
91.9	12.4	1.3E-08	2.3E-09												
102.3	13.3	1.3E-08	4.8E-10												
113.0	14.9	1.3E-08	5.3E-10												
125.3	15.6	1.3E-08	1.1E-09												
139.0	15.8	1.2E-08	5.6E-10												
152.6	14.4	1.2E-08	1.1E-09												
166.9	13.0	9.8E-09	1.2E-09												
182.5	13.0	9.8E-09	1.2E-09												
198.8	12.8	9.5E-09	9.8E-10												
214.8	13.9														
231.2	16.1					8.1E-09	1.7E-09	8.0E-09	2.7E-10						
250.2	18.1					1.8E-08	5.5E-09	1.3E-08	4.1E-09						
270.9	16.2					3.4E-08	1.1E-08	2.3E-08	7.0E-09	1.0E-08	3.7E-10				
293.7	14.3					6.8E-08	1.9E-08	4.9E-08	1.1E-08	1.5E-08	5.1E-09			4.5E-09	7.8E-11
318.9	14.2			6.8E-09	4.6E-09	1.3E-07	2.9E-08	8.4E-08	1.7E-08	2.1E-08	4.1E-10			4.6E-09	9.1E-11
344.6	13.9			1.7E-08	4.0E-09	2.0E-07	4.2E-08	1.1E-07	2.3E-08	2.6E-08	5.5E-09			7.7E-09	5.4E-09
368.6	14.2			2.4E-08	1.4E-08	2.5E-07	3.4E-08	1.5E-07	1.8E-08	2.6E-08	5.8E-09	7.6E-09	3.1E-09	1.9E-08	4.1E-09
390.9	15.8			2.9E-08	9.4E-09	2.7E-07	4.4E-08	1.5E-07	2.4E-08	2.6E-08	2.9E-09	2.0E-08	3.9E-09	4.2E-08	1.0E-08
413.0	16.8			3.3E-08	4.9E-09	2.4E-07	3.1E-08	1.1E-07	1.8E-08	2.6E-08	2.9E-09	2.8E-08	4.2E-09	5.9E-08	1.6E-08
432.7	13.8			3.1E-08	5.9E-09	1.8E-07	2.4E-08	8.5E-08	1.9E-08	1.4E-08	3.4E-09	3.2E-08	1.9E-09	5.9E-08	5.7E-09
450.1	11.8			2.7E-08	4.3E-09	1.3E-07	1.9E-08	6.5E-08	1.2E-08			3.2E-08	4.0E-09	5.5E-08	7.1E-09
467.4	11.0			2.2E-08	3.1E-09	9.4E-08	2.0E-08	5.0E-08	4.5E-09			3.2E-08	3.6E-09	4.3E-08	2.4E-09
484.3	10.0			1.9E-08	3.7E-09	6.7E-08	1.2E-08	4.5E-08	5.3E-09			2.9E-08	1.2E-09	3.1E-08	3.1E-09
500.2	10.3			1.3E-08	2.5E-09	5.8E-08	7.0E-09	3.4E-08	8.5E-09			2.3E-08	4.3E-09	2.6E-08	2.0E-09
516.4	11.5			1.2E-08	6.5E-09	4.8E-08	6.9E-09	2.9E-08	8.6E-09			2.0E-08	6.1E-10	1.9E-08	2.2E-09
532.3	12.0			1.0E-08	5.2E-09	4.2E-08	6.1E-09	2.0E-08	5.2E-10			1.7E-08	1.5E-09	1.8E-08	3.4E-09
547.9	12.6			7.9E-09	2.6E-09	3.6E-08	4.8E-09	1.7E-08	6.2E-09			1.4E-08	1.7E-09	1.2E-08	2.5E-10
563.2	11.7			7.8E-09	2.3E-09	2.9E-08	5.7E-09	1.9E-08	1.6E-09			1.3E-08	2.2E-09	1.2E-08	4.1E-10
578.1	10.5			6.5E-09	1.2E-09	2.7E-08	4.3E-09	1.4E-08	4.0E-09			1.0E-08	2.7E-10	9.1E-09	2.8E-09
594.2	10.9			6.3E-09	1.2E-09	2.4E-08	2.6E-09	1.4E-08	5.2E-09			9.4E-09	9.0E-10	7.4E-09	1.4E-09
610.2	11.0			6.1E-09	9.5E-10	2.0E-08	4.3E-09	1.2E-08	4.5E-09			7.3E-09	2.0E-09	6.8E-09	1.1E-09
625.1	12.2			5.7E-09	1.2E-09	1.8E-08	3.7E-09	1.1E-08	2.8E-09			7.3E-09	2.0E-09	5.8E-09	3.6E-10
639.4	13.4			5.2E-09	2.0E-10	1.8E-08	3.4E-09					6.3E-09	2.0E-09	5.7E-09	2.3E-10
654.7	12.9			5.1E-09	6.2E-11	1.5E-08	1.6E-09					6.2E-09	2.3E-09	5.6E-09	6.9E-11

		2-Propanol		Xylene		Cresol		Dimethyl Phenol		Trimethyl Phenol		Benzene		Toluene	
T / °C	± °C	moles ·°C^{-1}	SD (1σ)	moles ·°C^{-1}	SD (1σ)	moles ·°C^{-1}	SD (1σ)	moles ·°C^{-1}	SD (1σ)	moles ·°C^{-1}	SD (1σ)	moles ·°C^{-1}	SD (1σ)	moles ·°C^{-1}	SD (1σ)
670.2	11.0			4.9E-09	1.9E-10	1.4E-08	2.4E-09					5.9E-09	2.0E-09	5.4E-09	2.1E-10
685.6	8.8			6.3E-09	2.2E-09	1.4E-08	2.8E-09					6.1E-09	2.1E-09	5.5E-09	1.0E-10
701.9	7.9			6.5E-09	2.2E-09	1.3E-08	3.9E-09								
717.9	6.8			6.2E-09	2.3E-09	1.1E-08	3.2E-09								
733.3	7.6					1.1E-08	2.7E-09								
748.1	9.7					9.6E-09	2.2E-09								
763.9	11.4					9.0E-09	2.6E-09								
781.1	11.8					9.0E-09	2.6E-09								
798.0	10.2					9.1E-09	2.6E-09								
815.1	8.7					9.0E-09	2.7E-09								
833.1	8.7														
851.0	9.2														
867.4	9.1														
882.9	11.0														
899.6	13.5														
916.1	13.9														
932.0	14.6														
948.8	16.3														
965.4	18.1														
980.9	18.5														
995.3	20.4														
1010.9	23.5														
1026.3	25.1														
1041.6	27.0														
1057.8	28.7														
1073.7	30.0														
1088.8	30.1														
1103.0	31.2														
1118.2	33.6														
1133.9	34.8														
1148.3	35.1														
1161.7	34.0														
1174.6	30.7														
1186.5	27.3														

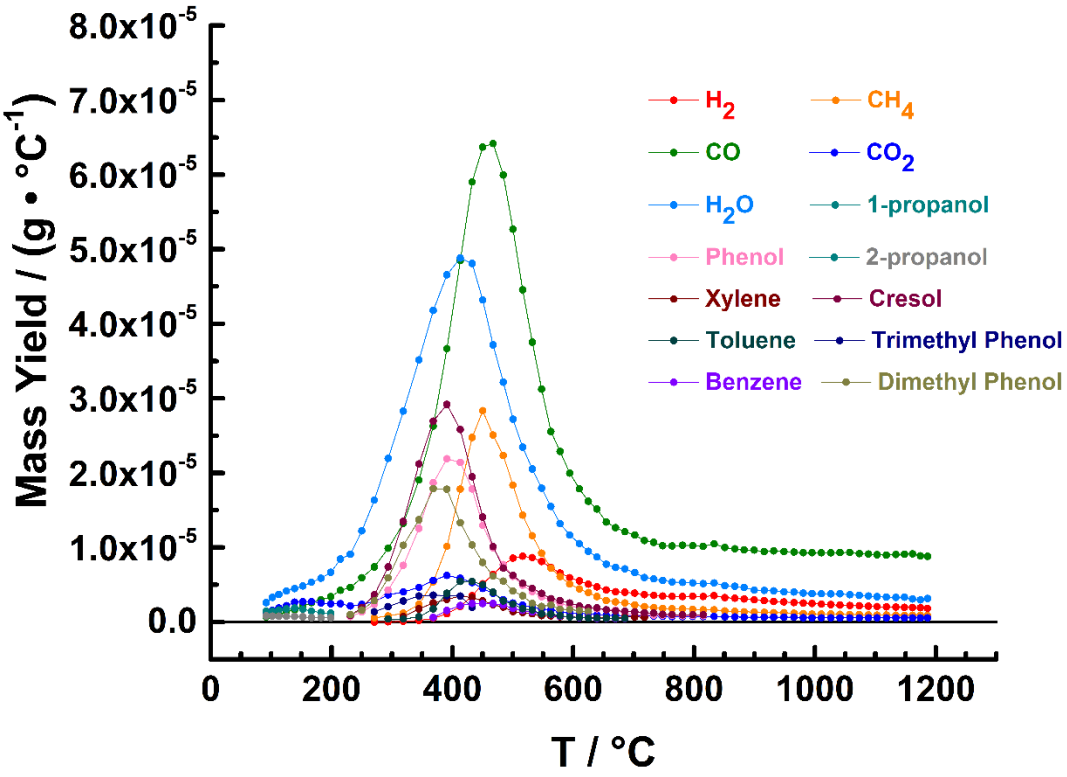

Figure B.21. Mass yields of pyrolysis products as a function of nominal heating rate of PICA, measured during the pyrolysis of PICA with a nominal heating rate of 6.1 °C s^{-1}.

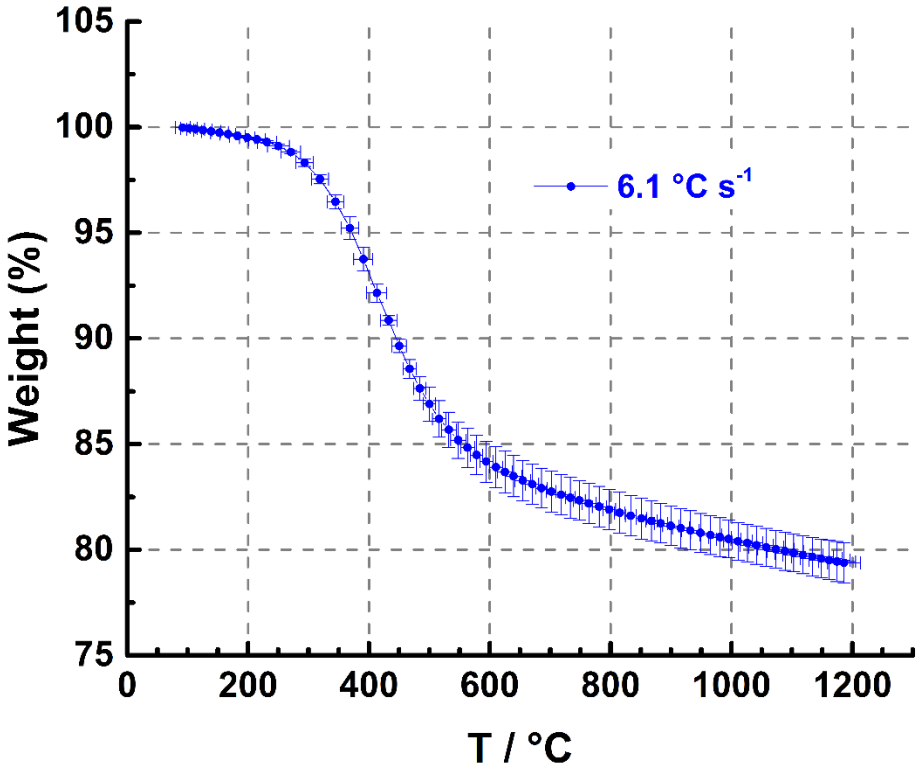

Figure B.22. Simulated thermogravimetric analysis (TGA) curve of PICA, with at a nominal heating rate of 6.1 °C s^{-1}.

Table B.T.6. TGA data collected with a nominal heating rate of 6.1 °C s^{-1}.

T / °C	± °C	% Weight	± % Weight
91.9	12.4	100.0	0.0
102.3	13.3	99.9	0.0
113.0	14.9	99.9	0.0
125.3	15.6	99.9	0.0
139.0	15.8	99.8	0.0
152.6	14.4	99.7	0.0
166.9	13.0	99.7	0.0
182.5	13.0	99.6	0.0
198.8	12.8	99.5	0.0
214.8	13.9	99.4	0.0
231.2	16.1	99.3	0.1
250.2	18.1	99.1	0.1
270.9	16.2	98.8	0.1
293.7	14.3	98.3	0.2
318.9	14.2	97.5	0.2
344.6	13.9	96.5	0.3
368.6	14.2	95.2	0.5
390.9	15.8	93.8	0.6
413.0	16.8	92.1	0.4
432.7	13.8	90.9	0.2
450.1	11.8	89.6	0.3
467.4	11.0	88.6	0.4
484.3	10.0	87.6	0.5
500.2	10.3	86.9	0.8
516.4	11.5	86.2	0.9
532.3	12.0	85.7	0.8
547.9	12.6	85.2	0.9
563.2	11.7	84.8	0.9
578.1	10.5	84.5	0.9
594.2	10.9	84.2	1.0
610.2	11.0	83.9	1.0
625.1	12.2	83.7	1.0
639.4	13.4	83.5	1.0
654.7	12.9	83.3	1.0
	SD (1σ)		SD (1σ)

T / °C	± °C	% Weight	± % Weight
670.2	11.0	83.1	1.0
685.6	8.8	82.9	1.0
701.9	7.9	82.8	1.0
717.9	6.8	82.6	1.0
733.3	7.6	82.5	1.0
748.1	9.7	82.3	0.9
763.9	11.4	82.2	0.9
781.1	11.8	82.0	1.0
798.0	10.2	81.9	1.0
815.1	8.7	81.8	1.0
833.1	8.7	81.6	1.0
851.0	9.2	81.5	1.0
867.4	9.1	81.4	1.0
882.9	11.0	81.3	0.9
899.6	13.5	81.1	0.9
916.1	13.9	81.0	0.9
932.0	14.6	80.9	0.9
948.8	16.3	80.8	0.9
965.4	18.1	80.7	0.9
980.9	18.5	80.6	0.9
995.3	20.4	80.5	0.9
1010.9	23.5	80.4	0.9
1026.3	25.1	80.3	0.9
1041.6	27.0	80.2	0.9
1057.8	28.7	80.1	0.9
1073.7	30.0	80.0	0.9
1088.8	30.1	79.9	0.9
1103.0	31.2	79.8	0.9
1118.2	33.6	79.8	0.9
1133.9	34.8	79.7	0.9
1148.3	35.1	79.6	0.9
1161.7	34.0	79.5	0.9
1174.6	30.7	79.4	0.9
1186.5	27.3	79.4	1.0
	SD (1σ)		SD (1σ)

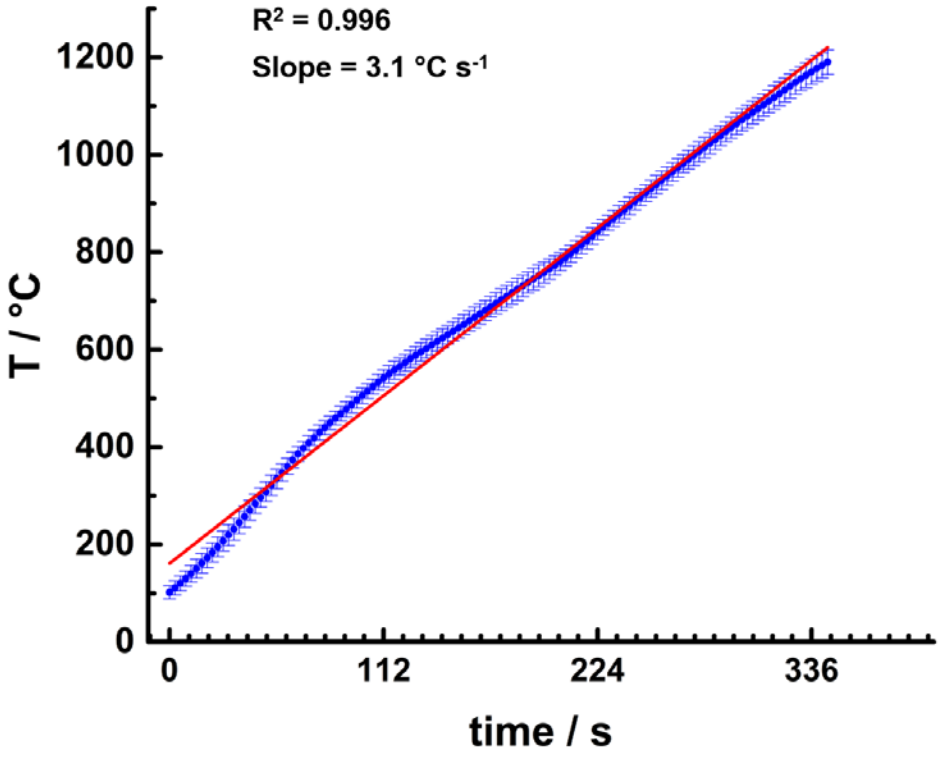

Figure B.23. Heating profile for PICA, with a nominal heating rate of 3.1 °C s^{-1}.

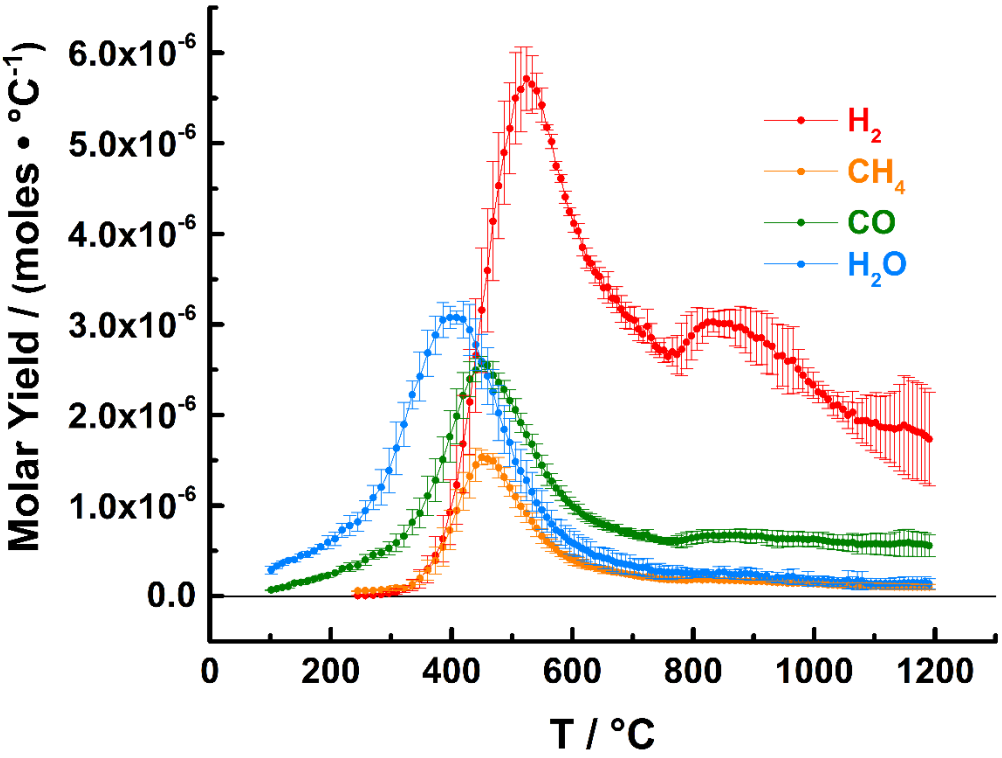

Figure B.24. Molar yields of H_2, CH_4, CO, and H_2O, measured during the pyrolysis of PICA with a nominal heating rate of 3.1 °C s^{-1}.

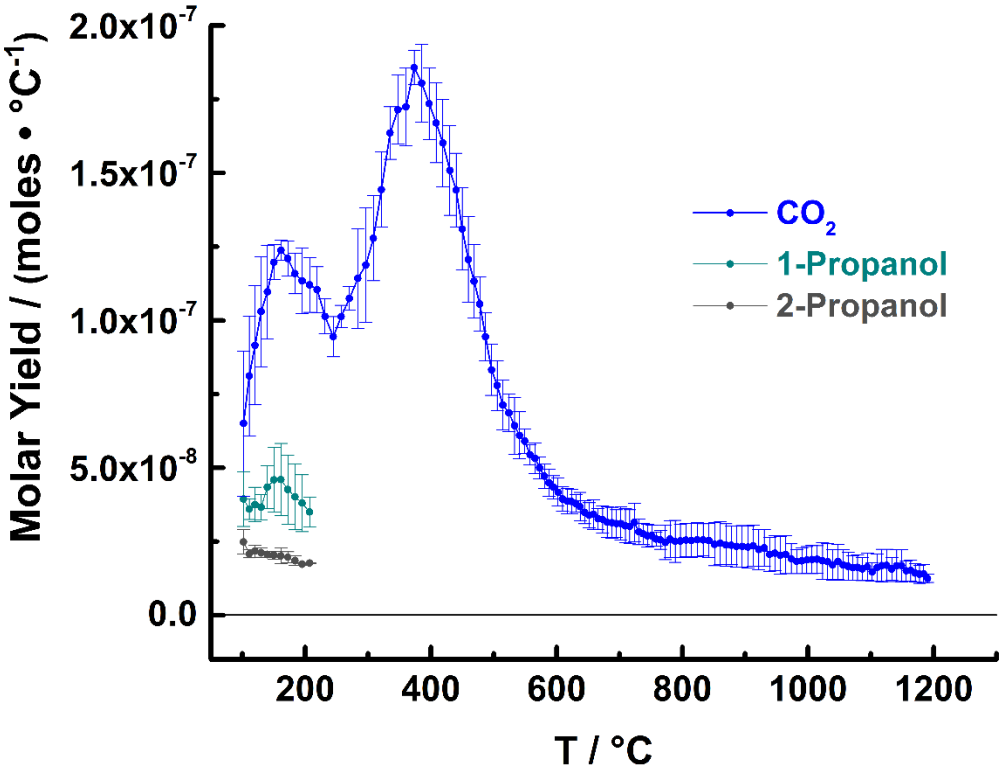

Figure B.25. Molar yields of CO_2, 1-propanol, and 2-propanol, measured during the pyrolysis of PICA with a nominal heating rate of 3.1 °C s^{-1}.

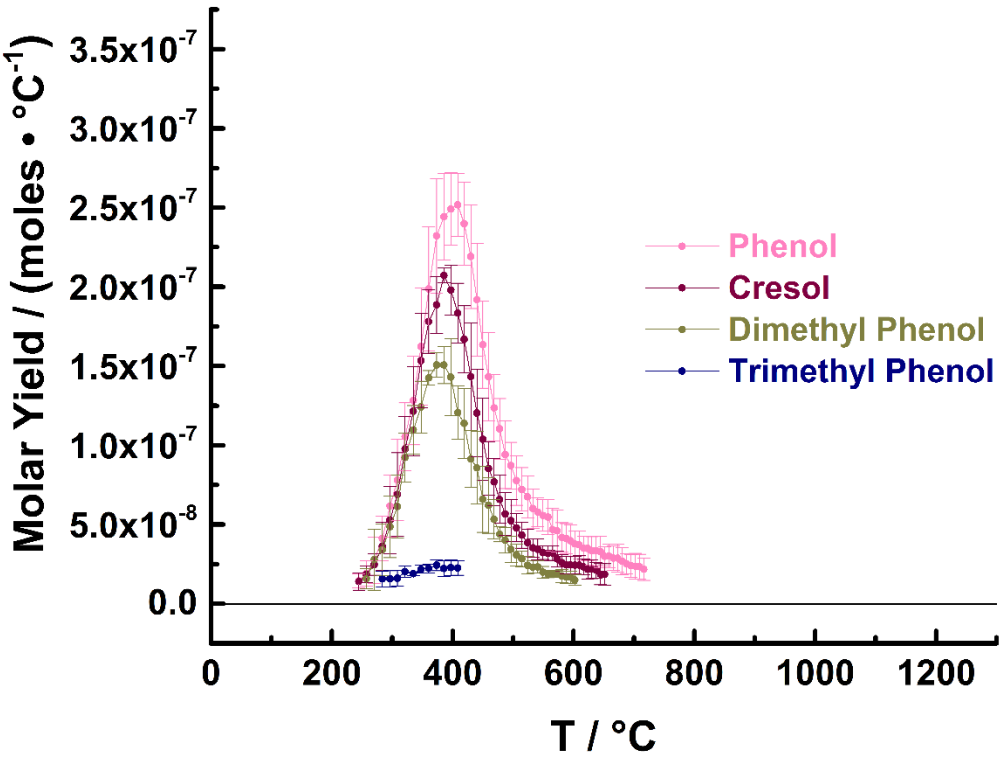

Figure B.26. Molar yields of phenol and its derivatives, measured during the pyrolysis of PICA with a nominal heating rate of 3.1 °C s^{-1}.

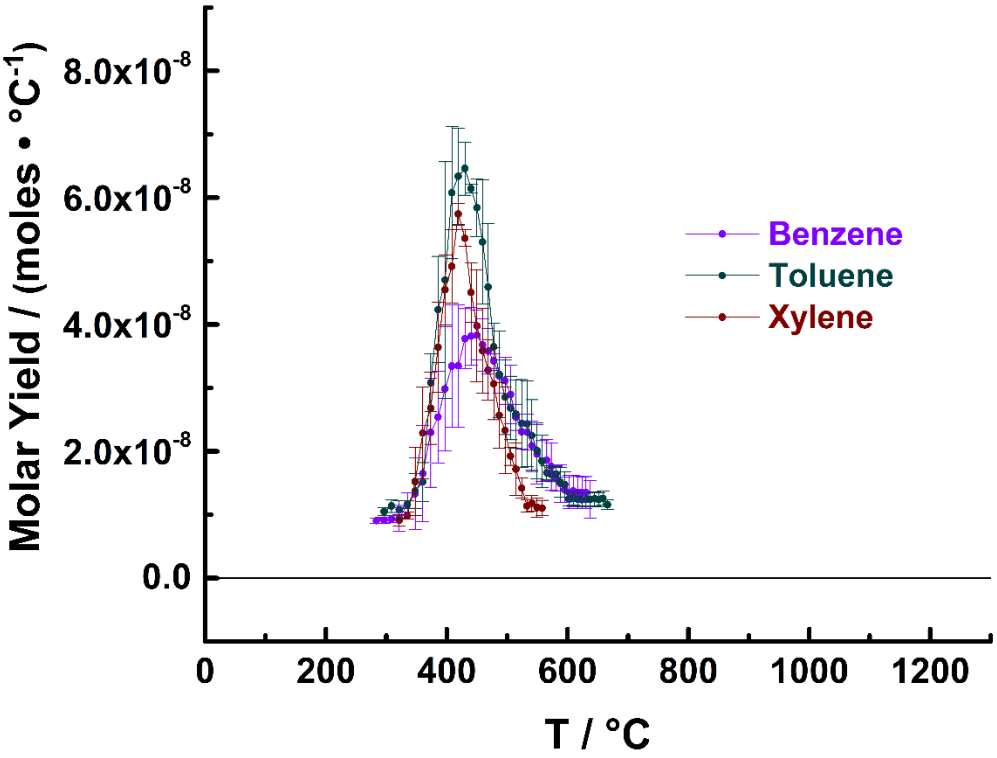

Figure B.27. Molar yields of benzene and its derivatives, measured during the pyrolysis of PICA with a nominal heating rate of 3.1 °C s^{-1}.

Table B.T.7. Molar yields of pyrolysis products, measured during the pyrolysis of PICA with a nominal heating rate of 3.1 °C s^{-1}.

		H_2		CH_4		CO		CO_2		Phenol		H_2O		1-Propanol	
T / °C	± °C	moles ·°C^{-1}	SD (1σ)	moles ·°C^{-1}	SD (1σ)	moles ·°C^{-1}	SD (1σ)	moles ·°C^{-1}	SD (1σ)	moles ·°C^{-1}	SD (1σ)	moles ·°C^{-1}	SD (1σ)	moles ·°C^{-1}	SD (1σ)
101.8	13.4					6.8E-08	3.7E-09	6.5E-08	2.5E-08			2.9E-07	4.3E-08	3.9E-08	9.3E-09
111.0	14.4					8.2E-08	1.3E-08	8.1E-08	2.0E-08			3.3E-07	2.9E-08	3.6E-08	3.5E-09
120.2	15.0					9.5E-08	1.6E-08	9.2E-08	2.0E-08			3.6E-07	2.4E-08	3.8E-08	5.9E-09
129.8	15.7					1.1E-07	2.0E-08	1.0E-07	1.9E-08			3.9E-07	1.8E-08	3.7E-08	4.4E-09
139.9	17.5					1.4E-07	1.6E-08	1.1E-07	1.6E-08			4.0E-07	2.3E-08	4.3E-08	7.3E-09
150.2	19.3					1.5E-07	2.2E-08	1.2E-07	5.9E-09			4.5E-07	1.7E-08	4.6E-08	1.1E-08
161.4	20.4					1.7E-07	2.3E-08	1.2E-07	3.5E-09			4.6E-07	3.2E-08	4.6E-08	1.2E-08
172.4	20.2					1.9E-07	2.2E-08	1.2E-07	6.0E-09			5.0E-07	3.4E-08	4.3E-08	1.2E-08
183.6	19.8					2.1E-07	1.9E-08	1.2E-07	6.9E-09			5.4E-07	2.6E-08	4.0E-08	1.1E-08
195.1	19.9					2.3E-07	2.0E-08	1.1E-07	1.1E-08			5.9E-07	7.2E-08	3.8E-08	9.6E-09
207.0	20.2					2.5E-07	1.2E-08	1.1E-07	9.3E-09			6.3E-07	7.3E-08	3.5E-08	5.0E-09
219.1	21.6					3.0E-07	3.2E-08	1.1E-07	7.8E-09			7.3E-07	7.7E-08		
231.5	22.8					3.2E-07	4.8E-08	1.0E-07	6.0E-09			7.8E-07	1.1E-07		
244.7	22.8	7.1E-09	4.5E-10	5.8E-08	5.2E-09	3.4E-07	5.0E-08	9.4E-08	6.8E-09	1.4E-08	4.4E-09	8.2E-07	1.0E-07		
257.3	21.7	7.2E-09	2.8E-10	6.0E-08	7.4E-09	4.0E-07	5.9E-08	1.0E-07	3.8E-09	1.9E-08	7.8E-09	9.4E-07	1.1E-07		
270.2	20.5	1.2E-08	4.9E-09	6.3E-08	6.0E-09	4.5E-07	4.8E-08	1.1E-07	4.0E-09	2.8E-08	1.5E-08	1.1E-06	1.3E-07		
283.8	20.2	1.8E-08	1.2E-08	6.8E-08	8.3E-09	4.8E-07	5.2E-08	1.1E-07	1.7E-08	4.1E-08	1.4E-08	1.2E-06	2.0E-07		
296.4	19.9	3.1E-08	1.8E-08	7.7E-08	1.3E-08	5.3E-07	7.0E-08	1.2E-07	1.9E-08	6.2E-08	2.0E-08	1.4E-06	2.4E-07		
308.4	20.1	4.8E-08	2.9E-08	9.2E-08	2.9E-08	5.9E-07	9.8E-08	1.3E-07	1.4E-08	7.8E-08	2.6E-08	1.6E-06	2.9E-07		
321.3	20.6	8.1E-08	3.8E-08	9.0E-08	1.7E-08	6.6E-07	1.2E-07	1.4E-07	1.3E-08	1.1E-07	2.1E-08	1.9E-06	2.4E-07		
334.9	19.8	1.2E-07	6.4E-08	1.3E-07	4.8E-08	8.2E-07	1.4E-07	1.6E-07	8.9E-09	1.3E-07	2.8E-08	2.2E-06	1.5E-07		
347.7	18.2	1.9E-07	1.0E-07	2.0E-07	7.4E-08	9.2E-07	1.7E-07	1.7E-07	1.2E-08	1.6E-07	3.7E-08	2.4E-06	2.7E-07		
360.3	16.6	3.0E-07	1.5E-07	2.9E-07	1.1E-07	1.1E-06	2.2E-07	1.7E-07	1.3E-08	2.0E-07	3.9E-08	2.7E-06	2.6E-07		
373.4	16.0	4.5E-07	2.1E-07	3.9E-07	1.5E-07	1.3E-06	2.4E-07	1.9E-07	5.9E-09	2.3E-07	3.6E-08	2.9E-06	2.1E-07		
385.5	15.1	6.3E-07	2.6E-07	5.4E-07	2.1E-07	1.5E-06	2.5E-07	1.8E-07	1.3E-08	2.4E-07	2.7E-08	3.0E-06	1.9E-07		
397.1	14.5	9.3E-07	3.6E-07	7.3E-07	2.2E-07	1.8E-06	2.8E-07	1.7E-07	1.2E-08	2.5E-07	2.3E-08	3.1E-06	1.2E-07		
408.3	15.4	1.2E-06	4.3E-07	9.5E-07	2.3E-07	2.0E-06	3.0E-07	1.7E-07	1.4E-08	2.5E-07	2.0E-08	3.1E-06	7.2E-08		
419.0	15.7	1.7E-06	5.4E-07	1.2E-06	2.1E-07	2.2E-06	2.5E-07	1.6E-07	1.5E-08	2.4E-07	2.6E-08	3.1E-06	2.0E-07		
430.1	15.3	2.1E-06	5.8E-07	1.3E-06	2.4E-07	2.4E-06	1.9E-07	1.5E-07	1.5E-08	2.2E-07	3.3E-08	2.9E-06	2.8E-07		
440.1	14.3	2.7E-06	6.3E-07	1.5E-06	1.8E-07	2.5E-06	1.3E-07	1.4E-07	1.2E-08	1.9E-07	3.6E-08	2.8E-06	2.8E-07		
449.9	13.5	3.2E-06	6.9E-07	1.5E-06	8.3E-08	2.6E-06	7.9E-08	1.3E-07	1.4E-08	1.6E-07	2.7E-08	2.6E-06	3.0E-07		
459.5	14.0	3.6E-06	6.8E-07	1.5E-06	5.4E-08	2.6E-06	4.4E-08	1.2E-07	1.5E-08	1.4E-07	2.8E-08	2.4E-06	3.1E-07		
468.7	14.9	4.1E-06	6.6E-07	1.5E-06	8.6E-08	2.4E-06	1.5E-07	1.1E-07	1.3E-08	1.2E-07	2.1E-08	2.3E-06	2.5E-07		
477.7	15.8	4.5E-06	5.8E-07	1.4E-06	1.1E-07	2.4E-06	1.1E-07	1.1E-07	9.1E-09	1.1E-07	1.9E-08	2.0E-06	3.1E-07		
		H_2		CH_4		CO		CO_2		Phenol		H_2O		1-Propanol	
T / °C	± °C	moles ·°C^{-1}	SD (1σ)	moles ·°C^{-1}	SD (1σ)	moles ·°C^{-1}	SD (1σ)	moles ·°C^{-1}	SD (1σ)	moles ·°C^{-1}	SD (1σ)	moles ·°C^{-1}	SD (1σ)	moles ·°C^{-1}	SD (1σ)
486.8	16.6	4.9E-06	5.7E-07	1.3E-06	1.0E-07	2.3E-06	1.0E-07	9.4E-08	8.1E-09	9.4E-08	2.1E-08	1.8E-06	2.6E-07		
496.5	16.9	5.2E-06	5.0E-07	1.2E-06	9.0E-08	2.2E-06	1.2E-07	8.3E-08	8.6E-09	8.7E-08	1.5E-08	1.7E-06	2.7E-07		
505.5	16.0	5.5E-06	5.0E-07	1.1E-06	1.2E-07	2.1E-06	1.2E-07	7.8E-08	8.5E-09	7.8E-08	1.6E-08	1.5E-06	2.1E-07		
514.6	15.2	5.6E-06	4.7E-07	9.9E-07	1.1E-07	1.9E-06	1.1E-07	7.1E-08	8.4E-09	7.2E-08	1.4E-08	1.4E-06	2.4E-07		
524.2	15.3	5.7E-06	3.5E-07	9.2E-07	1.0E-07	1.8E-06	1.1E-07	6.9E-08	6.4E-09	6.7E-08	1.3E-08	1.3E-06	2.2E-07		
533.0	16.2	5.7E-06	3.2E-07	8.3E-07	9.6E-08	1.7E-06	1.1E-07	6.4E-08	9.6E-09	6.0E-08	1.2E-08	1.2E-06	2.2E-07		
541.1	17.3	5.6E-06	2.0E-07	7.5E-07	9.4E-08	1.6E-06	1.3E-07	6.1E-08	8.0E-09	5.8E-08	9.1E-09	1.0E-06	1.6E-07		
549.4	17.8	5.4E-06	1.9E-07	6.6E-07	8.0E-08	1.4E-06	1.1E-07	5.9E-08	4.2E-09	5.6E-08	9.9E-09	9.5E-07	2.1E-07		
557.9	18.1	5.2E-06	2.7E-08	6.0E-07	7.4E-08	1.3E-06	1.2E-07	5.4E-08	3.4E-09	5.5E-08	1.1E-08	8.7E-07	1.6E-07		
565.5	17.5	5.0E-06	8.0E-08	5.6E-07	7.0E-08	1.3E-06	8.2E-08	5.3E-08	5.2E-09	4.7E-08	1.3E-08	7.9E-07	1.5E-07		
573.0	17.2	4.8E-06	5.1E-08	5.2E-07	4.7E-08	1.2E-06	8.4E-08	5.0E-08	3.7E-09	4.6E-08	1.3E-08	7.3E-07	1.2E-07		
580.8	17.5	4.6E-06	4.0E-08	4.7E-07	3.2E-08	1.1E-06	7.9E-08	4.7E-08	4.2E-09	4.2E-08	9.4E-09	7.0E-07	1.4E-07		
588.1	18.2	4.4E-06	6.8E-08	4.5E-07	4.5E-08	1.1E-06	7.5E-08	4.5E-08	4.6E-09	4.1E-08	9.5E-09	6.5E-07	1.3E-07		
595.3	18.9	4.2E-06	4.6E-08	4.2E-07	5.0E-08	1.0E-06	6.4E-08	4.3E-08	3.9E-09	4.0E-08	9.9E-09	6.0E-07	1.4E-07		
602.3	19.3	4.1E-06	9.6E-08	4.0E-07	5.5E-08	9.8E-07	6.8E-08	4.2E-08	4.8E-09	3.8E-08	8.1E-09	5.8E-07	1.3E-07		
609.4	19.7	4.0E-06	8.4E-08	3.8E-07	4.9E-08	9.6E-07	5.5E-08	3.9E-08	4.1E-09	3.7E-08	9.0E-09	5.6E-07	1.2E-07		
616.8	19.9	3.9E-06	9.7E-08	3.6E-07	4.8E-08	9.1E-07	5.2E-08	3.9E-08	4.2E-09	3.5E-08	7.6E-09	5.2E-07	1.3E-07		
623.6	19.5	3.7E-06	1.1E-07	3.4E-07	3.6E-08	8.7E-07	4.9E-08	3.9E-08	4.2E-09	3.5E-08	7.6E-09	5.1E-07	1.3E-07		
630.4	18.9	3.7E-06	8.2E-08	3.3E-07	3.4E-08	8.6E-07	5.1E-08	3.8E-08	3.0E-09	3.3E-08	9.0E-09	4.7E-07	1.2E-07		
637.4	19.5	3.6E-06	1.2E-07	3.2E-07	3.2E-08	8.3E-07	5.5E-08	3.7E-08	4.8E-09	3.4E-08	9.3E-09	4.4E-07	9.7E-08		
644.5	20.2	3.5E-06	9.8E-08	3.1E-07	3.6E-08	8.1E-07	4.7E-08	3.5E-08	3.9E-09	3.3E-08	9.9E-09	4.4E-07	9.9E-08		
651.6	20.4	3.4E-06	1.2E-07	2.9E-07	4.2E-08	7.9E-07	5.1E-08	3.4E-08	4.2E-09	3.0E-08	6.1E-09	4.2E-07	1.1E-07		
658.7	20.8	3.4E-06	1.7E-07	2.9E-07	3.6E-08	7.8E-07	5.2E-08	3.4E-08	5.0E-09	3.0E-08	7.5E-09	4.1E-07	1.1E-07		
666.1	21.1	3.3E-06	9.9E-08	2.7E-07	2.6E-08	7.5E-07	4.3E-08	3.3E-08	3.5E-09	2.9E-08	7.6E-09	3.9E-07	1.1E-07		
673.2	20.7	3.3E-06	1.4E-07	2.6E-07	2.8E-08	7.5E-07	4.4E-08	3.2E-08	4.6E-09	2.9E-08	8.7E-09	3.7E-07	1.1E-07		
680.5	20.5	3.2E-06	1.5E-07	2.6E-07	2.5E-08	7.1E-07	4.4E-08	3.2E-08	5.2E-09	2.7E-08	8.6E-09	3.6E-07	1.1E-07		
688.1	20.9	3.1E-06	1.4E-07	2.5E-07	2.5E-08	7.1E-07	4.6E-08	3.1E-08	5.2E-09	2.5E-08	6.4E-09	3.5E-07	1.1E-07		
695.2	21.6	3.1E-06	1.2E-07	2.4E-07	2.7E-08	7.0E-07	4.2E-08	3.1E-08	4.7E-09	2.4E-08	7.2E-09	3.5E-07	1.1E-07		
702.3	22.4	3.0E-06	1.5E-07	2.3E-07	2.2E-08	6.8E-07	4.1E-08	3.1E-08	5.6E-09	2.4E-08	8.2E-09	3.3E-07	8.8E-08		
709.4	22.6	2.9E-06	1.2E-07	2.2E-07	1.8E-08	6.7E-07	3.7E-08	3.0E-08	5.8E-09	2.3E-08	7.9E-09	3.2E-07	8.5E-08		
716.4	22.8	2.9E-06	9.1E-08	2.1E-07	2.4E-08	6.7E-07	5.5E-08	3.0E-08	5.7E-09	2.2E-08	7.0E-09	3.2E-07	9.7E-08		
723.8	22.8	3.0E-06	1.9E-07	2.1E-07	2.9E-08	6.8E-07	5.9E-08	3.1E-08	6.6E-09			3.2E-07	9.7E-08		
730.7	22.2	2.9E-06	1.5E-07	2.0E-07	2.2E-08	6.4E-07	4.0E-08	2.8E-08	4.4E-09			2.8E-07	8.2E-08		
737.7	21.6	2.8E-06	9.1E-08	2.0E-07	2.1E-08	6.3E-07	2.6E-08	2.8E-08	3.6E-09			2.7E-07	7.8E-08		

Table B.T.7. - Continued

		H_2		CH_4		CO		CO_2		Phenol		H_2O		1-Propanol	
T / °C	± °C	moles ·°C^{-1}	SD (1σ)	moles ·°C^{-1}	SD (1σ)	moles ·°C^{-1}	SD (1σ)	moles ·°C^{-1}	SD (1σ)	moles ·°C^{-1}	SD (1σ)	moles ·°C^{-1}	SD (1σ)	moles ·°C^{-1}	SD (1σ)
744.6	22.1	2.7E-06	8.1E-08	1.9E-07	2.2E-08	6.2E-07	2.8E-08	2.7E-08	3.9E-09			2.8E-07	8.9E-08		
751.4	22.6	2.7E-06	1.3E-07	1.9E-07	1.6E-08	6.1E-07	3.5E-08	2.7E-08	3.6E-09			2.6E-07	7.2E-08		
758.3	21.8	2.6E-06	6.1E-08	1.8E-07	2.4E-08	6.1E-07	2.9E-08	2.6E-08	2.4E-09			2.6E-07	7.3E-08		
765.3	20.9	2.7E-06	1.6E-07	1.8E-07	2.3E-08	6.1E-07	4.6E-08	2.6E-08	3.2E-09			2.6E-07	7.9E-08		
773.0	19.8	2.7E-06	2.1E-07	1.8E-07	2.1E-08	6.1E-07	6.4E-08	2.5E-08	5.8E-09			2.7E-07	7.0E-08		
780.6	18.3	2.7E-06	2.9E-07	1.8E-07	2.5E-08	6.1E-07	7.7E-08	2.6E-08	6.3E-09			2.6E-07	6.5E-08		
788.7	17.0	2.8E-06	2.9E-07	1.8E-07	1.4E-08	6.3E-07	7.8E-08	2.5E-08	7.1E-09			2.6E-07	5.9E-08		
797.0	17.5	2.9E-06	2.7E-07	1.8E-07	1.6E-08	6.4E-07	7.1E-08	2.5E-08	5.6E-09			2.5E-07	4.8E-08		
805.8	18.0	3.0E-06	2.3E-07	1.9E-07	1.4E-08	6.5E-07	6.9E-08	2.5E-08	5.7E-09			2.5E-07	3.5E-08		
814.8	17.7	3.0E-06	1.9E-07	1.8E-07	9.4E-09	6.6E-07	6.9E-08	2.5E-08	5.8E-09			2.5E-07	4.9E-08		
823.7	17.6	3.0E-06	1.5E-07	1.8E-07	1.0E-08	6.7E-07	5.9E-08	2.6E-08	5.7E-09			2.5E-07	4.3E-08		
833.3	17.4	3.0E-06	1.1E-07	1.8E-07	8.5E-09	6.7E-07	6.4E-08	2.6E-08	5.5E-09			2.4E-07	2.8E-08		
842.4	16.6	3.0E-06	1.4E-07	1.7E-07	6.4E-09	6.6E-07	7.0E-08	2.5E-08	5.8E-09			2.6E-07	6.4E-08		
851.3	15.8	3.0E-06	1.5E-07	1.8E-07	5.0E-09	6.7E-07	6.3E-08	2.4E-08	7.3E-09			2.6E-07	6.8E-08		
860.6	15.8	3.0E-06	1.6E-07	1.8E-07	9.6E-09	6.7E-07	6.7E-08	2.4E-08	7.2E-09			2.4E-07	4.7E-08		
869.4	16.6	3.0E-06	2.0E-07	1.7E-07	8.0E-09	6.7E-07	6.9E-08	2.4E-08	7.2E-09			2.4E-07	5.3E-08		
878.0	17.6	3.0E-06	2.3E-07	1.7E-07	6.5E-09	6.7E-07	7.2E-08	2.4E-08	6.6E-09			2.4E-07	5.8E-08		
886.6	17.7	2.9E-06	2.5E-07	1.7E-07	9.2E-09	6.6E-07	7.6E-08	2.3E-08	7.0E-09			2.5E-07	7.0E-08		
895.2	17.8	2.9E-06	2.9E-07	1.7E-07	1.0E-08	6.6E-07	7.8E-08	2.3E-08	7.1E-09			2.4E-07	6.7E-08		
904.4	17.9	2.8E-06	3.0E-07	1.6E-07	1.0E-08	6.6E-07	7.6E-08	2.3E-08	7.2E-09			2.4E-07	6.0E-08		
913.0	17.2	2.9E-06	3.0E-07	1.6E-07	8.7E-09	6.6E-07	7.6E-08	2.3E-08	7.0E-09			2.1E-07	3.3E-08		
921.7	16.7	2.8E-06	3.3E-07	1.6E-07	1.3E-08	6.5E-07	8.1E-08	2.2E-08	6.8E-09			2.3E-07	5.0E-08		
930.4	17.6	2.8E-06	3.1E-07	1.6E-07	1.1E-08	6.4E-07	8.6E-08	2.3E-08	6.2E-09			1.9E-07	3.2E-08		
938.9	18.8	2.7E-06	3.6E-07	1.5E-07	1.1E-08	6.3E-07	9.3E-08	2.1E-08	5.7E-09			2.1E-07	5.8E-08		
947.5	18.9	2.7E-06	3.4E-07	1.5E-07	1.2E-08	6.4E-07	8.2E-08	2.1E-08	5.9E-09			2.0E-07	4.0E-08		
956.1	19.0	2.6E-06	3.6E-07	1.4E-07	1.6E-08	6.3E-07	8.9E-08	2.0E-08	6.3E-09			2.1E-07	7.5E-08		
965.0	19.3	2.6E-06	3.7E-07	1.4E-07	1.4E-08	6.3E-07	8.3E-08	2.1E-08	6.5E-09			2.1E-07	8.5E-08		
973.4	18.7	2.5E-06	2.2E-07	1.5E-07	1.4E-08	6.4E-07	8.1E-08	1.9E-08	5.1E-09			1.9E-07	4.4E-08		
981.8	18.3	2.4E-06	1.8E-07	1.4E-07	1.4E-08	6.3E-07	8.0E-08	1.8E-08	4.1E-09			1.8E-07	4.9E-08		
990.1	19.3	2.4E-06	1.5E-07	1.4E-07	1.7E-08	6.3E-07	8.0E-08	1.8E-08	4.3E-09			1.9E-07	8.2E-08		
998.2	20.5	2.3E-06	1.5E-07	1.4E-07	1.8E-08	6.3E-07	7.7E-08	1.9E-08	4.5E-09			1.7E-07	5.4E-08		
1006.5	20.7	2.3E-06	1.2E-07	1.3E-07	2.2E-08	6.2E-07	7.8E-08	1.9E-08	4.8E-09			1.7E-07	5.3E-08		
1014.7	21.0	2.2E-06	9.7E-08	1.3E-07	2.1E-08	6.2E-07	9.0E-08	1.9E-08	4.6E-09			1.7E-07	5.3E-08		
1023.3	21.3	2.2E-06	1.0E-07	1.3E-07	2.3E-08	6.1E-07	8.3E-08	1.8E-08	6.2E-09			1.6E-07	5.2E-08		
		H_2		CH_4		CO		CO_2		Phenol		H_2O		1-Propanol	
T / °C	± °C	moles ·°C^{-1}	SD (1σ)	moles ·°C^{-1}	SD (1σ)	moles ·°C^{-1}	SD (1σ)	moles ·°C^{-1}	SD (1σ)	moles ·°C^{-1}	SD (1σ)	moles ·°C^{-1}	SD (1σ)	moles ·°C^{-1}	SD (1σ)
1031.2	20.7	2.1E-06	1.1E-07	1.2E-07	2.3E-08	6.0E-07	8.2E-08	1.8E-08	6.1E-09			1.6E-07	5.1E-08		
1039.1	20.3	2.1E-06	1.4E-07	1.2E-07	2.4E-08	5.9E-07	8.1E-08	1.7E-08	5.1E-09			1.6E-07	5.0E-08		
1047.8	20.5	2.1E-06	1.4E-07	1.2E-07	2.8E-08	5.9E-07	8.5E-08	1.8E-08	6.0E-09			1.6E-07	5.1E-08		
1055.9	21.5	2.0E-06	1.5E-07	1.2E-07	3.0E-08	5.9E-07	9.4E-08	1.7E-08	5.2E-09			1.8E-07	1.0E-07		
1063.8	22.5	2.0E-06	2.3E-07	1.2E-07	2.9E-08	5.9E-07	1.0E-07	1.7E-08	4.7E-09			1.5E-07	6.2E-08		
1071.4	22.8	1.9E-06	2.0E-07	1.1E-07	3.0E-08	5.7E-07	1.0E-07	1.6E-08	4.1E-09			1.7E-07	9.9E-08		
1078.8	23.1	1.9E-06	2.5E-07	1.1E-07	3.2E-08	5.7E-07	1.1E-07	1.6E-08	4.3E-09			1.7E-07	1.0E-07		
1086.6	23.4	1.9E-06	2.8E-07	1.1E-07	3.6E-08	5.8E-07	1.1E-07	1.6E-08	3.9E-09			1.4E-07	6.0E-08		
1094.4	23.0	1.9E-06	3.0E-07	1.1E-07	3.5E-08	5.8E-07	1.1E-07	1.6E-08	4.6E-09			1.4E-07	5.6E-08		
1102.1	22.4	1.9E-06	3.3E-07	1.1E-07	3.4E-08	5.8E-07	1.2E-07	1.5E-08	3.1E-09			1.4E-07	5.7E-08		
1109.8	23.3	1.9E-06	3.4E-07	1.1E-07	3.3E-08	5.8E-07	1.2E-07	1.6E-08	4.5E-09			1.4E-07	5.7E-08		
1117.6	24.1	1.9E-06	3.5E-07	1.1E-07	3.5E-08	5.7E-07	1.2E-07	1.7E-08	5.5E-09			1.4E-07	5.7E-08		
1125.4	24.3	1.9E-06	3.8E-07	1.1E-07	3.5E-08	5.7E-07	1.2E-07	1.7E-08	5.5E-09			1.4E-07	5.7E-08		
1133.2	24.6	1.8E-06	4.2E-07	1.0E-07	3.3E-08	5.8E-07	1.3E-07	1.6E-08	3.8E-09			1.4E-07	6.0E-08		
1141.2	25.0	1.9E-06	4.8E-07	1.0E-07	3.5E-08	5.9E-07	1.4E-07	1.7E-08	5.4E-09			1.4E-07	6.1E-08		
1148.9	24.6	1.9E-06	5.5E-07	1.0E-07	3.5E-08	5.9E-07	1.5E-07	1.7E-08	5.5E-09			1.5E-07	6.6E-08		
1156.3	24.3	1.9E-06	5.6E-07	1.0E-07	3.4E-08	5.9E-07	1.5E-07	1.5E-08	3.4E-09			1.5E-07	6.7E-08		
1163.5	25.4	1.8E-06	5.4E-07	1.0E-07	3.3E-08	5.8E-07	1.4E-07	1.5E-08	3.5E-09			1.5E-07	6.7E-08		
1170.6	26.3	1.8E-06	5.4E-07	1.0E-07	3.2E-08	5.7E-07	1.3E-07	1.4E-08	3.1E-09			1.5E-07	6.7E-08		
1177.5	26.4	1.8E-06	5.3E-07	1.0E-07	3.2E-08	5.7E-07	1.3E-07	1.4E-08	3.1E-09			1.5E-07	6.7E-08		
1183.9	26.0	1.8E-06	5.3E-07	1.0E-07	3.1E-08	5.7E-07	1.3E-07	1.4E-08	3.1E-09			1.5E-07	6.7E-08		
1190.2	25.0	1.7E-06	5.2E-07	1.0E-07	3.3E-08	5.6E-07	1.2E-07	1.2E-08	1.4E-09			1.4E-07	5.5E-08		

Table B.T.7. - Continued

		2-Propanol		Xylene		Cresol		Dimethyl Phenol		Trimethyl Phenol		Benzene		Toluene	
T / °C	± °C	moles ·°C^{-1}	SD (1σ)	moles ·°C^{-1}	SD (1σ)	moles ·°C^{-1}	SD (1σ)	moles ·°C^{-1}	SD (1σ)	moles ·°C^{-1}	SD (1σ)	moles ·°C^{-1}	SD (1σ)	moles ·°C^{-1}	SD (1σ)
101.8	13.4	2.5E-08	4.2E-09												
111.0	14.4	2.1E-08	1.4E-09												
120.2	15.0	2.2E-08	2.0E-09												
129.8	15.7	2.1E-08	1.6E-09												
139.9	17.5	2.1E-08	9.7E-10												
150.2	19.3	2.0E-08	1.3E-09												
161.4	20.4	2.0E-08	2.6E-09												
172.4	20.2	2.0E-08	1.9E-09												
183.6	19.8	1.9E-08	1.7E-09												
195.1	19.9	1.7E-08	3.1E-10												
207.0	20.2	1.8E-08	1.6E-10												
219.1	21.6														
231.5	22.8														
244.7	22.8					1.4E-08	5.5E-09								
257.3	21.7					1.9E-08	5.4E-09	1.6E-08	6.5E-09						
270.2	20.5					2.5E-08	6.7E-09	2.8E-08	1.9E-08						
283.8	20.2					3.6E-08	1.5E-08	3.4E-08	1.6E-08	1.6E-08	4.8E-09	9.1E-09	4.6E-10		
296.4	19.9					5.3E-08	2.1E-08	4.9E-08	1.9E-08	1.6E-08	5.1E-09	9.1E-09	5.2E-10	1.0E-08	5.9E-10
308.4	20.1					6.9E-08	2.6E-08	6.1E-08	2.0E-08	1.6E-08	5.0E-09	9.3E-09	5.1E-10	1.1E-08	1.0E-09
321.3	20.6			9.1E-09	9.3E-10	9.8E-08	2.1E-08	9.2E-08	1.5E-08	2.0E-08	3.5E-09	9.4E-09	2.0E-09	1.1E-08	1.4E-09
334.9	19.8			9.8E-09	5.7E-10	1.2E-07	2.8E-08	1.1E-07	1.5E-08	1.9E-08	1.1E-09	1.2E-08	1.8E-09	1.2E-08	5.7E-10
347.7	18.2			1.5E-08	5.4E-09	1.5E-07	3.0E-08	1.2E-07	1.6E-08	2.2E-08	2.4E-09	1.3E-08	5.7E-09	1.4E-08	2.8E-09
360.3	16.6			2.3E-08	7.3E-09	1.8E-07	2.0E-08	1.4E-07	4.7E-09	2.2E-08	2.7E-09	1.6E-08	7.6E-09	1.5E-08	3.1E-09
373.4	16.0			2.7E-08	5.7E-09	1.9E-07	1.8E-08	1.5E-07	7.8E-09	2.4E-08	3.4E-09	2.3E-08	8.6E-09	3.1E-08	4.6E-09
385.5	15.1			3.6E-08	7.1E-09	2.1E-07	4.8E-09	1.5E-07	1.2E-08	2.2E-08	4.9E-09	2.5E-08	7.2E-09	4.2E-08	8.4E-09
397.1	14.5			4.5E-08	5.5E-09	2.0E-07	1.6E-08	1.4E-07	2.4E-08	2.3E-08	5.0E-09	3.0E-08	9.8E-09	4.7E-08	1.9E-08
408.3	15.4			4.9E-08	5.8E-09	1.8E-07	1.9E-08	1.2E-07	1.7E-08	2.3E-08	4.6E-09	3.3E-08	9.6E-09	6.1E-08	1.0E-08
419.0	15.7			5.7E-08	1.7E-09	1.7E-07	2.1E-08	1.1E-07	2.2E-08	0.0E+00	0.0E+00	3.3E-08	9.7E-09	6.3E-08	7.6E-09
430.1	15.3			5.4E-08	1.3E-09	1.4E-07	3.4E-08	9.1E-08	1.8E-08	0.0E+00	0.0E+00	3.8E-08	4.7E-09	6.5E-08	4.2E-09
440.1	14.3			4.5E-08	4.7E-09	1.2E-07	2.8E-08	8.6E-08	2.3E-08	0.0E+00	0.0E+00	3.8E-08	4.6E-09	6.1E-08	6.9E-10
449.9	13.5			4.0E-08	8.8E-09	1.0E-07	2.6E-08	6.6E-08	2.1E-08	0.0E+00	0.0E+00	3.8E-08	3.9E-09	5.8E-08	4.6E-09
459.5	14.0			3.6E-08	6.7E-09	8.5E-08	1.7E-08	6.2E-08	1.8E-08	0.0E+00	0.0E+00	3.7E-08	4.1E-09	5.3E-08	9.8E-09
468.7	14.9			3.3E-08	4.7E-09	7.7E-08	1.5E-08	5.3E-08	1.2E-08	0.0E+00	0.0E+00	3.6E-08	3.6E-09	4.6E-08	1.0E-08
477.7	15.8			3.1E-08	5.7E-09	6.6E-08	1.5E-08	4.4E-08	4.9E-09	0.0E+00	0.0E+00	3.4E-08	1.2E-09	3.6E-08	3.8E-09

		2-Propanol		Xylene		Cresol		Dimethyl Phenol		Trimethyl Phenol		Benzene		Toluene	
T / °C	± °C	moles ·°C^{-1}	SD (1σ)	moles ·°C^{-1}	SD (1σ)	moles ·°C^{-1}	SD (1σ)	moles ·°C^{-1}	SD (1σ)	moles ·°C^{-1}	SD (1σ)	moles ·°C^{-1}	SD (1σ)	moles ·°C^{-1}	SD (1σ)
486.8	16.6			2.6E-08	5.2E-09	5.7E-08	1.4E-08	4.0E-08	8.0E-09			3.2E-08	2.6E-09	3.2E-08	6.8E-09
496.5	16.9			2.3E-08	6.8E-09	5.2E-08	1.3E-08	3.4E-08	8.4E-09			3.1E-08	3.7E-09	2.9E-08	5.9E-09
505.5	16.0			1.9E-08	1.4E-09	4.8E-08	8.9E-09	3.1E-08	6.9E-09			2.9E-08	4.6E-09	2.7E-08	5.0E-09
514.6	15.2			1.7E-08	4.1E-09	4.3E-08	8.1E-09	2.8E-08	5.1E-09			2.5E-08	2.1E-09	2.6E-08	5.4E-09
524.2	15.3			1.4E-08	1.6E-09	3.9E-08	8.7E-09	2.4E-08	5.6E-09			2.3E-08	2.8E-09	2.4E-08	6.9E-09
533.0	16.2			1.1E-08	9.8E-10	3.5E-08	5.8E-09	2.3E-08	3.9E-09			2.3E-08	2.8E-09	2.4E-08	6.8E-09
541.1	17.3			1.2E-08	1.2E-09	3.4E-08	6.7E-09	2.3E-08	3.9E-09			2.1E-08	3.9E-09	2.2E-08	5.7E-09
549.4	17.8			1.1E-08	1.5E-09	3.2E-08	4.2E-09	2.0E-08	3.7E-09			2.0E-08	4.7E-09	2.0E-08	4.4E-09
557.9	18.1			1.1E-08	1.2E-09	3.2E-08	4.7E-09	1.9E-08	2.4E-09			1.8E-08	3.2E-09	1.8E-08	4.2E-09
565.5	17.5					3.2E-08	4.5E-09	1.9E-08	2.1E-09			1.9E-08	3.3E-09	1.7E-08	1.1E-09
573.0	17.2					2.8E-08	5.0E-09	1.9E-08	2.2E-09			1.8E-08	3.7E-09	1.6E-08	1.2E-09
580.8	17.5					2.6E-08	5.2E-09	1.7E-08	4.3E-09			1.6E-08	2.0E-09	1.6E-08	1.1E-09
588.1	18.2					2.4E-08	5.5E-09	1.7E-08	3.8E-09			1.5E-08	3.0E-09	1.5E-08	2.4E-09
595.3	18.9					2.4E-08	5.5E-09	1.7E-08	3.8E-09			1.4E-08	2.0E-09	1.5E-08	1.9E-09
602.3	19.3					2.4E-08	5.7E-09	1.5E-08	3.4E-09			1.4E-08	2.6E-09	1.2E-08	1.0E-09
609.4	19.7					2.4E-08	6.0E-09					1.4E-08	2.5E-09	1.3E-08	1.2E-09
616.8	19.9					2.3E-08	4.8E-09					1.4E-08	2.5E-09	1.2E-08	1.1E-09
623.6	19.5					2.2E-08	6.0E-09					1.3E-08	2.5E-09	1.2E-08	1.1E-09
630.4	18.9					2.2E-08	5.9E-09					1.3E-08	2.5E-09	1.2E-08	1.1E-09
637.4	19.5					2.1E-08	5.0E-09					1.2E-08	2.9E-09	1.2E-08	1.1E-09
644.5	20.2					1.9E-08	6.7E-09							1.2E-08	1.1E-09
651.6	20.4					1.9E-08	6.7E-09							1.2E-08	1.1E-09
658.7	20.8													1.3E-08	1.1E-09
666.1	21.1													1.2E-08	7.3E-10
673.2	20.7														
680.5	20.5														
688.1	20.9														
695.2	21.6														
702.3	22.4														
709.4	22.6														
716.4	22.8														
723.8	22.8														
730.7	22.2														
737.7	21.6														

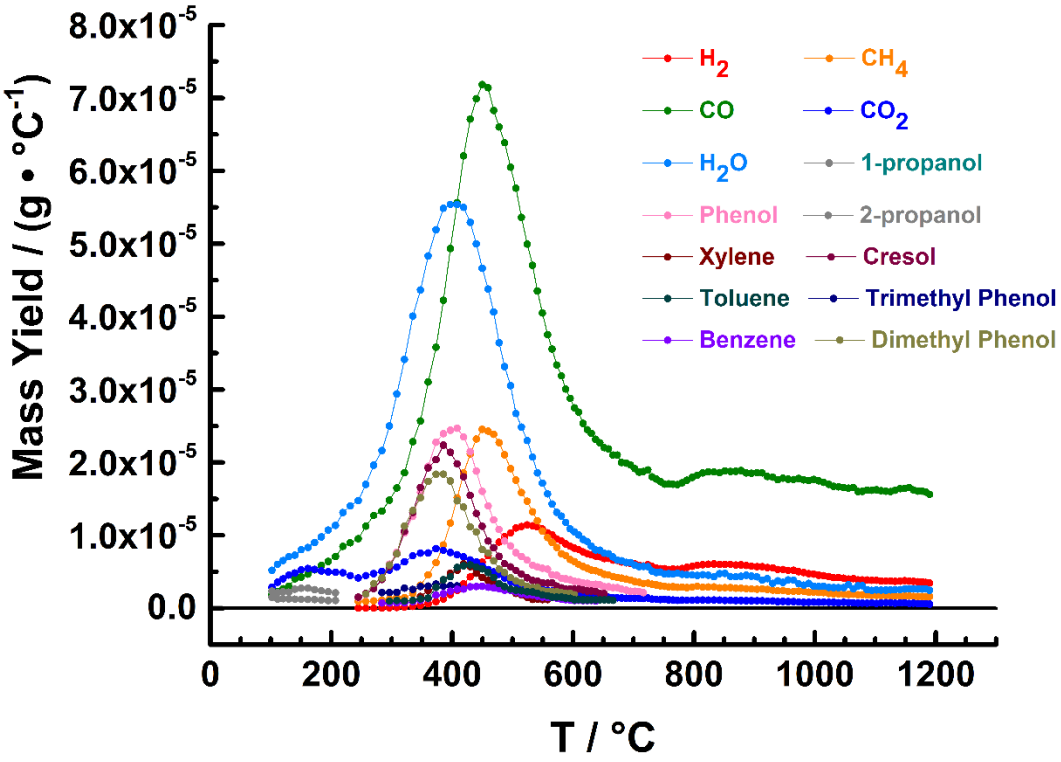

Figure B.28. Mass yields of pyrolysis products as a function of nominal heating rate of PICA, measured during the pyrolysis of PICA with a nominal heating rate of 3.1 °C s^{-1}.

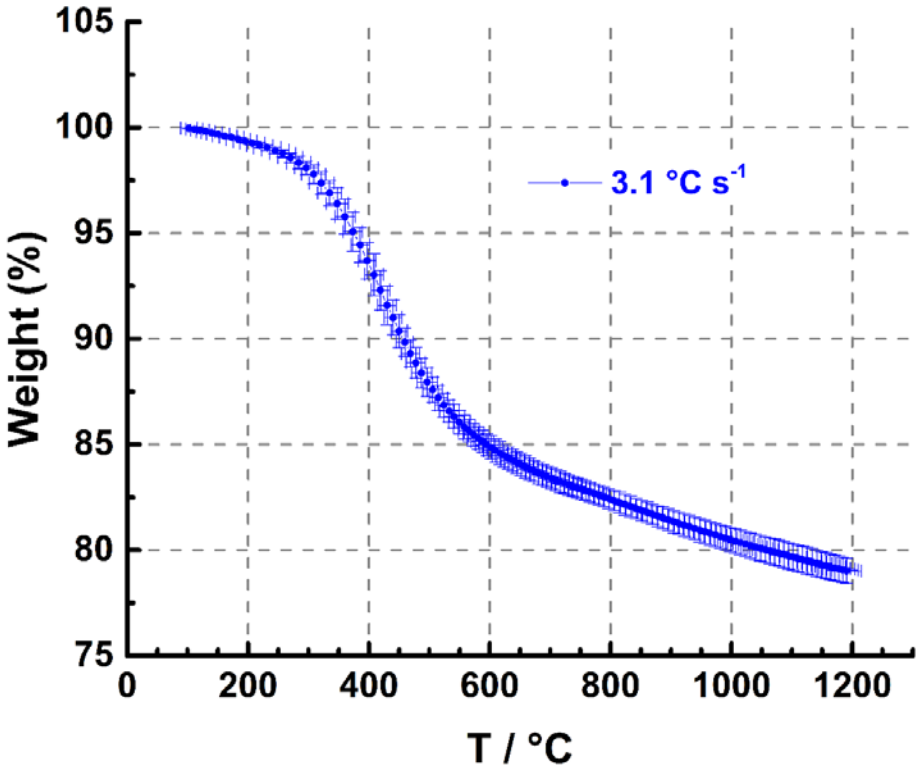

Figure B.29. Simulated thermogravimetric analysis (TGA) curve of PICA, with a nominal heating rate of 3.1 °C s^{-1}.

Table B.T.8. TGA data collected with a nominal heating rate of 3.1 °C s^{-1}.

T / °C	± °C	% Weight	± % Weight
101.8	13.4	100.0	0.0
111.0	14.4	99.9	0.0
120.2	15.0	99.9	0.0
129.8	15.7	99.8	0.0
139.9	17.5	99.8	0.0
150.2	19.3	99.7	0.1
161.4	20.4	99.6	0.1
172.4	20.2	99.5	0.1
183.6	19.8	99.4	0.1
195.1	19.9	99.4	0.1
207.0	20.2	99.3	0.1
219.1	21.6	99.2	0.1
231.5	22.8	99.0	0.1
244.7	22.8	98.9	0.2
257.3	21.7	98.8	0.2
270.2	20.5	98.6	0.2
283.8	20.2	98.3	0.3
296.4	19.9	98.1	0.3
308.4	20.1	97.8	0.4
321.3	20.6	97.4	0.5
334.9	19.8	96.9	0.6
347.7	18.2	96.4	0.7
360.3	16.6	95.8	0.8
373.4	16.0	95.1	0.9
385.5	15.1	94.4	0.8
397.1	14.5	93.7	0.9
408.3	15.4	93.0	1.0
419.0	15.7	92.3	0.9
430.1	15.3	91.6	0.9
440.1	14.3	91.0	0.8
449.9	13.5	90.4	0.8
459.5	14.0	89.8	0.7
468.7	14.9	89.3	0.6
477.7	15.8	88.9	0.7

T / °C	± °C	% Weight	± % Weight
486.8	16.6	88.4	0.7
496.5	16.9	88.0	0.7
505.5	16.0	87.6	0.6
514.6	15.2	87.2	0.6
524.2	15.3	86.9	0.6
533.0	16.2	86.6	0.5
541.1	17.3	86.3	0.6
549.4	17.8	86.1	0.6
557.9	18.1	85.8	0.6
565.5	17.5	85.7	0.5
573.0	17.2	85.5	0.5
580.8	17.5	85.3	0.5
588.1	18.2	85.1	0.5
595.3	18.9	85.0	0.5
602.3	19.3	84.9	0.5
609.4	19.7	84.7	0.5
616.8	19.9	84.6	0.5
623.6	19.5	84.5	0.5
630.4	18.9	84.4	0.5
637.4	19.5	84.3	0.5
644.5	20.2	84.1	0.5
651.6	20.4	84.0	0.5
658.7	20.8	83.9	0.5
666.1	21.1	83.8	0.5
673.2	20.7	83.7	0.5
680.5	20.5	83.6	0.5
688.1	20.9	83.6	0.5
695.2	21.6	83.5	0.5
702.3	22.4	83.4	0.5
709.4	22.6	83.3	0.5
716.4	22.8	83.2	0.5
723.8	22.8	83.2	0.5
730.7	22.2	83.1	0.5
737.7	21.6	83.0	0.5

Table B.T.8. - Continued

T / °C	± °C	% Weight	± % Weight
744.6	22.1	82.9	0.5
751.4	22.6	82.9	0.5
758.3	21.8	82.8	0.5
765.3	20.9	82.7	0.5
773.0	19.8	82.7	0.5
780.6	18.3	82.6	0.5
788.7	17.0	82.5	0.5
797.0	17.5	82.4	0.5
805.8	18.0	82.3	0.5
814.8	17.7	82.3	0.5
823.7	17.6	82.2	0.5
833.3	17.4	82.1	0.5
842.4	16.6	82.0	0.5
851.3	15.8	81.9	0.5
860.6	15.8	81.8	0.5
869.4	16.6	81.7	0.5
878.0	17.6	81.6	0.5
886.6	17.7	81.5	0.5
895.2	17.8	81.4	0.5
904.4	17.9	81.3	0.5
913.0	17.2	81.3	0.5
921.7	16.7	81.2	0.5
930.4	17.6	81.1	0.5
938.9	18.8	81.0	0.5
947.5	18.9	80.9	0.6
956.1	19.0	80.9	0.6
965.0	19.3	80.8	0.6
973.4	18.7	80.7	0.6
981.8	18.3	80.6	0.6
990.1	19.3	80.6	0.6
998.2	20.5	80.5	0.6
1006.5	20.7	80.4	0.6
1014.7	21.0	80.4	0.6
1023.3	21.3	80.3	0.6

T / °C	± °C	% Weight	± % Weight
1031.2	20.7	80.2	0.6
1039.1	20.3	80.2	0.6
1047.8	20.5	80.1	0.6
1055.9	21.5	80.0	0.6
1063.8	22.5	80.0	0.6
1071.4	22.8	79.9	0.6
1078.8	23.1	79.8	0.6
1086.6	23.4	79.8	0.6
1094.4	23.0	79.7	0.6
1102.1	22.4	79.7	0.6
1109.8	23.3	79.6	0.6
1117.6	24.1	79.6	0.6
1125.4	24.3	79.5	0.6
1133.2	24.6	79.4	0.6
1141.2	25.0	79.4	0.6
1148.9	24.6	79.3	0.6
1156.3	24.3	79.3	0.6
1163.5	25.4	79.2	0.6
1170.6	26.3	79.2	0.6
1177.5	26.4	79.1	0.6
1183.9	26.0	79.1	0.6
1190.2	25.0	79.0	0.6

APPENDIX C

DATA TABLES AND FIGURES FOR D.E.N. 438 AND COMPOSITE MATERIAL

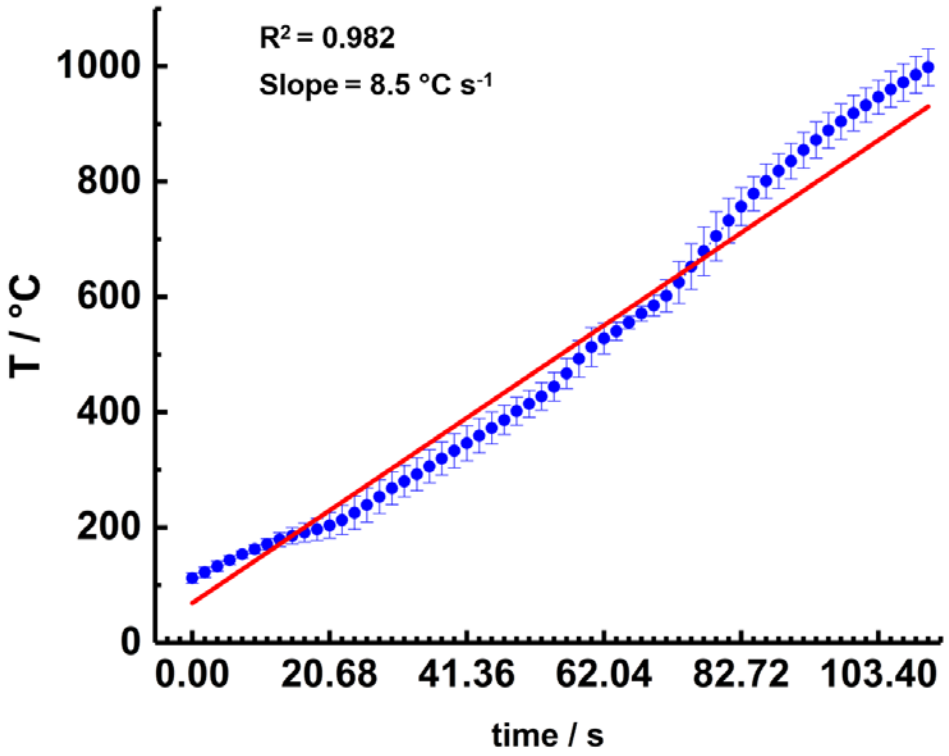

Figure C.1. Heating profile for D.E.N. 438, with a nominal heating rate of 8.5 °C s^{-1}.

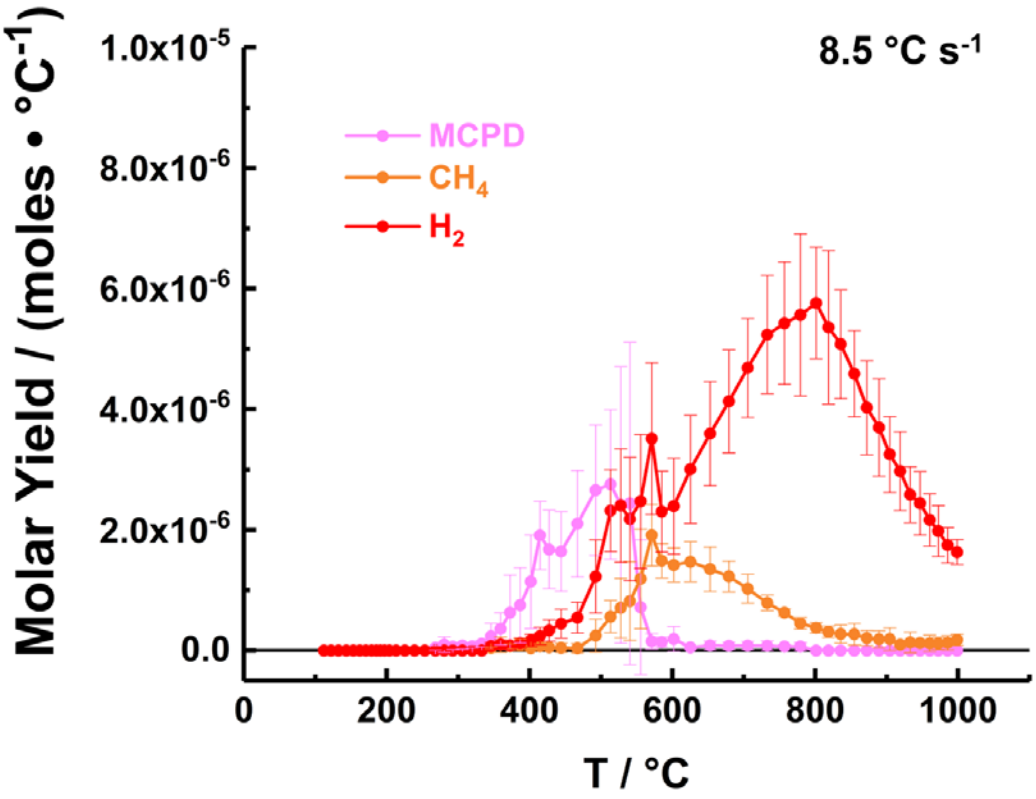

Figure C.2. Molar yields of H_2, CH_4, and MCPD, with a nominal heating rate of 8.5 °C s^{-1}.

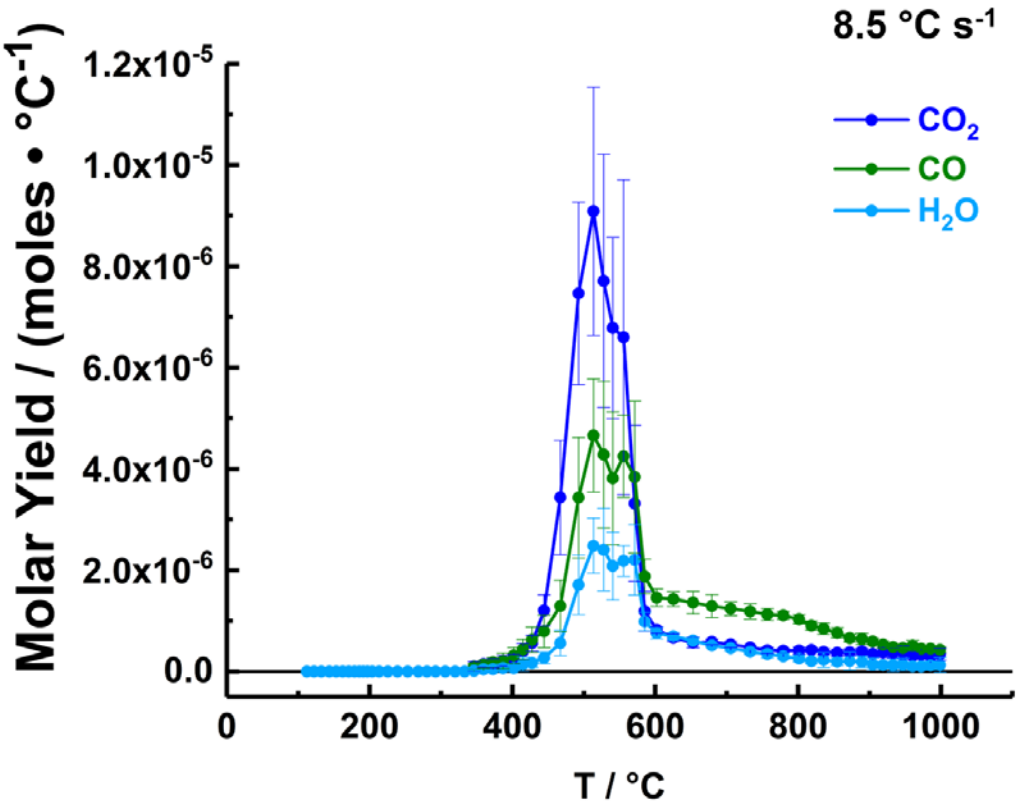

Figure C.3. Molar yields of H_2O, CO, and CO_2, with a nominal heating rate of 8.5 °C s^{-1}.

Table C.T.1. Molar yields of pyrolysis products, measured during the pyrolysis of D.E.N. 438 with a nominal heating rate of 8.5 °C s^{-1}.

		H_2		CH_4		H_2O		CO		CO_2		MCPD	
T / °C	± °C	moles ·°C^{-1}	SD (1σ)	moles ·°C^{-1}	SD (1σ)	moles ·°C^{-1}	SD (1σ)	moles ·°C^{-1}	SD (1σ)	moles ·°C^{-1}	SD (1σ)	moles ·°C^{-1}	SD (1σ)
112.1	9.2	0.0E+00	0.0E+00	0.0E+00	0.0E+00	0.0E+00	0.0E+00	0.0E+00	0.0E+00	0.0E+00	0.0E+00	0.0E+00	0.0E+00
122.2	9.2	0.0E+00	0.0E+00	0.0E+00	0.0E+00	0.0E+00	0.0E+00	0.0E+00	0.0E+00	0.0E+00	0.0E+00	0.0E+00	0.0E+00
132.5	8.7	0.0E+00	0.0E+00	0.0E+00	0.0E+00	0.0E+00	0.0E+00	0.0E+00	0.0E+00	0.0E+00	0.0E+00	0.0E+00	0.0E+00
143.4	7.6	0.0E+00	0.0E+00	0.0E+00	0.0E+00	0.0E+00	0.0E+00	0.0E+00	0.0E+00	0.0E+00	0.0E+00	0.0E+00	0.0E+00
153.3	6.8	0.0E+00	0.0E+00	0.0E+00	0.0E+00	0.0E+00	0.0E+00	0.0E+00	0.0E+00	0.0E+00	0.0E+00	0.0E+00	0.0E+00
162.4	7.8	0.0E+00	0.0E+00	0.0E+00	0.0E+00	0.0E+00	0.0E+00	0.0E+00	0.0E+00	0.0E+00	0.0E+00	0.0E+00	0.0E+00
170.9	9.6	0.0E+00	0.0E+00	0.0E+00	0.0E+00	0.0E+00	0.0E+00	0.0E+00	0.0E+00	0.0E+00	0.0E+00	0.0E+00	0.0E+00
178.9	12.2	0.0E+00	0.0E+00	0.0E+00	0.0E+00	0.0E+00	0.0E+00	0.0E+00	0.0E+00	0.0E+00	0.0E+00	0.0E+00	0.0E+00
185.6	14.1	0.0E+00	0.0E+00	0.0E+00	0.0E+00	0.0E+00	0.0E+00	0.0E+00	0.0E+00	0.0E+00	0.0E+00	0.0E+00	0.0E+00
191.1	16.1	0.0E+00	0.0E+00	0.0E+00	0.0E+00	0.0E+00	0.0E+00	0.0E+00	0.0E+00	0.0E+00	0.0E+00	0.0E+00	0.0E+00
196.8	19.1	0.0E+00	0.0E+00	0.0E+00	0.0E+00	0.0E+00	0.0E+00	0.0E+00	0.0E+00	0.0E+00	0.0E+00	0.0E+00	0.0E+00
203.6	22.1	0.0E+00	0.0E+00	0.0E+00	0.0E+00	0.0E+00	0.0E+00	0.0E+00	0.0E+00	0.0E+00	0.0E+00	0.0E+00	0.0E+00
213.1	25.4	0.0E+00	0.0E+00	0.0E+00	0.0E+00	0.0E+00	0.0E+00	0.0E+00	0.0E+00	0.0E+00	0.0E+00	0.0E+00	0.0E+00
225.4	28.8	0.0E+00	0.0E+00	0.0E+00	0.0E+00	0.0E+00	0.0E+00	0.0E+00	0.0E+00	0.0E+00	0.0E+00	0.0E+00	0.0E+00
239.0	29.9	0.0E+00	0.0E+00	0.0E+00	0.0E+00	0.0E+00	0.0E+00	0.0E+00	0.0E+00	0.0E+00	0.0E+00	0.0E+00	0.0E+00
253.4	29.5	1.0E+00	0.0E+00	0.0E+00	0.0E+00	0.0E+00	0.0E+00	0.0E+00	0.0E+00	0.0E+00	0.0E+00	0.0E+00	0.0E+00
268.0	28.4	0.0E+00	0.0E+00	0.0E+00	0.0E+00	0.0E+00	0.0E+00	0.0E+00	0.0E+00	0.0E+00	0.0E+00	4.3E-08	3.7E-08
280.3	27.6	0.0E+00	0.0E+00	0.0E+00	0.0E+00	0.0E+00	0.0E+00	0.0E+00	0.0E+00	0.0E+00	0.0E+00	9.8E-08	1.3E-07
292.3	28.4	0.0E+00	0.0E+00	0.0E+00	0.0E+00	0.0E+00	0.0E+00	0.0E+00	0.0E+00	0.0E+00	0.0E+00	6.0E-08	4.6E-08
306.0	28.7	0.0E+00	0.0E+00	0.0E+00	0.0E+00	0.0E+00	0.0E+00	0.0E+00	0.0E+00	0.0E+00	0.0E+00	7.8E-08	5.6E-08
319.8	28.6	0.0E+00	0.0E+00	0.0E+00	0.0E+00	0.0E+00	0.0E+00	0.0E+00	0.0E+00	0.0E+00	0.0E+00	6.7E-08	2.3E-08
333.1	29.6	0.0E+00	0.0E+00	0.0E+00	0.0E+00	0.0E+00	0.0E+00	0.0E+00	0.0E+00	0.0E+00	0.0E+00	1.1E-07	5.5E-08
346.2	30.5	7.0E-08	5.7E-08	4.4E-08	1.7E-08	1.5E-08	1.8E-08	9.8E-08	5.7E-08	1.0E-07	9.8E-08	2.4E-07	2.1E-07
359.3	29.7	1.0E-07	7.2E-08	9.8E-08	1.3E-07	4.3E-08	6.4E-08	1.4E-07	7.2E-08	1.5E-07	6.0E-08	3.6E-07	2.6E-07
372.6	27.6	8.2E-08	6.7E-08	6.8E-08	4.0E-08	4.5E-08	5.2E-08	1.8E-07	9.0E-08	1.6E-07	8.9E-08	6.3E-07	6.2E-07
386.7	25.2	1.2E-07	8.5E-08	8.7E-08	9.8E-08	6.8E-08	7.5E-08	2.1E-07	1.5E-07	2.1E-07	1.1E-07	7.5E-07	6.3E-07
401.8	23.8	1.7E-07	1.0E-07	3.9E-08	2.9E-08	6.7E-08	4.0E-08	3.2E-07	1.6E-07	2.4E-07	9.0E-08	1.1E-06	7.8E-07
414.6	23.2	2.4E-07	1.4E-07	6.9E-08	4.4E-08	1.5E-07	1.4E-07	4.4E-07	2.0E-07	4.0E-07	1.6E-07	1.9E-06	5.6E-07
427.3	24.0	3.3E-07	1.8E-07	5.3E-08	1.4E-08	1.7E-07	8.4E-08	6.3E-07	2.5E-07	5.6E-07	1.6E-07	1.7E-06	6.5E-07
444.1	24.5	4.4E-07	2.4E-07	4.4E-08	7.6E-08	2.7E-07	1.1E-07	7.9E-07	3.2E-07	1.2E-06	3.1E-07	1.6E-06	6.6E-07
467.1	25.9	5.4E-07	2.5E-07	3.9E-08	7.7E-08	5.6E-07	2.5E-07	1.3E-06	5.1E-07	3.4E-06	1.1E-06	2.1E-06	8.8E-07
492.6	31.8	1.2E-06	6.1E-07	2.5E-07	2.7E-07	1.7E-06	5.9E-07	3.4E-06	1.2E-06	7.5E-06	1.8E-06	2.7E-06	1.1E-06
513.3	33.9	2.3E-06	6.8E-07	5.6E-07	2.7E-07	2.5E-06	5.5E-07	4.7E-06	1.1E-06	9.1E-06	2.5E-06	2.8E-06	1.2E-06
527.8	26.8	2.4E-06	9.4E-07	7.1E-07	4.9E-07	2.4E-06	8.1E-07	4.3E-06	1.4E-06	7.7E-06	2.5E-06	2.4E-06	2.3E-06
540.6	15.8	2.2E-06	1.0E-06	8.2E-07	6.5E-07	2.1E-06	6.7E-07	3.8E-06	1.3E-06	6.8E-06	1.8E-06	2.4E-06	2.7E-06
555.6	11.2	2.5E-06	1.1E-06	1.2E-06	8.3E-07	2.2E-06	3.0E-07	4.3E-06	8.1E-07	6.6E-06	3.1E-06	7.2E-07	1.1E-06
571.0	12.8	3.5E-06	1.3E-06	1.9E-06	5.1E-07	2.2E-06	6.9E-07	3.8E-06	1.5E-06	3.3E-06	1.5E-06	1.5E-07	1.3E-07
585.2	18.1	2.3E-06	6.7E-07	1.5E-06	2.8E-07	9.9E-07	1.8E-07	1.9E-06	3.4E-07	1.2E-06	3.9E-07	1.4E-07	8.2E-08
602.0	27.8	2.4E-06	7.9E-07	1.4E-06	2.8E-07	7.5E-07	1.1E-07	1.5E-06	1.7E-07	8.2E-07	6.3E-08	1.9E-07	2.1E-07
625.2	36.5	3.0E-06	9.0E-07	1.5E-06	3.3E-07	7.0E-07	7.4E-08	1.4E-06	1.4E-07	6.7E-07	7.2E-08	4.9E-08	2.4E-08
652.8	39.3	3.6E-06	8.6E-07	1.3E-06	3.7E-07	6.1E-07	5.9E-08	1.4E-06	2.2E-07	5.7E-07	1.0E-07	8.2E-08	7.2E-08
679.3	42.1	4.1E-06	8.5E-07	1.2E-06	2.5E-07	5.2E-07	3.6E-08	1.3E-06	2.3E-07	5.9E-07	5.5E-08	7.6E-08	6.2E-08
705.5	42.6	4.7E-06	8.2E-07	1.0E-06	2.4E-07	4.6E-07	5.7E-08	1.2E-06	1.3E-07	5.4E-07	6.3E-08	8.0E-08	6.8E-08
732.7	38.9	5.2E-06	9.8E-07	7.9E-07	1.3E-07	3.9E-07	4.3E-08	1.2E-06	1.5E-07	4.7E-07	3.9E-08	7.8E-08	7.8E-08
756.9	33.0	5.4E-06	1.0E-06	6.3E-07	5.8E-08	3.5E-07	7.5E-08	1.1E-06	1.2E-07	4.2E-07	6.0E-08	6.5E-08	3.0E-08
779.3	29.4	5.6E-06	1.3E-06	4.5E-07	9.5E-08	3.0E-07	5.5E-08	1.1E-06	7.6E-08	4.1E-07	4.6E-08	6.4E-08	6.7E-08
801.2	29.6	5.8E-06	9.3E-07	3.8E-07	9.0E-08	2.6E-07	6.6E-08	1.0E-06	9.0E-08	4.2E-07	7.0E-08	4.0E-08	3.3E-08
818.7	30.2	5.4E-06	1.3E-06	3.1E-07	9.6E-08	2.0E-07	5.4E-08	9.1E-07	9.1E-08	4.3E-07	4.7E-08	0.0E+00	0.0E+00
835.6	30.9	5.1E-06	9.0E-07	2.7E-07	1.5E-07	2.3E-07	1.5E-07	8.5E-07	1.1E-07	3.9E-07	6.4E-08	0.0E+00	0.0E+00
854.6	31.0	4.6E-06	7.1E-07	2.7E-07	1.8E-07	1.9E-07	7.3E-08	7.6E-07	9.9E-08	3.7E-07	6.8E-08	0.0E+00	0.0E+00
872.4	31.1	4.0E-06	7.8E-07	2.0E-07	1.3E-07	2.1E-07	1.8E-07	6.6E-07	7.9E-08	3.8E-07	6.7E-08	0.0E+00	0.0E+00
889.2	30.7	3.7E-06	8.1E-07	1.9E-07	1.4E-07	1.9E-07	1.1E-07	6.4E-07	1.1E-07	4.0E-07	6.2E-08	0.0E+00	0.0E+00
904.4	30.6	3.3E-06	6.3E-07	1.9E-07	1.9E-07	1.4E-07	1.2E-07	5.9E-07	6.1E-08	3.5E-07	4.8E-08	0.0E+00	0.0E+00
919.0	30.9	3.0E-06	6.5E-07	9.8E-08	5.9E-08	1.3E-07	6.2E-08	5.3E-07	7.2E-08	3.7E-07	9.2E-08	0.0E+00	0.0E+00
932.9	30.0	2.6E-06	4.6E-07	1.3E-07	1.7E-07	1.2E-07	1.2E-07	4.8E-07	1.1E-08	3.7E-07	9.7E-08	0.0E+00	0.0E+00
946.8	29.4	2.4E-06	5.3E-07	1.2E-07	5.9E-08	1.4E-07	1.2E-07	4.6E-07	2.4E-08	3.7E-07	1.3E-07	0.0E+00	0.0E+00
960.4	31.3	2.2E-06	4.3E-07	1.2E-07	1.4E-07	1.0E-07	3.8E-08	5.1E-07	1.0E-07	3.1E-07	5.9E-08	0.0E+00	0.0E+00
972.3	32.2	2.0E-06	4.2E-07	1.2E-07	1.0E-07	9.6E-08	7.3E-08	4.5E-07	4.5E-08	3.3E-07	7.9E-08	0.0E+00	0.0E+00
985.3	31.8	1.7E-06	2.9E-07	1.3E-07	1.2E-07	1.2E-07	8.5E-08	4.5E-07	5.1E-08	3.0E-07	2.9E-08	0.0E+00	0.0E+00
998.7	32.3	1.6E-06	2.1E-07	1.8E-07	9.3E-08	1.3E-07	1.5E-07	4.3E-07	5.6E-08	3.4E-07	1.2E-07	0.0E+00	0.0E+00

Table C.T.2. TGA data collected with a nominal heating rate of 8.5 °C s^{-1}.

T / °C	± °C	% Mass Loss	± % Weight
112.1	9.2	100.0	0.0
122.2	9.2	100.0	0.0
132.5	8.7	100.0	0.0
143.4	7.6	100.0	0.0
153.3	6.8	100.0	0.0
162.4	7.8	100.0	0.0
170.9	9.6	100.0	0.0
178.9	12.2	100.0	0.0
185.6	14.1	100.0	0.0
191.1	16.1	100.0	0.0
196.8	19.1	100.0	0.0
203.6	22.1	100.0	0.0
213.1	25.4	100.0	0.0
225.4	28.8	100.0	0.0
239.0	29.9	99.9	0.1
253.4	29.5	99.8	0.1
268.0	28.4	99.7	0.2
280.3	27.6	99.6	0.3
292.3	28.4	99.4	0.4
306.0	28.7	99.3	0.6
319.8	28.6	99.1	0.7
333.1	29.6	99.0	0.7
346.2	30.5	98.8	0.8
359.3	29.7	98.5	0.8
372.6	27.6	98.1	0.9
386.7	25.2	97.5	0.8
401.8	23.8	96.7	0.9
414.6	23.2	95.7	1.2
427.3	24.0	94.1	1.9
444.1	24.5	91.4	3.1
467.1	25.9	83.6	6.6
492.6	31.8	71.0	11.3
513.3	33.9	60.7	10.3
527.8	26.8	53.7	7.7
540.6	15.8	47.7	3.1
555.6	11.2	40.6	1.1
571.0	12.8	36.8	2.7
585.2	18.1	34.9	2.8
602.0	27.8	32.7	2.9
625.2	36.5	30.0	3.0
652.8	39.3	27.3	3.1
679.3	42.1	25.1	3.3
705.5	42.6	22.7	2.9
732.7	38.9	20.6	2.6
756.9	33.0	19.0	2.1
779.3	29.4	17.5	2.0
801.2	29.6	16.3	1.8
818.7	30.2	15.5	1.9
835.6	30.9	14.4	1.8
854.6	31.0	13.6	1.6
872.4	31.1	12.8	1.5
889.2	30.7	12.1	1.4
904.4	30.6	11.5	1.3
919.0	30.9	11.0	1.2
932.9	30.0	10.5	1.0
946.8	29.4	10.0	0.9
960.4	31.3	9.6	0.9
972.3	32.2	9.3	0.9
985.3	31.8	8.8	0.9
998.7	32.3	8.4	0.9

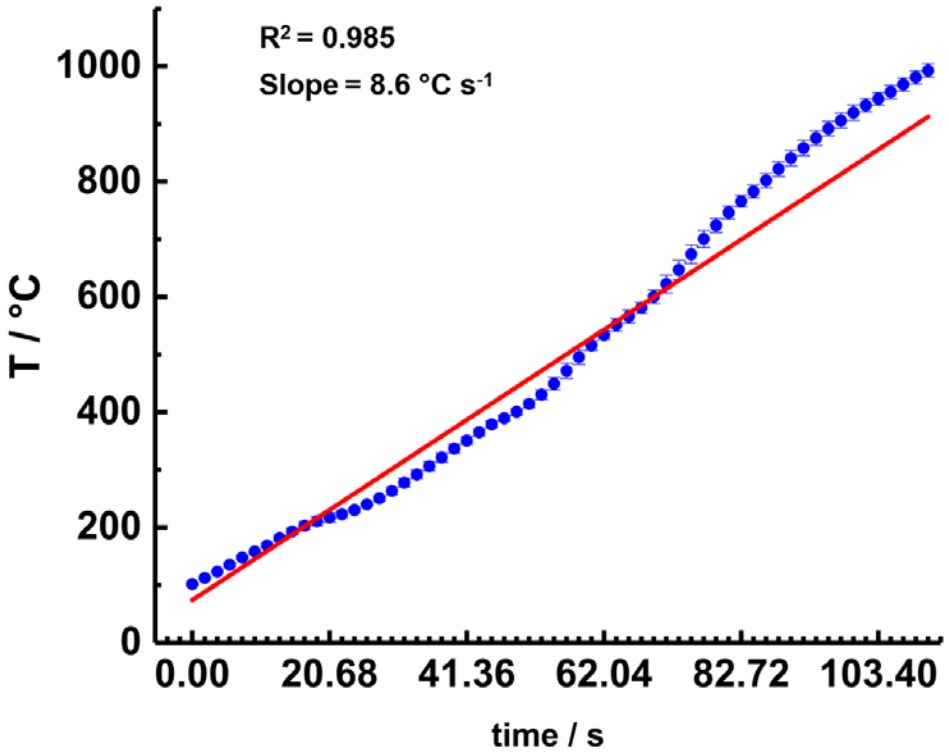

Figure C.4. Heating profile for D.E.N. 438 + 5.6 wt%, with a nominal heating rate of 8.6 °C s^{-1}.

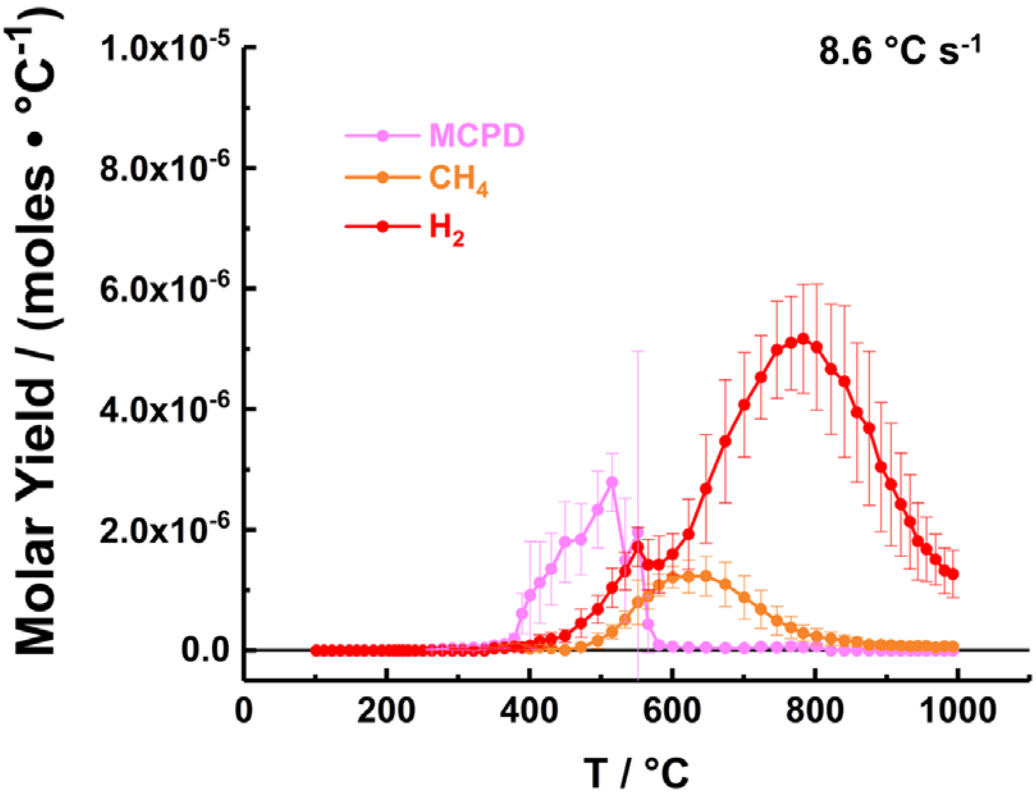

Figure C.5. Molar yields of H_2, CH_4, and MCPD with a nominal heating rate of 8.5 °C s^{-1}.

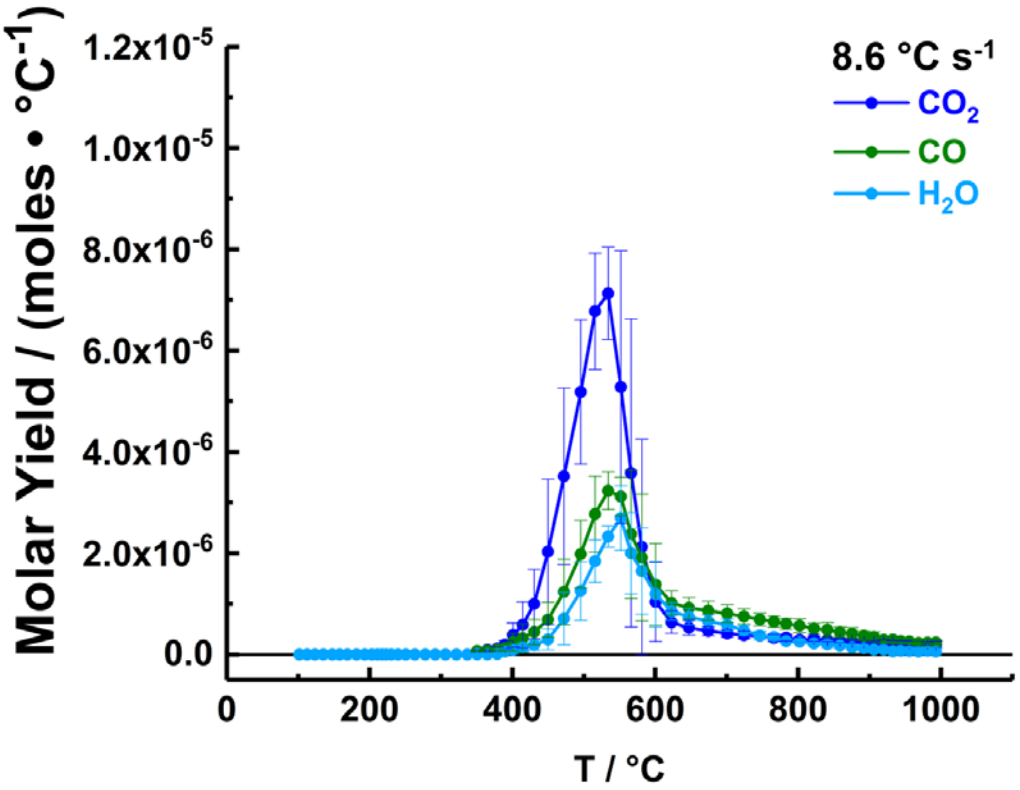

Figure C.6. Molar yields of H_2O, CO, and CO_2, with a nominal heating rate of 8.5 °C s^{-1}.

Table C.T.3 Molar yields of pyrolysis products, measured during the pyrolysis of the composite material with a nominal heating rate of 8.6 °C s^{-1}.

		H_2		CH_4		H_2O		CO		CO_2		MCPD	
T / °C	± °C	moles ·°C^{-1}	SD (1σ)	moles ·°C^{-1}	SD (1σ)	moles ·°C^{-1}	SD (1σ)	moles ·°C^{-1}	SD (1σ)	moles ·°C^{-1}	SD (1σ)	moles ·°C^{-1}	SD (1σ)
101.7	2.2	0.0E+00	0.0E+00	0.0E+00	0.0E+00	0.0E+00	0.0E+00	0.0E+00	0.0E+00	0.0E+00	0.0E+00	0.0E+00	0.0E+00
112.4	2.1	0.0E+00	0.0E+00	0.0E+00	0.0E+00	0.0E+00	0.0E+00	0.0E+00	0.0E+00	0.0E+00	0.0E+00	0.0E+00	0.0E+00
123.3	2.4	0.0E+00	0.0E+00	0.0E+00	0.0E+00	0.0E+00	0.0E+00	0.0E+00	0.0E+00	0.0E+00	0.0E+00	0.0E+00	0.0E+00
135.1	3.2	0.0E+00	0.0E+00	0.0E+00	0.0E+00	0.0E+00	0.0E+00	0.0E+00	0.0E+00	0.0E+00	0.0E+00	0.0E+00	0.0E+00
147.8	3.1	0.0E+00	0.0E+00	0.0E+00	0.0E+00	0.0E+00	0.0E+00	0.0E+00	0.0E+00	0.0E+00	0.0E+00	0.0E+00	0.0E+00
158.1	2.5	0.0E+00	0.0E+00	0.0E+00	0.0E+00	0.0E+00	0.0E+00	0.0E+00	0.0E+00	0.0E+00	0.0E+00	0.0E+00	0.0E+00
168.8	3.6	0.0E+00	0.0E+00	0.0E+00	0.0E+00	0.0E+00	0.0E+00	0.0E+00	0.0E+00	0.0E+00	0.0E+00	0.0E+00	0.0E+00
181.5	5.3	0.0E+00	0.0E+00	0.0E+00	0.0E+00	0.0E+00	0.0E+00	0.0E+00	0.0E+00	0.0E+00	0.0E+00	0.0E+00	0.0E+00
193.1	6.2	0.0E+00	0.0E+00	0.0E+00	0.0E+00	0.0E+00	0.0E+00	0.0E+00	0.0E+00	0.0E+00	0.0E+00	0.0E+00	0.0E+00
203.1	7.3	0.0E+00	0.0E+00	0.0E+00	0.0E+00	0.0E+00	0.0E+00	0.0E+00	0.0E+00	0.0E+00	0.0E+00	0.0E+00	0.0E+00
210.9	8.1	0.0E+00	0.0E+00	0.0E+00	0.0E+00	0.0E+00	0.0E+00	0.0E+00	0.0E+00	0.0E+00	0.0E+00	0.0E+00	0.0E+00
217.2	7.9	0.0E+00	0.0E+00	0.0E+00	0.0E+00	0.0E+00	0.0E+00	0.0E+00	0.0E+00	0.0E+00	0.0E+00	0.0E+00	0.0E+00
223.0	6.3	0.0E+00	0.0E+00	0.0E+00	0.0E+00	0.0E+00	0.0E+00	0.0E+00	0.0E+00	0.0E+00	0.0E+00	0.0E+00	0.0E+00
230.3	3.6	0.0E+00	0.0E+00	0.0E+00	0.0E+00	0.0E+00	0.0E+00	0.0E+00	0.0E+00	0.0E+00	0.0E+00	0.0E+00	0.0E+00
239.9	1.5	0.0E+00	0.0E+00	0.0E+00	0.0E+00	0.0E+00	0.0E+00	0.0E+00	0.0E+00	0.0E+00	0.0E+00	0.0E+00	0.0E+00
250.4	4.8	0.0E+00	0.0E+00	0.0E+00	0.0E+00	0.0E+00	0.0E+00	0.0E+00	0.0E+00	0.0E+00	0.0E+00	0.0E+00	0.0E+00
263.3	7.0	0.0E+00	0.0E+00	0.0E+00	0.0E+00	0.0E+00	0.0E+00	0.0E+00	0.0E+00	0.0E+00	0.0E+00	1.4E-08	9.8E-09
277.9	7.6	0.0E+00	0.0E+00	0.0E+00	0.0E+00	0.0E+00	0.0E+00	0.0E+00	0.0E+00	0.0E+00	0.0E+00	2.6E-08	9.1E-09
291.8	7.8	0.0E+00	0.0E+00	0.0E+00	0.0E+00	0.0E+00	0.0E+00	0.0E+00	0.0E+00	0.0E+00	0.0E+00	3.2E-08	2.2E-08
306.3	8.1	0.0E+00	0.0E+00	0.0E+00	0.0E+00	0.0E+00	0.0E+00	0.0E+00	0.0E+00	0.0E+00	0.0E+00	3.3E-08	2.2E-08
321.6	8.1	0.0E+00	0.0E+00	0.0E+00	0.0E+00	0.0E+00	0.0E+00	0.0E+00	0.0E+00	0.0E+00	0.0E+00	4.2E-08	4.0E-08
336.7	7.7	0.0E+00	0.0E+00	0.0E+00	0.0E+00	0.0E+00	0.0E+00	0.0E+00	0.0E+00	0.0E+00	0.0E+00	4.0E-08	2.4E-08
350.6	7.0	3.7E-08	2.6E-08	3.2E-08	2.0E-08	1.5E-09	2.7E-09	6.9E-08	9.2E-09	6.9E-08	1.8E-08	8.1E-08	6.4E-08
365.0	6.5	4.1E-08	2.6E-08	4.9E-08	4.2E-08	2.0E-09	3.9E-09	7.7E-08	2.5E-08	9.1E-08	1.6E-08	9.9E-08	5.6E-08
378.8	5.5	5.9E-08	3.6E-08	6.4E-08	5.0E-08	8.7E-09	1.1E-08	9.3E-08	2.3E-08	1.1E-07	3.8E-08	1.9E-07	8.2E-08
389.6	4.7	5.0E-08	2.3E-08	5.1E-08	4.2E-08	5.9E-08	4.0E-08	1.3E-07	5.5E-08	1.9E-07	8.1E-08	6.1E-07	3.4E-07
400.7	5.5	7.8E-08	4.1E-08	3.1E-08	2.4E-08	8.8E-08	7.7E-08	2.5E-07	1.7E-07	3.9E-07	2.4E-07	9.1E-07	8.9E-07
414.4	6.6	1.5E-07	1.1E-07	5.1E-08	4.7E-08	1.4E-07	7.7E-08	3.2E-07	2.8E-07	5.9E-07	4.6E-07	1.1E-06	6.7E-07
430.5	8.4	1.8E-07	1.2E-07	3.8E-08	2.8E-08	1.8E-07	1.0E-07	4.4E-07	2.5E-07	1.0E-06	6.8E-07	1.4E-06	6.0E-07
449.6	10.9	2.4E-07	1.1E-07	9.0E-09	1.8E-08	3.0E-07	2.0E-07	6.9E-07	3.5E-07	2.0E-06	1.4E-06	1.8E-06	6.7E-07
472.0	13.0	4.5E-07	2.3E-07	5.7E-08	5.9E-08	7.1E-07	5.2E-07	1.2E-06	6.5E-07	3.5E-06	1.7E-06	1.8E-06	5.9E-07
495.6	12.4	6.8E-07	2.3E-07	1.6E-07	1.3E-07	1.3E-06	5.8E-07	2.0E-06	6.7E-07	5.2E-06	1.4E-06	2.3E-06	6.4E-07
515.7	8.0	1.0E-06	3.3E-07	3.1E-07	1.1E-07	1.8E-06	4.2E-07	2.8E-06	7.5E-07	6.8E-06	1.1E-06	2.8E-06	4.8E-07
533.9	7.6	1.3E-06	3.1E-07	5.1E-07	1.4E-07	2.3E-06	2.1E-07	3.2E-06	3.7E-07	7.1E-06	9.1E-07	1.5E-06	1.0E-06
551.7	10.9	1.7E-06	3.3E-07	8.0E-07	3.7E-07	2.7E-06	6.4E-07	3.1E-06	3.8E-07	5.3E-06	2.7E-06	2.0E-06	3.0E-06
566.0	11.2	1.4E-06	4.2E-07	9.0E-07	2.1E-07	2.0E-06	8.0E-07	2.4E-06	1.3E-06	3.6E-06	3.0E-06	4.4E-07	4.8E-07
581.1	9.4	1.4E-06	4.7E-07	1.1E-06	1.8E-07	1.6E-06	8.5E-07	1.9E-06	1.3E-06	2.1E-06	2.1E-06	8.9E-08	5.0E-08
600.5	11.7	1.6E-06	3.4E-07	1.2E-06	1.8E-07	1.2E-06	6.5E-07	1.4E-06	8.1E-07	1.0E-06	7.8E-07	6.2E-08	2.1E-08
622.7	15.8	1.9E-06	5.8E-07	1.2E-06	2.7E-07	8.5E-07	1.7E-07	1.0E-06	2.4E-07	6.4E-07	2.2E-07	5.1E-08	2.5E-08
647.1	16.9	2.7E-06	9.0E-07	1.2E-06	3.2E-07	7.5E-07	1.6E-07	9.2E-07	2.0E-07	5.3E-07	1.5E-07	4.9E-08	4.5E-08
674.1	16.0	3.5E-06	1.0E-06	1.1E-06	3.6E-07	6.5E-07	1.3E-07	8.7E-07	1.9E-07	4.6E-07	8.9E-08	4.1E-08	4.4E-08
700.6	14.9	4.1E-06	8.7E-07	8.8E-07	3.6E-07	5.8E-07	1.2E-07	8.1E-07	1.7E-07	4.2E-07	7.4E-08	3.7E-08	3.5E-08
724.1	12.4	4.5E-06	6.9E-07	6.8E-07	3.1E-07	4.8E-07	9.9E-08	7.5E-07	1.5E-07	3.8E-07	7.9E-08	6.0E-08	3.7E-08
746.5	11.3	5.0E-06	8.1E-07	4.9E-07	2.4E-07	3.7E-07	8.1E-08	6.9E-07	1.3E-07	3.7E-07	8.1E-08	5.1E-08	5.3E-08
766.2	10.2	5.1E-06	7.7E-07	3.8E-07	1.8E-07	3.5E-07	6.8E-08	6.5E-07	1.1E-07	3.3E-07	7.2E-08	6.4E-08	6.4E-08
783.3	10.9	5.2E-06	9.0E-07	2.9E-07	1.3E-07	2.7E-07	4.0E-08	6.1E-07	1.1E-07	3.3E-07	6.4E-08	5.4E-08	6.5E-08
802.0	12.5	5.0E-06	1.0E-06	2.3E-07	1.3E-07	2.5E-07	2.4E-08	5.7E-07	1.4E-07	2.9E-07	5.4E-08	6.4E-08	5.7E-08
822.0	12.9	4.7E-06	1.1E-06	2.0E-07	1.1E-07	2.2E-07	2.8E-08	5.1E-07	1.0E-07	3.1E-07	5.1E-08	7.0E-08	0.0E+00
840.9	13.7	4.5E-06	1.3E-06	1.6E-07	8.4E-08	2.0E-07	7.1E-08	4.9E-07	1.5E-07	2.9E-07	3.1E-08	9.3E-08	0.0E+00
858.4	13.3	3.9E-06	1.2E-06	1.4E-07	7.2E-08	1.7E-07	4.7E-08	4.4E-07	1.0E-07	2.8E-07	4.8E-08	8.8E-08	0.0E+00
875.6	12.6	3.7E-06	1.3E-06	9.5E-08	5.5E-08	1.5E-07	5.8E-08	4.1E-07	1.2E-07	2.6E-07	4.0E-08	6.8E-08	0.0E+00
892.0	12.6	3.0E-06	1.1E-06	9.1E-08	5.1E-08	1.2E-07	4.9E-08	3.7E-07	8.9E-08	2.5E-07	3.1E-08	7.1E-08	0.0E+00
906.1	13.2	2.8E-06	1.0E-06	8.5E-08	6.0E-08	9.6E-08	4.0E-08	3.5E-07	1.0E-07	2.5E-07	2.1E-08	1.1E-07	0.0E+00
919.8	13.6	2.4E-06	8.5E-07	7.6E-08	5.1E-08	9.3E-08	3.6E-08	2.9E-07	7.4E-08	2.5E-07	4.1E-08	8.1E-08	0.0E+00
932.6	11.8	2.1E-06	7.8E-07	6.7E-08	3.3E-08	6.2E-08	5.0E-08	2.9E-07	7.3E-08	2.4E-07	4.0E-08	1.0E-07	0.0E+00
943.7	11.1	1.8E-06	6.4E-07	7.4E-08	3.1E-08	7.2E-08	2.4E-08	2.6E-07	5.0E-08	2.4E-07	3.7E-08	1.1E-07	0.0E+00
955.7	11.7	1.7E-06	5.4E-07	7.4E-08	2.5E-08	7.1E-08	5.5E-08	2.6E-07	5.0E-08	2.2E-07	4.7E-08	1.0E-07	0.0E+00
968.6	11.4	1.5E-06	4.2E-07	4.9E-08	3.1E-08	6.0E-08	3.8E-08	2.3E-07	5.1E-08	2.2E-07	5.1E-08	1.3E-07	0.0E+00
981.1	11.6	1.3E-06	3.8E-07	6.6E-08	4.5E-08	7.5E-08	5.9E-08	2.3E-07	7.1E-08	2.2E-07	2.8E-08	7.5E-08	0.0E+00
993.0	11.9	1.3E-06	3.9E-07	6.2E-08	3.5E-08	6.0E-08	6.1E-08	2.4E-07	4.0E-08	2.0E-07	6.3E-08	9.4E-08	0.0E+00

Table C.T.4 TGA data collected with a nominal heating rate of 8.6 °C s^{-1}.

T / °C	± °C	% Mass Loss	± % Weight
101.7	2.2	100.0	0.0
112.4	2.1	100.0	0.0
123.3	2.4	100.0	0.0
135.1	3.2	100.0	0.0
147.8	3.1	100.0	0.0
158.1	2.5	100.0	0.0
168.8	3.6	100.0	0.0
181.5	5.3	100.0	0.0
193.1	6.2	100.0	0.0
203.1	7.3	100.0	0.0
210.9	8.1	100.0	0.0
217.2	7.9	100.0	0.0
223.0	6.3	100.0	0.0
230.3	3.6	100.0	0.0
239.9	1.5	100.0	0.0
250.4	4.8	99.9	0.0
263.3	7.0	99.9	0.0
277.9	7.6	99.8	0.0
291.8	7.8	99.7	0.1
306.3	8.1	99.6	0.1
321.6	8.1	99.5	0.1
336.7	7.7	99.4	0.2
350.6	7.0	99.3	0.2
365.0	6.5	99.1	0.2
378.8	5.5	98.9	0.2
389.6	4.7	98.6	0.3
400.7	5.5	97.9	0.9
414.4	6.6	96.6	2.2
430.5	8.4	94.4	3.8
449.6	10.9	90.2	7.0
472.0	13.0	82.6	10.6
495.6	12.4	73.0	11.0
515.7	8.0	63.9	8.8
533.9	7.6	53.7	8.8
551.7	10.9	47.3	10.1
566.0	11.2	43.4	7.0
581.1	9.4	39.8	4.2
600.5	11.7	37.1	3.3
622.7	15.8	34.8	3.2
647.1	16.9	32.5	3.0
674.1	16.0	30.1	2.6
700.6	14.9	28.2	2.2
724.1	12.4	26.7	1.7
746.5	11.3	25.2	1.3
766.2	10.2	24.3	1.5
783.3	10.9	23.4	1.2
802.0	12.5	22.4	1.1
822.0	12.9	21.5	0.9
840.9	13.7	20.8	0.9
858.4	13.3	20.1	0.9
875.6	12.6	19.5	0.8
892.0	12.6	19.0	0.8
906.1	13.2	18.6	0.7
919.8	13.6	18.2	0.7
932.6	11.8	18.0	0.8
943.7	11.1	17.7	0.8
955.7	11.7	17.4	0.8
968.6	11.4	17.1	0.8
981.1	11.6	16.8	0.8
993.0	11.9	16.6	0.8